Development of multifunctional mannan nanogel

Sílvia Alexandra Rodrigues Mendes Ferreira

UMinho | 2012

Universidade do Minho
Escola de Engenharia

Sílvia Alexandra Rodrigues Mendes Ferreira

Development of multifunctional mannan nanogel

April 2012

Universidade do Minho
Escola de Engenharia

Sílvia Alexandra Rodrigues Mendes Ferreira

Development of multifunctional mannan nanogel

Thesis for PhD Degree in Biomedical Engineering

PhD Research Supervision
Supervisor: **Miguel Gama, PhD**
Co-supervisor: **Manuel Vilanova, PhD**

April 2012

Universidade do Minho, ___/___/______

Assinatura: ____

Agradecimentos

Com o aproximar desta meta importante, o meu doutoramento, olho para traz e sinto uma enorme felicidade porque no caminho percorrido fui guiada de perto por muitos que serão sempre por mim lembrados e aos quais aqui registo o meu reconhecimento e gratidão.

Começo por agradecer ao meu orientador Prof. Dr. Miguel Gama e ao meu co-orientador Prof. Dr. Manuel Vilanova pela confiança, orientação, dedicação, apoio científico e amizade.

Aos amigos e colegas do FUNCARB e do DEB-UM, em especial Paula Pereira, Vera Carvalho, Catarina Gonçalves, Renata Pértile, Fábia Andrade, Susana Moreira, Joana Carvalho, Reinaldo Ramos, Joana Silva, Maria Molinos, Carla Oliveira, Dina Silva, Sílvia Pedrosa, Jorge Padrão, Alexandre Leitão, João Pedro Silva, Ana Cristina Rodrigues, João Machado, Madalena Vieira entre muitos outros.

Aos amigos e colegas do ICBAS-UP, em especial Alexandra Correia, Pedro Madureira, Adília Ribeiro, Prof. Dr. Paula Ferreira, Filipe Cerca, Luzia Teixeira, Elva Andrade, Pedro Ferreirinha, Liliana Oliveira e Joana Alves.

Aos Professores Doutores Paulo Coutinho (DF-UM), Paula Sampaio (DB-UM), João Paulo Teixeira (INSA), José Alberto Martins (DQ-UM), Paula Gameiro (FCUP), Arwyn Jones (Universidade de Cardiff) e África González Fernández (UVigo); e ainda a Carla Costa (INSA), Merce Peleteiro Olmedo (UVigo), Goreti Pinto (ICVS-UM), Sandra Barros (Xana), Miguel Ferreira, Arsénio Sá, André Fontes, Elisa Pinto (DQ-UM) e Ana Sofia Abreu (DF-UM).

Aos amigos e colegas da Universidade de Lund, em especial Tommy Cedervall, Prof. Dr. Sara Linse, Risto Cuckalevski, Birgitta Frohm, Gleb Solomentsev, Erik Hellstrand, Olga Szczepankiewicz, Petra Behnen, Martin Lundqvist, Célia Cabaleiro, Cecilia Oslakovic, Prof. Dr. Björn Dahlbäck, Mikael Bauer, Michal Respondek, Johan Qvist, Carl Diehl e Ulrich Weininger. Obrigada por me terem feito sentir em casa na terra dos Vikings e como elemento da equipa.

A todos acima mencionados, agradeço a pronta ajuda, o saber transmitido, o companheirismo e todos os bons momentos dos quais tenho e terei sempre muita saudade. Sem vocês e as vossas sugestões e amizade tudo teria sido menos feliz e muito mais difícil.

À minha família que felizmente é grande e muito unida, em particular aos meus pais pelo apoio incondicional, pelo amor e por me terem permitido sonhar e alimentar os sonhos vivendo sempre intensamente novos desafios… Não há palavras! É mesmo único e excelente ser vossa filha!

Finalmente, ao International Iberian Nanotechnology Laboratory (INL) pela bolsa de doutoramento, à Fundação para a Ciência e Tecnologia (FCT) pelo apoio financeiro através do projeto PTDC e ainda à bolsa da Fundação Europeia para a Ciência (ESF) no âmbito do projeto europeu intitulado “Mapping the detailed composition of Surface-Absorbed Protein Layers on Biomaterials and Nanoparticles” (EpitopeMap).

Aos meus pais

Abstract

Development of multifunctional mannan nanogel

Self-assembled nanogels made of hydrophobized mannan or pullulan were obtained using a versatile, simple, reproducible and low-cost method. In a first reaction pullulan or mannan were modified with hydroxyethyl methacrylate or vinyl methacrylate, further modified in the second reaction with 1-hexadecanethiol. The resultant amphiphilic material self-assembles in water *via* the hydrophobic interaction among alkyl chains, originating the nanogel. Structural features, size, shape, surface charge and stability of the nanogels were studied using hydrogen nuclear magnetic resonance, cryo-field emission scanning electron microscopy and dynamic light scattering. Above the critical micellar concentration (cmc), evaluated by fluorescence spectroscopy with Nile red and pyrene, spherical polydisperse nanogels reveal long-term colloidal stability in aqueous medium up to six months, with a nearly neutral negative surface charge and mean hydrodynamic diameter in the nanoscale range, depending on the polymer degree of substitution. Nanogel based on vinyl methacrylated mannan was selected for further characterization among others because its synthesis is much easier, cheaper and less time consuming, its cmc and size are smaller, it is less polydisperse, and more stable at pH 3–8, in salt or urea solutions being consequently more suitable for biological applications.

Proteins (bovine serum albumin or ovalbumin) and hydrophobic drugs (curcumin) are spontaneously incorporated in the mannan nanogel, being stabilized by the hydrophobic domains randomly distributed within the nanogel, opening the possibility for the development of applications as potential delivery systems for therapeutic molecules.

No cytotoxicity is detected up to about 0.4 mg/mL of mannan nanogel in mouse embryo fibroblast cell line 3T3 and mouse bone marrow-derived macrophages (BMDM) using cell proliferation, lactate dehydrogenase and Live/Dead assays. Comet assay, under the tested conditions, reveals no DNA damage in fibroblasts, which seems to occur in the case of BMDM.

The internalization kinetics, uptake mechanisms and intracellular trafficking pathways of mannan nanogel in mouse BMDM was assessed by flow cytometry and confocal laser scanning microscopy, using fluorescently conjugated nanogel. A time-, concentration- and energy-dependent uptake profile of the mannan nanogel is observed. Inhibition analysis unraveled mannose receptor-mediated phagocytosis and clathrin-mediated endocytosis to be involved in nanogel uptake. The mannan nanogel is also visualized in the cytosol suggesting that a fraction was able to escape from the endolysosomal system.

The protein corona formed in human plasma around mannan nanogel was characterized by mass spectrometry after size exclusion chromatography or centrifugation followed by sodium dodecyl sulphate polyacrylamide gel electrophoresis. It consists of a very specific set of proteins, apolipoproteins B-100, A-I and E and human serum albumin, slowly formed following a dynamic protein exchange process.

The mannan nanogel does not affect blood coagulation, does not induce complement activation and retards the fibril formation of both Alzheimer's disease-associated amyloid β peptide and haemodialysis-associated amyloidosis β2 microglobulin, as was assessed by fluorometric thrombin generation assay, Western blot, and continuous thioflavin T fluorescence assay, respectively.

Mannan nanogel has potential immunological adjuvant activity, as evaluated on the specific immune response to ovalbumin in intradermally immunized BALB/c mice. Elicited ovalbumin-specific antibodies were predominantly of IgG1 subclass indicating a T helper 2-type bias.

Physicochemical characteristics, loading ability of biological agents, cytocompatibility and uptake of mannan nanogel by mouse BMDM, biosafety and biocompatibility studied at molecular level, and adjuvant activity are pronounced hints of the potential applicability of this nanosystem for macrophages targeted delivery of vaccines or drugs, acting as promising nanomedicines, always with the key goal of preventing and/or treating diseases.

Resumo

Desenvolvimento de um nanogel de manano multifuncional

Nanogéis poliméricos auto-organizados foram obtidos a partir de manano e pululano hidrofobicamente modificados por um método versátil, simples, reprodutível e económico. Numa primeira reação, manano ou pululano foram enxertados com hidroxietil metacrilato ou vinil metacrilato, que por sua vez foram substituídos numa segunda reação com 1-hexadecanetiol. O material anfifílico resultante auto-organiza-se em água através da associação das cadeias alquílicas hidrofóbicas, originando o nanogel. As características estruturais, o tamanho, a forma, a carga de superfície e a estabilidade dos nanogéis foram estudados por espectroscopia de ressonância magnética nuclear ^{1}H, microscopia crio-eletrónica de varrimento e dispersão dinâmica de luz. Acima da concentração micelar critica (cmc), avaliada por espectroscopia de fluorescência usando o vermelho de Nilo e o pireno, os nanogéis esféricos polidispersos revelam longa estabilidade coloidal em meios aquosos até seis meses, com carga de superfície negativa praticamente neutra, e diâmetro médio num intervalo nanométrico, cujo valor depende do grau de substituição do polímero. Dos nanogéis produzidos, o nanogel baseado em manano enxertado com vinil metacrilato foi selecionado para uma caracterização mais aprofundada porque a sua síntese é mais fácil, económica e rápida, a cmc e o tamanho são menores, é menos polidisperso e mais estável no intervalo de pH 3–8 bem como na presença de sal e ureia, sendo consequentemente mais apropriado para aplicações biológicas.

Proteínas (albumina sérica bovina ou ovalbumina) e drogas hidrofóbicas (curcumina) são incorporadas espontaneamente no nanogel de manano, sendo estabilizados nos domínios hidrofóbicos aleatoriamente distribuídos no interior do nanogel, abrindo perspetivas para o desenvolvimento de aplicações em sistemas de libertação de moléculas terapêuticas.

Nenhuma citotoxicidade é detetada com o nanogel de manano até 0.4 mg/mL na linha celular de fibroblastos de embrião de ratinho 3T3 e nos macrófagos derivados da medula óssea de ratinho usando ensaios de proliferação celular, lactato desidrogenase e “Live/Dead”. O ensaio cometa nas condições testadas, não revela dano no ADN dos fibroblastos, que possivelmente ocorre, no entanto, no caso dos macrófagos.

A cinética de internalização, os mecanismos de internalização e as vias de tráfego intracelular do nanogel de manano nos macrófagos derivados da medula óssea de ratinho foram avaliados por citometria de fluxo e microscopia de confocal de varrimento laser, usando o nanogel conjugado com um fluorocromo. O perfil de internalização do nanogel é dependente do tempo, da concentração e de energia. A análise com inibidores revelou que a fagocitose mediada pelo receptor da manose e a endocitose mediada por clatrina estão envolvidos na internalização do nanogel. O nanogel de manano é também visualizado no citosol sugerindo que uma fração é capaz de escapar do sistema endolisossomal.

A corona de proteínas formada no plasma humano em redor do nanogel de manano foi caracterizada por espectrometria de massa, após cromatografia de exclusão por tamanho ou centrifugação, seguidas de eletroforese em gel de poliacrilamida na presença de dodecil sulfato de sódio. A corona consiste num conjunto específico de proteínas, apoliproteínas B-100, A-I e E e albumina sérica humana, que se forma após um lento e dinâmico processo de troca de proteínas.

O nanogel de manano não afeta a coagulação do sangue, não induz ativação do complemento e retarda a formação de fibras do péptido β amiloide associado à doença de Alzheimer e de β2 microglobulina na amiloidose associada à hemodiálise, como foi avaliado por teste fluorimétrico de geração de trombina, Western blot e análise continua da fluorescência de tioflavina T, respectivamente.

O nanogel de manano tem potencial atividade adjuvante, avaliada na resposta imune específica para ovalbumina em ratinhos BALB/c imunizados por via intradérmica. Os anticorpos específicos para ovalbumina induzidos foram predominantemente da subclasse IgG1, o que indica uma propensão para induzir uma resposta mediada por células “T helper” tipo 2.

As características físico-químicas, a capacidade de incorporação de agentes biológicos, a citocompatibilidade e a internalização do nanogel de manano por macrófagos derivados da medula óssea de ratinho, a biossegurança e biocompatibilidade estudadas a nível molecular, e a atividade adjuvante deixam entrever a potencial aplicação deste nanosistema na libertação direcionada a macrófagos, quer de vacinas quer de fármacos, atuando como promissores nanomedicamentos, sempre com o objetivo chave de prevenir e/ou tratar doenças.

Publications

This thesis is based on the following review and original research articles:

Ferreira, S. A.; Vilanova, M.; Gama, F. M. **Polymeric nanogels as vaccine delivery systems.** *Submitted* (Chapter 1)

Ferreira, S. A.; Coutinho, P. J. G.; and Gama, F. M. **Synthesis and characterization of self-assembled nanogels made of pullulan.** *Materials* **2011**, 4, 601-620. (Chapter 2)*

Ferreira, S. A.; Coutinho, P. J. G.; Gama, F. M. **Self-assembled nanogel made of mannan: synthesis and characterization.** *Langmuir* **2010**, 26, 11413-11420. (Chapter 3)*

Ferreira, S. A.; Pereira, P.; Sampaio, P.; Coutinho, P. J. G.; Gama, F. M. **Supramolecular assembled nanogel made of mannan.** *J Colloid Interface Sci* **2011**, 361, 97-108. (Chapter 4)*

Ferreira, S.A.; Carvalho, V.; Costa, C.; Teixeira, J. P.; Vilanova, M.; Gama, F. M. **Self-assembled mannan nanogel: cytocompatibility and cell localization.** *J Biomed Nanotechnol* **2012**, accepted (Chapter 5)*

Ferreira, S. A.; Correia, A.; Madureira, P.; Vilanova, M.; Gama, F. M. **Unraveling the uptake mechanism of mannan nanogel in bone-marrow derived macrophages.** *Submitted* (Chapter 6)

Ferreira, S. A.; Oslakovic, C.; Cuckalevski, R.; Frohm, B.; Dahlbäck, B.; Linse, S.; Gama, F. M.; Cedervall, T. **Biocompatibility of mannan nanogel – safe interaction with plasma proteins.** *Biochim Biophys Acta* **2012**, accepted (Chapter 7)*

Ferreira, S. A.; Correia, A.; Vilanova, M.; Gama, F. M. **Adjuvant effect of mannan nanogel on the immune responses to ovalbumin in mice.** *Work still in progress* (Chapter 8)

** According to article 8 paragraph 2 of the Portuguese Decree-Law No. 388/70, this thesis is based on the publications discriminated.*

Table of contents

Chapter 1 1

General Introduction: Polymeric nanogels as vaccine delivery systems

Chapter 2 35

Synthesis and characterization of self-assembled nanogels made of pullulan

Chapter 3 57

Self-assembled nanogel made of mannan: synthesis and characterization

Chapter 4 79

Supramolecular assembled nanogel made of mannan

Chapter 5 107

Self-assembled mannan nanogel: cytocompatibility and cell localization

Chapter 6 127

Unraveling the uptake mechanism of mannan nanogel in bone marrow-derived macrophages

Chapter 7 149

Biocompatibility of mannan nanogel – safe interaction with plasma proteins

List of figures

Chapter 1 1

Chapter 2 35

Chapter 3 57

List of tables

Chapter 1 1

Chapter 2 35

Chapter 3 57

Chapter 4 79

Chapter 5 107

Chapter 6 127

Chapter 8 175

List of schemes

List of abbreviations and nomenclature

A549	Human lung adenocarcinoma cell line
Aβ(M1-40)	Amyloid β peptide
Alum	Aluminum salts
ANOVA	Analysis of variance
APC	Antigen-presenting cells
apoA-I	Apolipoprotein A-I
AS03 and AS04	Adjuvant System 03 and Adjuvant System 04
ATCC	American Type Culture Collection
ATP	Adenosine triphosphate
ATPase	Enzyme that binds and hydrolyzes adenosine triphosphate
BCA	Bicinchoninic acid
BCIP	5-bromo-4-chloro-3-indolyl phosphate
BMDC	Bone marrow-derived dendritic cells
BMDM	Bone morrow-derived macrophages
BSA	Bovine serum albumin
C	Number of colocalized pixels
C_{16} or SC_{16}	C_{16} aliphatic chain; 1-hexadecanethiol
C1q	Complement component 1q
C3	Complement component 3
C3b	Complement component 3b
cac	Critical aggregation concentration
CD (in cells)	Cluster of differentiation
CD	Circular dichroism
C_G	Colocalization coefficient in green pixels area
CHM	Cholesterol-bearing mannan
CHP	Cholesterol-bearing pullulan
CLSM	Confocal laser scanning microscopy
cmc	Critical micellar concentration
con A	Concanavalin A
CPI	Cell proliferation index
C_R	Colocalization coefficient in red pixels area
cRPMI	RPMI complete medium
Cryo-FESEM	Cryo-field emission scanning electron microscopy
C_T	Colocalization coefficient in total pixels area
CT-26	Mouse colon carcinoma cell line
CTB	Cholera toxin B subunit
CVB3	Coxsackievirus B3
D_2O	Deuterium oxide
DAPI	4'-6-diamidino-2-phenylindole
DC	Dendritic cells
DC-SIGN	Dendritic cell-specific intercellular adhesion molecule 3-grabbing non-integrin

DEC-205	Dendritic and epithelial cells, 205 kDa integral membrane glycoprotein (CD205)
DIC	Differential interference contrast
DLS	Dynamic light scattering
DLVO	Derjaguin-Landau-Verwey-Overbeek
DMAP	4-(N,N-dimethylamino)pyridine
DMEM	Dulbecco's modified Eagle's media
DMSO	Dimethyl sulfoxide
DNA	Deoxyribonucleic acid
DS	Degree of substitution
DS_{C16}	Degree of substitution with the hydrophobic alkyl chains
$DS_{HEMA\ or}$ DS_{VMA}	Degree of substitution with methacrylate groups
DT	Diphtheria toxoid
EDTA	Ethylenediaminetetraacetic acid
E.G7	Ovalbumin-expressing tumor cell line
λ_{em}	Wavelength of emission
ELISA	Enzyme-linked immunosorbent assay
EphA2	Ephrin type-A receptor 2
ER	Endoplasmic reticulum
Eriss	Endoplasmic reticulum-insertion signal sequence
λ_{ex}	Wavelength of excitation
FACS	Fluorescence-activated cell sorting; flow cytometric
FBS	Fetal bovine serum
FDA	Food and Drug Administration
FM 4-64	N-(3-triethylammoniumpropyl)-4-(p-diethylaminophenyl-hexatrienyl) pyridinium dibromide
G	Number of green pixels
GM-CSF	Granulocyte-macrophage colony stimulating factor
gp	Glycoprotein
GTPase	Enzyme that binds and hydrolyzes guanine triphosphate
ΔH	Enthalpy
^{1}H NMR	Hydrogen nuclear magnetic resonance
H3N2	Influenza A virus subtype (surface coated by 3 hemagglutinin and 2 neuraminidase)
HA	Hemagglutinin
HASMCs	Human arterial smooth muscle cells
HBcAg	Hepatitis B core antigen
HBS	HEPES buffered saline
HBSS	Hank´s balanced salt solution
HBsAg	Hepatitis B surface antigen
HBSBSA	HEPES buffered saline supplemented with bovine serum albumin
HDL	High-density lipoprotein
HeLa	Human epithelial carcinoma cell line
HEMA	Hydroxyethyl methacrylate
HEMA-CI	CDI-activated hydroxyethyl methacrylate or hydroxyethyl methacrylate-

	imidazolyl carbamate
HEPES	4-(2-hydroxyethyl)-1-piperazineethanesulfonic acid
HepG2	Human hepatoma cell line
HER2	Human epidermal growth factor receptor 2
HIV	Human immunodeficiency virus
HLA	Human leukocyte antigen
γ-hPGA	Hydrophobically modified poly-(γ-glutamic acid)
HSA	Human serum albumin
I-1140 or Z-Gly-Gly-Arg-AMC · HCl	Z-Glycine-Glycine-Argynin-7-amino-4-methylcoumarin · hydrochloric acid
i.d.	Intradermally
IFN	Interferon
Ig	Immunoglobulin
IL	Interleukin
i.m.	Intramuscularly
i.n.	Intranasally
i.p.	Intraperitonealy
ITC	Isothermal titration calorimetry
i.v.	Intravenously
J774	Mouse macrophage-like cell line
K_D	Dissociation constant
KDa	Kilodalton
LCCM	L929 cell conditioned medium
LDH	Lactate dehydrogenase
LPS	Lipopolysaccharide
LTK63	Nontoxic mutant of *Escherichia coli*
β2m	β2 microglobulin
M cells	Microfold cells
MAC-1	Macrophage-1 antigen receptor
MAGE-3	Melanoma-associated antigen 3
MALDI-TOF	Matrix-assisted laser desorption/ionization - time of flight
MALT	Mucosa-associated lymphoid tissues
Mannan-C_{16}	Amphiphilic mannan or hydrophobized mannan
Mannan-HEMA	Hydroxyethyl methacrylated mannan
Mannan-VMA	Vinyl methacrylated mannan
MAPK	Mitogen-activated protein kinase
MCC	Mono-*N*-carboxymethyl chitosan
MCF-7	Human breast adenocarcinoma cell line
MDP	Muramyl dipeptide
MFC	Mouse forestomach carcinoma cell line
MFI	Mean fluorescence intensity
MHC	Major histocompatibility complex
MHC_{16}	Amphiphilic molecules mannan-HEMA-C_{16}
MO5	Ovalbumin-expressing murine B16 melanoma

MPL	Monophosphoryl lipid A
MPs	Microparticles
MR	Mannose receptor
mRNA	Messenger RNA
MS	Mass spectrometry
MSP-1	Merozoite surface protein 1
MTS	3-(4,5-dimethylthiazol-2-yl)-5-(3-carboxymethoxyphenyl)-2-(4-sulfophenyl)-2H-tetrazolium
MTT	3-(4,5-dimethylthiazol-2-yl)-2,5-diphenyltetrazolium bromide
MVC$_{16}$	Amphiphilic molecules mannan-VMA-C$_{16}$
MWCO	Molecular weight cut-off
MyD88	Myeloid differentiation factor-88
NF-κB	Nuclear factor kappa-light-chain-enhancer of activated B cells
NIPAM	*N*-isopropylacrylamide
NIPAM:BAM	*N*-isopropylacrylamide:*N*-*tert*-butylacrylacrylamide
NLRP3	NOD-like receptor family, pyrin domain containing 3
NPs	Nanoparticles
NR	Nile red
NY	New York
NY-ESO-1	New York-esophageous 1 protein
OVA	Ovalbumin
PAM$_3$CSK$_4$	Tripalmitoyl cysteinyl seryl tetralysine lipopeptide
PAMP	Pathogen-associated molecular patterns
PBS	Phosphate buffered saline
PCL	Poly(ε-caprolactone)
PdI	Polydispersity index
PEG	Poly(ethylene glycol)
PEI	Poly(ethylenimine)
PGA	Poly(glycolic acid)
γ-PGA	Poly-(γ-glutamic acid)
PHC$_{16}$	Amphiphilic molecules pullulan-HEMA-C$_{16}$
PI	Propidium iodide
PLA	Poly(D,L-lactic acid)
PLGA	Poly(D,L-lactic-co-glycolic acid)
PLL	Poly-L-lysine
PMMA	Poly(methyl methacrylate)
PMS	Phenazine methosulfate
poly-U	Poly(uridylic acid)
PRR	Pattern-recognition receptors
PS-PE-PC	Phosphatidylserine-phosphatidylethanolamine-phosphatidylcholine
Pullulan-C$_{16}$	Amphiphilic pullulan or hydrophobized pullulan
Pullulan-HEMA	Hydroxyethyl methacrylated pullulan
Pullulan-VMA	Vinyl methacrylated pullulan
PVC$_{16}$	Amphiphilic molecules pullulan-VMA-C$_{16}$

PVDF	Polyvinylidene fluoride
Py	Pyrene
R	Overlap coefficient
R	Number of red pixels
RAW 264.7	Murine macrophage cell line
ROIs	Regions of interest
RNA	Ribonucleic acid
Rp	Pearson's correlation coefficient
RPMI	Roswell Park Memorial Institute medium
RSV	Respiratory syncytial virus
SAMSA fluorescein	5-((2-(and-3)-*S*-(acetylmercapto)succinoyl)amino)fluorescein
s.c.	Subcutaneously
S.D.	Standard deviation
SDS	Sodium dodecyl sulphate
SDS-PAGE	Sodium dodecyl sulphate polyacrylamide gel electrophoresis
SEC	Size exclusion chromatography
SI	Stimulation index
sIgA	Secretory immunoglobulin A
SHIV-KU-2	Simian and human immunodeficiency chimeric virus
3T3	Mouse embryo fibroblast cell line
T	Number of total pixels
TAA	Tumor-associated antigen
TEA	Triethylamine
T_H	T helper
THP-1	Human acute monocytic leukemia cell line
ThT	Thioflavin T
TLR	Toll-like receptors
TMC	*N*-trimethyl chitosan
TNF	Tumor-necrosis factor
TRP-2	Tyrosinase related protein-2
TST	Tris-buffered saline
TT	Tetanus toxoid
UK	United Kingdom
USA	United States of America
UV-Vis	Ultraviolet-visible
VEGF	Vascular endothelium growth factor
VMA	Vinyl methacrylate
VP1	Viral protein 1

Aims and thesis outline

Polymeric nanogels plenty of remarkable intrinsic properties have been extensively and successfully exploited as promising biomedical formulations arising as great alternatives with potential applicability in vaccination and in new therapeutic approaches.

The prime motivation of this work was to design self-assembled mannan and pullulan nanogels in order to supply a vaccine or therapeutic delivery platform based on the bioactive properties of mannan to target mannose receptor expressed on the surface of antigen-presenting cells and of pullulan to target asialoglycoprotein receptor expressed on the sinusoidal surface of the hepatocytes, combined with the performance of polymeric nanogels as carriers of biologically active agents.

Chapter 1 covers the recent published data concerning the modulation of innate and adaptive immune responses using engineered polymeric nanogels and their potential application as delivery systems in vaccination.

Chapters 2, 3 and 4 describe the synthesis of self-assembled mannan and pullulan nanogels by Michael addition and report their characterization in terms of structure, size, shape, surface charge and stability. Achieved results conducted to the selection of nanogel based on hydrophobized vinyl methacrylated mannan to be further studied to evaluate its potential for biological applications.

Chapter 5 provides details of mannan nanogel cytocompatibility in mouse embryo fibroblast cell line 3T3 and bone marrow-derived macrophages.

Chapter 6 unravels the mannan nanogel uptake profile in mouse bone marrow-derived macrophages.

Chapter 7 reveals the protein corona around mannan nanogel formed in human plasma, and the effect of mannan nanogel on blood coagulation and in protein fibrillation.

In chapter 8, the mannan nanogel potential as an adjuvant/delivery system is evaluated in a preliminary immunization study in mice using ovalbumin as a model antigen.

In the final chapter, chapter 8, a summary of the main conclusions and some future perspectives are portrayed.

Chapter 1

General Introduction: Polymeric nanogels as vaccine delivery systems

Polymeric nanogels find a relevant field of application in the formulation of a new generation of therapeutic and preventive vaccines, aiming the fine-tuned modulation of the immune response. Intrinsic properties of polymeric nanogels, such as material chemistry, size and shape, surface charge, and hydrophobicity/hydrophilicity may be determining factors in shaping the induced immune response. These materials can thus work as synthetic adjuvants, which can also be conjugated with immunostimulants. Polymeric nanogels protect vaccine antigens from degradation *in vivo* and, surface-conjugated with antibodies or specific ligands could increase active targeting specificity. This review covers the recent published data concerning the modulation of innate and adaptive immune responses by engineered polymeric nanogels and their potential application as delivery systems in vaccination.

The induction of an antigen-specific immune response is a key principle of vaccination. Usually, immunogenicity depends on the action of antigen-presenting cells (APC) into which antigens must be carried to be internally processed for surface presentation to T-cells. In addition to antigen presentation, APC-dependent activation of the T-cells also needs the up-regulated expression of surface co-stimulatory molecules or secreted factors such as cytokines (Figure 1). Cytokines released from APC drive the differentiation of T-cells, which acquire effector functions including antigen-specific cytotoxicity or specific help to cellular or humoral immunity. In naturally occurring immunizations, especially in the course of infection, the up-regulated expression of T-cell co-stimulatory molecules or cytokines by APC is triggered by ligands characteristic of invading pathogens, generally designated as pathogen-associated molecular patterns (PAMP). These may be recognized by specific pattern-recognition receptors (PRR) on the surface, in the cytosol or inside intracellular compartments, of which Toll-like receptors (TLR) are the prototypical example.[1] When PAMP are absent in subunit vaccine formulations, adjuvants might be necessary to potentiate such mechanisms of T-cell stimulation and therefore immunogenicity. Some adjuvants can act on APC by engaging specific PRR, thus mimicking signals usually provided by pathogens.[2] In addition, some delivery systems, e.g., liposomes or virus-like particles preparations, can combine adjuvant activity with the targeted delivery of antigens to APC.[3] Only a few adjuvants are currently licensed for human vaccines, which include alum (aluminum salts), MF59™, Adjuvant System 03 (AS03), Montanide™ ISA 51, Adjuvant System 04 (AS04), and virosomes.[2, 4, 5] Approved adjuvants are mostly used in preventive vaccines of diseases caused by virus or extracellular bacteria, for which specific antibodies provide significant protection.[5] This illustrates one of the limitations of current vaccines, i.e., their efficacy mostly relies on the induction of protective antibodies rather than on cell-mediated immunity.[6] This may hamper the immune-based prevention of diseases caused by intracellular pathogens or cancer, where cellular immunity is a key effector mechanism.[7] To overcome the mentioned limitation and improve vaccine performance or potency as well, novel compounds or formulations are currently being rationally designed. Among them, polymeric nanogels have potential to arise as safe and effective alternatives to the current way of vaccine delivery being able to induce not only strong and long-lasting antibody responses but also potent cell mediated immunity based on $CD4^+$ and $CD8^+$ T-cell responses. Polymeric nanogels may combine immunomodulatory properties with targeted antigen delivery features, working as integrated adjuvants.[8, 9]

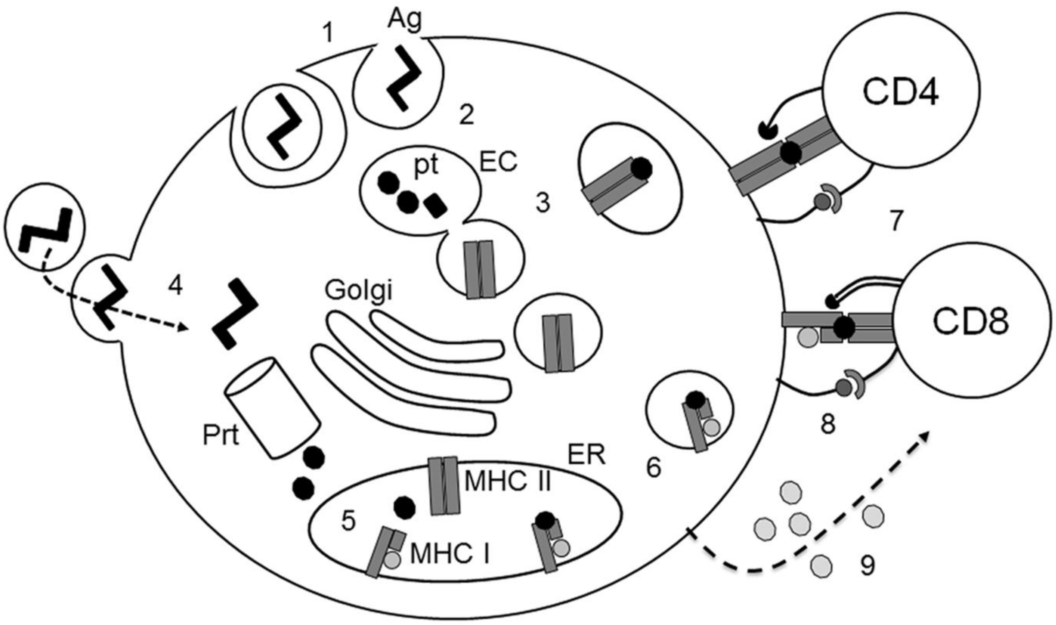

Figure 1. Vaccination antigens (Ag), e.g., purified proteins, may be internalized by APC from the external millieu by phagocytosis or other endocytic processes (1). Within endocytic compartments (EC), antigen is processed at acidic pH into peptide fragments (pt) (2). Peptides are then loaded to major histocompatibility complex class II molecules (MHC II) transported into endocytic compartments in Golgi apparatus (Golgi)-originated vesicles (3). Mature endosomes fuse with the plasma membrane where peptides loaded to MHC class II molecules are exposed. Antigens may also be delivered to the cytosol and cleaved within the proteasome (Prt) originating peptides (4). These are transported into the endoplasmic reticulum (ER) where they are loaded to MHC class I molecules (MHC I) in a chaperone-assisted process (5). Peptide-loaded MHC class I molecules are transported to the cell membrane (6), where they can be recognized by specific CD8$^+$ T-cells, whereas CD4$^+$ T-cells recognize peptides presented in the context of MHC class II molecules (7). APC also provide co-stimulatory stimuli by either surface molecules (8) or soluble factors such as cytokines (9).

Polymeric nanogels as vaccine delivery/adjuvant systems

Nanometer-sized polymeric hydrogels, i.e., nanogels or hydrogel nanoparticles (NPs; size from 1 to 1000 nm) are swollen networks composed of amphiphilic or hydrophilic polyionic polymers, either natural or synthetic. Nanogels are promising multifunctional polymeric NPs with potential as delivery systems because of their *sui generis* properties. These include tunable chemical and physical structures, flexible nanosize, large surface area for multivalent conjugation, high water content, biocompatibility,[10, 11] loading capacity, stability, ability to target specific cells and specific cell compartments, immunomodulatory properties and responsiveness to environmental factors.[12] As nanocarriers must be delivered to specific sites upon injected into body fluids, the possibility to modulate the chemical and physical properties of NPs could be most helpful in the overcoming of major biological barriers such as the reticuloendothelial system, clearance through kidney glomeruli and nonspecific accumulation in different organs.

Nanogels have been designed using different approaches, which can be divided into physical self-assembly of interactive polymers, polymerization of monomers in a homogeneous phase or in a micro- or nanoscale heterogeneous environment, cross-linking of preformed polymers, and template-assisted nanofabrication.[13] Several natural biopolymers have been commonly used to develop nanogels, e.g., dextran, dextrin, pullulan, mannan, chitosan, poly-L-lysine (PLL), poly-(γ-glutamic acid) (γ-PGA), heparin, hyaluronic acid, and alginate. Synthetic biodegradable and biocompatible polymers, e.g., poly(methyl methacrylate) (PMMA), poly(D,L-lactic acid) (PLA), poly(glycolic acid) (PGA), poly(D,L-lactic-co-glycolic acid) (PLGA), and poly(ε-caprolactone) (PCL), approved for human administration by the USA FDA,[14] have been frequently used in the development of potential vaccine delivery systems.

NPs may be engineered as to either stimulate or suppress the triggered immune response, thus providing the appropriate activity: upregulation or downregulation of the immune response, respectively in the prevention or treatment of infections and cancer or of allergies and autoimmune diseases.[15] A compilation of studies in which different NPs have been used as antigen- or nucleic acid-delivery systems in different experimental or clinical settings is presented in Table 1. The interaction of particulate delivery systems with APC may stimulate these cells in a way resembling the one triggered by pathogens, which are commonly recognized, phagocytozed, and processed by professional APC. *In vitro* studies have shown that exposing dendritic cells (DC) to polymeric NPs resulted in their activation and maturation, as evidenced by upregulated surface expression of major histocompatibility complex (MHC) class II or co-stimulatory molecules (CD40, CD80, CD83, and CD86),[16-18] secretion of cytokines[19] and chemokines, and expression of chemokine receptors.[20] Activated DC migrate to regional lymph nodes where they present antigen to T-cells, thereby triggering cellular immunity, which in turn may provide help to humoral immunity. The intrinsic adjuvant properties of NPs to stimulate APC may thus be an additional advantage towards their usage as antigen-delivery systems for vaccination. In vaccination, the relationship between the rate of antigen availability and the induction of the immune response is poorly understood as, apparently, no clear or direct correlation could be found between *in vitro* antigen release profile and the antigen-specific *in vivo* immune response. Indeed, both rapid and extended *in vitro* antigen release profiles have been shown to induce similar immune responses in animal studies upon intranasal (i.n.) administration.[21, 22] Continuous antigen delivery is usually considered to be more effective in inducing immunity, as prolonged antigen exposure allows enough time for affinity maturation and isotype switching to occur, and immune memory to be generated.[23] Moreover, in a DNA-based vaccine delivery system, controlled release of DNA in synchrony with the natural development of the immune response seems to be crucial for the efficacy of the vaccine.[24] However, it has been suggested that antigen presentation by APC to naïve and effector T-cells may only be required over the first few days for an efficient induction of T-cell expansion and differentiation, and that antigen presentation for weeks or months may instead lead to T-cell death, decreased effector expansion and reduced cytokine production by recovered effectors.[25]

Table 1. Usage of polymeric nanogels as antigen- or nucleic acid-delivery systems

Polymeric nanogels (+ *immunostimulant*)	**Antigen/nucleic acid**	**Model**	**Response**	**Route(s)**	**Ref**
CHP	HER2	Human	IgG, $CD4^+$, $CD8^+$ T-cells	s.c.	105, 106, 110
CHP	NY-ESO-1	Human	IgG, $CD4^+$, $CD8^+$ T-cells	s.c.	107, 108, 110
chitosan-deoxycholic acid	MAGE-3 peptide	615 mice	IFN-γ, cytotoxic T-cells	s.c.	99
chitosan	TT	BALB/c	IgG, IgA	i.n.	67
chitosan	TT	BALB/c	IFN-γ, IgG	i.n.	114
chitosan	HBsAg	BALB/c	IgG	i.m./i.n.	115
chitosan-alginate (+ *CpG*)	HBsAg	BALB/c	IgG, IgA	i.n.	93
chitosan	*Leishmania* superoxide dismutase	BALB/c	IgG	s.c.	113
chitosan	plasmid DNA encoding peanut allergen	AKR/J mice	decreased IgE	oral	149
chitosan	plasmid DNA encoding HBsAg	BALB/c	IFN-γ, IL-2, IgG, IgA	i.n.	140
chitosan	plasmid DNA encoding *M. tuberculosis* peptides	HLA-A2 transgenic mice	IFN-γ	i.m./pulmonary	18
chitosan	plasmid DNA encoding VP1 of CVB3	BALB/c	IgG, IgA, cytotoxic T-cell	i.n.	65
chitosan	plasmid DNA encoding RSV antigens	BALB/c	IFN-γ, IgG, IgA, cytotoxic T-cells	i.n.	66
chitosan/TMC	OVA	BALB/c	IgG	intraduodenally	118
TMC	OVA	BALB/c	IgG	i.d.	17

Table 1. *cont.*

Polymeric nanogels (+ *immunostimulant*)	**Antigen/nucleic acid**	**Model**	**Response**	**Route(s)**	**Ref**
TMC	OVA	BALB/c	IgG	i.m.	88, 119
TMC	OVA	BALB/c	IgG, IgA	i.n.	119
TMC (+*LPS/CTB/* PAM$_3$CSK$_4$*/MDP/CpG*)	OVA	BALB/c	IgG, IgA	i.d./i.n.	87
TMC-hyaluronic acid	OVA	BALB/c	IgG	i.n./i.d.	120
TMC	HBsAg	BALB/c	IgG/IgA	i.n.	117
TMC	DT	BALB/c	IgG	i.d.	17
TMC	influenza A subunit H3N2	C57BL/6	IgG/IgA	i.m./i.n	22
TMC-MCC	TT	BALB/c	IgG	i.n.	70
TMC-alginate	urease	Kunming mice	IgG/IgA	s.c./oral	49
γ-hPGA	listerolysin peptide	C57BL/6	survival	rear footpad	73
γ-hPGA	Tax peptide	C3H mice	cytotoxic T-cells	s.c.	100
γ-hPGA	gp100 peptide	C57BL/6	IFN-γ	s.c.	100
γ-hPGA	EphA2 peptide	C57BL/6	IFN-γ, cytotoxic T-cells	i.p.	101
γ-hPGA	OVA	C57BL/6	cytotoxic T-cells	s.c.	124
γ-hPGA	OVA	C57BL/6	IgG, cytotoxic T-cells	rear footpad	73
γ-hPGA	HIV-1 gp120	BALB/c	IFN-γ, cytotoxic T-cells	i.n.	36
γ-hPGA	HIV-1 p24	BALB/c	IFN-γ, IgG	s.c.	121
γ-hPGA	influenza HA	BALB/c	IFN-γ, IL-4, IL-6, IgG, cytotoxic T-cells	s.c.	122
γ-hPGA	influenza HA	BALB/c	IFN-γ, IL-4, IL-6, IgG/IgA	s.c./i.n.	123
PEI/γ-PGA	plasmid DNA encoding *P. yoelii* MSP-1 C-terminal	C57BL/6	IFN-γ, IL12p40, IgG	i.v.	143, 144

Table 1. cont.

Polymeric nanogels (+ *immunostimulant*)	**Antigen/nucleic acid**	**Model**	**Response**	**Route(s)**	**Ref**
PLA (+ *poly-U)*	OVA	C57BL/6	IFN-γ, IgG	s.c.	[90]
PLA	HIV-1 p24 and/or gp120	BALB/c	IL-2, IL-6, IL-10, IgG, cytotoxic T-cells	s.c.	[127, 128]
PLA	HBsAg	Wistar Rats	IFN-γ, IgG	i.m.	[54]
PLGA (+ *7-acyl lipid A*)	TRP-2 peptide	C57BL/6	$CD8^+$-derived IFN-γ	s.c.	[102]
PLGA, PLGA/TMC	OVA	BALB/c	IgG	i.m.	[119]
PLGA (+ *7-acyl lipid A*)	OVA	BALB/c	IFN-γ, $CD4^+$, $CD8^+$ T-cells	i.p./s.c.	[133]
PLGA (+ *MPL*)	OVA	BALB/c	IgG, IgA	oral	[134]
PLGA (+ *CpG)*	TT	C57BL/6	IFN-γ, IgG	s.c.	[85]
PLGA	*B. pertussis* toxoid and filamentous HA	BALB/c	IFN-γ, IL-5, IgG	i.p./oral	[55]
PLGA	BSA	BALB/c	IgG	s.c./oral/i.n.	[57]
PLGA	protein from *N. meningitides* type B	CD1 mice	IgG	i.m./i.p.	[58]
PLGA (+ *LTK63*)	HIV-1 gp140	BALB/c	IgG	i.n.+i.m.	[58]
PLGA (+ *MPL)*	HBcAg	C57BL/6	IFN-γ	s.c.	[131]
PLGA-PEI	Rv1733c DNA /protein	BALB/c	IFN-γ	i.m./pulmonary	[19]
PCL, PLGA, PLGA-PCL	DT	BALB/c	IFN-γ, IL-6, IgG	i.n./i.m.	[71]
PCL-based (+ *CTB*)	*S. equi* proteins	BALB/c	IL-2, IL-4, IgG	i.n.	[92]
acid-degradable polyacrylamide (+ *CpG*)	OVA	C57BL/6	cytotoxic T-cells	s.c.	[16, 29, 30]
PMMA-Eudragit L100-55	HIV-1 Tat protein	BALB/c	IFN-γ, IL-4, IgG, cytotoxic T-cells	i.n.	[136]

ref, references; BALB/c and C57BL/6 are mice strains unless otherwise indicated.

Properties of the nanodevice vs immune response

Nanogels themselves may be intrinsically immunologically active, by virtue of their particular character or as a result of protein adsorption, being recognized as a “danger” signal. Properties of the nanodelivery systems, such as material chemistry, size and shape, surface charge, and hydrophobicity/hydrophilicity are determining factors on the induced immunity and will be discussed below.

Material Chemistry

The molecular weight and the copolymer composition can modulate the load release mechanism; higher polymer molecular weight results in slower *in vitro* release of the biological agent.[26] On the other hand, the functional groups at the nanogel surface can be modified with various targeting moieties for site-specific vaccine delivery. A number of materials chemistries have been engineered to promote release of NPs payload within the endolysosomal compartments, attending both pH and the reductive-oxidative gradient experienced during endolysosomal processing.[27] Nanomaterials sensitive to acid hydrolysis (orthoesters, hydrazide or acetal bonds)[28-30] or to reduction (glutathione-responsive)[31] have been investigated for endosomal release of biological agents. Whereas the endosomal/phagosomal compartment is the aimed target for MHC class II loading, MHC class I presentation requires the antigen payload to be present in the cytosol.[32] Thus, disruption of the endosomal membrane barrier in order that exogenous antigens could gain access the cytosol is an important target and a challenging problem. Endosomal disruption is also necessary for DNA-based vaccination, in which plasmid DNA must be expressed to produce the antigen.[33] To avoid lysosomal trafficking, “smart” polymers have been designed. Both pH-sensitive and reductive-sensitive nanomaterials release oligonucleotides and peptides into the cytosol as the endosome is acidified, avoiding the lysosomal fusion. As a consequence, antigen processing may occur through the cytosolic (MHC class I) pathway instead of the exogenous (MHC class II) pathway, thus promoting cross-presentation. Indeed, endosomal escape following uptake of PLGA NPs loaded with ovalbumin (OVA) have been linked to an increase in the presence of antigen in the cytosol and promoted cross-presentation, enhancing and sustaining antigen presentation *via* MHC class I to a much higher degree than soluble antigen, in murine bone marrow-derived dendritic cells (BMDC).[34] Protamine-coated PLGA NPs stimulated murine BMDC and enhanced the cross-presentation of encapsulated exogenous antigen (OVA) by facilitating antigen uptake and lysosomal escape.[35] Moreover, HIV envelope glycoprotein (gp)120 loaded in hydrophobically modified γ-PGA (γ-hPGA, γ-PGA-graft-L-phenylalanine copolymers) NPs have shown induced antigen specific effector and CD8$^+$ T-cell memory response in i.n.-immunized mice.[36] Acid-degradable particles, which components exert an osmotic pressure on the endosomal/phagosomal membrane leading to its rupture, have been used to enhance antigen presentation *in vitro* and vaccination *in vivo.*[16, 37, 38] CD205 (dendritic and epithelial cells, 205-kDa integral membrane glycoprotein (DEC-205))-targeted acid-degradable acetal-cross-linked OVA-loaded particles enhanced antigen presentation by DC *via* both MHC class I and II pathways, leading to an improved cellular immune response.[37] Codelivery with adjuvants (unmethylated CpG and anti-interleukin-10 anti-sense oligonucleotides) increased secretion of interleukin (IL)-12 and maximized the elicited cellular immune response.[38] Acid-degradable acetal-cross-linked NPs encapsulating both OVA and CpG (TLR9 agonist) induced an OVA-specific CD8$^+$ T-cell response.[16] Same system but with CpG covalently attached, enhanced the efficacy of antigen presentation *via* MHC class I leading to a greater cytotoxic T-cell activity, as compared with particles subcutaneously (s.c.) coadministered with adjuvant in an unbound form in mice.[30] This system effectively showed to induce protective immunity using the MO5 murine melanoma model until the moment when the cancer cells apparently stopped expressing the antigen, due to *in vivo* selection pressure.[30]

Immune potentiation can also be achieved by activating the complement system. Triggering of complement activates a series of proteins and enzymes that can promote inflammation, macrophage phagocytosis, anaphylaxis, B-cell activation, and T-cell response, as well as enhance antigen presentation to B-cells by follicular DC.[9] Certain primary hydroxyls[39] or amine groups[40] on the pathogen molecules or on the material surface can bind to the exposed thioester of C3b to activate complement by alternative pathway.[39, 41] Furthermore, activating materials also facilitate the binding of Factor B to C3b, forming the C3 convertase, which catalyzes the cleavage of more C3, thus amplifying the response.[41] Interestingly, C1q binds to hydrophobic molecules or aggregates, such as lipopolysaccharide (LPS) and liposomes.[42] Hence, the incorporation of hydrophobic domains could activate complement through the classical pathway. In summary, although much of biomaterials research seeks to avoid interactions with the complement system, immunobioengineering may exploit surface-mediated complement activation and of diverse ways in which it could affect innate and adaptive immunity.

Size and Shape

The size of the polymeric particulate vaccine delivery systems and their interactions with APC influence the immune response both qualitatively and quantitatively.[13] The nanoscale size is advantageous in vaccine delivery, improving the safety, stability and targeted delivery of biological agents, enhancing the transport across biological barriers and hence the bioavailability, extending the effect in the target tissue.[12]

Particle size is the critical factor for lymphatic uptake from the interstitial space.[43] Therefore, particles greater than 100 nm frequently remain near the administration site and are internalized by immature peripheral DC that then migrate to lymph nodes, mature and present antigen to T-cells. Particles smaller than 50 nm in diameter are more efficiently carried into lymphatic vessels by the interstitial flow and transported to regional draining lymph nodes, where concentrated populations of resident immature DC internalize them.[39, 44, 45] Therefore the size of particles is determinant for their applicability towards targeting peripheral versus lymph-node DC. Interestingly, size may also affect internalization of targeted biomaterials by APC. DC have been described to internalize PLGA-based DC-SIGN-targeted NPs and microparticles (MPs; size from 1 to 1000 µm) more effectively than nontargeted controls. However, NPs were more effectively targeted than MPs, as demonstrated by the relatively high nonspecific uptake of MPs by DC. Contrastingly, scavenging by other phagocytes occurred more efficiently for targeted MPs rather than for NPs.[46]

Transport across mucosal surfaces may also be affected by particle size. Mucosae are both an appealing and challenging route for vaccination. NPs must gain access to the mucosal epithelia for antigen delivery or transfection. Therefore, they must be able to penetrate the mucous layer. The mucus consists of a physically cross-linked, viscoelastic hydrogel, with mesh sizes in the order of 10–100 nm.[47] Barrier penetration has been shown largely restricted for particles greater in diameter than a few hundred nanometers,[47, 48] whereas particles of about 50 nm could diffuse in mucus almost as freely as in water.[47] NPs have been described to improve transmucosal transport and transcytosis by microfold (M) cells.[49] Indeed, NPs crossed the mucosal epithelium better than MPs, since not only M cells overlaying the mucosa-associated lymphoid tissues (MALT) but also the epithelial cells were involved in the transport of NPs.[21] A better uptake by Peyer's patches was observed for negatively charged PLGA particles having a mean diameter of 1 µm or less.[50]

Nanomaterial size may also determine its immunological activity, by influencing uptake by APC and their maturation.[51] Indeed, it has been shown that cell uptake of NPs was relatively high, when compared to that of MPs.[52, 53] The NPs size-dependent immunomodulation is a key feature towards their usage in vaccination. Immunization with PLA NPs entrapping hepatitis B surface antigen (HBsAg) has been previously linked with higher levels of interferon (IFN)-γ production and with antibody isotypes associated with T helper (T_H)1-type immune response. Conversely, immunization with MPs promoted IL-4 secretion and favored T_H2-type immune response.[54] However, immunization with PLGA MPs loaded with *Bordetella pertussis* antigens elicited a marked T_H1 immune response, whereas similarly loaded NPs favored a T_H2 immune response.[55] In another model, synthetic peptide malaria vaccine SPf66-loaded PLGA NPs showed to be poorly immunogenic while SPf66-loaded MPs elicited potent, long lasting systemic antibody levels and mixed T_H1/T_H2 immune response in i.n.-immunized mice.[56] Therefore, the type of size-dependent polarization of the immune response may also depend or be affected by the particular loaded antigen or other NPs characteristics.

In addition to its type, the intensity of the humoral immune response seems to be also affected by particle size, as significant variations on antibody titers were observed after a single immunization, using differently sized PLA particles entrapping HBsAg.[54] NPs have been shown to be efficiently taken up by macrophages but elicited lower antibody titers in comparison to MPs. PLA MPs eliciting the highest and long-lasting antibody titers after single immunization were found attached to the macrophage cell surface, not being internalized.[54] Bovine serum albumin (BSA)-loaded PGLA particles (1 µm) induced a higher humoral response, immunoglobulin (Ig)G-mediated, than smaller particles administered by oral and i.n. routes.[57] Other studies did not reveal the same size-dependent effect. PLGA NPs and MPs vaccine systems delivering a recombinant protein antigen from *Neisseria meningitidis* type B (intramuscularly (i.m.) or intraperitonealy (i.p.)), and a HIV-1 envelop gp140 (i.n. followed by an i.m. boost) elicited comparable immune response in mice.[58]

Although it is not obvious how one specific size range could be optimal for particular vaccine formulations, it is however clear that controlling the size of a vaccine particle could be a mean to bias the immune response.[59, 60]

The particle geometry has been described as a strategic feature regarding transport through the vasculature, circulation half-life, targeting efficiency, endocytosis, and subsequent intracellular transport.[61, 62] Spherical and cylindrical particles have been described to be phagocytozed more effectively than the ellipsoid or disc-shaped. Elongated particles have been reported to avoid phagocytosis and remained in circulation for longer times, whereas both elongated and flat particles targeted the diseased site better than their spherical counterparts.[61]

Surface charge

Surface charge may affect bioadhesivity, entrapment efficiency, percent loading, stability and *in vivo* immunogenic performance of a vaccine formulation.[63] Due to the supercoiled structure and negative charge, the entrapment efficiency and stability of DNA-based vaccine formulations is usually low. Cationic nanomaterials complex plasmid DNA by electrostatic interactions, increasing stability and entrapment efficiency.[64, 65] A net positive surface charge can facilitate transfection by favoring the interaction with the negatively charged glycoproteins at the cell membrane. However, electrostatic interactions with solutes or proteins from blood and interstitial fluid can lead to competitive binding, destabilization of the carrier, and subsequent premature release of the nucleic acid payload.[33] These cationic delivery systems have been shown to enhance mucosal and systemic immunogenicity, including the generation of efficient mucosal antibody response and cytotoxic T-cells after i.n. administration,[66] hence providing an attractive alternative to parenteral administration. It is therefore critical to control the cationic charge density to minimize toxicity – frequently associated to polycationic materials, e.g., poly(ethylenimine) (PEI) – while attaining high immune response.

The electrostatic interactions between the mucus – an anionic polyelectrolyte – and the cationic NPs, resulting in mucoadhesion, may provide sufficient residence time for an efficient antigen uptake. Mucoadhesive, hydrophilic NPs have received much attention to deliver protein antigens *via* the nasal route.[21, 67-69] Mucoadhesive NPs improve mucosal absorption, because they strongly attach to the mucosa and increase the viscosity of mucin. Thereby they significantly decrease the nasal mucociliary clearance rate and, thus, increase the residence time of the formulation in the nasal cavity. For instance, carriers of chitosan and derivatives – polyampholyte mono-*N*-carboxymethyl chitosan (MCC) and positively charged *N*-trimethyl chitosan (TMC) – loading tetanus toxoid (TT) have shown enhanced mucosal immune response in i.n.-immunized mice.[68] MCC induced relatively lower IgG titers for TT when compared with TMC and chitosan, yet producing the smallest NPs, with narrower size distribution and higher loading capacity.[68] TT loaded TMC/MCC NPs, obtained without using any organic solvent or cross-linker, induced both mucosal and systemic immune responses in i.n.-immunized mice.[70]

Hydrophobicity/hydrophilicity

Certain material features can mimic pathogen surfaces leading to the activation of innate immune pathways. Some biomaterials, particularly polymers that contain hydrophobic domains, exhibit natural adjuvant behavior. A positive correlation was observed between hydrophobicity of diphtheria toxoid (DT)-loaded PLGA, PCL and PLGA-PCL NPs, their *in vitro* uptake and the serum levels of antigen-specific IgG achieved in i.n.-immunized mice.[71] The mechanism(s) by which biomaterials hydrophobicity affects the inflammatory and antibody responses, although not fully elucidated, may involve the complement system and/or TLR. TLR4 binds to a variety of structurally dissimilar ligands, many of them, including LPS and bacterial fimbriae, having hydrophobic domains. The hydrophobic domains of these ligands might be sensed as a “danger signal” by TLR to initiate innate immune response.[72] Similarly, hydrophobic portions of polymers in vehicles might interact specifically with TLR and induce DC maturation and adaptive immunity.[42] For example, LPS-free γ-hPGA NPs stimulated DC through TLR2 and TLR4, possibly through the hydrophobic regions.[20] This was reached through MyD88-mediated NF-κB activation and p38 mitogen-activated protein kinase (MAPK) pathways, in a manner somewhat similar to LPS signaling through TLR4.[20, 73-75]

Once exposed to a biological environment, hydrophobic material surfaces are obscured by protein adsorption faster than the hydrophilic ones,[33] affecting the phagocytosis and clearance by macrophages (e.g., through scavenger receptor) and hence potentially affecting distribution and delivery to the intended target sites.[76] Immunoglobulins, complement components or other opsonins adsorption might be advantageous to induce immunity.[76] A study with DC-SIGN-targeted PLGA NPs, coated with hydrophilic poly(ethylene glycol) (PEG) of various chain lengths in order to shield non-specific interactions, demonstrated that PEG chains cannot be extended beyond a certain length without compromising the efficacy of targeted delivery.[77] The addition of PEG and other hydrophilic polymers can also result in lower transfection efficiency.[33]

An hydrophilic surface (e.g., PEG, poly(ethylene oxide), Pluronic or poloxamers) is relevant to withstand aggregation and adsorption of particles to components of the mucus and permit their transport as individual particles. Shorter, denser graft layers of PEG tend to sterically stabilize the NPs surface whereas longer, sparser grafts allow interpenetration of the grafted chains and the mucous network, leading to adhesion to the mucus, associated with entanglement and disentanglement, and unfavorable slower NPs penetration.[78] Therefore, PEG chains long enough (2 KDa)[48] to prevent adsorption, but not long enough (10 KDa)[78] to lead to entanglement, are desirable. PEG coating of PGLA

NPs have shown to enhance diffusion in human cervical mucus in a manner strongly dependent on PEG molecular weight and density;[79] in PLA NPs, PEG coating has favored penetration across rat nasal mucosa.[27] The role of the hydrophobicity/hydrophilicity of the transmucosal nanocarriers is controversial in different reports and remains a dilemma.[80]

Multifunctional vaccine delivery systems

A range of technologies and approaches have been used for the development of nano-sized vaccine delivery systems, aiming at improving preventive and therapeutic vaccination methods.[26] They are designed to protect antigen from enzymatic degradation,[12, 18, 81] to extend antigen release,[23] to closely mimic the size, shape, surface molecular organization,[82] composition, and immunological processing of actual pathogens; to actively or passively target APC for efficient delivery;[83] direct the nature of the resulting immune response and at last, to induce APC maturation by interacting with elements of the innate immune system, such as TLR.[59, 82] Polymeric vehicles also have the significant benefit of reducing the toxicity due to inflammatory cytokines often observed after injection, a common side effect of immunostimulants, by directly targeting APC.[84]

Vaccines may include synthetic peptides representing an epitope of a pathogen protein; a full-length protein carrying several epitopes that may be recognizable by B- and T-cells, produced either by pathogens, synthetically or recombinantly; or a gene encoding a particular protein fused into a DNA or RNA plasmid. These vaccines offer considerable advantages over traditional empiric vaccines, based in live-attenuated, inactivated or killed pathogens, in terms of safety, stability and production cost. However, in most cases, subunit vaccines have limited immunogenicity and require the addition of adjuvants to induce a protective and long-lasting effective immune response.[38, 59] Antigens in subunit vaccines are taken up by DC but usually lack the necessary “danger signals” to induce DC maturation. Several immunostimulants may therefore be coadministrated either by coinjection, or by physical linkage to the carrier *via* surface adsorption and coencapsulation.[85-87] An antigen-adjuvant mixture stimulates the activation of immature DC, but an antigen-adjuvant conjugate increases the chance of simultaneous uptake of both adjuvant and antigen to the same endocytic compartment, resulting in higher numbers of mature antigen-carrying DC,[88] which are necessary to ensure optimal antigen presentation to $CD4^+$ T-cells, cross-presentation and induction of $CD8^+$ T-cell response,[89] and increased humoral immune response.[88, 90]

Adjuvants are molecules, compounds or macromolecular complexes that evoke or enhance the potency and longevity of a specific immune response against coinoculated antigens.[4, 6, 26] The adjuvants choice should follow several criteria, like target site, antigens, type of desired immune response, route of administration, animal species to be vaccinated, duration of immunity, prevention of adverse effects or stability of the vaccine.[4, 91] An optimally formulated adjuvant must be able to promote an antigen specific immune response and should be safe, intrinsically non-immunogenic, biocompatible, readily biodegraded and eliminated, inexpensive to produce, stable before administration, and physicochemically well-defined to facilitate quality control important to ensure reproducible manufacturing and activity.[4, 6]

Multivalent vaccines that encapsulate not only a combination of multiple antigens,[66, 92] necessary in many diseases associated with multi-antigenic variability and shedding, but that also combine the synergy between different adjuvant mechanisms,[87, 93] using mixtures of immunostimulants and delivery systems have been under preclinical studies.

Peptide-based vaccines

Peptide-epitopes might be recognized by antibody or immune cells. Synthetic peptide-based immunogens are easily produced, free of bacterial/viral contaminating substances as well as devoid of oncogenic potential, present low adverse reactions, low cross-reactivity and high stability but also poor inherent immunogenicity.[26] Peptide-based vaccines can include several peptide-epitopes corresponding to subtypes of a pathogen, different stages in the life cycle of a pathogen or even epitopes from multiple pathogens.[94]

In order to overcome the limitations of using single cytotoxic T-cell epitopes imposed by MHC polymorphism, mixtures of separate peptides or polytope vaccines have been designed by producing recombinant proteins consisting of a combination of T_H and/or cytotoxic T-cell epitopes. Physical linking of T_H and cytotoxic T-cell peptide-epitopes further increased the magnitude of the cytotoxic T-cell response suggesting that presentation of both T_H and cytotoxic T-cell peptide-epitopes on a single APC is more efficient than when the two epitopes are presented on different APC, which may occur when these epitopes are delivered as a mixture.[95, 96]

Peptide-based vaccine efficacy is determined by how the peptides are recognized by the immune system. Specific immune response can be significantly affected by the presence of T_H epitopes, peptide concentration, multivalency, secondary structure,[59] geometry,[97, 98] orientation (N-terminus or C-terminus of B-cell epitopes could determine antibody specificity), chemical linkage between separately synthesized peptide modules,[96] association with adjuvants (self-adjuvanting lipopeptides, such as tripalmitoyl-S-glyceryl cysteine coupled to appropriate synthetic epitopes) and size. Long synthetic peptides are not able to bind directly to MHC class I or II molecules and are, therefore, taken up, processed and presented by APC.[59]

The induction of robust CD8$^+$ T-cell response requires a sustained presentation of antigen in a stimulatory context. Carrier induced epitope suppression and *in vivo* biodegradation should be avoided. Biodegradation escape can be achieved by using non-natural "protease-resistant" derivatives of cytotoxic T-cell epitopes that still retain the antigenicity and immunogenicity of the parental peptide, or by using a high number of repetitive injections with minimal cytotoxic T-cell peptide-epitopes within a week and for several courses.[95] While vaccines of small peptides can be rapidly biodegraded, larger peptides are relatively protected and may actually benefit from additional extracellular processing.[95]

Some examples of polymeric nanogels tested as potential peptide-based vaccine delivery systems with chitosan, γ-PGA and PLGA will be summarized below.

Chitosan

Chitosan conjugated with deoxycholic acid NPs self-assembled with melanoma-associated antigen 3 (MAGE-3)-derived CD4$^+$-CD8$^+$ T-cell peptide-epitopes, in s.c.-immunized mice, have been linked to the generation of MAGE-3-targeted cytotoxic T-cells, killing MAGE-3-specific tumor cells and causing regression of the growth of mouse forestomach carcinoma cell line (MFC).[99]

γ-PGA

Mice immunized with γ-hPGA NPs carrying the listerolysin$_{296–307}$ CD8$^+$ T-cell peptide-epitope have shown to be protected from a lethal infection with *Listeria monocytogenes* without the need of additional adjuvant.[73] γ-hPGA NPs entrapping an endoplasmic reticulum (ER)-transport system containing an ER-insertion signal sequence (Eriss)-conjugated antigenic peptides (Tax$_{38–46}$ peptide derived from human T-cell leukemia virus type-I and gp100$_{25-35}$ human melanoma peptide) markedly amplified and activated cytotoxic T-cells and IFN-γ-secreting cells specific for the antigen in s.c.-immunized mice.[100] Additionally, in a murine model of tumor metastasis, i.p.-vaccination with γ-hPGA NPs loaded with the tumor-associated antigen (TAA)-derived peptide, the ephrin type-A receptor 2 (EphA2), have been reported to exhibit an enhanced EphA2-specific CD8$^+$ T-cell activation and have demonstrated an antitumor effect by eliciting immunity equivalent to that of the antigen administered with complete Freund's adjuvant.[101]

PLGA

PLGA NPs encapsulating both the tyrosinase related protein-2 (TRP-2)$_{180\text{-}188}$ (self-TAA peptide) and 7-acyl lipid A (TLR4 agonist) have demonstrated to induce therapeutic immunity against highly aggressive B16 melanoma, in s.c.-immunized mice, breaking immunotolerance to cancer-associated self-antigens and leading to tumor growth control through the induction of TRP-2-specific cytotoxic T-cells. Activated TRP2-specific CD8$^+$ T-cells have shown to secrete IFN-γ in the lymph nodes and spleens of the vaccinated mice. Within the tumor microenvironment there was reversal of the immune suppressive milieu through an up-regulation of T_H1 cytokines (IL-6, IL-12, IFN-γ, tumor-necrosis factor (TNF)-α) and a down-regulation of the proangiogenic vascular endothelium growth factor (VEGF).[102]

Protein-based vaccines

A suitable vaccine must elicit a T-cell response in a background of many different human leukocyte antigen (HLA) class I and II alleles. Vaccines providing the immune system with complete proteins are ideal over single peptide-epitope vaccines, since the latter may not contain all important epitopes suitable to be loaded on antigen-presenting molecules of individuals with different HLA haplotypes.[95] Intact recombinant proteins are thus more likely to bear peptide sequences and to originate peptides that could bind MHC class I or II molecules of more than one HLA haplotype.

Some examples of polymeric nanogels currently being tested as potential protein-based vaccine delivery systems will be summarized below according to the main modified polymer – mannan and pullulan, chitosan and derivatives, γ-PGA, PLA and PLGA, PCL or PMMA.

Mannan and pullulan

Cholesterol-bearing mannan or pullulan (CHM or CHP) complexed with human epidermal growth factor receptor 2 (HER2) oncoprotein have been successfully used to induce CD8$^+$ cytotoxic T-cells against HER2$^+$ tumors. Mice s.c.-immunized with CHM-HER2 or CHP-HER2 before or early after tumor challenge successfully rejected HER2-transfected tumors.[103, 104] In addition, vaccination with CHM-HER2 complexes led to a strongly enhanced production of IgG against HER2.[103] In another study, CHP was used in combination with New York-esophageous 1 (NY-ESO-1) protein (CHP-NY-ESO-1) to pulse DC, which efficiently activated both CD4$^+$ and CD8$^+$ T-cells *in vitro.*[89] This further indicated the suitability of CHP to be used as a vaccine delivery system in cancer therapy. The evaluation of CHP-based protein vaccine in clinical trials yields encouraging results. In a phase I clinical trial conducted in HER2-expressing cancer patients, the CHP-HER2 complex vaccine, s.c. administered, showed to be safe and to induce HER2-specific CD8$^+$ and/or CD4$^+$ T-cell immune responses;[105] in a second clinical trial with this vaccine, it was further shown to induce a HER2-specific humoral immune response that was increased by co-administration of granulocyte-macrophage colony stimulating factor (GM-CSF).[106] Despite the CHP-HER2 formulation was effective in raising the production of antibodies specific for the immunogen used, these antibodies were not able to bind to or promote the lysis of HER2-expressing tumor cells. Their usefulness however could reside in their usage as surrogate markers for the T-cell mediated immune response.[106] In a phase I clinical trial, CHP-NY-ESO-1 vaccine elicited potent humoral[107] and increased CD4$^+$ and CD8$^+$ T-cell responses in immunized cancer patients.[108] In cancer patients despite CHP-NY-ESO-1 induced NY-ESO-1 specific immunity, tumor growth was nevertheless observed upon vaccination.[109] Combined CHP-NY-ESO-1 and CHP-HER2 vaccines s.c. administered to esophageal cancer patients elicited limited mild adverse events.[110] Targeting multiple tumor antigens showed to be feasible, without antigenic interactions. The combination vaccine elicited a response to NY-ESO-1 comparable to that obtained with the single vaccine, while inducing a lower antibody production specific for HER2.[110] Although the induction of antigen-specific T-cell responses upon vaccination is a promising result, further studies will be necessary to fully understand the true potential or effectiveness of CHP and CHM based cancer vaccination. The identification of immunologic biomarkers that could allow a more accurate evaluation of the clinical response to cancer immunotherapeutic approaches[111] will certainly be useful in this regard.

Chitosan and derivatives

Chitosan-based vaccines have shown superb effectiveness in preclinical models and promising results in clinical trials. Nevertheless, further optimizations for these systems will be necessary for clinical approval.[69, 112] Formulations of superoxide dismutase B1 in chitosan NPs s.c. administered to mice have been described to increase their immunogenicity towards cell-mediated immunity (T_H1 cells, IgG2a) and to be effective against *Leishmania*.[113] Hydrophobic NPs (PLA or PLGA) coated with hydrophilic polymers (PEG or chitosan) and NPs made solely of hydrophilic polymers have proved suitable to deliver proteins across the nasal and intestinal mucosae,[114] as exemplified by chitosan NPs loaded with TT, which elicited high and long-lasting IgG[67, 114] and secretory immunoglobulin A (sIgA) response in i.n.-immunized mice.[67] The association of recombinant HBsAg with the alginate-coated chitosan NPs, in i.n.-immunized mice, showed to be able to elicit a mucosal but not a systemic humoral immune response. However, antigen-specific systemic antibodies of T_H1-associated isotypes were detected when NPs were used together with CpG.[93] In other study, the recombinant HBsAg-loaded chitosan NPs induced anti-HBsAg IgG levels up to 9-fold the alum-adsorbed vaccine in i.m.-immunized mice.[115] Colloidal polyelectrolyte complexes, free of chemical cross-linkers and surfactants, were obtained by chitosan and dextran sulfate macromolecular assembly and loaded with HIV-1 p24. In the murine model, upon s.c.-vaccination with these NPs, a strong, specific anti-p24 antibody production and cytokine release suggested that both arms of immunity have been stimulated, though the immune response could be T_H2 biased.[116]

TMC NPs carrying monovalent influenza A subunit H3N2 have been described to significantly enhance systemic IgG and local sIgA immune responses, compared to soluble influenza vaccine, in mice (i.m. or i.n.).[22] Urease, a target antigen used in vaccination against *Helicobacter pylori* infection, loaded into TMC NPs, have elicited specific IgG and sIgA when oral administrated, but only IgG in s.c.-immunized mice.[49] TMC NPs have induced humoral and mucosal immune responses against recombinant HBsAg in i.n.-immunized mice.[117] Another study described that TMC based formulations containing either OVA or DT were able to elicit high titers of IgG specific for both antigens, in intradermally (i.d.)-immunized mice.[17] TMC-OVA conjugate (OVA covalently linked to TMC) caused higher OVA-specific IgG levels than plain OVA or a physical mixture of TMC and OVA in i.m.-immunized mice, and slightly elevated levels when compared to those achieved with TMC/OVA NPs obtained by ionic complexation.[88] Intraduodenal vaccination of mice with OVA-loaded chitosan and TMC NPs led to significantly higher antibody response than immunization with OVA alone. TMC NPs could induce anti-OVA antibodies after only a priming dose. TMC NPs but not chitosan or PLGA NPs had intrinsic adjuvant effect on DC.[118] Among similar sized OVA-loaded PLGA, TMC and TMC-coated PLGA (PLGA/TMC) NPs, only mucoadhesive TMC was able to increase the nasal residence time of OVA compared to OVA alone. All nanosystems i.m. administered induced higher IgG titers than OVA alone, PLGA and TMC being superior to PLGA/TMC. Slow antigen releasing PLGA and PLGA/TMC NPs did not induce detectable antibody titers whereas positively charged, fast antigen releasing TMC NPs led to high sIgA and serum antibody titers in i.n.-immunized mice. Therefore, particle charge and antigen release pattern of OVA-loaded NPs have to be adapted to the intended route of administration.[119] Additionally, covalently stabilized TMC-hyaluronic acid NPs loaded with OVA have shown adequate loading efficiency, particle integrity to a higher extent and enhanced adjuvanticity as evidenced by higher IgG titers compared with non-stabilized particles in i.n.- and i.d.-immunized mice.[120]

γ-PGA

The potential of using self-assembled γ-hPGA NPs in triggering murine immunity has been demonstrated for several protein antigens, such as HIV-1 p24,[121] HIV-1 gp120,[36, 52] influenza hemagglutinin (HA),[122, 123] and OVA.[73, 74, 124] In macaques (i.n. and s.c.), HIV-1 gp120 carrying γ-hPGA NPs have presented great potential for the induction of specific cellular and humoral immunity. However, the macaques intravenously (i.v.) challenged with simian and human immunodeficiency chimeric virus (SHIV)-KU-2, have presented an increased viral load when immunized with those NPs. Thus, the induced immune response has not been effective for protection, actually enhanced the infection in rhesus macaques.[125] Furthermore, γ-hPGA NPs showed to be promising adjuvants and allergen-delivery systems for allergen-specific immunotherapy; human monocyte-derived DC from allergic subjects stimulated *in vitro* with a mixture of γ-hPGA NPs and extract of grass pollen allergen *Phleum pratense* increased allergen-specific IL-10 production and proliferation of autologous $CD4^+$ memory T-cells.[20] More recently, OVA/benzalkonium chloride/γ-PGA complex s.c. administered to mice have been described to induced IgG1, IgG2b − T_H2-type − IgG2a and IgG3 − T_H1-type − indicating the ability of this complex to induce humoral and cellular responses. This complex was able to inhibit the growth of OVA-expressing tumor cell line E.G7 and caused the complete tumor rejection.[126]

PLA and PLGA

PLA NPs coated with HIV-1 p24 have been described to induce enhanced cellular and humoral immune responses in mice, rabbits and macaques immunized by the s.c. route.[127] Coadsorption of HIV-1 p24 and gp120 to these NPs preserved their antigenicity and immunogenicity.[128] In other study where mice were also s.c.-immunized, OVA and poly(uridylic acid) (poly-U, a TLR7/8 agonist) coencapsulated in PLA NPs, increased the specific humoral immune response and the levels of IFN-γ secreting T-cells.[90]

PLGA NPs have been reported as effective vehicles for sustained and targeted antigen delivery to APC by efficiently trafficking through local lymphoid tissues.[129, 130] Codelivery of hepatitis B core antigen (HBcAg) and monophosphoryl lipid A (MPL) in PLGA NPs promoted HBcAg-specific T_H1 cellular immune response with IFN-γ production in a murine model s.c.-immunized.[131] Encapsulated West Nile virus envelope protein antigen conferred host protection in a murine model of viral encephalitis.[132] In other study, PLGA particulate delivery of OVA and 7-acyl lipid A to DC led to an increased antigen-specific $CD8^+$ and $CD4^+$ T-cell-mediated response.[133] The expanded T-cells were capable of cytokine secretion and displayed an activation and memory surface phenotype.[133] Oral administration to mice of OVA and MPL codelivered in PLGA NPs showed to induce both systemic and mucosal immune responses.[134] LPS-modified PLGA NPs, in s.c.-immunized mice were able to effectively enter APC eliciting both humoral and cellular immunity against encapsulated OVA, without toxicity, therefore proving to be an effective vaccine vector through both TLR and inflammasome activation.[132] DEC-205-targeted OVA-loaded PLGA NPs have demonstrated to induce DC to produce IL-10, with levels correlating with the amount of anti-DEC-205 monoclonal antibodies conjugated on the particle surface, both *in vitro* and in i.p.-immunized mice.[135] This delivery system induced DC and T-cells to produce both pro-inflammatory (IL-12, IL-5, IFN-γ) and anti-inflammatory (IL-10) cytokines. The DEC-205-associated pathway elicited the DC production of IL-10 and T-cell production of IL-10 and IL-5 without impeding IL-12-mediated DC priming of a T_H1-type response characterized by IFN-γ production, due to the PLGA component. Multivalent cross-linking of the DEC-205 receptors was required for the response, and was associated with the upregulation of the scavenger receptor CD36 on the DC.[135]

PCL

PCL NPs modified by different adjuvants (mucoadhesive polymers – alginate or glycolchitosan – and absorption enhancers – spermine, oleic acid), with *Streptococcus equi equi* (*S. equi*) surface proteins adsorbed or encapsulated, have shown to induce significantly higher specific systemic and mucosal immune responses to *S. equi* antigens in i.n.-immunized mice.[92] The inclusion of cholera toxin B subunit (CTB) in the formulations further activated the pathways leading to T_H1 and T_H2 cells differentiation.[92]

PMMA

Vaccine formulations composed of HIV-1 Tat protein and anionic surfactant-free polymeric core-shell NPs and MPs with an inner core constituted by PMMA and a hydrophilic outer shell composed of a hydrosoluble co-polymer (Eudragit L100-55) have demonstrated to induce robust and long-lasting cellular and humoral immune responses in mice after systemic and/or mucosal immunization.[136]

DNA-based vaccines

In DNA-based vaccines, the peptide/protein targets of immune response are encoded in DNA and produced within the body own cells, which can mimic actual infection more closely than injection of traditional nonreplicating vaccines.[137] The DNA vector is made of a bacterial-derived plasmid equipped with eukaryotic or viral promoter/enhancer transcription elements and a gene encoding the antigen of interest followed by a transcript termination/polyadenylation sequence.[138]

DNA-based vaccines accumulate desirable qualities, such as immunogenicity (expression of multiple antigens or epitopes in a single vector inducing antigen-specific humoral and cellular immune responses), safety (low cytotoxicity and reduced immunogenic reactions), versatility (vaccine targets can be simply, rapidly and economically changed by selecting the appropriate sequence of the plasmid DNA), easy to scale-up and manufacture (low cost and reproducible large-scale production and isolation), stability (long shelf-life) and mobility (ease of storage and transport, likely not to require a cold chain).[33, 138, 139] The principal drawback rely on the challenging intracellular delivery of DNA in the appropriate cell-type, APC or a bystander cell, and the low levels of transfection that may consequently limit the immune response.[33] The approach of coinoculating plasmids coding for different cytokines, costimulatory factors or other fusion constructs to enhance or modify the immune response generated by the vaccine plasmid has been used successfully.[139]

Different polymers have been extensively studied as non-viral DNA carriers for vaccine delivery[83] and some examples will be summarized below.

Chitosan

Chitosan NPs containing a cocktail of DNA encoding nine immunogenic antigens of respiratory syncytial virus (RSV) have demonstrated to elevate the production of IFN-γ in the lungs, and to induce high levels of IgG and sIgA and cytotoxic T-cells with antiviral action in a mice model.[66] Plasmid DNA expressing different *Mycobacterium tuberculosis* epitopes loaded on chitosan NPs, when pulmonary administered in mice, showed to increase IFN-γ secretion from T-cells.[18] Chitosan NPs loaded with DNA encoding VP1, a major structural protein of coxsackievirus B3 (CVB3) induced high levels of IgG and sIgA and a strong cytotoxic T-cell response that effectively eliminated CVB3 viruses in i.n.-immunized mice.[65] The chitosan complexes with plasmid DNA encoding HBcAg in i.m.-immunized mice displayed stronger immunogenicity than naked DNA vaccines, with a higher value of specific antibody, elevated IFN-γ secretion and increased specific cell lysis.[81] Plasmid DNA encoding HBsAg loaded on chitosan NPs induced humoral, both systemic and mucosal, and cellular immune responses in i.n.-immunized mice.[140] Low molecular weight chitosan, although having lower binding affinity to plasmid DNA encoding human cholesteryl ester transfer protein C-terminal fragment, mediated higher transfection efficiency, elicited significant systemic immune response, modulated plasma lipoprotein profile and attenuated the progression of atherosclerosis in i.n.-immunized rabbits.[141] Oral delivery of chitosan-DNA vaccine encoding mite dust allergen from *Dermatophagoides pteronyssinus* generated high gene expression levels in mice, and preferentially activated a specific T_H1 immune response, thus preventing subsequent sensitization towards T_H2 cell-regulated specific IgE response.[142]

γ-PGA

DNA vaccination with PEI/γ-PGA NPs loaded with a plasmid encoding *Plasmodium yoelii* merozoite surface protein (MSP)-1 C-terminal, i.v. administered in mice, have been shown to generate an antigen-specific IgG response dominated by IgG1 and IgG2b and to induce weak T_H1 (IFN-γ and IL-12p40) and strong T_H2 (IL-4) cytokines responses.[143] In other study, same complex when i.p. and i.v. administered caused complete protection against lethal challenge with significant increase in levels of immunoglobulins and T_H1 and T_H2 cytokines, but in s.c. vaccinated group, only half of mice were protected and marginal levels of specific antibody were measured.[144]

PLA and PLGA

A single dose of plasmid DNA encoding β-galactosidase encapsulated in PLA-PEG NPs, showed to induced in i.n.-immunized mice a significant systemic antibody response to the encoded protein.[27] Multifunctional core-shell polymeric NPs – comprising hydrophobic PLGA core loaded with fluorescent quantum dots and a reporter gene electrostatically adsorbed onto the positively-charged glycol chitosan shell – could be delivered transdermally in a mouse model *via* gene gun bombardment. The loaded DNA was intracellularly released *via* a pH-mediated mechanism, directly into epidermal Langerhans cells, which then migrated and expressed the encoded gene products in the skin draining lymph nodes.[145]

The PLGA-PEI NPs combined with DNA encoding *Mycobacterium tuberculosis* latency antigen Rv1733c when applied to the lungs increased T-cell proliferation and IFN-γ production more potently than the same formulations given i.m. to mice. The strongest immunogenicity was obtained by pulmonary priming with NPs-adsorbed Rv1733c DNA followed by boosting with Rv1733c protein.[19]

RNA-based vaccines

Significant challenges continue with respect to delivery of RNA-based nanoparticles.[146] The RNA-based vaccines, in contrast to those of DNA, offer a simpler delivery directed to the cytoplasm, thus bypassing dependence on cellular transcription machinery and transport of nucleic acids to and from the nucleus, excluding any potential for integration into host chromosomes. Nevertheless, RNA is relatively labile and expensive to manufacture at a commercial scale.

Efficient transfection of DC with mRNA expressing TAA, followed by vaccination with the RNA-pulsed DC, has shown promising results in murine models and lately in humans. In this context, prior identification and characterization of individual gene sequences encoding the TAA seems to be nonessential, as preparations of total mRNA isolated directly from tumors may also be used.[147]

The mRNA-based vaccines *in vivo* may have to deal with potency issues related to limited transfected mRNA copies into each cell and deficient expressed protein antigen levels to stimulate the desirable immune response. A smart strategy to increase the intracellular levels of mRNA comprises the incorporation of replication elements derived from RNA viruses (alphaviruses, flaviviruses and picornaviruses), which together program the cytoplasmic self-amplification of RNA within transfected cells. In order to avoid the production of any detrimental infectious virus, essential virus genes such as those encoding the structural “coat” proteins are excluded, originating modified RNA vaccine vectors, termed “replicons”.[147]

Biodegradable core-shell NPs – comprising a pH-responsive poly(β-amino ester) core, selected to promote endosome disruption, enveloped by a phospholipid bilayer shell to reduce the polycation core toxicity – were designed for *in vivo* mRNA delivery with possible usage in noninvasive delivery of mRNA-based vaccines. These NPs loaded with luciferase-encoding mRNA led to the expression of the reporter protein luciferase, statistically significant above naked mRNA treatment group, when i.n. administrated into mice.[148]

In conclusion, polymeric nanogels effectively perform as targeted carriers protecting vaccine antigens from degradation *in vivo*. Following internalization of the biomaterial vehicles by APC, the loaded antigens are released intracellularly entering MHC class II- and class I-dependent antigen presentation pathways and, therefore, can induce both CD4$^+$ and CD8$^+$ T-cell-mediated immunity. Moreover, the surface of the biomaterial vehicle can be conjugated with antibodies or other specific ligands to improve tissue, cellular or subcellular targeting specificity, steer specific immune response by improving the efficacy achieved at a much lower antigen dose, and/or reduce inflammatory side effects associated to some “danger signals”. Biomaterials themselves can function as synthetic adjuvants, which can also be conjugated with immunostimulants that activate APC and induce subsequent T-cell immunity. Advantages in the usage of polymeric nanogels as antigen-delivery systems comprise their simplicity of formulation, loading capacity, stability of the resulting dispersion, nontoxicity, economical, and easiness of manufacture and scale up.

Despite currently less developed than DNA- or protein-based vaccines, major advances in peptide- and RNA-based vaccines can be expected in the near future. A comprehensive evaluation of all of the latest vaccination concepts, together with a better understanding of disease pathology, advances in biomaterials science and technology, and regulated systematic experiments will provide more proved safe, effective, and targeted delivery systems that really make preventive and therapeutic vaccines advancing to the next level, as a major goal in global public health.

References

1. Schenten, D.; Medzhitov, R. The control of adaptive immune responses by the innate immune system. *Adv Immunol* **2011**, 109, 87-124.

2. Leroux-Roels, G. Unmet needs in modern vaccinology: adjuvants to improve the immune response. *Vaccine* **2010**, 28 Suppl 3, C25-36.

3. Brunner, R.; Jensen-Jarolim, E.; Pali-Scholl, I. The ABC of clinical and experimental adjuvants-a brief overview. *Immunol Lett* **2010**, 128, 29-35.

4. Reed, S. G.; Bertholet, S.; Coler, R. N.; Friede, M. New horizons in adjuvants for vaccine development. *Trends Immunol* **2009**, 30, 23-32.

5. Mbow, M. L.; De Gregorio, E.; Valiante, N. M.; Rappuoli, R. New adjuvants for human vaccines. *Curr Opin Immunol* **2010**, 22, 411-416.

6. Guy, B. The perfect mix: recent progress in adjuvant research. *Nat Rev Microbiol* **2007**, 5, 505-517.

7. Disis, M. L.; Bernhard, H.; Jaffee, E. M. Use of tumour-responsive T cells as cancer treatment. *The Lancet* **2009**, 373, 673-683.

8. De Temmerman, M. L.; Rejman, J.; Demeester, J.; Irvine, D. J.; Gander, B.; De Smedt, S. C. Particulate vaccines: on the quest for optimal delivery and immune response. *Drug Discov Today* **2011**, 16, 569-582.

9. Look, M.; Bandyopadhyay, A.; Blum, J. S.; Fahmy, T. M. Application of nanotechnologies for improved immune response against infectious diseases in the developing world. *Adv Drug Deliv Rev* **2010**, 62, 378-393.

10. Oh, J. K.; Lee, D. I.; Park, J. M. Biopolymer-based microgels/nanogels for drug delivery applications. *Prog Polym Sci* **2009**, 34, 1261-1282.

11. Oh, J. K. Engineering of nanometer-sized cross-linked hydrogels for biomedical applications. *Can J Chern* **2010**, 88, 173-184.

12. Hubbell, J. A.; Thomas, S. N.; Swartz, M. A. Materials engineering for immunomodulation. *Nature* **2009**, 462, 449-460.

13. Kabanov, A. V.; Vinogradov, S. V. Nanogels as pharmaceutical carriers: finite networks of infinite capabilities. *Angew Chem Int Ed Engl* **2009**, 48, 5418-5429.

14. Mishra, B.; Patel, B. B.; Tiwari, S. Colloidal nanocarriers: a review on formulation technology, types and applications toward targeted drug delivery. *Nanomedicine* **2010**, 6, 9-24.

15. Dobrovolskaia, M. A.; McNeil, S. E. Immunological properties of engineered nanomaterials. *Nat Nano* **2007**, 2, 469-478.

16. Standley, S. M.; Mende, I.; Goh, S. L.; Kwon, Y. J.; Beaudette, T. T.; Engleman, E. G.; Frechet, J. M. Incorporation of CpG oligonucleotide ligand into protein-loaded particle vaccines promotes antigen-specific CD8 T-cell immunity. *Bioconjug Chem* **2007**, 18, 77-83.

17. Bal, S. M.; Slütter, B.; van Riet, E.; Kruithof, A. C.; Ding, Z.; Kersten, G. F.; Jiskoot, W.; Bouwstra, J. A. Efficient induction of immune responses through intradermal vaccination with N-trimethyl chitosan containing antigen formulations. *J Control Release* **2010**, 142, 374-383.

18. Bivas-Benita, M.; van Meijgaarden, K. E.; Franken, K. L. M. C.; Junginger, H. E.; Borchard, G.; Ottenhoff, T. H. M.; Geluk, A. Pulmonary delivery of chitosan-DNA nanoparticles enhances the immunogenicity of a DNA vaccine encoding HLA-A*0201-restricted T-cell epitopes of Mycobacterium tuberculosis. *Vaccine* **2004**, 22, 1609-1615.

19. Bivas-Benita, M.; Lin, M. Y.; Bal, S. M.; van Meijgaarden, K. E.; Franken, K. L. M. C.; Friggen, A. H.; Junginger, H. E.; Borchard, G.; Klein, M. R.; Ottenhoff, T. H. M. Pulmonary delivery of DNA encoding Mycobacterium tuberculosis latency antigen Rv1733c associated to PLGA-PEI nanoparticles enhances T cell responses in a DNA prime/protein boost vaccination regimen in mice. *Vaccine* **2009**, 27, 4010-4017.

20. Broos, S.; Lundberg, K.; Akagi, T.; Kadowaki, K.; Akashi, M.; Greiff, L.; Borrebaeck, C. A.; Lindstedt, M. Immunomodulatory nanoparticles as adjuvants and allergen-delivery system to human dendritic cells: Implications for specific immunotherapy. *Vaccine* **2010**, 28, 5075-5085.

21. Amidi, M.; Romeijn, S. G.; Borchard, G.; Junginger, H. E.; Hennink, W. E.; Jiskoot, W. Preparation and characterization of protein-loaded N-trimethyl chitosan nanoparticles as nasal delivery system. *J Control Release* **2006**, 111, 107-116.

22. Amidi, M.; Romeijn, S. G.; Verhoef, J. C.; Junginger, H. E.; Bungener, L.; Huckriede, A.; Crommelin, D. J.; Jiskoot, W. N-trimethyl chitosan (TMC) nanoparticles loaded with influenza subunit antigen for intranasal vaccination: biological properties and immunogenicity in a mouse model. *Vaccine* **2007**, 25, 144-153.

23. Lofthouse, S. Immunological aspects of controlled antigen delivery. *Adv Drug Deliv Rev* **2002**, 54, 863-870.

24. Wang, C.; Ge, Q.; Ting, D.; Nguyen, D.; Shen, H.-R.; Chen, J.; Eisen, H. N.; Heller, J.; Langer, R.; Putnam, D. Molecularly engineered poly(ortho ester) microspheres for enhanced delivery of DNA vaccines. *Nat Mater* **2004**, 3, 190-196.

25. Jelley-Gibbs, D. M.; Lepak, N. M.; Yen, M.; Swain, S. L. Two distinct stages in the transition from naive CD4 T cells to effectors, early antigen-dependent and late cytokine-driven expansion and differentiation. *J Immunol* **2000**, 165, 5017-5026.

26. Liang, M. T.; Davies, N. M.; Blanchfield, J. T.; Toth, I. Particulate systems as adjuvants and carriers for peptide and protein antigens. *Curr Drug Deliv* **2006**, 3, 379-388.

27. Vila, A.; Sánchez, A.; Pérez, C.; Alonso, M. J. PLA-PEG nanospheres: new carriers for transmucosal delivery of proteins and plasmid DNA. *Polym Adv Technol* **2002**, 13, 851-858.

28. Hu, Y.; Atukorale, P. U.; Lu, J. J.; Moon, J. J.; Um, S. H.; Cho, E. C.; Wang, Y.; Chen, J.; Irvine, D. J. Cytosolic delivery mediated via electrostatic surface binding of protein, virus, or siRNA cargos to pH-responsive core-shell gel particles. *Biomacromolecules* **2009**, 13, 756-765.

29. Cohen, J. A.; Beaudette, T. T.; Tseng, W. W.; Bachelder, E. M.; Mende, I.; Engleman, E. G.; Fréchet, J. M. T-cell activation by antigen-loaded pH-sensitive hydrogel particles in vivo: the effect of particle size. *Bioconjug Chem* **2009**, 20, 111-119.

30. Beaudette, T. T.; Bachelder, E. M.; Cohen, J. A.; Obermeyer, A. C.; Broaders, K. E.; Frechet, J. M.; Kang, E. S.; Mende, I.; Tseng, W. W.; Davidson, M. G.*, et al.* In vivo studies on the effect of co-encapsulation of CpG DNA and antigen in acid-degradable microparticle vaccines. *Mol Pharm* **2009**, 6, 1160-1169.

31. Cheng, R.; Feng, F.; Meng, F.; Deng, C.; Feijen, J.; Zhong, Z. Glutathione-responsive nano-vehicles as a promising platform for targeted intracellular drug and gene delivery. *J Control Release* **2011**, 152, 2-12.

32. Blander, J. M.; Medzhitov, R. On regulation of phagosome maturation and antigen presentation. *Nat Immunol* **2006**, 7, 1029-1035.

33. Nguyen, D.; Green, J.; Chan, J.; Langer, R.; Anderson, D. Polymeric materials for gene delivery and DNA vaccination. *Adv Mater* **2009**, 21, 847-867.

34. Shen, H.; Ackerman, A. L.; Cody, V.; Giodini, A.; Hinson, E. R.; Cresswell, P.; Edelson, R. L.; Saltzman, W. M.; Hanlon, D. J. Enhanced and prolonged cross-presentation following endosomal escape of exogenous antigens encapsulated in biodegradable nanoparticles. *Immunology* **2006**, 117, 78-88.

35. Han, R.; Zhu, J.; Yang, X.; Xu, H. Surface modification of poly(D,L-lactic-co-glycolic acid) nanoparticles with protamine enhanced cross-presentation of encapsulated ovalbumin by bone marrow-derived dendritic cells. *J Biomed Mater Res A* **2011**, 96, 142-149.

36. Wang, X.; Uto, T.; Akagi, T.; Akashi, M.; Baba, M. Induction of potent CD8+ T-cell responses by novel biodegradable nanoparticles carrying human immunodeficiency virus type 1 gp120. *J Virol* **2007**, 81, 10009-10016.

37. Kwon, Y. J.; James, E.; Shastri, N.; Frechet, J. M. In vivo targeting of dendritic cells for activation of cellular immunity using vaccine carriers based on pH-responsive microparticles. *Proc Natl Acad Sci USA* **2005**, 102, 18264-18268.

38. Kwon, Y. J.; Standley, S. M.; Goh, S. L.; Fréchet, J. M. J. Enhanced antigen presentation and immunostimulation of dendritic cells using acid-degradable cationic nanoparticles. *J Control Release* **2005**, 105, 199-212.

39. Reddy, S. T.; van der Vlies, A. J.; Simeoni, E.; Angeli, V.; Randolph, G. J.; O'Neil, C. P.; Lee, L. K.; Swartz, M. A.; Hubbell, J. A. Exploiting lymphatic transport and complement activation in nanoparticle vaccines. *Nat Biotechnol* **2007**, 25, 1159-1164.

40. Toda, M.; Iwata, H. Effects of hydrophobicity and electrostatic charge on complement activation by amino groups. *ACS Appl Mater Interfaces* **2010**, 2, 1107-1113.

41. Andersson, J.; Ekdahl, K. N.; Larsson, R.; Nilsson, U. R.; Nilsson, B. C3 adsorbed to a polymer surface can form an initiating alternative pathway convertase. *J Immunol* **2002**, 168, 5786-5791.

42. Seong, S. Y.; Matzinger, P. Hydrophobicity: an ancient damage-associated molecular pattern that initiates innate immune responses. *Nat Rev Immunol* **2004**, 4, 469-478.

43. Swartz, M. A.; Hubbell, J. A.; Reddy, S. T. Lymphatic drainage function and its immunological implications: From dendritic cell homing to vaccine design. *Semin Immunol* **2008**, 20, 147-156.

44. Reddy, S. T.; Berk, D. A.; Jain, R. K.; Swartz, M. A. A sensitive in vivo model for quantifying interstitial convective transport of injected macromolecules and nanoparticles. *J Appl Physiol* **2006**, 101, 1162-1169.

45. Reddy, S. T.; Rehor, A.; Schmoekel, H. G.; Hubbell, J. A.; Swartz, M. A. In vivo targeting of dendritic cells in lymph nodes with poly(propylene sulfide) nanoparticles. *J Control Release* **2006**, 112, 26-34.

46. Cruz, L. J.; Tacken, P. J.; Fokkink, R.; Joosten, B.; Stuart, M. C.; Albericio, F.; Torensma, R.; Figdor, C. G. Targeted PLGA nano- but not microparticles specifically deliver antigen to human dendritic cells via DC-SIGN in vitro. *J Control Release* **2010**, 144, 118-126.

47. Cone, R. A. Barrier properties of mucus. *Adv Drug Deliv Rev* **2009**, 61, 75-85.

48. Lai, S. K.; Wang, Y. Y.; Hanes, J. Mucus-penetrating nanoparticles for drug and gene delivery to mucosal tissues. *Adv Drug Deliv Rev* **2009**, 61, 158-171.

49. Chen, F.; Zhang, Z.-R.; Yuan, F.; Qin, X.; Wang, M.; Huang, Y. In vitro and in vivo study of N-trimethyl chitosan nanoparticles for oral protein delivery. *Int J Pharm* **2008**, 349, 226-233.

50. Shakweh, M.; Besnard, M.; Nicolas, V.; Fattal, E. Poly(lactide-co-glycolide) particles of different physicochemical properties and their uptake by Peyer's patches in mice. *Eur J Pharm Biopharm* **2005**, 61, 1-13.

51. Kim, H.; Uto, T.; Akagi, T.; Baba, M.; Akashi, M. Amphiphilic poly(amino acid) nanoparticles induce size-dependent dendritic cell maturation. *Adv Funct Mater* **2010**, 20, 3925-3931.

52. Akagi, T.; Wang, X.; Uto, T.; Baba, M.; Akashi, M. Protein direct delivery to dendritic cells using nanoparticles based on amphiphilic poly(amino acid) derivatives. *Biomaterials* **2007**, 28, 3427-3436.

53. Yue, H.; Wei, W.; Yue, Z.; Lv, P.; Wang, L.; Ma, G.; Su, Z. Particle size affects the cellular response in macrophages. *Eur J Pharm Sci* **2010**, 41, 650-657.

54. Kanchan, V.; Panda, A. K. Interactions of antigen-loaded polylactide particles with macrophages and their correlation with the immune response. *Biomaterials* **2007**, 28, 5344-5357.

55. Conway, M. A.; Madrigal-Estebas, L.; McClean, S.; Brayden, D. J.; Mills, K. H. Protection against Bordetella pertussis infection following parenteral or oral immunization with antigens entrapped in biodegradable particles: effect of formulation and route of immunization on induction of Th1 and Th2 cells. *Vaccine* **2001**, 19, 1940-1950.

56. Carcaboso, A. M.; Hernández, R. M.; Igartua, M.; Rosas, J. E.; Patarroyo, M. E.; Pedraz, J. L. Potent, long lasting systemic antibody levels and mixed Th1/Th2 immune response after nasal immunization with malaria antigen loaded PLGA microparticles. *Vaccine* **2004**, 22, 1423-1432.

57. Gutierro, I.; Hernández, R. M.; Igartua, M.; Gascón, A. R.; Pedraz, J. L. Size dependent immune response after subcutaneous, oral and intranasal administration of BSA loaded nanospheres. *Vaccine* **2002**, 21, 67-77.

58. Wendorf, J.; Chesko, J.; Kazzaz, J.; Ugozzoli, M.; Vajdy, M.; O'Hagan, D.; Singh, M. A comparison of anionic nanoparticles and microparticles as vaccine delivery systems. *Hum Vaccin* **2008**, 4, 44-49.

59. Black, M.; Trent, A.; Tirrell, M.; Olive, C. Advances in the design and delivery of peptide subunit vaccines with a focus on toll-like receptor agonists. *Expert Rev Vaccines* **2010**, 9, 157-173.

60. Oyewumi, M. O.; Kumar, A.; Cui, Z. Nano-microparticles as immune adjuvants: correlating particle sizes and the resultant immune responses. *Expert Rev Vaccines* **2010**, 9, 1095-1107.

61. Doshi, N.; Mitragotri, S. Designer biomaterials for nanomedicine. *Adv Funct Mater* **2009**, 19, 3843-3854.

62. Yoo, J.-W.; Doshi, N.; Mitragotri, S. Endocytosis and intracellular distribution of PLGA particles in endothelial cells: effect of particle geometry. *Macromol Rapid Commun* **2010**, 31, 142-148.

63. Sharma, S.; Mukkur, T. K.; Benson, H. A.; Chen, Y. Pharmaceutical aspects of intranasal delivery of vaccines using particulate systems. *J Pharm Sci* **2009**, 98, 812-843.

64. Mao, H. Q.; Roy, K.; Troung-Le, V. L.; Janes, K. A.; Lin, K. Y.; Wang, Y.; August, J. T.; Leong, K. W. Chitosan-DNA nanoparticles as gene carriers: synthesis, characterization and transfection efficiency. *J Control Release* **2001**, 70, 399-421.

65. Xu, W.; Shen, Y.; Jiang, Z.; Wang, Y.; Chu, Y.; Xiong, S. Intranasal delivery of chitosan-DNA vaccine generates mucosal sIgA and anti-CVB3 protection. *Vaccine* **2004**, 22, 3603-3612.

66. Kumar, M.; Behera, A. K.; Lockey, R. F.; Zhang, J.; Bhullar, G.; De La Cruz, C. P.; Chen, L. C.; Leong, K. W.; Huang, S. K.; Mohapatra, S. S. Intranasal gene transfer by chitosan-DNA nanospheres protects BALB/c mice against acute respiratory syncytial virus infection. *Hum Gene Ther* **2002**, 13, 1415-1425.

67. Vila, A.; Sanchez, A.; Janes, K.; Behrens, I.; Kissel, T.; Vila Jato, J. L.; Alonso, M. J. Low molecular weight chitosan nanoparticles as new carriers for nasal vaccine delivery in mice. *Eur J Pharm Biopharm* **2004**, 57, 123-131.

68. Sayin, B.; Somavarapu, S.; Li, X. W.; Thanou, M.; Sesardic, D.; Alpar, H. O.; Senel, S. Mono-N-carboxymethyl chitosan (MCC) and N-trimethyl chitosan (TMC) nanoparticles for non-invasive vaccine delivery. *Int J Pharm* **2008**, 363, 139-148.

69. Amidi, M.; Mastrobattista, E.; Jiskoot, W.; Hennink, W. E. Chitosan-based delivery systems for protein therapeutics and antigens. *Adv Drug Deliv Rev* **2010**, 62, 59-82.

70. Sayin, B.; Somavarapu, S.; Li, X. W.; Sesardic, D.; Senel, S.; Alpar, O. H. TMC-MCC (N-trimethyl chitosan-mono-N-carboxymethyl chitosan) nanocomplexes for mucosal delivery of vaccines. *Eur J Pharm Sci* **2009**, 38, 362-369.

71. Singh, J.; Pandit, S.; Bramwell, V. W.; Alpar, H. O. Diphtheria toxoid loaded poly-([epsilon]-caprolactone) nanoparticles as mucosal vaccine delivery systems. *Methods* **2006**, 38, 96-105.

72. Botos, I.; Segal, David M.; Davies, David R. The structural biology of Toll-like receptors. *Structure* **2011**, 19, 447-459.

73. Uto, T.; Wang, X.; Sato, K.; Haraguchi, M.; Akagi, T.; Akashi, M.; Baba, M. Targeting of antigen to dendritic cells with poly(gamma-glutamic acid) nanoparticles induces antigen-specific humoral and cellular immunity. *J Immunol* **2007**, 178, 2979-2986.

74. Uto, T.; Akagi, T.; Hamasaki, T.; Akashi, M.; Baba, M. Modulation of innate and adaptive immunity by biodegradable nanoparticles. *Immunol Lett* **2009**, 125, 46-52.

75. Uto, T.; Akagi, T.; Yoshinaga, K.; Toyama, M.; Akashi, M.; Baba, M. The induction of innate and adaptive immunity by biodegradable poly(gamma-glutamic acid) nanoparticles via a TLR4 and MyD88 signaling pathway. *Biomaterials* **2011**, 32, 5206-5212.

76. Dobrovolskaia, M. A.; Aggarwal, P.; Hall, J. B.; McNeil, S. E. Preclinical studies to understand nanoparticle interaction with the immune system and its potential effects on nanoparticle biodistribution. *Mol Pharm* **2008**, 5, 487-495.

77. Cruz, L. J.; Tacken, P. J.; Fokkink, R.; Figdor, C. G. The influence of PEG chain length and targeting moiety on antibody-mediated delivery of nanoparticle vaccines to human dendritic cells. *Biomaterials* **2011**, 32,

78. Huang, Y. B.; Leobandung, W.; Foss, A.; Peppas, N. A. Molecular aspects of muco- and bioadhesion: tethered structures and site-specific surfaces. *J Control Release* **2000**, 65, 63-71.

79. Cu, Y.; Saltzman, W. M. Controlled surface modification with poly(ethylene)glycol enhances diffusion of PLGA nanoparticles in human cervical mucus. *Mol Pharm* **2008**, 6, 173-181.

80. Vila, A.; Gill, H.; McCallion, O.; Alonso, M. J. Transport of PLA-PEG particles across the nasal mucosa: effect of particle size and PEG coating density. *J Control Release* **2004**, 98, 231-244.

81. Jiang, L.; Qian, F.; He, X.; Wang, F.; Ren, D.; He, Y.; Li, K.; Sun, S.; Yin, C. Novel chitosan derivative nanoparticles enhance the immunogenicity of a DNA vaccine encoding hepatitis B virus core antigen in mice. *J Gene Med* **2007**, 9, 253-264.

82. Bachmann, M. F.; Jennings, G. T. Vaccine delivery: a matter of size, geometry, kinetics and molecular patterns. *Nat Rev Immunol* **2010**, 10, 787-796.

83. Xiang, S. D.; Selomulya, C.; Ho, J.; Apostolopoulos, V.; Plebanski, M. Delivery of DNA vaccines: an overview on the use of biodegradable polymeric and magnetic nanoparticles. *Wiley Interdiscip Rev Nanomed Nanobiotechnol* **2010**, 2, 205-218.

84. Lingnau, K.; Egyed, A.; Schellack, C.; Mattner, F.; Buschle, M.; Schmidt, W. Poly-arginine synergizes with oligodeoxynucleotides containing CpG-motifs (CpG-ODN) for enhanced and prolonged immune responses

and prevents the CpG-ODN-induced systemic release of pro-inflammatory cytokines. *Vaccine* **2002**, 20, 3498-3508.

85. Diwan, M.; Tafaghodi, M.; Samuel, J. Enhancement of immune responses by co-delivery of a CpG oligodeoxynucleotide and tetanus toxoid in biodegradable nanospheres. *J Control Release* **2002**, 85, 247-262.

86. Elamanchili, P.; Diwan, M.; Cao, M.; Samuel, J. Characterization of poly(D,L-lactic-co-glycolic acid) based nanoparticulate system for enhanced delivery of antigens to dendritic cells. *Vaccine* **2004**, 22, 2406-2412.

87. Bal, S. M.; Slutter, B.; Verheul, R.; Bouwstra, J. A.; Jiskoot, W. Adjuvanted, antigen loaded N-trimethyl chitosan nanoparticles for nasal and intradermal vaccination: Adjuvant- and site-dependent immunogenicity in mice. *Eur J Pharm Sci* **2011**, 45, 475-481.

88. Slütter, B.; Soema, P. C.; Ding, Z.; Verheul, R.; Hennink, W.; Jiskoot, W. Conjugation of ovalbumin to trimethyl chitosan improves immunogenicity of the antigen. *J Control Release* **2010**, 143, 207-214.

89. Hasegawa, K.; Noguchi, Y.; Koizumi, F.; Uenaka, A.; Tanaka, M.; Shimono, M.; Nakamura, H.; Shiku, H.; Gnjatic, S.; Murphy, R.*, et al.* In vitro stimulation of CD8 and CD4 T cells by dendritic cells loaded with a complex of cholesterol-bearing hydrophobized pullulan and NY-ESO-1 protein: Identification of a new HLA-DR15-binding CD4 T-cell epitope. *Clin Cancer Res* **2006**, 12, 1921-1927.

90. Westwood, A.; Elvin, S. J.; Healey, G. D.; Williamson, E. D.; Eyles, J. E. Immunological responses after immunisation of mice with microparticles containing antigen and single stranded RNA (polyuridylic acid). *Vaccine* **2006**, 24, 1736-1743.

91. Harandi, A. M.; Medaglini, D.; Shattock, R. J. Vaccine adjuvants: a priority for vaccine research. *Vaccine* **2010**, 28, 2363-2366.

92. Florindo, H. F.; Pandit, S.; Lacerda, L.; Gonçalves, L. M. D.; Alpar, H. O.; Almeida, A. J. The enhancement of the immune response against S. equi antigens through the intranasal administration of poly-[epsilon]-caprolactone-based nanoparticles. *Biomaterials* **2009**, 30, 879-891.

93. Borges, O.; Cordeiro-da-Silva, A.; Tavares, J.; Santarem, N.; de Sousa, A.; Borchard, G.; Junginger, H. E. Immune response by nasal delivery of hepatitis B surface antigen and codelivery of a CpG ODN in alginate coated chitosan nanoparticles. *Eur J Pharm Biopharm* **2008**, 69, 405-416.

94. Skwarczynski, M.; Toth, I. Peptide-based subunit nanovaccines. *Curr Drug Deliv* **2011**, 8, 282-289.

95. van der Burg, S. H.; Bijker, M. S.; Welters, M. J.; Offringa, R.; Melief, C. J. Improved peptide vaccine strategies, creating synthetic artificial infections to maximize immune efficacy. *Adv Drug Deliv Rev* **2006**, 58, 916-930.

96. Zeng, W.; Ghosh, S.; Macris, M.; Pagnon, J.; Jackson, D. C. Assembly of synthetic peptide vaccines by chemoselective ligation of epitopes: influence of different chemical linkages and epitope orientations on biological activity. *Vaccine* **2001**, 19, 3843-3852.

97. Calvo-Calle, J. M.; Oliveira, G. A.; Watta, C. O.; Soverow, J.; Parra-Lopez, C.; Nardin, E. H. A linear peptide containing minimal T- and B-cell epitopes of Plasmodium falciparum circumsporozoite protein elicits protection against transgenic sporozoite challenge. *Infect Immun* **2006**, 74, 6929-6939.

98. Renaudet, O.; Dasgupta, G.; Bettahi, I.; Shi, A.; Nesburn, A. B.; Dumy, P.; BenMohamed, L. Linear and branched glyco-lipopeptide vaccines follow distinct cross-presentation pathways and generate different magnitudes of antitumor immunity. *PLoS ONE* **2010**, 5, e11216.

99. Yang, J.; Li, Z. H.; Zhou, J. J.; Chen, R. F.; Cheng, L. Z.; Zhou, Q. B.; Yang, L. Q. Preparation and antitumor effects of nanovaccines with MAGE-3 peptides in transplanted gastric cancer in mice. *Chin J Cancer* **2010**, 29, 359-364.

100. Matsuo, K.; Yoshikawa, T.; Oda, A.; Akagi, T.; Akashi, M.; Mukai, Y.; Yoshioka, Y.; Okada, N.; Nakagawa, S. Efficient generation of antigen-specific cellular immunity by vaccination with poly([gamma]-glutamic acid) nanoparticles entrapping endoplasmic reticulum-targeted peptides. *Biochem Bioph Res Co* **2007**, 362, 1069-1072.

101. Yamaguchi, S.; Tatsumi, T.; Takehara, T.; Sasakawa, A.; Yamamoto, M.; Kohga, K.; Miyagi, T.; Kanto, T.; Hiramastu, N.; Akagi, T.*, et al.* EphA2-derived peptide vaccine with amphiphilic poly(gamma-glutamic acid) nanoparticles elicits an anti-tumor effect against mouse liver tumor. *Cancer Immunol Immun* **2010**, 59, 759-767.

102. Hamdy, S.; Molavi, O.; Ma, Z.; Haddadi, A.; Alshamsan, A.; Gobti, Z.; Elhasi, S.; Samuel, J.; Lavasanifar, A. Co-delivery of cancer-associated antigen and Toll-like receptor 4 ligand in PLGA nanoparticles induces potent CD8+ T cell-mediated anti-tumor immunity. *Vaccine* **2008**, 26, 5046-5057.

103. Gu, X. G.; Schmitt, M.; Hiasa, A.; Nagata, Y.; Ikeda, H.; Sasaki, Y.; Akiyoshi, K.; Sunamoto, J.; Nakamura, H.; Kuribayashi, K.*, et al.* A novel hydrophobized polysaccharide/oncoprotein complex vaccine induces in vitro and in vivo cellular and humoral immune responses against HER2-expressing murine sarcomas. *Cancer Res* **1998**, 58, 3385-3390.

104. Shiku, H.; Wang, L.; Ikuta, Y.; Okugawa, T.; Schmitt, M.; Gu, X.; Akiyoshi, K.; Sunamoto, J.; Nakamura, H. Development of a cancer vaccine: peptides, proteins, and DNA. *Cancer Chemoth Pharm* **2000**, 46 Suppl, S77-82.

105. Kitano, S.; Kageyama, S.; Nagata, Y.; Miyahara, Y.; Hiasa, A.; Naota, H.; Okumura, S.; Imai, H.; Shiraishi, T.; Masuya, M.*, et al.* HER2-specific T-cell immune responses in patients vaccinated with truncated HER2 protein complexed with nanogels of cholesteryl pullulan. *Clin Cancer Res* **2006**, 12, 7397-7405.

106. Kageyama, S.; Kitano, S.; Hirayama, M.; Nagata, Y.; Imai, H.; Shiraishi, T.; Akiyoshi, K.; Scott, A. M.; Murphy, R.; Hoffman, E. W.*, et al.* Humoral immune responses in patients vaccinated with 1-146 HER2 protein complexed with cholesteryl pullulan nanogel. *Cancer Sci* **2008**, 99, 601-607.

107. Kawabata, R.; Wada, H.; Isobe, M.; Saika, T.; Sato, S.; Uenaka, A.; Miyata, H.; Yasuda, T.; Doki, Y.; Noguchi, Y.*, et al.* Antibody response against NY-ESO-1 in CHP-NY-ESO-1 vaccinated patients. *Int J Cancer* **2007**, 120, 2178-2184.

108. Uenaka, A.; Wada, H.; Isobe, M.; Saika, T.; Tsuji, K.; Sato, E.; Sato, S.; Noguchi, Y.; Kawabata, R.; Yasuda, T.*, et al.* T cell immunomonitoring and tumor responses in patients immunized with a complex of cholesterol-bearing hydrophobized pullulan (CHP) and NY-ESO-1 protein. *Cancer Immun* **2007**, 7, 9.

109. Wada, H.; Sato, E.; Uenaka, A.; Isobe, M.; Kawabata, R.; Nakamura, Y.; Iwae, S.; Yonezawa, K.; Yamasaki, M.; Miyata, H.*, et al.* Analysis of peripheral and local anti-tumor immune response in esophageal cancer patients after NY-ESO-1 protein vaccination. *Int J Cancer* **2008**, 123, 2362-2369.

110. Aoki, M.; Ueda, S.; Nishikawa, H.; Kitano, S.; Hirayama, M.; Ikeda, H.; Toyoda, H.; Tanaka, K.; Kanai, M.; Takabayashi, A.*, et al.* Antibody responses against NY-ESO-1 and HER2 antigens in patients vaccinated with combinations of cholesteryl pullulan (CHP)-NY-ESO-1 and CHP-HER2 with OK-432. *Vaccine* **2009**, 27, 6854-6861.

111. Disis, M. L. Immunologic biomarkers as correlates of clinical response to cancer immunotherapy. *Cancer Immunol Immunother* **2011**, 60, 433-442.

112. Dash, M.; Chiellini, F.; Ottenbrite, R. M.; Chiellini, E. Chitosan-A versatile semi-synthetic polymer in biomedical applications. *Prog Polym Sci* **2011**, 36, 981-1014.

113. Danesh-Bahreini, M. A.; Shokri, J.; Samiei, A.; Kamali-Sarvestani, E.; Barzegar-Jalali, M.; Mohammadi-Samani, S. Nanovaccine for leishmaniasis: preparation of chitosan nanoparticles containing Leishmania superoxide dismutase and evaluation of its immunogenicity in BALB/c mice. *Int J Nanomedicine* **2011**, 6, 835–842.

114. Vila, A.; Sánchez, A.; Toblo, M.; Calvo, P.; Alonso, M. J. Design of biodegradable particles for protein delivery. *J Control Release* **2002**, 78, 15-24.

115. Prego, C.; Paolicelli, P.; Diaz, B.; Vicente, S.; Sanchez, A.; Gonzalez-Fernandez, A.; Alonso, M. J. Chitosan-based nanoparticles for improving immunization against hepatitis B infection. *Vaccine* **2010**, 28, 2607-2614.

116. Weber, C.; Drogoz, A.; David, L.; Domard, A.; Charles, M.-H.; Verrier, B.; Delair, T. Polysaccharide-based vaccine delivery systems: Macromolecular assembly, interactions with antigen presenting cells, and in vivo immunomonitoring. *J Biomed Mater Res A* **2009**, 93A, 1322-1334.

117. Mangal, S.; Pawar, D.; Garg, N. K.; Jain, A. K.; Vyas, S. P.; Rao, D. S.; Jaganathan, K. S. Pharmaceutical and immunological evaluation of mucoadhesive nanoparticles based delivery system(s) administered intranasally. *Vaccine* **2011**, 29, 4953-4962.

118. Slütter, B.; Plapied, L.; Fievez, V.; Sande, M. A.; des Rieux, A.; Schneider, Y. J.; Van Riet, E.; Jiskoot, W.; Preat, V. Mechanistic study of the adjuvant effect of biodegradable nanoparticles in mucosal vaccination. *J Control Release* **2009**, 138, 113-121.

119. Slütter, B.; Bal, S.; Keijzer, C.; Mallants, R.; Hagenaars, N.; Que, I.; Kaijzel, E.; van Eden, W.; Augustijns, P.; Lowik, C.*, et al.* Nasal vaccination with N-trimethyl chitosan and PLGA based nanoparticles: nanoparticle characteristics determine quality and strength of the antibody response in mice against the encapsulated antigen. *Vaccine* **2010**, 28, 6282-6291.

120. Verheul, R. J.; Slütter, B.; Bal, S. M.; Bouwstra, J. A.; Jiskoot, W.; Hennink, W. E. Covalently stabilized trimethyl chitosan-hyaluronic acid nanoparticles for nasal and intradermal vaccination. *J Control Release* **2011**, 156, 46-52.

121. Wang, X.; Uto, T.; Akagi, T.; Akashi, M.; Baba, M. Poly(gamma-glutamic acid) nanoparticles as an efficient antigen delivery and adjuvant system: potential for an AIDS vaccine. *J Med Virol* **2008**, 80, 11-19.

122. Okamoto, S.; Yoshii, H.; Akagi, T.; Akashi, M.; Ishikawa, T.; Okuno, Y.; Takahashi, M.; Yamanishi, K.; Mori, Y. Influenza hemagglutinin vaccine with poly([gamma]-glutamic acid) nanoparticles enhances the protection against influenza virus infection through both humoral and cell-mediated immunity. *Vaccine* **2007**, 25, 8270-8278.

123. Okamoto, S.; Matsuura, M.; Akagi, T.; Akashi, M.; Tanimoto, T.; Ishikawa, T.; Takahashi, M.; Yamanishi, K.; Mori, Y. Poly(gamma-glutamic acid) nano-particles combined with mucosal influenza virus hemagglutinin vaccine protects against influenza virus infection in mice. *Vaccine* **2009**, 27, 5896-5905.

124. Yoshikawa, T.; Okada, N.; Oda, A.; Matsuo, K.; Matsuo, K.; Kayamuro, H.; Ishii, Y.; Yoshinaga, T.; Akagi, T.; Akashi, M.*, et al.* Nanoparticles built by self-assembly of amphiphilic [gamma]-PGA can deliver antigens to antigen-presenting cells with high efficiency: A new tumor-vaccine carrier for eliciting effector T cells. *Vaccine* **2008**, 26, 1303-1313.

125. Himeno, A.; Akagi, T.; Uto, T.; Wang, X.; Baba, M.; Ibuki, K.; Matsuyama, M.; Horiike, M.; Igarashi, T.; Miura, T.*, et al.* Evaluation of the immune response and protective effects of rhesus macaques vaccinated with biodegradable nanoparticles carrying gp120 of human immunodeficiency virus. *Vaccine* **2010**, 28, 5377-5385.

126. Kurosaki, T.; Kitahara, T.; Nakamura, T.; Nishida, K.; Fumoto, S.; Kodama, Y.; Nakagawa, H.; Higuchi, N.; Sasaki, H. Development of effective cancer vaccine using targeting system of antigen protein to APCs. *Pharm Res* **2011**, 1-7.

127. Ataman-Önal, Y.; Munier, S.; Ganée, A.; Terrat, C.; Durand, P.-Y.; Battail, N.; Martinon, F.; Le Grand, R.; Charles, M.-H.; Delair, T.*, et al.* Surfactant-free anionic PLA nanoparticles coated with HIV-1 p24 protein induced enhanced cellular and humoral immune responses in various animal models. *J Control Release* **2006**, 112, 175-185.

128. Lamalle-Bernard, D.; Munier, S.; Compagnon, C.; Charles, M. H.; Kalyanaraman, V. S.; Delair, T.; Verrier, B.; Ataman-Onal, Y. Coadsorption of HIV-1 p24 and gp120 proteins to surfactant-free anionic PLA nanoparticles preserves antigenicity and immunogenicity. *J Control Release* **2006**, 115, 57-67.

129. Lu, J. M.; Wang, X.; Marin-Muller, C.; Wang, H.; Lin, P. H.; Yao, Q.; Chen, C. Current advances in research and clinical applications of PLGA-based nanotechnology. *Expert Rev Mol Diagn* **2009**, 9, 325-341.

130. Hamdy, S.; Haddadi, A.; Hung, R. W.; Lavasanifar, A. Targeting dendritic cells with nano-particulate PLGA cancer vaccine formulations. *Adv Drug Deliv Rev* **2011**, 63, 943-955.

131. Chong, C. S. W.; Cao, M.; Wong, W. W.; Fischer, K. P.; Addison, W. R.; Kwon, G. S.; Tyrrell, D. L.; Samuel, J. Enhancement of T helper type 1 immune responses against hepatitis B virus core antigen by PLGA nanoparticle vaccine delivery. *J Control Release* **2005**, 102, 85-99.

132. Demento, S. L.; Eisenbarth, S. C.; Foellmer, H. G.; Platt, C.; Caplan, M. J.; Mark Saltzman, W.; Mellman, I.; Ledizet, M.; Fikrig, E.; Flavell, R. A.*, et al.* Inflammasome-activating nanoparticles as modular systems for optimizing vaccine efficacy. *Vaccine* **2009**, 27, 3013-3021.

133. Hamdy, S.; Elamanchili, P.; Alshamsan, A.; Molavi, O.; Satou, T.; Samuel, J. Enhanced antigen-specific primary CD4+ and CD8+ responses by codelivery of ovalbumin and toll-like receptor ligand monophosphoryl lipid A in poly(D,L-lactic-co-glycolic acid) nanoparticles. *J Biomed Mater Res A* **2007**, 81, 652-662.

134. Sarti, F.; Perera, G.; Hintzen, F.; Kotti, K.; Karageorgiou, V.; Kammona, O.; Kiparissides, C.; Bernkop-Schnurch, A. In vivo evidence of oral vaccination with PLGA nanoparticles containing the immunostimulant monophosphoryl lipid A. *Biomaterials* **2011**, 32, 4052-4057.

135. Bandyopadhyay, A.; Fine, R. L.; Demento, S.; Bockenstedt, L. K.; Fahmy, T. M. The impact of nanoparticle ligand density on dendritic-cell targeted vaccines. *Biomaterials* **2011**, 32, 3094-3105.

136. Caputo, A.; Castaldello, A.; Brocca-Cofano, E.; Voltan, R.; Bortolazzi, F.; Altavilla, G.; Sparnacci, K.; Laus, M.; Tondelli, L.; Gavioli, R.*, et al.* Induction of humoral and enhanced cellular immune responses by novel core-shell nanosphere- and microsphere-based vaccine formulations following systemic and mucosal administration. *Vaccine* **2009**, 27, 3605-3615.

137. Rice, J.; Ottensmeier, C. H.; Stevenson, F. K. DNA vaccines: precision tools for activating effective immunity against cancer. *Nat Rev Cancer* **2008**, 8, 108-120.

138. Ingolotti, M.; Kawalekar, O.; Shedlock, D. J.; Muthumani, K.; Weiner, D. B. DNA vaccines for targeting bacterial infections. *Expert Rev Vaccines* **2010**, 9, 747-763.

139. Chadwick, S.; Kriegel, C.; Amiji, M. Delivery strategies to enhance mucosal vaccination. *Expert Opin Biol Ther* **2009**, 9, 427-440.

140. Khatri, K.; Goyal, A. K.; Gupta, P. N.; Mishra, N.; Vyas, S. P. Plasmid DNA loaded chitosan nanoparticles for nasal mucosal immunization against hepatitis B. *Int J Pharm* **2008**, 354, 235-241.

141. Yang, X.; Yuan, X.; Cai, D.; Wang, S.; Zong, L. Low molecular weight chitosan in DNA vaccine delivery via mucosa. *Int J Pharm* **2009**, 375, 123-132.

142. Li, G.; Liu, Z.; Liao, B.; Zhong, N. Induction of Th1-type immune response by chitosan nanoparticles containing plasmid DNA encoding house dust mite allergen Der p 2 for oral vaccination in mice. *Cell Mol Immunol* **2009**, 6, 45-50.

143. Shuaibu, M. N.; Cherif, M. S.; Kurosaki, T.; Helegbe, G. K.; Kikuchi, M.; Yanagi, T.; Sasaki, H.; Hirayama, K. Effect of nanoparticle coating on the immunogenicity of plasmid DNA vaccine encoding P. yoelii MSP-1 C-terminal. *Vaccine* **2011**, 29, 3239-3247.

144. Cherif, M. S.; Shuaibu, M. N.; Kurosaki, T.; Helegbe, G. K.; Kikuchi, M.; Yanagi, T.; Tsuboi, T.; Sasaki, H.; Hirayama, K. Immunogenicity of novel nanoparticle-coated MSP-1 C-terminus malaria DNA vaccine using different routes of administration. *Vaccine* **2011**, 29, 9038-9050.

145. Lee, P. W.; Hsu, S. H.; Tsai, J. S.; Chen, F. R.; Huang, P. J.; Ke, C. J.; Liao, Z. X.; Hsiao, C. W.; Lin, H. J.; Sung, H. W. Multifunctional core-shell polymeric nanoparticles for transdermal DNA delivery and epidermal Langerhans cells tracking. *Biomaterials* **2010**, 31, 2425-2434.

146. Shukla, G. C.; Haque, F.; Tor, Y.; Wilhelmsson, L. M.; Toulmeȉ, J.-J.; Isambert, H.; Guo, P.; Rossi, J. J.; Tenenbaum, S. A.; Shapiro, B. A. A boost for the emerging field of RNA nanotechnology. *ACS Nano* **2011**, 5, 3405-3418.

147. Vajdy, M.; Srivastava, I.; Polo, J.; Donnelly, J.; O'Hagan, D.; Singh, M. Mucosal adjuvants and delivery systems for protein-, DNA- and RNA-based vaccines. *Immunol Cell Biol* **2004**, 82, 617-627.

148. Su, X.; Fricke, J.; Kavanagh, D. G.; Irvine, D. J. In vitro and in vivo mRNA delivery using lipid-enveloped pH-responsive polymer nanoparticles. *Mol Pharm* **2011**, 8, 774-787.

149. Roy, K.; Mao, H.Q.; Huang, S.K.; Leong, K.W. Oral gene delivery with chitosan-DNA nanoparticles generates immunologic protection in a murine model of peanut allergy. *Nat Med* **1999**, 5, 387-391.

150. Scholl, I.; Weissenbock, A.; Forster-Waldl, E.; Untersmayr, E.; Walter, F.; Willheim, M.; Boltz-Nitulescu, G.; Scheiner, O.; Gabor, F.; Jensen-Jarolim, E. Allergen-loaded biodegradable poly(D,L-lactic-co-glycolic) acid nanoparticles down-regulate an ongoing Th2 response in the BALB/c mouse model. *Clin Exp Allergy* **2004**, 34, 315-321.

Chapter 2

Synthesis and characterization of self-assembled nanogels made of pullulan

Self-assembled nanogels made of hydrophobized pullulan were obtained using a versatile, simple, reproducible and low-cost method. In a first reaction pullulan was modified with hydroxyethyl methacrylate or vinyl methacrylate, further modified in the second step with hydrophobic 1-hexadecanethiol, resulting as an amphiphilic material, which self-assembles in water *via* the hydrophobic interaction among alkyl chains. Structural features, size, shape, surface charge and stability of the nanogels were studied using hydrogen nuclear magnetic resonance, fluorescence spectroscopy, cryo-field emission scanning electron microscopy and dynamic light scattering. Above the critical aggregation concentration spherical polydisperse macromolecular micelles revealed long-term colloidal stability in aqueous medium, with a nearly neutral negative surface charge and mean hydrodynamic diameter in the range 100–400 nm, depending on the polymer degree of substitution. Good size stability was observed when nanogels were exposed to potential destabilizing pH conditions. While the size stability of the nanogel made of pullulan with vinyl methacrylate and more hydrophobic chains grafted was affected by the ionic strength and urea, nanogel made of pullulan with hydroxyethyl methacrylate and fewer hydrophobic chains grafted remained stable.

Adapted from: *Materials* **2011**, 4, 601-620.

Introduction

Pullulan is a water soluble, linear, neutral extracellular biodegradable homopolysaccharide of glucose produced by the fungus *Aureobasidium pullulans* (*Pullularia pullulans*).[1-4] Pullulan consists of maltotriosyl units connected by α-D-1,6-glycoside linkages.[3, 5] Pullulan is extensively used in food, cosmetic and pharmaceutical industries because it is easily modifiable chemically, non-toxic, non-immunogenic, non-mutagenic, and non-carcinogenic.[5, 6] Furthermore, pullulan has good mechanical properties and attractive functional properties, such as adhesiveness, film formability, and enzymatically-mediated degradability.[7] In the form of self-assembled nanogels, it has been shown to exhibit chaperon like activity, thus being a promising technique for protein refolding.[8] It has been studied as a blood-plasma expander and substitute.[9] Pullulan arose as a promising polymer for various biomedical applications,[10] such as surface modification of polymeric materials to improve blood compatibility (bioinert surfaces),[11, 12] for gene[13, 14] and drug delivery,[5, 15-19] as a carrier for quantum dots for intracellular labeling to be used as a fluorescent probe for diagnostic bioimaging[20] and tissue engineering.[21] Self-assembled biotinylated pullulan acetate nanoparticles loading Adriamycin were described as targeted anti-cancer drug delivery systems, internalized by human hepatoma cell line (HepG2). The drug loading and release rate were accessed with a dialysis method.[18] Adriamycin loaded pullulan acetate/sulfonamide conjugate nanoparticles responding to tumor pH revealed pH-dependent cell interaction, internalization and cytotoxicity in *in vitro* studies using a breast tumor cell line (MCF-7). The drug loading profile was evaluated using a dialysis method.[19] Non-toxicity, efficient internalization and transfection *in vitro* of hydrogel pullulan nanoparticles encapsulating pBUDLacZ plasmid showed this system to be an efficient gene delivery carrier.[14] Pullulan potentially targets and accumulates in the liver because it is recognized by the asialoglycoprotein receptor expressed on the sinusoidal surface of the hepatocytes.[22] The asialoglycoprotein receptor was reported to be involved in pullulan receptor-mediated endocytosis.[23]

The production of hydrophobically modified pullulan nanogels, using an approach similar to the one presented in this work, was achieved by other authors using cholesteryl group-bearing pullulan. The resulting nanogels were monodisperse, with a diameter of 20–30 nm and stable in water. Their size and density were controlled by the pullulan degree of substitution with cholesterol and the molecular weights of parent pullulan.[24] This nanogel was utilized in molecular complexation with bovine serum albumin (BSA),[25] insulin,[26] lipase,[27] human epidermal growth factor receptor 2 (HER2),[28-30] interleukin (IL)-

12,[31, 32] among other therapeutic molecules, proving this system to be useful as a therapeutic delivery system. Self-assembled hydrogel nanoparticles of cholesterol-bearing pullulan spontaneously release insulin from the complex and thermal denaturation/aggregation were effectively suppressed upon complexation.[26] Cholesteryl group-bearing pullulan complexed with the truncated HER2 protein, delivered a HER2 oncoprotein containing an epitope peptide to the major histocompatibility complex class I pathway, and was able to induce CD8$^+$ cytotoxic T lymphocytes against HER2$^+$ tumors and caused complete rejection of tumors. The results suggested this hydrophobized polysaccharide may help soluble proteins to induce cellular immunity with potential benefit in cancer prevention and cancer therapy.[30] The subcutaneous injection of cholesterol-bearing pullulan complexed with recombinant murine IL-12 led to a prolonged elevation of IL-12 concentration in the serum. Repetitive administrations of the complex induced drastic growth retardation of reestablished subcutaneous fibrosarcoma, without causing toxicity.[31] Raspberry-like assembly of nanogels encapsulated IL-12 efficiently (96%) and kept it stable in the presence of BSA (50 mg/mL) and showed high potential to maintain a high IL-12 level in plasma after subcutaneous injection in mice.[32] Cationic derivative, ethylenediamine group functionalization of cholesteryl group-bearing pullulan, was developed as an effective intracellular protein delivery system.[33] The same research group designed hybrid hydrogels with self-assembled nanogels as cross-linkers to achieve interaction with proteins and chaperone-like activity.[32, 34, 35]

Nanogel formulations, described as potential drug and vaccine delivery systems, have the potential to modify the drug, gene, protein, peptide, oligosaccharide or immunogen profile and the ability to cross biological barriers, the biodistribution and pharmacokinetics, improving their efficacy and safety, as well as the patient compliance.[36]

In the present work, hydrophobized pullulan was obtained with a two-step synthesis. The resultant self-assembled nanogels were characterized in terms of structure, size, shape, surface charge and stability by hydrogen nuclear magnetic resonance (^{1}H NMR), fluorescence spectroscopy, cryo-field emission scanning electron microscopy (cryo-FESEM) and dynamic light scattering (DLS).

Experimental

Materials

CDI-activated hydroxyethyl methacrylate (HEMA-CI) was produced as described elsewhere.[37] Pullulan (Mw = 100,000 g/mol), vinyl methacrylate (VMA), dimethyl sulfoxide (DMSO), 4-(N,N-dimethylamino)pyridine (DMAP), triethylamine (TEA), 1-hexadecanethiol (C_{16}), deuterium oxide (D_2O), dimethyl sulfoxide-d_6 (DMSO-d_6), pyrene (Py), 9-(diethylamino)-5H-benzo[α]phenoxazin-5-one (Nile red, NR) were purchased from Sigma-Aldrich. Pyrene was purified by appropriate recrystallization from absolute ethanol. Phosphotungstic acid was purchased from Riedel-de Haën. Regenerated cellulose tubular membranes, with a 12,000−14,000 nominal molecular weight cut-off (MWCO), were obtained from Membrane Filtration Products. Water was purified with a Milli-Q system (Millipore) with resistivity equal to 18.2 MΩ.cm. Other organic and inorganic chemicals were purchased from Sigma-Aldrich and used without further purification.

Synthesis of amphiphilic pullulan-C_{16}

Hydroxyethyl methacrylate-derivatized pullulan (pullulan-HEMA) was prepared as described by Van Dijk-Wolthuis *et al.*[37] Briefly, pullulan was dissolved in dry DMSO in a nitrogen atmosphere with different calculated amounts of HEMA-CI, resulting in 0.20, 0.25 and 0.4 molar ratios of HEMA-CI to glucose residues. The reaction catalyzed by DMAP (2 mol equiv to HEMA-CI) was allowed to proceed and the mixture was stirred at room temperature for 4 days. The reaction was terminated with concentrated HCl (2% v/v), which neutralized DMAP and imidazole. The mixture was then dialyzed against frequently changed distilled water at 4 °C for 3 days. After being lyophilized, pullulan-HEMA resulted as a white fluffy product, which was stored at −20 °C.

Vinyl methacrylated pullulan (pullulan-VMA) was synthesized by transesterification of pullulan with VMA, overall as described by Ferreira *et al.* [38] but without enzymes.[39] Briefly, pullulan was dissolved in dry DMSO, with calculated amounts of VMA resulting in 0.25 and 0.5 molar ratios of VMA to glucose residues. After stirring at 50 °C for 2 days, the resulting mixture was dialyzed for 3 days against frequently changed distilled water, at room temperature (~25 °C). Each sample of modified pullulan after being lyophilized resulted as a white fluffy product that was stored at room temperature.

Finally, the amphiphilic molecules pullulan-HEMA-C_{16} (PHC_{16}) and pullulan-VMA-C_{16} (PVC_{16}) were produced as described elsewhere.[40] In brief, Pullulan-HEMA or Pullulan-VMA reacted in dry DMSO (equivalent HEMA or VMA = 0.03 M) with C_{16}. The reaction was catalyzed by TEA in a 2 molar ratio of TEA to HEMA or VMA. After stirring for 3.5 days at 50 °C, the resulting mixture was dialyzed, lyophilized and stored as described above.

Characterization of pullulan-C_{16} nanogels

^{1}H NMR spectroscopy

Lyophilized reaction products were dispersed in D_2O (5 mg/mL). The pullulan-C_{16} was also dispersed in DMSO-d_6 and in 10% D_2O in DMSO-d_6 (5 mg/mL). Samples were stirred overnight at 50 °C to obtain a clear dispersion, which was transferred to 5 mm NMR tubes. One-dimensional ^{1}H NMR measurements were performed in a Varian Unity Plus 300 spectrometer operating at 299.94 MHz. One-dimensional ^{1}H NMR spectra were recorded at 298 K with 256 scans, a spectral width of 5000 Hz, a relaxation delay of 1 s between scans, and an acquisition time of 2.8 s.

Fluorescence spectroscopy

The cac of the pullulan-C_{16} was fluorometrically investigated using hydrophobic guest molecules, such as Py and NR. The fluorescence intensity change of these guest molecules was calculated as a function of the pullulan-C_{16} concentration. Briefly, lyophilized pullulan-C_{16} was dispersed in ultrapure water (1 mg/mL) with stirring for 3–5 days at 50 °C. Consecutive dilutions of 1 mL of each sample were prepared in ultrapure water. In the case of Py, a volume of 5 µL of a 1.2×10^{-4} M Py stock solution in ethanol was added, giving a constant concentration of 6×10^{-7} M in 0.5 % ethanol/water for all Py fluorescence measurements. In case of NR, a volume of 5 µL of a 4×10^{-5} M NR stock solution in ethanol was then added, giving a constant concentration of 2×10^{-7} M in 0.5 % ethanol/water for all NR fluorescence measurements. The samples were stirred overnight. Fluorescence measurements were performed with a Spex Fluorolog 3 spectrofluorimeter, at room temperature. The slit width was set at 5 nm for excitation and 5 nm for emission. All spectra were corrected for the instrumental response of the system. The signal obtained for each sample was subtracted with the signal obtained with negative control, which corresponded to pullulan derivatives at exactly the same experimental conditions but without the guest NR or Py molecules. The cac was calculated using both the Py fluorescence intensity ratio of the third (384–385 nm) and first vibrational bands (372–374 nm) (I_3/I_1) of the emission spectra (λ_{ex} 339 nm) and the maximum emission intensity of NR

(λ_{ex} 570 nm) in the pullulan-C_{16}/water system as a function of pullulan-C_{16} concentration; in both cases, the cac was estimated as the interception of two trend lines.

Cryo-FESEM

Each colloidal dispersion of pullulan-C_{16} was prepared with stirring of the lyophilized pullulan-C_{16} in ultrapure water for 3–5 days at 50 °C (1 mg/mL) followed by filtration (pore size 0.45 μm), with insignificant material lost, as confirmed with the phenol-sulfuric acid method, using glucose as standard.[41] The colloidal dispersions were concentrated by ultrafiltration (Amicon Ultra-4 Centrifugal Filter Units, MWCO, 1×10^5) and negatively stained with phosphotungstic acid (0.01% w/v). Samples were placed into brass rivets, plunged frozen into slush nitrogen at −200 °C and transferred to the cryo stage (Gatan, Alto 2500, UK) of an electronic microscope (SEM/EDS: FESEM JEOL JSM6301F/Oxford Inca Energy 350). Each sample was fractured on the cryo stage with a knife. Once in the microscope, sublimation of ice was carried out in the cryo chamber for 10 min at −95 °C, allowing the exposure of the nanogel particles. The samples were sputter coated with gold and palladium at −140 °C, using an accelerating voltage of 10 kV. The antipollutant of copper covers and protects the sample. The samples were observed at −140 °C at 15 kV. The solvent used in the preparation of the samples (water and phosphotungstic acid) was also observed as a negative control.

DLS

The size distribution and zeta potential measurements for each colloidal dispersion, prepared as described above for cryo-FESEM, were performed in a Malvern Zetasizer NANO ZS (Malvern Instruments Limited, UK) using a He-Ne laser wavelength of 633 nm, a detector angle of 173 ° and a refractive index of 1.33.

Size. For each sample (1 mL), the polydispersity index (PdI) and z-average diameter, which corresponds to the mean hydrodynamic diameter, were evaluated in 10 repeated measurements performed periodically during six months of storage in a polystyrene cell at 25 °C. The size distribution of each sample dispersed in ultrapure water (0.05–2 mg/mL), phosphate-buffered saline (PBS 1×, pH 7.4), phosphate-citrate buffer (pH 2.2–8.0), NaCl (0–0.6 M) or in urea (0–7 M) was executed at 37 °C in three independent experiments, three repeated measurements being performed in each one.

Zeta Potential. Each sample dispersed in ultrapure water (0.05–2 mg/mL), PBS 1×, pH 7.4 or in phosphate-citrate buffer (pH 2.2–8.0) was analyzed at 37 °C in a folded capillary cell. The zeta potential values reported were calculated using the Smoluchowski equation with three independent experiments, three repeated measurements being performed in each one.

Results and discussion

Synthesis of pullulan-C_{16}

According to the literature and in the same way as other reported methacrylates, hydroxyethyl methacrylate (HEMA) and vinyl methacrylate (VMA) should be grafted on the ^{6}C of the glucose residues.[42] Then, by the Michael addition mechanism, the thiol from 1-hexadecanethiol (C_{16}) acting as a nucleophile reacts with grafted methacrylate (Scheme 1).

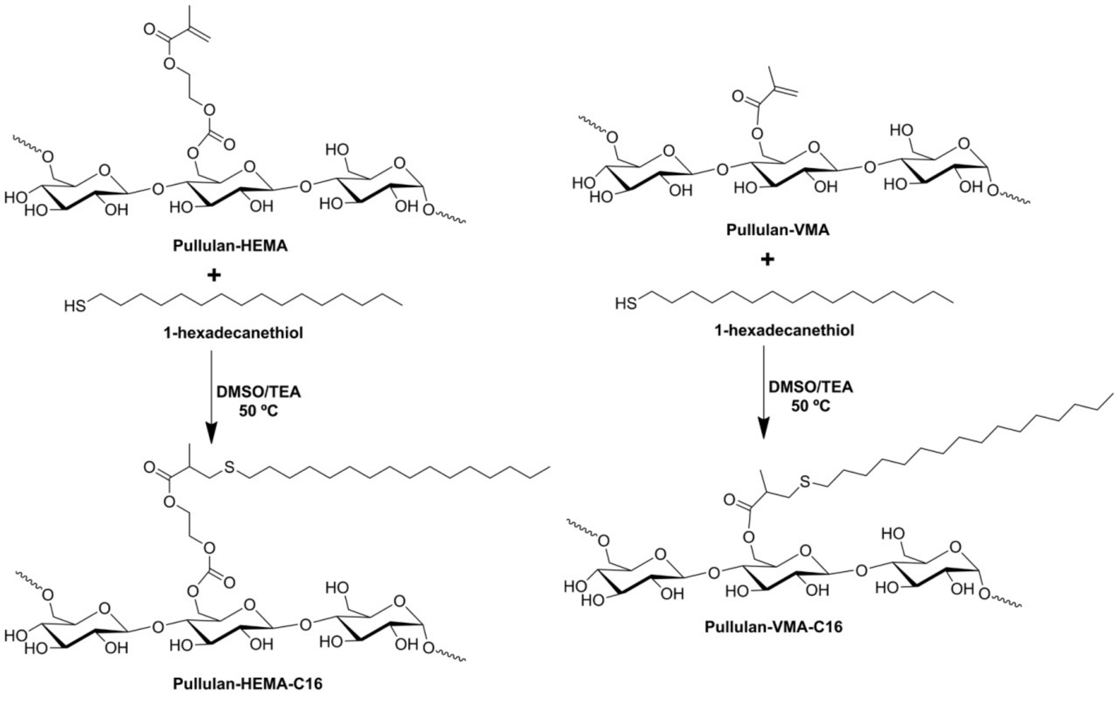

Scheme 1. Synthesis of pullulan-C_{16}.

The success of the synthesis, purity, chemical structure and polymer degree of substitution of the reaction products were controlled using ^{1}H NMR spectra in D_2O (Figure 1 and Table 1). Different independent batches of hydrophobized pullulan (pullulan-C_{16}) with various degree of substitution with the methacrylated groups and hydrophobic alkyl chains (DS_{HEMA} or DS_{VMA} and DS_{C16}, defined as the percentage of grafted HEMA or VMA or C_{16} moieties relative to the glucose residues, respectively), were synthesized by varying the molar ratios of methacrylate groups to glucose residues and the molar ratios of C_{16} to methacrylated groups. The synthetic procedure adopted proves to be versatile, simple and reproducible (Table 1).

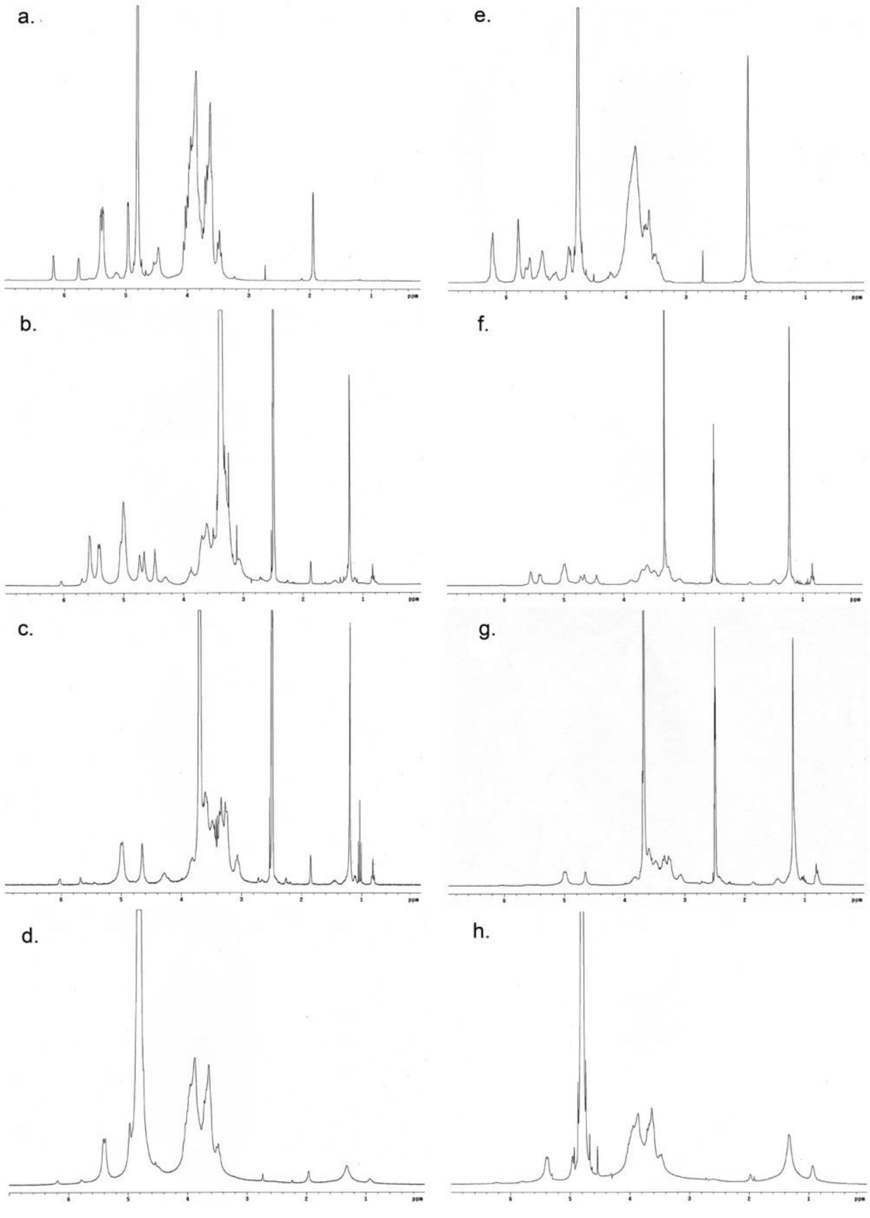

Figure 1. ^1H NMR spectra of (*a*) pullulan-HEMA and (*e*) pullulan-VMA in D_2O. ^1H NMR spectra of PHC_{16}-5.6-1.3 and PVC_{16}-10-7 in (*b, f*) DMSO-d_6, (*c, g*) 10% D_2O in DMSO-d_6 and (*d, h*) D_2O, respectively.

Table 1. Characteristics of pullulan-C_{16}

$t\mathrm{DS}_{\mathrm{HEMA}}$ or $t\mathrm{DS}_{\mathrm{VMA}}$ [a]	$\mathrm{DS}_{\mathrm{HEMA}}$ or $\mathrm{DS}_{\mathrm{VMA}}$ [b]	$t\mathrm{DS}_{\mathrm{C16}}$ [c]	$\mathrm{DS}_{\mathrm{C16}}$ [d]	$\mathrm{DS}_{\mathrm{C16}}/\mathrm{DS}_{\mathrm{HEMA}}$ or $\mathrm{DS}_{\mathrm{C16}}/\mathrm{DS}_{\mathrm{VMA}}$ [e]	Pullulan-C_{16} [f]
		Pullulan-HEMA-C_{16}			
20	5.6	120	1.3	23.2	PHC_{16}-5.6-1.3
25	8	80	4.6	57.5	PHC_{16}-8-4.6
		200	4.3	53.8	PHC_{16}-8-4.3
40	10	80	1.2	12	PHC_{16}-10-1.2
		200	5.9	59	PHC_{16}-10-5.9
		Pullulan-VMA-C_{16}			
25	8.8	200	6	68.2	PVC_{16}-8.8-6
50	10	200	7	70	PVC_{16}-10-7

[a] Theoretical $\mathrm{DS}_{\mathrm{HEMA}}$ or $\mathrm{DS}_{\mathrm{VMA}}$ calculated as the molar ratio of HEMA or VMA to glucose residue (×100) in the reaction mixture. [b] Calculated from the ^{1}H NMR spectra in D_2O of pullulan-HEMA or pullulan-VMA in D_2O with the equation $(I_a)/(I_{H1})\times100$, in which I_a is the average integral of the protons of the unsaturated carbons of the acrylate groups (around 6 ppm)[37, 38] and I_{H1} is the integral of the anomeric protons (4.86, 5.28 and 5.30 ppm).[4, 43] [c] Theoretical $\mathrm{DS}_{\mathrm{C16}}$ calculated as the molar ratio of C_{16} to methacrylated groups (×100) in the reaction mixture. [d] Calculated from the ^{1}H NMR spectra of pullulan-C_{16} in D_2O with the equation $(7X)/(37Y)\times100$, in which X is the average integral corresponding to the protons from alkyl moieties (1.8–0.6 ppm)[40] and Y is the integral of all pullulan protons (3.3–4.0 ppm and 4.86, 5.28 and 5.30 ppm).[4, 43] [e] Obtained $\mathrm{DS}_{\mathrm{C16}}$ relative to methacrylated groups calculated using the following equation: $\mathrm{DS}_{\mathrm{C16}}/\mathrm{DS}_{\mathrm{HEMA}}$ (×100) or $\mathrm{DS}_{\mathrm{C16}}/\mathrm{DS}_{\mathrm{VMA}}$ (×100). [f] Pullulan-HEMA-SC_{16} synthesized: PHC_{16}-$\mathrm{DS}_{\mathrm{HEMA}}$-$\mathrm{DS}_{\mathrm{C16}}$; or Pullulan-VMA-$SC_{16}$ synthesized: PVC_{16}-$\mathrm{DS}_{\mathrm{VMA}}$-$\mathrm{DS}_{\mathrm{C16}}$. The table presents the values (%) obtained in each set of conditions.

Self-assembly of pullulan-C_{16}

The self-assembly of amphiphilic pullulan-C_{16} in water was studied using ^{1}H NMR and fluorescence spectroscopy. Analyzing the ^{1}H NMR spectra of pullulan-C_{16} (Figure 1), it can be observed that while the mobility of the polysaccharide skeleton was maintained in environments of different polarity, the shape and width of the proton signals of the methyl (0.8 ppm) and methylene (1.1 ppm) groups of C_{16} depended on the polarity of the solvent used. In DMSO-d_6, pullulan-C_{16} was soluble, and the C_{16} signals were sharp, as all hydrophobic chains were exposed to the solvent, having the same mobility (Figure 1b, f).[40] Increasing the percentage of D_2O in DMSO-d_6, the base of those signals broadened (Figure 1c, g). In pure D_2O, a large broadening was obvious, which represents the superposition of peaks of chemically identical species, yet possessing various degrees of mobility (Figure 1d, h).[44] These results give evidence that pullulan-C_{16} dispersed in water has part of the alkyl chains exposed to hydrophobic domains, while others might have been exposed to the hydrophilic solvent. Differences in the environment and/or mobility of the molecules thus explain the broad peak observed for the aliphatic protons. Therefore, pullulan-C_{16} nanogels are obtained upon self-assembly in water through the association of the hydrophobic alkyl chains in hydrophobic domains.

The critical aggregation concentration (cac) or critical micelle concentration (cmc) of pullulan-C_{16} was studied by fluorescence spectroscopy using hydrophobic dyes, Pyrene (Py)[45, 46] and Nile red (NR),[47] whose solubility and fluorescence are weak in water but high in hydrophobic environments.

The intensity of Py increased with increasing concentrations of pullulan-C_{16}, and a red shift occurred in the excitation spectra (Figure 2a, b). Above cac, in the emission spectra (Figure 2a, b), some bands in the 450 nm region associated to the presence of Py dimers are detected in pullulan-C_{16}, suggesting high water penetration into the nanogel, which is in agreement with the ^1H NMR measurements. The intensity ratio of the third and first vibrational bands, $I_3/I_{1,}$ rapidly augmented above the cac, which was 0.06 mg/mL for PHC_{16}-5.6-1.3 and for PVC_{16}-10-7. This transition of intensity translated the transference of Py to a less polar and hydrophobic domain that was coincident to the onset of supramolecular formation of pullulan-C_{16} nanogels (Figure 2c). A lower I_3/I_1 ratio obtained for PHC_{16}-5.6-1.3 indicates the location of Py in a more hydrophilic environment, while a higher I_3/I_1 ratio for PVC_{16}-10-7 indicates the location of Py in a more hydrophobic environment (Figure 2c).[45] This is confirmed by a better defined vibronic structure of Py emission in the case of PVC_{16}-10-7. Surprisingly, the resulting cac is the same for both nanogels despite their different DS_{C16} relative to methacrylated groups (70% for PVC_{16}-10-7 and 23% for PHC_{16}-5.6-1.3).

The area-normalized fluorescence emission intensity of NR was constant, without any shift in the maximum emission wavelength, for lower concentrations of pullulan-C_{16} because individual molecules exist as premicelles in aqueous environment (Figure 3; zone A). In contrast, for concentrations greater than the cac, fluorescence intensity increased and the maximum emission wavelength was blue-shifted due to the transfer of NR to the hydrophobic domains of the nanogels. The resultant cac was 0.04 mg/mL and 0.01 mg/mL for PHC_{16}-5.6-1.3 and PVC_{16}-10-7, respectively (Figure 3). This variation is consistent with the C_{16} loading of the studied pullulan nanogels as higher hydrophobicity results in lower cac. The PVC_{16}-10-7 hydrophobic domains are dissimilar to those present in a typical surfactant system and have two types of hydration levels (Figure 3b; zones B and C), while in PHC_{16}-5.6-1.3 only a type of hydrophobic domains is observed (Figure 3a; zone C). This observation shows a slight dependence of the formed hydrophobic domains on the type of linker used (HEMA or VMA).

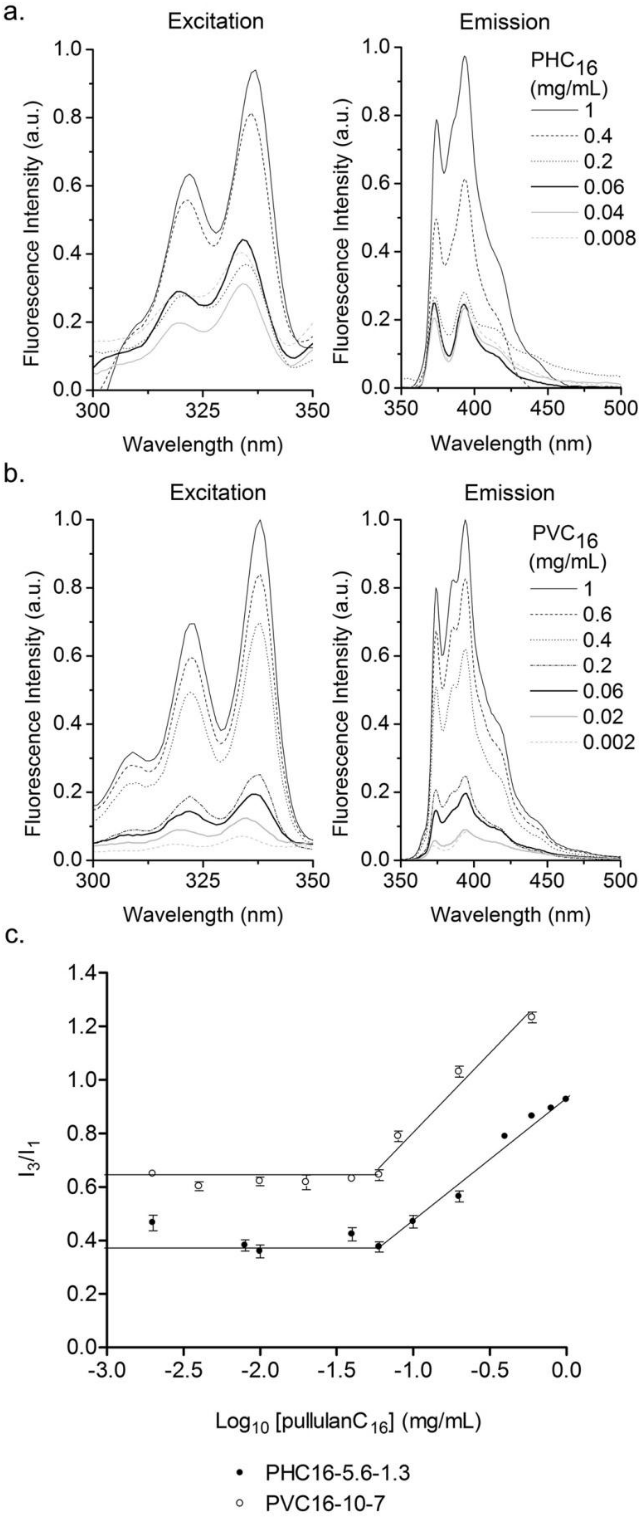

Figure 2. Determination of the cac of pullulan-C_{16} using fluorescence excitation (λ_{em} 390 nm) and emission (λ_{ex} 339 nm) spectra of Py (6×10^{-7} M) in the pullulan-C_{16}/water system as a function of the (*a*) PHC_{16}-5.6-1.3 and (*b*) PVC_{16}-10-7 concentration; (*c*) Intensity ratio I_3/I_1 as a function of the pullulan-C_{16} concentration. The cac obtained for both materials was 0.06 mg/mL.

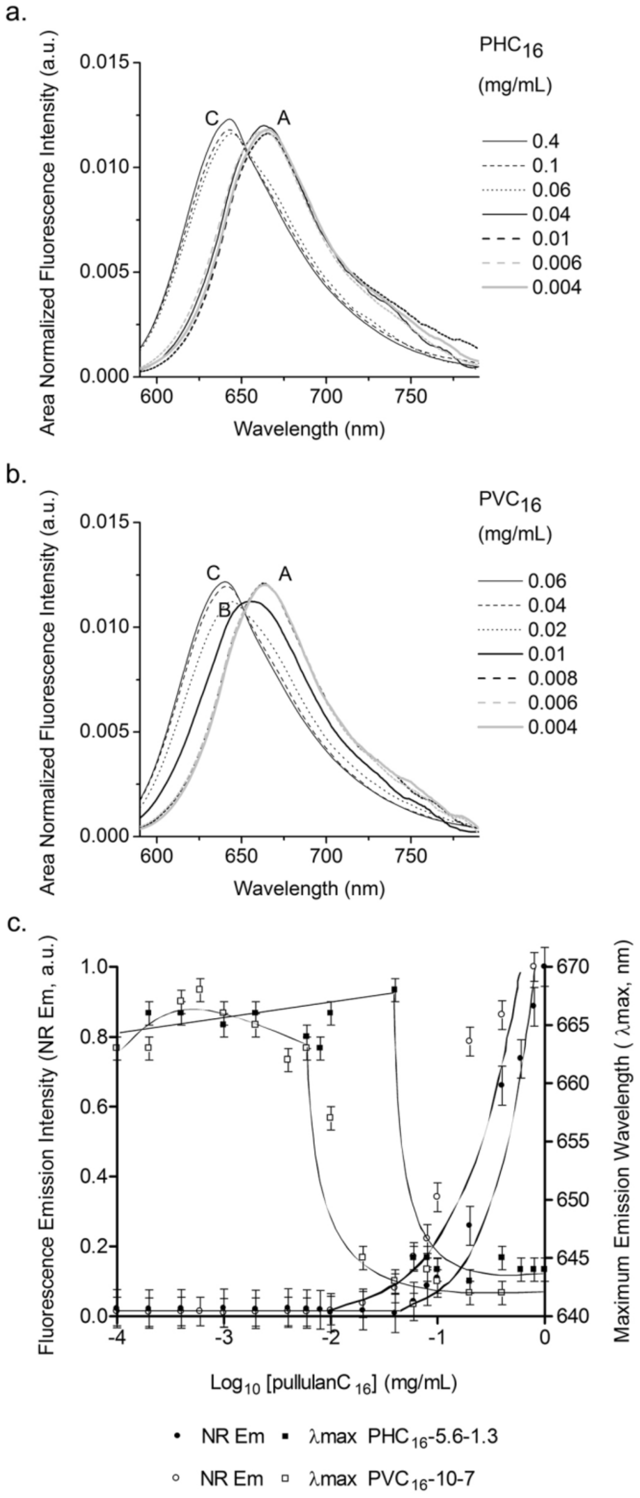

Figure 3. Determination of the cac of pullulan-C$_{16}$ using area normalized fluorescence emission (λ_{ex} 570 nm) spectra of NR (2×10^{-7} M) in the pullulan-C$_{16}$/water system as a function of (*a*) PHC$_{16}$-5.6-1.3 and (*b*) PVC$_{16}$-10-7 concentration; (*c*) area normalized fluorescence emission intensity and position of maximum emission wavelength of NR in the pullulan-C$_{16}$/water system as a function of pullulan-C$_{16}$ concentration. The cac obtained for PHC$_{16}$-5.6-1.3 was 0.04 mg/mL and for PVC$_{16}$-10-7 was 0.01 mg/mL.

In the case of PHC$_{16}$-5.6-1.3, the determined cac values are similar for both fluorescent probes. But that is not the case for PVC$_{16}$-10-7. This is explainable by the fact that as Py molecules already start at a low hydrated pre-micellar environment they are unable to detect the micellar domains of type B, which have higher hydration levels than those domains of type C. For the last ones there is a sufficient variation of hydration level that can be detected by Py I_3/I_1 ratio resulting in a cac value above the real one. We thus conclude that NR is a more sensitive fluorescence probe as it was able to follow all the variations in hydration level that occurred in the self-aggregation process of PVC$_{16}$-10-7. For PHC$_{16}$-5.6-1.3 the absence of B type micellar domains and the higher hydration of the premicellar environment, also seen in NR emission in zone A, allowed compatible determinations of cac for both probes.

As pullulan-C$_{16}$ concentration augments above the cac, more hydrophobic domains are formed, solubilizing more Py and NR, which consequently increases the fluorescence detected, not occurring the typical second plateau (Figures 2c, 3c). The highest concentration of pullulan-C$_{16}$ used was insufficient to enclose all of the hydrophobic dyes – this might be caused by the continued redistribution of Py and NR molecules to the less hydrated hydrophobic domains and by the formation of Py dimers in the hydrophobic domains with greater hydration level.

Characterization of pullulan-C$_{16}$ nanogels

Size and shape

The hydrophobic forces that sequester the hydrophobic chains in the core and the excluded volume repulsion between the chains mostly establish the micellar size.[48] The pullulan-C$_{16}$ nanogels appeared spherical in cryo-FESEM micrographs, with a large size distribution in the range of 100–700 nm for PHC$_{16}$-5.6-1.3 and 200–300 nm for PVC$_{16}$-10-7 (Figure 4).

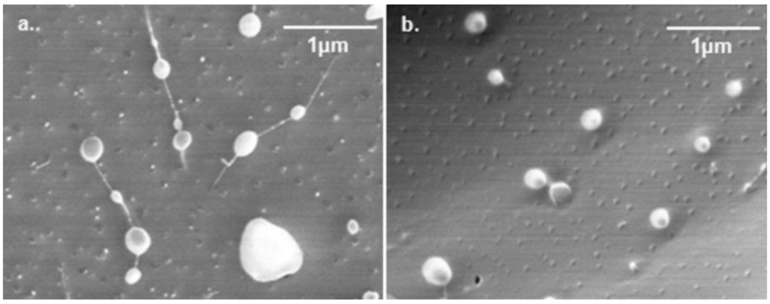

Figure 4. Cryo-FESEM negatively stained micrographs (magnification 30,000×) of (*a*) PHC$_{16}$-5.6-1.3 and (*b*) PVC$_{16}$-10-7.

Storage

The mean hydrodynamic diameter obtained using DLS for pullulan-C_{16} nanogels dispersed in ultrapure water oscillated between 162 nm and 335 nm for PHC_{16}-5.6-1.3 and between 115 nm and 369 nm for PVC_{16}-10-7, over a six month storage period at room temperature (25 °C). Both materials exhibited fairly high polydispersity, with an average PdI of 0.59 ± 0.11 for PHC_{16}-5.6-1.3 and 0.43 ± 0.23 for PVC_{16}-10-7, which means that there may be macromolecular micelles with a distribution of sizes and shapes, as also revealed by the cryo-FESEM micrographs (Figure 5).

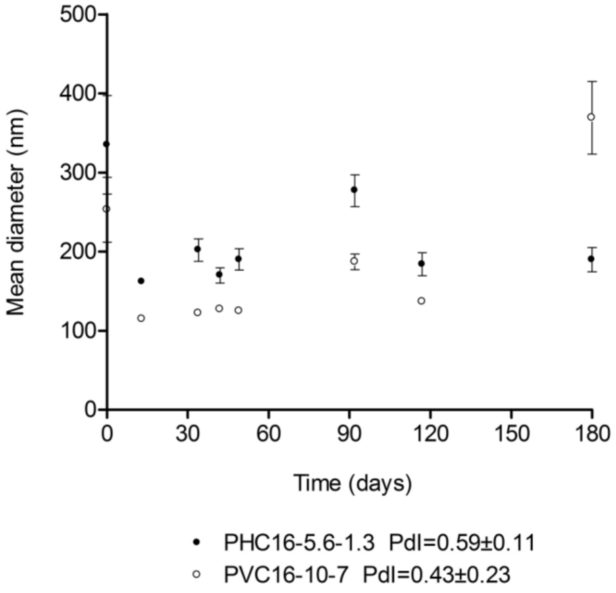

Figure.5. Size of pullulan-C_{16} water dispersions (1 mg/mL) over a six month storage period at room temperature (25 °C). Size was measured periodically in DLS (mean ± S.D., *n* = 10).

Effect of the concentration of pullulan-C_{16}

The mean hydrodynamic diameter tended to be much larger for lower concentrations of pullulan-C_{16}, especially when closer to the cac. It appears that, for higher concentrations of the polymer, the remaining solvent is gradually released from the hydrophobic core, resulting in a decrease in size. In contrast, occasionally exposed hydrophobic domains within a less mobile shell formed by hydrophilic chains may originate secondary aggregation enlarging the resultant macromolecular micelles.[48] The zeta potential values were always negative and close to zero, never lower than −20 mV. Once zeta potential approaches zero, electrostatic repulsion becomes small compared to the ever-present van der Waals attraction. In these conditions, eventually, instability may arise, causing aggregation followed by sedimentation and phase separation. However, the pullulan-C_{16} nanogels preserved their nanosize with the exception of PVC_{16}-10-7 at 0.5 mg/mL that formed aggregates out of the nanoscale (Figure 6).

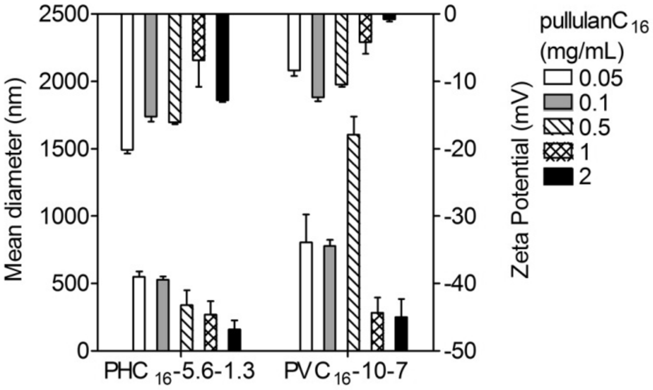

Figure 6. Influence of concentration on the size and zeta potential of pullulan-C_{16} nanogels (0.05–2 mg/mL) measured at 37 °C in DLS (mean ± S.D., *n* = 3).

Effect of urea

Urea is known for its ability to break intramolecular hydrogen bonds and to destabilize hydrophobic domains.[49, 50] Urea and its derivatives are very efficient as modifiers of the aqueous solution properties participating at the level of the micellar solvation layer because it enhances the polarity and the hydrophilic character of water. An increased accessibility from the aqueous phase at higher urea concentrations could result in a stronger solvation of the polar groups in micellar aggregates by urea-water mixture than water alone. Urea is related to the enhancement of the solubility of hydrocarbon tails favoring their solvation and to the weakening of the hydrophobic interactions responsible for the formation and maintenance of the micellar assembly in aqueous solution. The action of urea on micellization depends on the way in which solvation occurs in a specific micellar system.[51] The results obtained show that urea did not affect the nanogel size of PHC_{16}-5.6-1.3. In contrast, urea caused concentration dependent destabilization of PVC_{16}-10-7, affecting the self-assembly of this amphiphilic system in water, leading to the formation of larger aggregates out of the nanoscale (Figure 7). Destabilization of PVC_{16}-10-7, resulting in higher particle size, may be tentatively assigned to improved solvation of the hydrophobic domains. This possibility is supported by the fact that PVC_{16} has a higher substitution degree than PHC_{16} (DS_{C16} of 7 *vs.* 1.3).

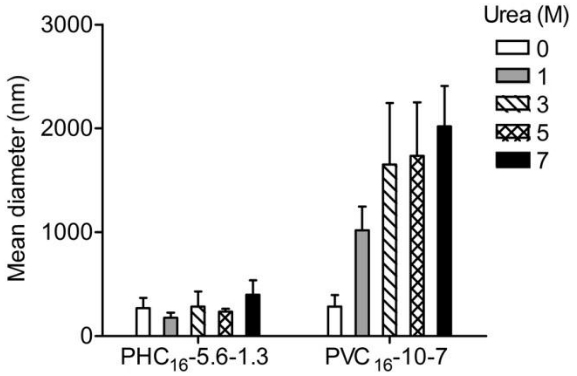

Figure 7. Influence of urea (0–7 M) on the size of pullulan-C_{16} nanogels (1 mg/mL) measured at 37 °C in DLS (mean ± S.D., *n* = 3).

Effect of ionic strength

Colloidal stability might be compromised in the absence of an electrostatic barrier. The addition of enough quantity of salt neutralizes the surface charge of the micelles in dispersion and compresses the surface double layer, facilitating the colloidal aggregation. Without the repulsive forces that keep macromolecular micelles separate, coagulation might occur due to attractive van der Waals forces. Compared to salt-free pullulan-C_{16} colloidal dispersion, while PHC$_{16}$-5.6-1.3 denoted stability, PVC$_{16}$-10-7 nanogel was larger as the ionic strength increased with increasing concentrations of NaCl (Figure 8).

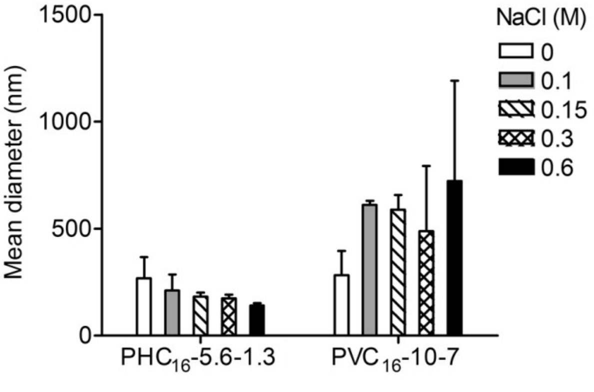

Figure 8. Influence of NaCl (0–0.6 M) on the size of pullulan-C_{16} nanogels (1 mg/mL) measured at 37 °C in DLS (mean ± S.D., *n* = 3).

Effect of pH

Size distributions and zeta potential of pullulan-C_{16} as a function of pH, using phosphate-citrate buffer (pH 2.2–8.0), were compared to values obtained in water and

PBS. The mean hydrodynamic diameter values obtained either for PHC_{16}-5.6-1.3 or PVC_{16}-10-7 were similar in the range of pH studied. The size stability, in the range of pH studied, demonstrates that the organization of hydrophobic alkyl chains, in hydrophobic domains with low water content, protect the amphiphilic molecules from the hydrolysis of the carbonate ester at alkaline pH and from the hydrolysis of the methacrylate ester at low pH.[52] For both materials, small negative values of zeta potential were obtained indicating little repulsion between macromolecular micelles to prevent aggregation. However, even with zeta potential close to zero, particles denoted only slight instability in the nanoscale (Figure 9). The nearly neutral charge is valuable for *in vivo* use, since large positively charged materials cause non-specific cell sticking, while large negatively charged materials are efficiently taken up by scavenger endothelial cells or "professional pinocytes" found in the liver, which results in a rapid clearance from the blood.[53]

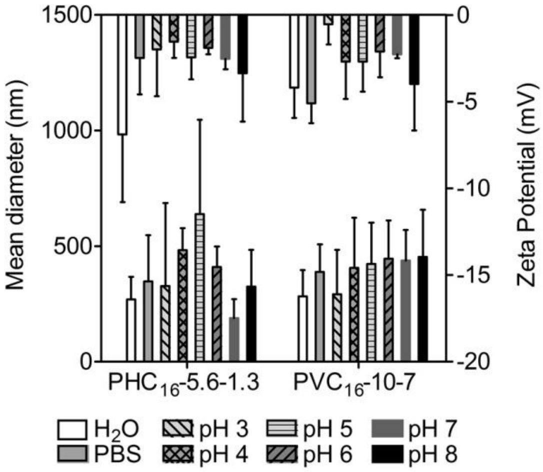

Figure 9. Influence of pH on the size and zeta potential of pullulan-C_{16} nanogels measured at 37 °C in DLS (mean ± S.D., *n* = 3).

Pullulan-based nanogels synthesized and characterized in this work have high water content, tunable size, interior network for possible incorporation of therapeutics, and large surface area for potential multivalent bioconjugation with cell-targeting ligands such as protein, peptides and antibodies. With these characteristics, described nanogels might be useful as polymeric carriers for therapeutic targeted delivery.

In our laboratory several nanogels are being developed, using different polysaccharides: dextrin, mannan, hyaluronic acid, glycolchitosan. The use of different polysaccharides allows the production of nanogels bearing different surface properties, namely size, charge and bioactivity. Among the applications envisaged for these materials, 1) the delivery of therapeutic proteins and of poorly water soluble pharmaceuticals, 2) vaccination, and 3) delivery of nucleic acid therapeutics are being developed. The comprehensive characterization of several nanogels provides a platform for the development of more sophisticated materials, with ability to perform as delivery systems. Recent results in our laboratory demonstrate the potential of dextrin nanogels for the delivery of cytokines, namely IL-10;[54] the association of the nanogels with injectable hydrogels is also a promising field of application of the self-assembled nanogels, allowing the incorporation of hydrophobic molecules in the highly hydrated environment of hydrogels. Ongoing work addresses the study of biodistribution and drainage of nanogels to the lymphatic nodes. Preliminary results using radioactively labeled nanogels and immunohistochemical analysis of the lymphatic nodes confirm the ability of the nanogels to reach the nodes, internalized in phagocytic cells. The use of mannan opens interesting possibilities concerning the use of the nanogels for vaccination purposes, acting as a delivery system and as an adjuvant. Self-assembled nanogels are thus very promising materials that bring together the essential requisites of biocompatibility and performance.

Conclusions

Hydrophobized pullulan nanogels were designed with a versatile, simple, reproducible and low-cost method. Above the cac, upon self-assembly in water, spherical polydisperse macromolecular micelles revealed long-term size stability in aqueous medium, with a nearly neutral negative surface charge and mean hydrodynamic diameter in the range 162–335 nm for PHC$_{16}$-5.6-1.3 and 115–369 nm for PVC$_{16}$-10-7. Size and zeta potential stability of pullulan-C$_{16}$ nanogels was maintained when exposed to potential destabilizing conditions of pH. While the size stability of the nanogel made of VMA with C$_{16}$ grafted, PVC$_{16}$-10-7, was affected by the ionic strength and urea, nanogel made of pullulan with HEMA and fewer C$_{16}$ grafted, PHC$_{16}$-5.6-1.3, remained more stable.

Pullulan-based nanogels have tunable size, high water content, interior network for possible incorporation of therapeutics, and large surface area for potential multivalent bioconjugation with cell-targeting ligands. With these characteristics, described nanogels might be useful as polymeric carriers for therapeutic targeted delivery. Further work is required to study molecular complexation, functionality and biocompatibility of these novel promising nanogels as drug and vaccine delivery systems.

References

1. Catley, B. J.; Whelan, W. J. Observations on the structure of pullulan. *Arch Biochem Biophys* **1971**, 143, 138-142.

2. Colson, P.; Jennings, H. J.; Smith, I. C. Composition, sequence, and conformation of polymers and oligomers of glucose as revealed by carbon-13 nuclear magnetic resonance. *J Am Chem Soc* **1974**, 96, 8081-8087.

3. Kasaai, M. R. Intrinsic viscosity-molecular weight relationship and hydrodynamic volume for pullulan. *J Appl Polym Sci* **2006**, 100, 4325-4332.

4. Jiao, Y. H.; Fu, Y.; Jiang, Z. H. Synthesis and characterization of poly(ethylene glycol) grafted on pullulan. *Abstracts of Papers of the American Chemical Society* **2003**, 225, U576-U576.

5. Masuda, K.; Sakagami, M.; Horie, K.; Nogusa, H.; Hamana, H.; Hirano, K. Evaluation of carboxymethylpullulan as a novel carrier for targeting immune tissues. *Pharm Res* **2001**, 18, 217-223.

6. Kimoto, T.; Shibuya, T.; Shiobara, S. Safety studies of a novel starch, pullulan: chronic toxicity in rats and bacterial mutagenicity. *Food Chem Toxicol* **1997**, 35, 323-329.

7. Shingel, K. I. Current knowledge on biosynthesis, biological activity, and chemical modification of the exopolysaccharide, pullulan. *Carbohydr Res* **2004**, 339, 447-460.

8. Nomura, Y.; Ikeda, M.; Yamaguchi, N.; Aoyama, Y.; Akiyoshi, K. Protein refolding assisted by self-assembled nanogels as novel artificial molecular chaperone. *Febs Letters* **2003**, 553, 271-276.

9. Shingel, K. I.; Petrov, P. T. Behavior of gamma-ray-irradiated pullulan in aqueous solutions of cationic (cetyltrimethylammonium hydroxide) and anionic (sodium dodecyl sulfate) surfactants. *Colloid Polym Sci* **2002**, 280, 176-182.

10. Leathers, T. D. Biotechnological production and applications of pullulan. *Appl Microbiol Biotechnol* **2003**, 62, 468-473.

11. Hasuda, H.; Kwon, O. H.; Kang, I. K.; Ito, Y. Synthesis of photoreactive pullulan for surface modification. *Biomaterials* **2005**, 26, 2401-2406.

12. Ito, Y.; Nogawa, M. Preparation of a protein micro-array using a photo-reactive polymer for a cell-adhesion assay. *Biomaterials* **2003**, 24, 3021-3026.

13. Hosseinkhani, H.; Aoyama, T.; Ogawa, O.; Tabata, Y. Liver targeting of plasmid DNA by pullulan conjugation based on metal coordination. *J Control Release* **2002**, 83, 287-302.

14. Gupta, M.; Gupta, A. K. Hydrogel pullulan nanoparticles encapsulating pBUDLacZ plasmid as an efficient gene delivery carrier. *J Control Release* **2004**, 99, 157-166.

15. Akiyoshi, K.; Kobayashi, S.; Shichibe, S.; Mix, D.; Baudys, M.; Kim, S. W.; Sunamoto, J. Self-assembled hydrogel nanoparticle of cholesterol-bearing pullulan as a carrier of protein drugs: Complexation and stabilization of insulin. *J Control Release* **1998**, 54, 313-320.

16. Suginoshita, Y.; Tabata, Y.; Matsumura, T.; Toda, Y.; Nabeshima, M.; Moriyasu, F.; Kada, Y.; Chiba, T. Liver targeting of human interferon-beta with pullulan based on metal coordination. *J Control Release* **2002**, 83, 75-88.

17. Nogusa, H.; Yamamoto, K.; Yano, T.; Kajiki, M.; Hamana, H.; Okuno, S. Distribution characteristics of carboxymethylpullulan-peptide-doxorubicin conjugates in tumor-bearing rats: Different sequence of peptide spacers and doxorubicin contents. *Biological & Pharmaceutical Bulletin* **2000**, 23, 621-626.

18. Na, K.; Bum Lee, T.; Park, K. H.; Shin, E. K.; Lee, Y. B.; Choi, H. K. Self-assembled nanoparticles of hydrophobically-modified polysaccharide bearing vitamin H as a targeted anti-cancer drug delivery system. *Eur J Pharm Sci* **2003**, 18, 165-173.

19. Na, K.; Seong Lee, E.; Bae, Y. H. Adriamycin loaded pullulan acetate/sulfonamide conjugate nanoparticles responding to tumor pH: pH-dependent cell interaction, internalization and cytotoxicity in vitro. *J Control Release* **2003**, 87, 3-13.

20. Hasegawa, U.; Nomura, S. M.; Kaul, S. C.; Hirano, T.; Akiyoshi, K. Nanogel-quantum dot hybrid nanoparticles for live cell imaging. *Biochem Biophys Res Commun* **2005**, 331, 917-921.

21. Na, K.; Shin, D.; Yun, K.; Park, K. H.; Lee, K. C. Conjugation of heparin into carboxylated pullulan derivatives as an extracellular matrix for endothelial cell culture. *Biotechnol Let* **2003**, 25, 381-385.

22. Yamaoka, T.; Tabata, Y.; Ikada, Y. Body distribution profile of polysaccharides after intravenous administration. *Drug Deliv* **1993**, 1, 75-82.

23. Kaneo, Y.; Tanaka, T.; Nakano, T.; Yamaguchi, Y. Evidence for receptor-mediated hepatic uptake of pullulan in rats. *Journal of Controlled Release* **2001**, 70, 365-373.

24. Akiyoshi, K.; Deguchi, S.; Moriguchi, N.; Yamaguchi, S.; Sunamoto, J. Self-aggregates of hydrophobized polysaccharides in water - formation and characteristics of nanoparticles. *Macromolecules* **1993**, 26, 3062-3068.

25. Nishikawa, T.; Akiyoshi, K.; Sunamoto, J. Macromolecular complexation between bovine serum albumin and the self-assembled hydrogel nanoparticle of hydrophobized polysaccharides. *J Am Chem Soc* **1996**, 118, 6110-6115.

26. Akiyoshi, K.; Kobayashi, S.; Shichibe, S.; Mix, D.; Baudys, M.; Kim, S. W.; Sunamoto, J. Self-assembled hydrogel nanoparticle of cholesterol-bearing pullulan as a carrier of protein drugs: complexation and stabilization of insulin. *J Control Release* **1998**, 54, 313-320.

27. Sawada, S. I.; Akiyoshi, K. Nano-encapsulation of lipase by self-assembled nanogels: induction of high enzyme activity and thermal stabilization. *Macromol Biosci* **2010**, 10, 353-358

28. Kitano, S.; Kageyama, S.; Nagata, Y.; Miyahara, Y.; Hiasa, A.; Naota, H.; Okumura, S.; Imai, H.; Shiraishi, T.; Masuya, M.*, et al.* HER2-specific T-cell immune responses in patients vaccinated with truncated HER2 protein complexed with nanogels of cholesteryl pullulan. *Clin Cancer Res* **2006**, 12, 7397-7405.

29. Gu, X. G.; Schmitt, M.; Hiasa, A.; Nagata, Y.; Ikeda, H.; Sasaki, Y.; Akiyoshi, K.; Sunamoto, J.; Nakamura, H.; Kuribayashi, K.*, et al.* A novel hydrophobized polysaccharide/oncoprotein complex vaccine induces in vitro and in vivo cellular and humoral immune responses against HER2-expressing murine sarcomas. *Cancer Res* **1998**, 58, 3385-3390.

30. Shiku, H.; Wang, L.; Ikuta, Y.; Okugawa, T.; Schmitt, M.; Gu, X.; Akiyoshi, K.; Sunamoto, J.; Nakamura, H. Development of a cancer vaccine: peptides, proteins, and DNA. *Cancer Chemother Pharmacol* **2000**, 46 Suppl, S77-82.

31. Shimizu, T.; Kishida, T.; Hasegawa, U.; Ueda, Y.; Imanishi, J.; Yamagishi, H.; Akiyoshi, K.; Otsuji, E.; Mazda, O. Nanogel DDS enables sustained release of IL-12 for tumor immunotherapy. *Biochem Biophys Res Commun* **2008**, 367, 330-335.

32. Hasegawa, U.; Sawada, S.; Shimizu, T.; Kishida, T.; Otsuji, E.; Mazda, O.; Akiyoshi, K. Raspberry-like assembly of cross-linked nanogels for protein delivery. *J Control Release* **2009**, 140, 312-317.

33. Ayame, H.; Morimoto, N.; Akiyoshi, K. Self-assembled cationic nanogels for intracellular protein delivery. *Bioconjug Chem* **2008**, 19, 882-890.

34. Morimoto, N.; Endo, T.; Iwasaki, Y.; Akiyoshi, K. Design of hybrid hydrogels with self-assembled nanogels as cross-linkers: interaction with proteins and chaperone-like activity. *Biomacromolecules* **2005**, 6, 1829-1834.

35. Hirakura, T.; Yasugi, K.; Nemoto, T.; Sato, M.; Shimoboji, T.; Aso, Y.; Morimoto, N.; Akiyoshi, K. Hybrid hyaluronan hydrogel encapsulating nanogel as a protein nanocarrier: new system for sustained delivery of protein with a chaperone-like function. *J Control Release* **2010***,* 142, 483-489.

36. Gonçalves, C.; Pereira, P.; Gama, M. Self-assembled hydrogel nanoparticles for drug delivery applications. *Materials* **2010**, 3, 1420-1460.

37. vanDijkWolthuis, W. N. E.; Tsang, S. K. Y.; KettenesvandenBosch, J. J.; Hennink, W. E. A new class of polymerizable dextrans with hydrolyzable groups: hydroxyethyl methacrylated dextran with and without oligolactate spacer. *Polymer* **1997**, 38, 6235-6242.

38. Ferreira, L.; Gil, M. H.; Dordick, J. S. Enzymatic synthesis of dextran-containing hydrogels. *Biomaterials* **2002**, 23, 3957-3967.

39. Carvalho, J.; Goncalves, C.; Gil, A. M.; Gama, F. M. Production and characterization of a new dextrin based hydrogel. *Eur Polym J* **2007**, 43, 3050-3059.

40. Goncalves, C.; Martins, J. A.; Gama, F. M. Self-assembled nanoparticles of dextrin substituted with hexadecanethiol. *Biomacromolecules* **2007**, 8, 392-398.

41. Dubois, M.; Gilles, K. A.; Hamilton, J. K.; Rebers, P. A.; Smith, F. Colorimetric method for determination of sugars and related substances. *Anal Chem* **1956**, 28, 350-356.

42. Masci, G.; Bontempo, D.; Crescenzi, V. Synthesis and characterization of thermoresponsive N-isopropylacrylamide/methacrylated pullulan hydrogels. *Polymer* **2002**, 43, 5587-5593.

43. Glinel, K.; Sauvage, J. P.; Oulyadi, H.; Huguet, J. Determination of substituents distribution in carboxymethylpullulans by NMR spectroscopy. *Carbohydr Res* **2000**, 328, 343-354.

44. Hrkach, J. S.; Peracchia, M. T.; Domb, A.; Lotan, N.; Langer, R. Nanotechnology for biomaterials engineering: Structural characterization of amphiphilic polymeric nanoparticles by H-1 NMR spectroscopy. *Biomaterials* **1997**, 18, 27-30.

45. Kalyanasundaram, K.; Thomas, J. K. Environmental effects on vibronic band intensities in pyrene monomer fluorescence and their application in studies of micellar systems. *J Am Chem Soc* **1977**, 99, 2039-2044.

46. Dong, D. C.; Winnik, M. A. The Py scale of solvent polarities. *Can J Chem* **1984**, 62, 2560-2565.

47. Coutinho, P. J. G.; Castanheira, E. M. S.; Rei, M. C.; Oliveira, M. E. C. D. R. Nile red and DCM fluorescence Anisotropy studies in C12E7/DPPC mixed systems. *J Phys Chem B* **2002**, 106, 12841-12846.

48. Jones, M. C.; Leroux, J. C. Polymeric micelles - a new generation of colloidal drug carriers. *Eur J Pharm Biopharm* **1999**, 48, 101-111.

49. Mukerjee, P.; Ray, A. Effect of urea on micelle formation and hydrophobic bonding. *J Phys Chem* **1963**, 67, 190-&.

50. Moore, D. R.; Mathias, L. J. Molecular composites *via* in situ polymerization - Poly(phenylene terephthalamide)-nylon 3. *J Appl Polym Sci* **1986**, 32, 6299-6315.

51. Hierrezuelo, J. M.; Molina-Bolívar, J. A.; Carnero Ruiz, C. On the urea action mechanism: a comparative study on the self-assembly of two sugar-based surfactants. *J Phys Chem B* **2009**, 113, 7178-7187.

52. Dijk-Wolthuis, W. N. E. v.; Steenbergen, M. J. v.; Underberg, W. J. M.; Hennink, W. E. Degradation kinetics of methacrylated dextrans in aqueous solution. *J Pharm Sci* **1997**, 86, 413-417.

53. Smedsrod, B. Clearance function of scavenger endothelial cells. *Comp Hepatol* **2004**, 3 Suppl 1, S22.

54. Carvalho, V.; Castanheira, P.; Faria, T. Q.; Goncalves, C.; Madureira, P.; Faro, C.; Domingues, L.; Brito, R. M.; Vilanova, M.; Gama, M. Biological activity of heterologous murine interleukin-10 and preliminary studies on the use of a dextrin nanogel as a delivery system. *Int J Pharm* **2010**, 400, 234-242.

Chapter 3

Self-assembled nanogel made of mannan: synthesis and characterization

Amphiphilic mannan (mannan-C_{16}) was synthesized by the Michael addition of hydrophobic 1-hexadecanethiol (C_{16}) to hydroxyethyl methacrylated mannan (mannan-HEMA). Mannan-C_{16} formed nanosized aggregates in water by self-assembly *via* the hydrophobic interaction among C_{16} molecules as confirmed by hydrogen nuclear magnetic resonance (^{1}H NMR), fluorescence spectroscopy, cryo-field emission scanning electron microscopy (cryo-FESEM) and dynamic light scattering (DLS). The mannan-C_{16} critical aggregation concentration (cac), calculated by fluorescence spectroscopy with Nile red and pyrene, ranged between 0.04 and 0.02 mg/mL depending on the polymer degree of substitution of C_{16} relative to methacrylated groups. Cryo-FESEM micrographs revealed that mannan-C_{16} formed irregular spherical macromolecular micelles, in this work designated as nanogels, with diameters ranging between 100 and 500 nm. The influence of the polymer degree of substitution, DS_{HEMA} and DS_{C16}, on the nanogel size and zeta potential was studied by DLS at different pH values and ionic strength and as a function of mannan-C_{16} and urea concentrations. Under all tested conditions, the nanogel was negatively charged with a zeta potential close to zero. Mannan-C_{16} with higher DS_{HEMA} and DS_{C16} values formed larger nanogels and were also less stable over a six months storage period and at concentrations close to cac. When exposed to solutions of different pH and to aggressive conditions of ionic strength and urea concentration, the size of mannan-C_{16} varied to some extent but was always in the nanoscale range.

Adapted from: *Langmuir* **2010**, 26, 11413-11420.

Introduction

The self-assembly phenomenon has been defined as the autonomous, spontaneous, and reversible organization of molecular units into structurally stable and well-defined aggregates in which defects are energetically rejected. This process is cost-effective, versatile, and facile.[1-3] Self-assembly occurs toward the system's thermodynamic minima and through a balance of attractive and repulsive interactions, which are generally weak and noncovalent, such as electrostatic, van der Waals, and Coulomb interactions, hydrophobic forces, and hydrogen bonds.[4]

Above critical aggregation concentration (cac), amphiphilic polymers can self-assemble in water because hydration forces, namely, intra- and/or intermolecular hydrophilic and hydrophobic interactions.[5] In other words, the nanostructure builds itself.

Recently, different hydrophobically modified polymers have been designed as new solutions for multifunctional pharmaceutical nanocarriers. A variety of molecules can be encapsulated within the particle core, entrapped in the polymer matrix, chemically attached, and/or physically adsorbed at the surface of the macromolecular micelles, also designated by some authors as nanogels. In this work, we adopt this terminology, with the term nanogel referring to the hydrogel-like – highly porous and hydrated – nanosized material. Through combining several useful properties in one nanogel, the possibility to enhance the efficacy of many therapeutic and diagnostic protocols arose.[6]

Various macromolecular polysaccharides have been reported as molecular carriers, including chitosan,[7] dextran,[8] dextrin,[9] mannan,[10, 11] pullulan,[10, 12, 13] hyaluronic acid,[14] either in their native forms or as carrier conjugates.[15] Among them, we selected mannan, from *Saccharomyces cerevisiae*, which consists of an α-1,6-linked mannose backbone with a high percentage of α-1,2- and α-1,3-side chains of different composition.[16] Mannan is a biodegradable, biocompatible polymer and has been described as a promising targeted delivery system.[10, 17-19] Mannan potentially targets antigen-presenting cells (APC) because dendritic cells and macrophages express on their surface mannose receptor, which recognizes carbohydrates present on the cell walls of infectious agents. The mannose receptor is part of the multilectin receptor proteins and provides a link between innate and adaptive immunity.[19-22]

In this study, we aimed to develop new amphiphilic conjugates by the Michael addition of hydrophobic 1-hexadecanethiol (C_{16}) to hydroxyethyl methacrylated mannan (mannan-HEMA), also produced in this work. We studied the self-assembly of mannan-C_{16} in an aqueous environment by ^{1}H NMR and fluorescence spectroscopy with hydrophobic fluorescent probes Nile red and pyrene. Relevant features such as the chemical structure, size, surface charge, and morphology of mannan-C_{16} nanogel were characterized using ^1H NMR spectroscopy, cryo-field emission scanning electron microscopy (cryo-FESEM) and dynamic light scattering (DLS).

Experimental

Materials

CDI-activated hydroxyethyl methacrylate (HEMA-CI) was produced as described by van Dijk-Wolthuis et al.[23] Mannan (from *S. cerevisiae*), dimethyl sulfoxide (DMSO), 4-(N,N-dimethylamino)pyridine (DMAP), triethylamine (TEA), 1-hexadecanethiol, deuterium oxide (D_2O), dimethyl sulfoxide-d_6 (DMSO-d_6), pyrene (Py), and 9-(diethylamino)-5H-benzo[α]phenoxazin-5-one (Nile red, NR) were purchased from Sigma-Aldrich. Pyrene was purified by appropriate recrystallization from absolute ethanol. Phosphotungstic acid was purchased from Riedel-de Haën. Regenerated cellulose tubular membranes, with a 12,000-14,000 nominal molecular weight cut-off (MWCO), were obtained from Membrane Filtration Products. Water was purified with a Milli-Q system (Millipore). Other organic and inorganic chemicals were purchased from Sigma-Aldrich and used without further purification.

Synthesis of amphiphilic mannan-C_{16}

HEMA-derivatized mannan (mannan-HEMA) was prepared as described by van Dijk-Wolthuis et al.[23] Briefly, mannan was dissolved in dry DMSO in a nitrogen atmosphere to a concentration of 3−5% w/v with different calculated amounts of HEMA-CI resulting in 0.25 and 0.4 molar ratios of HEMA-CI to mannose residues. The reaction catalyzed by DMAP (2 mol equiv to HEMA-CI) was allowed to proceed and the mixture was stirred at room temperature for 4 days. The reaction was terminated with concentrated HCl (2% v/v), which neutralized DMAP and imidazole. The mixture was then dialyzed against frequently changed distilled water at 4 °C for 3 days. After being lyophilized, mannan-HEMA resulted as a pallid-yellow, fluffy product that was stored at −20 °C. Finally, amphiphilic molecule mannan-HEMA-SC_{16} (mannan-C_{16}) was produced as described elsewhere.[9] Briefly, mannan-HEMA and C_{16} at 1, 1.2 and 2 molar ratios of C_{16} to HEMA-CI were mixed in DMSO (equivalent HEMA = 0.03 M). The reaction mixture catalyzed by TEA (2 mol equiv with respect to HEMA) was stirred for 3.5 days at 50 °C. The resulting mixture was dialyzed for 3 days against frequently changed distilled water at room temperature. After being lyophilized, mannan-C_{16} resulted as a pallid-yellow, fluffy product that was stored at −20 °C.

^{1}H NMR spectroscopy

Lyophilized reaction products were dispersed in D_2O (5 mg/mL). Mannan-C_{16} was also dispersed in DMSO-d_6 and in 10% D_2O-DMSO-d_6 (5 mg/mL). Samples were stirred overnight at 50 °C to obtain a clear dispersion, which was transferred to 5 mm NMR tubes. One-dimensional ^{1}H NMR measurements were performed with a Varian Unity Plus 300 spectrometer operating at 299.94 MHz. One-dimensional ^{1}H NMR spectra were recorded at 298 K with 256 scans, a spectral width of 5000 Hz, a relaxation delay of 1 s between scans, and an acquisition time of 2.8 s.

Fluorescence spectroscopy

The cac of mannan-C_{16} was fluorometrically investigated using hydrophobic guest molecules such as NR and Py, whose maximum solubility values in water are 1×10^{-6} M and 5×10^{-7} M, respectively. The fluorescence intensity change of these guest molecules was calculated as a function of the mannan-C_{16} concentration. Lyophilized mannan-C_{16} was dispersed in ultrapure water (1 mg/mL) with stirring for 3 days at 50 °C. Consecutive dilutions of 1 mL of each sample were prepared in ultrapure water where NR and Py were injected. A volume of 5 µL of a 4×10^{-5} M NR stock solution in ethanol was added, giving a constant concentration of 2×10^{-7} M in 0.5 % ethanol/water for all NR fluorescence measurements. A volume of 5 µL of a 1.2×10^{-4} M Py stock solution in ethanol was added, giving a constant concentration of 6×10^{-7} M in 0.5% ethanol/water for all Py fluorescence measurements. Samples were stirred overnight before fluorescence measurements, which were performed with a Spex Fluorolog 3 spectrofluorimeter at room temperature. The slit width was set at 5 nm for excitation and 5 nm for emission. All spectra were corrected for the instrumental response of the system. The cac was calculated using both the maximum emission intensity of NR (λ_{ex} 570 nm) and the Py fluorescence intensity ratio of the third (384–385 nm) and first vibrational bands (372–374 nm) (I_3/I_1) of the emission spectra (λ_{ex} 339 nm) in the mannan-C_{16}/water system as a function of mannan-C_{16} concentration; in both cases, the cac was estimated as the interception of two trend lines.

Sample preparation

Lyophilized mannan-C_{16} was dispersed in ultrapure water (1 mg/mL) with stirring for 3 days at 50 °C. The resulting milky colloidal dispersion was filtered through the membrane filter (pore size 0.45 μm). Material lost during filtration was residual, as verified using the phenol-sulfuric acid method.[24]

Cryo-FESEM

The mannan-C_{16} nanogel concentrated by ultrafiltration (Amicon Ultra-4 Centrifugal Filter Units, MWCO, 1×10^5) was negatively stained with phosphotungstic acid (0.01% w/v). Samples were placed into brass rivets and plunged frozen into slush nitrogen at −200 °C and then stored in liquid nitrogen and transferred to the cryo stage (Gatan, Alto 2500, UK) of electronic microscope (SEM/EDS: FESEM JEOL JSM6301F/Oxford Inca Energy 350). Each sample was fractured on the cryo stage with a knife. In microscope, the sublimation of any unwanted surface ice was carried out in the cryo chamber for 10 min at −95 °C. At −140 °C samples were sputter coated with gold and palladium using an accelerating voltage of 10 kV. The antipollutant of copper covers and protects the sample. The samples were observed at −140 °C at 15 kV. The solvent used in the preparation of the samples (water and phosphotungstic acid) was also observed as a negative control.

DLS

The size distribution and zeta potential measurements were performed in a Malvern Zetasizer NANO ZS (Malvern Instruments Limited, UK). For each sample (1 mL), the size was measured periodically during six months of storage in a polystyrene cell at 25 °C using a He-Ne laser with a 633 nm wavelength, a detector angle of 173°, and a refractive index of 1.33. The values reported correspond to the polydispersity index (PdI) and z-average diameter, that is, the mean hydrodynamic diameter, and represent the mean ± S.D. obtained after 10 repeated measurements. The zeta potential and size of each sample dispersed in phosphate buffered saline (PBS 1×, pH 7.4) and in phosphate-citrate buffer (pH 2.2–8.0) were analyzed at 37 °C in a folded capillary cell. The zeta potential values were calculated using the Smoluchowski equation. The size distribution of each sample dispersed in dilutions of NaCl (0–0.6 M) and of urea (0–7 M) was evaluated at 37 °C. The values reported for the mean hydrodynamic diameter and zeta potential represent the mean ± S.D. obtained with three independent experiments, with three repeated measurements being performed in each one.

Results and discussion

Synthesis of mannan-C_{16}

Amphiphilic mannan-C_{16} was synthesized in a two step reaction. In the first step, methacrylated mannan was obtained by coupling HEMA-Cl to mannan. A majority of HEMA groups, according to several authors, are likely coupled to the ^6C of the mannose residues of the grafts.[16, 25] In the second step, the thiol acting as a nucleophile reacted with grafted methacrylate by a Michael addition mechanism, as shown in Scheme 1.

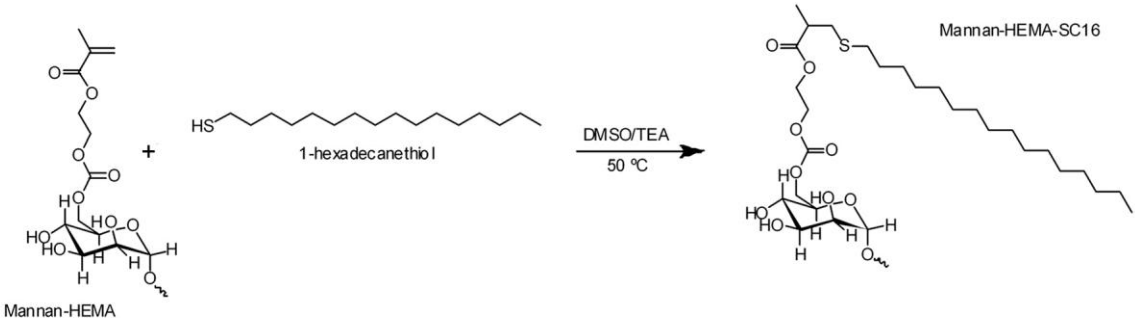

Scheme 1. Synthesis of mannan-C_{16}.

^{1}H NMR measurements

The purity, chemical structure, and polymer degree of substitution (DS) of the reaction products were controlled using ^1H NMR spectra in D_2O, as shown in Figure 1. The characteristic peaks of the protons of the unsaturated carbons of the acrylate groups of methacrylated mannan appeared in the range of 6.18 and 5.77 ppm.[23] The successful formation of mannan-C_{16} was confirmed by the peaks appearing between 1.8 and 0.6 ppm, which correspond to the grafted alkyl moiety.[9] In both spectra, the anomeric protons of mannan can be identified because their resonances lie in the range 4.9–5.5 ppm whereas the remaining protons of mannan appear in the range 3.5–4.5 ppm.[26] Mannan-C_{16} was washed with *n*-hexane, and the ^1H NMR analysis was repeated. Because no differences were observed, it was possible to conclude that the alkyl chain was covalently bound to the methacrylate group (data not shown).

The degree of substitution of methacrylate groups (DS_{HEMA}, defined as the number of methacrylate groups per 100 mannose residues), was calculated from the ^1H NMR spectra of mannan-HEMA in D_2O with the equation $(I_a)/(I_{H1})\times 100$, in which I_a is the average integral of the protons of the unsaturated carbons of the acrylate groups (around

6 ppm) and I_{H1} is the integral of the anomeric proton (4.9–5.5 ppm).[23] The degree of substitution with the hydrophobic alkyl chains (DS_{C16}, defined as the number of alkyl chains per 100 mannose residues) was calculated from the ^1H NMR spectra of mannan-C_{16} in D_2O as (7X)/(37Y)×100, in which X is the average integral corresponding to the protons from alkyl moieties (1.8–0.6 ppm) and Y is the integral of all mannan protons (3.5–5.5 ppm).[9]

By varying the molar ratio of HEMA-CI to mannose residues and the molar ratio of C_{16} to HEMA-CI, different independent batches of mannan-C_{16} with different DS_{HEMA} and DS_{C16} were obtained, indicating this method to be versatile, simple, and reproducible, as shown in Table 1.

The self-assembly of amphiphilic mannan-C_{16} in water was studied using ^1H NMR spectroscopy. The shape and width of the proton signals of C_{16} (1.8–0.6 ppm) depend on the polarity of the solvent used to record the ^1H NMR spectra, as shown in Figure 1. Therefore, the association of the hydrophobic alkyl chains forming nanogels can be detected by ^1H NMR. The signals provided by the methyl (0.8 ppm) and methylene (1.1 ppm) groups were sharp in DMSO-d_6 but tended to be gradually broadened at the base with an increase in the D_2O content in DMSO-d_6. A large amount of broadening was clear in pure D_2O, which is characteristic of the superposition of peaks representing a collection of chemically identical species yet possessing various degrees of mobility.[27] This result suggests that, when dispersed in water, part of the alkyl chains were exposed to hydrophobic microdomains (low mobility) but others might have been exposed to the hydrophilic solvent (high mobility). In DMSO-d_6, all hydrophobic chains were exposed to the solvent, having the same mobility, because the material is well dissolved.[9] In contrast, the mobility of the polysaccharide skeleton of mannan-C_{16} was kept in environments of different polarity. These data suggested that the mannan-C_{16} nanogel is obtained upon self-aggregation in water through the alkyl hydrophobic chains – partial water exclusion due to the hydrophobic interaction – and also owing to the relatively mobile shell of the hydrated polysaccharide skeleton on the outer surface of the nanogel.

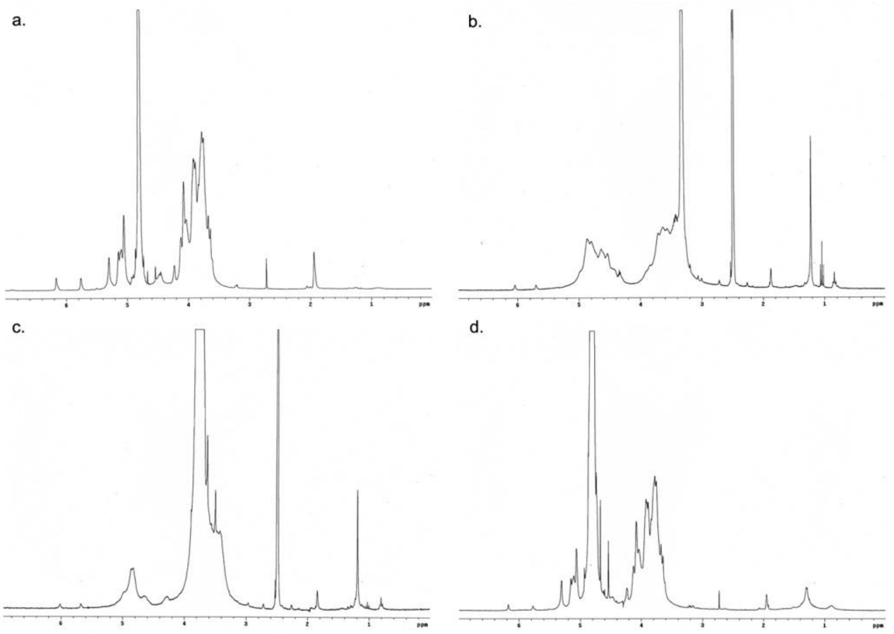

Figure 1. ^{1}H NMR spectrum of mannan-HEMA (5 mg/mL) in (*a*) D_2O and ^{1}H NMR spectra of mannan-C_{16} (5 mg/mL) in (*b*) DMSO-d_6, (*c*) 10% D_2O in DMSO-d_6 and (*d*) D_2O, using MHC$_{16}$-6.5-1.5 as an example.

Table 1. Characteristics of mannan-C_{16}

theoretical DS_{HEMA} [a] (%)	real DS_{HEMA} [b] (%)	theoretical DS_{C16} [c] (%)	real DS_{C16} [d] (%)	obtained DS_{C16} relative to methacrylated groups[e] (%)	efficiency [f] (%)	Mannan-C_{16} [g]
25	5	100	0.6	12	12	MHC$_{16}$-5-0.6
25	5	120	1.2	24	20	MHC$_{16}$-5-1.2
25	5	200	4.1	82	41	MHC$_{16}$-5-4.1
40	6.5	120	1.5	23	19	MHC$_{16}$-6.5-1.5
40	6.5	200	2.5	38	19	MHC$_{16}$-6.5-2.5

[a] Calculated as the molar ratio of HEMA-CI to mannose residue (×100) in the reaction mixture. [b] Calculated by ^{1}H NMR of mannan-HEMA in D_2O. [c] Calculated as the molar ratio of C_{16} to HEMA (×100) in the reaction mixture. [d] Calculated by ^{1}H NMR of mannan-C_{16} in D_2O. [e] Calculated using the following equation: real DS_{C16}/real DS_{HEMA} (×100). [f] Calculated as the ratio of the obtained to the theoretical DS_{C16} (×100). [g] mannan-HEMA-SC$_{16}$ synthesized: MHC$_{16}$-DS_{HEMA}-DS_{C16}.

Critical aggregation concentration of mannan-C_{16}

The self-assembly of mannan-C_{16} in aqueous solutions was also studied by fluorescence spectroscopy. The cac of mannan-C_{16} with different DS values was studied using hydrophobic dyes, NR[28] and Py,[29, 30] which are poorly soluble and weakly fluorescent in water. In contrast, their solubility and fluorescence dramatically increase in a hydrophobic medium.

The fluorescence measurements in Figures 2 and 4 showed that for lower concentrations of mannan-C_{16}, amphiphilic molecules exist in aqueous solutions as individual molecules (premicelle aqueous environment, zone A); the fluorescence intensity of NR remained constant, without any shift in the maximum emission wavelength. For higher concentrations, above the cac, an increase of intensity associated with a strong blue shift was observed, which is attributed to NR being close to (or inside) mannan-C_{16} hydrophobic domains. These hydrophobic domains are of two types with different hydration levels (zones B and C). However, the hydrophobic domains do not correspond to a typical surfactant system.

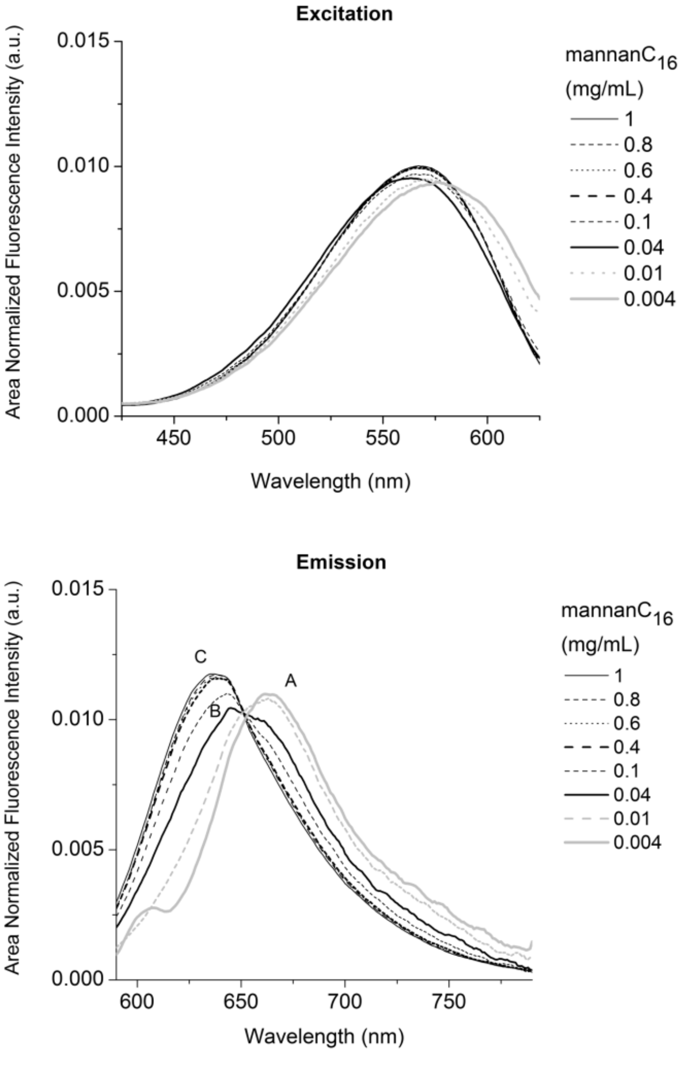

Figure 2. Area-normalized fluorescence excitation (λ_{em} 650 nm) and emission (λ_{ex} 570 nm) spectra of NR (2×10^{-7} M) in the mannan-C_{16}/water system as a function of mannan-C_{16} concentration obtained for MHC_{16}-5-0.6, as an example.

In the case of Py fluorescence, the spectra obtained in this study were typical of Py photophysical behavior. A red shift was observed in the excitation spectra, and intensity increased with increasing concentration of mannan-C_{16}, as shown in Figure 3. The I_3/I_1 oscillated with a linear trend below cac value but a small I_3/I_1 increase above this value was observed, as shown in Figure 4. This transition of intensity reflected the transference of Py to a less polar micellar domain, which was coincident with the onset of the supramolecular formation of mannan-C_{16}. However, some bands in the 450 nm region still appear above cac. This indicates the presence of Py dimers and can be explained by the high water penetration into the nanogel and is consistent with the ^{1}H NMR measurements.

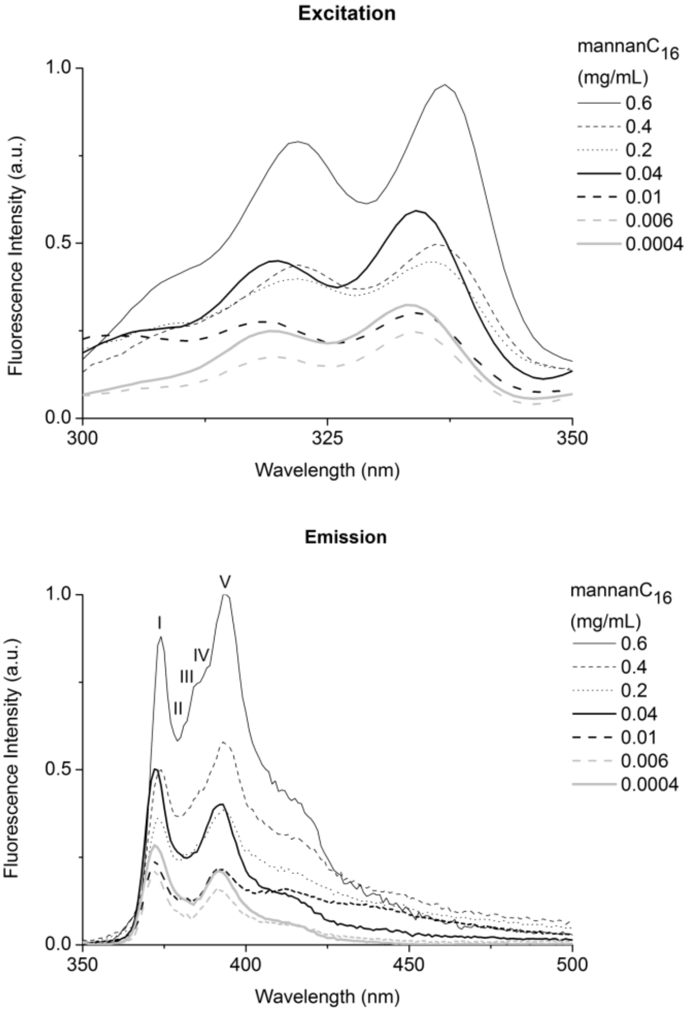

Figure 3. Fluorescence excitation (λ_{em} 390 nm) and emission (λ_{ex} 339 nm) spectra of Py (6×10^{-7} M) in the mannan-C_{16}/water system as a function of mannan-C_{16} concentration obtained for MHC_{16}-5-0.6, as an example.

The increase in the mannan-C_{16} concentration corresponds to an increased number of hydrophobic domains, allowing the solubility of more NR and Py; consequently, the fluorescence that is detected continues to increase. A second plateau is not achieved, as shown in Figure 4, either because the highest concentration of mannan-C_{16} used was not enough to enclose all of the hydrophobic dyes and saturation was not attained or because the NR or Py molecules, although enclosed in the hydrophobic domains, are sensitive to differences in the hydration level or different degrees of exposure to water and are still redistributing to hydrophobic domains with lower hydration levels as the mannan-C_{16} concentration increases above the cac. The effect is less defined in the case of Py, because of the formation of Py dimers in hydrophobic domains with greater hydration levels.

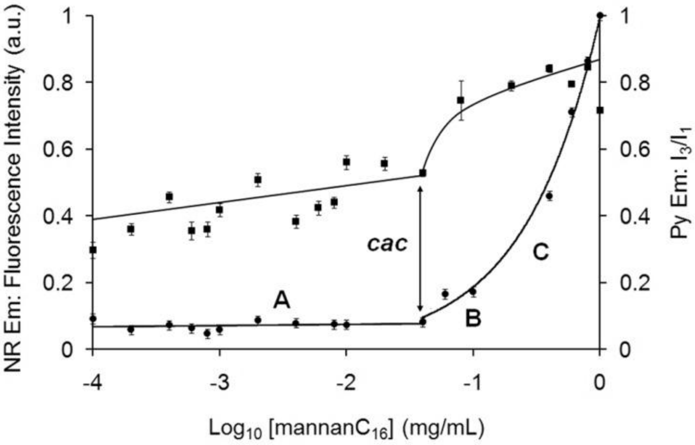

Figure 4. Maximum emission intensity of NR (circles; λ_{ex} 570 nm) and Py fluorescence intensity ratio I_3/I_1 (squares; λ_{ex} 339 nm) in the mannan-C_{16}/water system as a function of mannan-C_{16} concentration obtained for MHC_{16}-5-0.6, as an example.

The cac values obtained by fluorescence measurements with both dyes (Table 2) were consistent and exhibit a dependence on the obtained DS_{C16} relative to methacrylated groups, confirming that C_{16} governs the propensity of these molecules to self-assemble in water. The cac was 0.04 mg/mL for lower DS_{C16} relative to methacrylated group values (12% for MHC_{16}-5-0.6, 24% for MHC_{16}-5-1.2 and 38% for MHC_{16}-6.5-2.5). In contrast, for MHC_{16}-5-4.1 with DS_{C16} relative to acrylate groups of 82%, the cac decreased to 0.02 mg/mL.

Table 2. The cac (mg/mL) calculated for mannan-C_{16} by fluorescence spectroscopy using NR and Py

	NR cac	Py cac
MHC_{16}-5-0.6	0.04	0.04
MHC_{16}-5-1.2	0.04	0.04
MHC_{16}-6.5-2.5	0.04	0.04
MHC_{16}-5-4.1	0.02	0.02

Size and shape of mannan-C_{16} nanogel

Cryo-FESEM is the most valuable technique in the visualization of the colloidal systems. Indeed, using this technique, the samples may be observed to be close to their natural state.[31] The mannan-C_{16} nanogel was heterogeneous in terms of both size and shape, as shown in Figure 5. The majority of macromolecular micelles observed may be described as imperfect spheres, with diameters ranging between 100 and 500 nm for MHC_{16}-5-1.2 and between 200 and 500 nm for MHC_{16}-6.5-2.5.

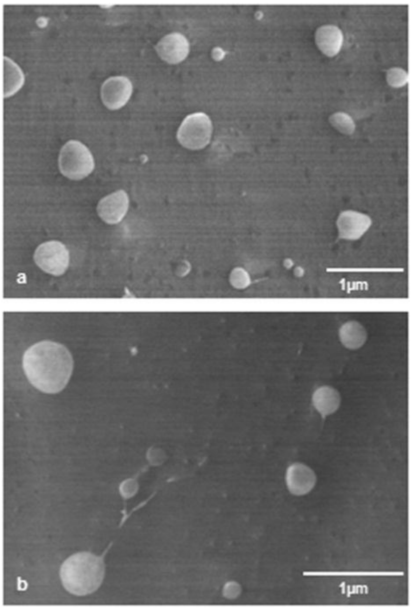

Figure 5. Cryo-FESEM negatively stained micrographs of mannan-C_{16} nanogel: (*a*) MHC_{16}-5-1.2 (magnification 15,000×) and (*b*) MHC_{16}-6.5-2.5 (magnification 30,000×).

Size and surface charge of mannan-C_{16} nanogel

The size and surface charge of mannan-C_{16} nanogel with different DS_{HEMA} and DS_{C16} were evaluated during storage and also in various environments as a function of pH and mannan-C_{16}, NaCl and urea concentrations by studying the variation of the mean hydrodynamic diameter and zeta potential obtained using DLS. The size and surface charge of the self-assembled particulate species play important roles in determining the stability in solution, the susceptibility to aggregate disassembly, coagulation and precipitation, and protein and cellular surface binding *in vivo*. Zeta potential values higher than 30 mV and lower than -30 mV are typical of colloids stabilized by electrostatic forces.

Storage

The size distribution of mannan-C_{16} nanogel with different DS values in ultrapure water was evaluated using DLS, over a storage period of six months, at room temperature (25 °C). The results are shown in Figure 6. Throughout the storage period, MHC_{16}-5-1.2 kept the mean hydrodynamic diameter stable, in the range of 108–234 nm; the MHC_{16}-6.5-2.5 size oscillated in the range of 218–429 nm. Both samples exhibited fairly high polydispersity, with an average PdI of 0.63. This result was consistent with the cryo-FESEM micrographs.

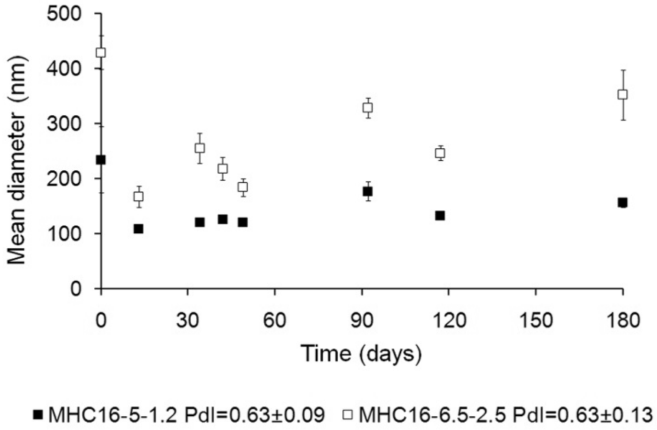

Figure 6. Size of mannan-C_{16} nanogel water dispersions (1 mg/mL) measured periodically in DLS (mean ± S.D., *n* = 10) over a storage period of six months at room temperature (25 °C).

Effect of the concentration of mannan-C_{16}

The micellar size is mainly determined by the hydrophobic forces that sequester the hydrophobic chains in the core and by the excluded volume repulsion between the chains that limits their size. The mean hydrodynamic diameter tended to be much larger for lower concentrations of mannan-C_{16}, and the material showed more instability. At 0.05 mg/mL, close to the cac, loose aggregates were formed that contained a significant quantity of solvent inside. For higher concentrations, the equilibrium favored nanogel formation.

Micelles adopt their low-energy-state configuration while the remaining solvent is gradually released from the hydrophobic core, resulting in a decrease in nanogel size.[32] These results are in agreement with the two types of hydrophobic environments with different hydration levels observed with NR and Py fluorescence. Amphiphilic mannan-C_{16} resulted in mannan being randomly substituted with hydrophobic alkyl chains. In randomly modified polymers, hydrophobic and hydrophilic parts are entangled together, which permits interaction between the core and the aqueous media. Exposed hydrophobic cores within a less mobile shell formed by hydrophilic chains may result in the secondary aggregation of polymeric micelles, which might explain the presence of large macromolecular micelles for lower concentrations of mannan-C_{16}.[32]

The zeta potential of mannan-C_{16} nanogel was apparently unaffected by the variation in concentration of mannan-C_{16} ranging between −8 mV and −26 mV, as shown in Figure 7. Thus, because the electrostatic forces are apparently not strong enough, the stability of the nanogel might be due to the hydration forces.

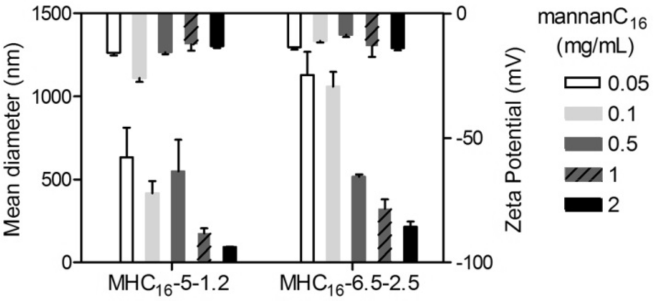

Figure 7. Influence of concentration on the size and zeta potential of mannan-C_{16} nanogel water dispersions (0.05–2 mg/mL) at 37 °C. The results shown were calculated by DLS (mean ± S.D., *n* = 3).

Effect of pH

The size distributions and zeta potential of mannan-C_{16} studied as a function of pH, using phosphate-citrate buffer (pH 2.2–8.0) were compared to values obtained in water and PBS (Figure 8). The mean hydrodynamic diameter values obtained for MHC$_{16}$-5-1.2 were larger in strong acidic solutions than in neutral, basic, and PBS solutions. The smallest size was observed at pH 6, although it was slightly larger than in water. The mean hydrodynamic diameter values for MHC$_{16}$-6.5-2.5 were smaller in pH 4 and 5 and PBS solutions; in other pH solutions, the nanogel presented a size as obtained in water yet with higher instability. For both materials, in all solutions, zeta potential values were found to be negative but still close to zero in the region of −2 mV to −13 mV. This is a relative small value indicating little repulsion between macromolecular micelles to prevent aggregation. However, even with the zeta potential close to zero in some environments, the nanogel is shown to be stable in nanoscale. The nearly neutral charge is valuable for *in vivo* use because large positive or negative charges may be rapidly cleared from the blood. Positively charged polymers and nanogels cause nonspecific cell sticking, while negatively charged polymers and nanogels are efficiently taken up by scavenger endothelial cells, or “professional pinocytes” found in liver.[33]

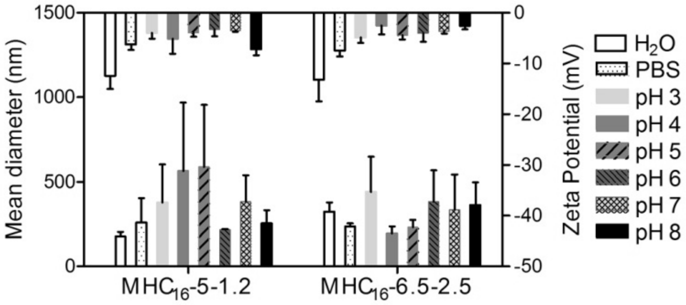

Figure 8. Influence of pH on size and zeta potential of mannan-C_{16} nanogel dispersions (1 mg/mL) at 37 ºC in water, PBS (pH 7.4) and phosphate-citrate buffer (pH 2.2–8.0). The results shown were calculated in DLS (mean ± S.D., *n* = 3).

Effect of ionic strength

Salts are known to have the ability to destabilize colloidal systems by removing the electrostatic barrier that prevents micelle aggregation. When added in enough quantity to a stable dispersion, salts may neutralize the surface charge of the macromolecular micelles, which removes the repulsive forces that keep micelles separate and allows for coagulation due to van der Waals forces. Compared to that in salt-free solution, the mean hydrodynamic diameter for MHC_{16}-5-1.2 decreased when the NaCl concentration was 0.3 and 0.6 M. A slight instability was observed for MHC_{16}-6.5-2.5 because the mean hydrodynamic diameter decreased when the NaCl concentration was between 0.1 and 0.3 M but leveled off when a higher concentration of NaCl (0.6 M) was applied, as shown in Figure 9. No flocculation was observed. The results obtained showed that NaCl, at tested concentrations, was not able to destabilize the size of mannan-C_{16} colloidal system.

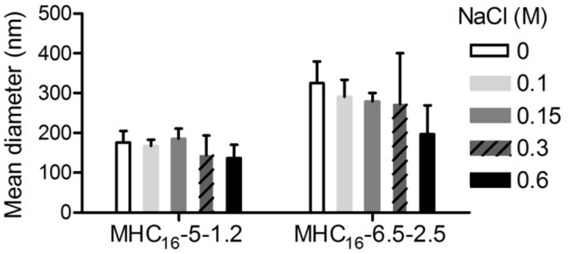

Figure 9. Influence of NaCl on the size of mannan-C_{16} nanogel dispersions (1 mg/mL) at 37 °C in NaCl solution (0–0.6 M). The results shown were calculated in DLS (mean ± S.D., *n* = 3).

Although the Derjaguin-Landau-Verwey-Overbeek (DLVO) theory effectively explains the long-range interaction forces observed in a large number of systems, when two surfaces or micelles are a few nanometers apart, the interactions between two solid surfaces in a liquid medium fail to be accounted for and can be much stronger. The other additional non-DLVO forces, such as the solvation force, hydrophobic force, or steric force, can be monotonically repulsive, monotonically attractive, or even oscillatory. The solvation forces referred to as hydration forces, when the solvent is water, depend both on the chemical and physical properties of the surfaces (e.g., wettability, crystal structure, surface morphology, and rigidity) and on the properties of the intervenient medium.[34] The physical mechanisms underlying the hydration force might be the anomalous polarization of water near the interfaces, which completely alters its dielectric response. Instead, the repulsive forces might be due to the entropic (osmotic) repulsion of thermally excited molecular groups that protrude from the surfaces, which explains many experimental observations in neutral systems.[34] The observed stability of the nanogel (no aggregation or flocculation is observed) with increasing in ionic strength thus suggests that non-DLVO forces are relevant to the colloidal behavior of this nanogel. Besides hydration forces, steric effects, which play a role whenever a reduction in the degree of freedom of the molecules in interacting colloids contributes to the stabilization of those colloids, may also be relevant in the present case.

Effect of urea

Urea has been described as being able to break intramolecular hydrogen bonds and to destabilize hydrophobic domains.[35, 36] The mean hydrodynamic diameter obtained for MHC_{16}-5-1.2 in water (176 nm) was similar to that obtained in urea 5 M, larger than that in 1 M and 3 M urea, and smaller than that in 7 M urea (214 nm). A stronger variability was observed for MHC_{16}-6.5-2.5 because the mean hydrodynamic diameter was smaller than in water (325 nm) for urea at concentrations between 1 and 5 M and significantly larger for urea at 7 M (519 nm), as shown in Figure 10. Although this changeability in the experimental results, urea did not significantly affect the self-assembly of the studied amphiphilic system in water and consequently nanogel formation.

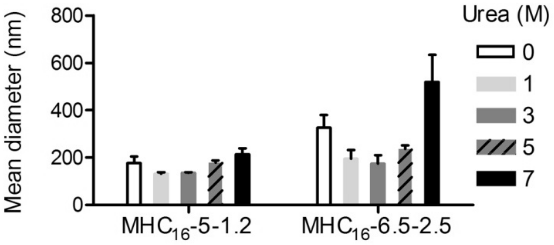

Figure 10. Influence of urea on size of mannan-C_{16} nanogel dispersions (1 mg/mL) at 37 °C in urea solution (0–7 M). The results shown were calculated in DLS (mean ± S.D., *n* = 3).

The nanogels have been developed as a key strategy to deliver conventional drugs, recombinant proteins, vaccines, and nucleotides transforming their kinetics, body distribution, and bioavailability. Nanoformulations will require controllable features, such as dimension (diameter < 200 nm), nearly neutral surface charge, stability for prolonged circulation in blood, nontoxicity to cells, proper degradability (to modulate the release of encapsulated biomolecules and to enable the removal of an empty device after drug release from the body), bioconjugation to targeted cells, high-loading efficiency, and controllable release of encapsulated therapeutics, reducing undesired side effects.[37-40]

The low cac values of mannan-C_{16} indicate the thermodynamic stability of self-aggregates under dilute conditions. The cac might be further reduced by increasing the hydrophobicity, augmenting $DS_{C16.}$ Because polymeric micelles suffer dilution upon intravenous administration (usually about a 25-fold dilution for a bolus injection or a much higher dilution at infusion), this low cac is advantageous as to maintain the micellar structure that facilitates prolonged circulation in the bloodstream.[41, 42] All polymers are characterized by a concentration window suitable for each delivery application because bellow cac the micelles may be destroyed early, releasing the encapsulated therapeutic molecule before attaining its target, and because above a critical value micelle aggregation and precipitation might occur.[42, 43]

Supramolecular self-assembled mannan-C_{16} might be useful in designing polymeric multifunctional nanocarriers (e.g., nanotheranostics, i.e., complementation of diagnostic tools with therapeutic modalities) because it bears functional groups for modification purposes, has adjustable chemical and mechanical properties, undergoes size alteration in a controlled manner depending on the DS of the amphiphile, and has a high water content.

Those nanogels have interior network for the possible incorporation of hydrophobic therapeutics, physically protecting them, by hydrophilic polymer chains, from degradation *in vivo*. The nanoencapsulation and controllable release of therapeutics will simplify their delivery or enhance their efficacy because therapeutics become more stable, or active, and are more efficiently delivered to targeted cells.

The mannan-C_{16} nanogel has a large surface area and functional groups for potential multivalent bioconjugation. The conjugation with cell-targeting ligands recognizing specific cellular receptors, in attempting to mimic endogenous immunoglobulins, is an approach for efficient systemic active targeted delivery to specific cells of encapsulated biological agents and drugs. As a polymer of mannose, mannan-C_{16} potentially targets the mannose receptor and possibly will activate professional APC. Cell-surface-bound receptors represent suitable attractive entry sites for delivery into cells by the receptor-mediated endocytosis of specific drugs, genes, or antigens conjugated with macromolecules or supramolecular structures.[19] Mannan-C_{16} originates imperfect spheres, and spherical particles are subject to more efficient phagocytosis than ellipsoid or disk-shaped ones, being captured by macrophages.[38] Therefore, this novel nanogel has the potential to serve as a universal protein-based vaccine adjuvant and carrier capable of inducing strong immune responses.

Further work is required to continue characterizing mannan-C_{16} nanogel and its potential as a multifunctional nanocarrier for biomedical applications.

Conclusions

The synthesis method used for amphiphilic mannan-C_{16} was showed to be versatile, simple, and reproducible. Above the cac, mannan-C_{16} formed nanosized aggregates under aqueous conditions by the association of the hydrophobic alkyl chains. The cac, determined by fluorescence spectroscopy with NR and Py, was consistent and dependent on the obtained DS_{C16} relative to methacrylated groups, ranging between 0.02 and 0.04 mg/mL. Cryo-FESEM revealed heterogeneous mannan-C_{16} macromolecular micelles to be similar to imperfect spheres with different diameters ranging from 100 nm to 500 nm. Mannan-C_{16} with higher DS_{HEMA} and DS_{C16} values presented larger values of the mean hydrodynamic diameter, in which oscillations denoted some instability during six months of storage at room temperature (25 °C). The mean hydrodynamic diameter tended to be much larger as the concentration decreased to close to the cac. For both materials, the size distribution varied on the nanoscale at different pH values. The effects of salt and urea were stronger for the highest concentrations tested and more marked for mannan-C_{16} with higher DS_{HEMA} and DS_{C16} but without avoiding nanogel formation and size stability. The mannan-C_{16} nanogel under tested conditions was always negatively charged with a zeta potential close to zero.

Further work is required to clarify and optimize the characteristics of these multifunctional nanogels made of mannan as a water-soluble delivery system for drugs or peptides and proteins acting, for example, like antigens or antibodies, as new strategies to target certain disease sites and thus increase the therapeutic benefit while minimizing side effects.

References

1. Whitesides, G. M.; Mathias, J. P.; Seto, C. T. Molecular self-assembly and nanochemistry: a chemical strategy for the synthesis of nanostructures. *Science* **1991**, 254, 1312-1319.

2. Whitesides, G. M.; Grzybowski, B. Self-assembly at all scales. *Science* **2002**, 295, 2418-2421.

3. Halley, J. D.; Winkler, D. A. Consistent concepts of self-organization and self-assembly. *Complexity* **2008**, 14, 10-17.

4. Whitesides, G. M.; Boncheva, M. Beyond molecules: self-assembly of mesoscopic and macroscopic components. *Proc Natl Acad Sci USA* **2002**, 99, 4769-4774.

5. Huie, J. C. Guided molecular self-assembly: a review of recent efforts. *Smart Mater Struct* **2003**, 12, 264-271.

6. Torchilin, V. P. Multifunctional nanocarriers. *Adv Drug Delivery Rev* **2006**, 58, 1532-1555.

7. Park, J. H.; Kwon, S. G.; Nam, J. O.; Park, R. W.; Chung, H.; Seo, S. B.; Kim, I. S.; Kwon, I. C.; Jeong, S. Y. Self-assembled nanoparticles based on glycol chitosan bearing 5 beta-cholanic acid for RGD peptide delivery. *J Control Release* **2004**, 95, 579-588.

8. Hennink, W. E.; Talsma, H.; Borchert, J. C. H.; DeSmedt, S. C.; Demeester, J. Controlled release of proteins from dextran hydrogels. *J Control Release* **1996**, 39, 47-55.

9. Goncalves, C.; Martins, J. A.; Gama, F. M. Self-assembled nanoparticles of dextrin substituted with hexadecanethiol. *Biomacromolecules* **2007**, 8, 392-398.

10. Gu, X. G.; Schmitt, M.; Hiasa, A.; Nagata, Y.; Ikeda, H.; Sasaki, Y.; Akiyoshi, K.; Sunamoto, J.; Nakamura, H.; Kuribayashi, K.*, et al.* A novel hydrophobized polysaccharide/oncoprotein complex vaccine induces in vitro and in vivo cellular and humoral immune responses against HER2-expressing murine sarcomas. *Cancer Res* **1998**, 58, 3385-3390.

11. Tang, C. K.; Lodding, J.; Minigo, G.; Pouniotis, D. S.; Plebanski, M.; Scholzen, A.; McKenzie, I. F.; Pietersz, G. A.; Apostolopoulos, V. Mannan-mediated gene delivery for cancer immunotherapy. *Immunology* **2007**, 120, 325-335.

12. Akiyoshi, K.; Kobayashi, S.; Shichibe, S.; Mix, D.; Baudys, M.; Kim, S. W.; Sunamoto, J. Self-assembled hydrogel nanoparticle of cholesterol-bearing pullulan as a carrier of protein drugs: complexation and stabilization of insulin. *J Control Release* **1998**, 54, 313-320.

13. Na, K.; Bae, Y. H. Self-assembled hydrogel nanoparticles responsive to tumor extracellular pH from pullulan derivative/sulfonamide conjugate: characterization, aggregation, and adriamycin release in vitro. *Pharm Res* **2002**, 19, 681-688.

14. Choi, K. Y.; Min, K. H.; Na, J. H.; Choi, K.; Kim, K.; Park, J. H.; Kwon, I. C.; Jeong, S. Y. Self-assembled hyaluronic acid nanoparticles as a potential drug carrier for cancer therapy: synthesis, characterization, and in vivo biodistribution. *J Mater Chem* **2009**, 19, 4102-4107.

15. Coviello, T.; Matricardi, P.; Marianecci, C.; Alhaique, F. Polysaccharide hydrogels for modified release formulations. *J Control Release* **2007**, 119, 5-24.

16. Nakajima, T.; Ballou, C. E. Structure of the linkage region between the polysaccharide and protein parts of Saccharomyces cerevisiae mannan. *J Biol Chem* **1974**, 249, 7685-7694.

17. Apostolopoulos, V.; Pietersz, G. A.; Loveland, B. E.; Sandrin, M. S.; McKenzie, I. F. Oxidative/reductive conjugation of mannan to antigen selects for T1 or T2 immune responses. *Proc Natl Acad Sci USA* **1995**, 92, 10128-10132.

18. Sihorkar, V.; Vyas, S. P. Potential of polysaccharide anchored liposomes in drug delivery, targeting and immunization. *J Pharm Pharm Sci* **2001**, 4, 138-158.

19. Gupta, A.; Gupta, R. K.; Gupta, G. S. Targeting cells for drug and gene delivery: Emerging applications of mannans and mannan binding lectins. *J Sci Ind Res* **2009**, 68, 465-483.

20. Avrameas, A.; McIlroy, D.; Hosmalin, A.; Autran, B.; Debre, P.; Monsigny, M.; Roche, A. C.; Midoux, P. Expression of a mannose/fucose membrane lectin on human dendritic cells. *Eur J Immunol* **1996**, 26, 394-400.

21. Fukasawa, M.; Shimizu, Y.; Shikata, K.; Nakata, M.; Sakakibara, R.; Yamamoto, N.; Hatanaka, M.; Mizuochi, T. Liposome oligomannose-coated with neoglycolipid, a new candidate for a safe adjuvant for induction of CD8+ cytotoxic T lymphocytes. *FEBS Lett* **1998**, 441, 353-356.

22. Apostolopoulos, V.; McKenzie, I. F. Role of the mannose receptor in the immune response. *Curr Mol Med* **2001**, 1, 469-474.

23. vanDijkWolthuis, W. N. E.; Tsang, S. K. Y.; KettenesvandenBosch, J. J.; Hennink, W. E. A new class of polymerizable dextrans with hydrolyzable groups: hydroxyethyl methacrylated dextran with and without oligolactate spacer. *Polymer* **1997**, 38, 6235-6242.

24. Dubois, M.; Gilles, K. A.; Hamilton, J. K.; Rebers, P. A.; Smith, F. Colorimetric method for determination of sugars and related substances. *Anal Chem* **1956**, 28, 350-356.

25. Arigita, C.; van den Berg, J.; Wensink, K.; van Steenbergen, M.; Hennink, W. E.; Crommelin, D. J. A.; Kersten, G. F. A.; Jiskoot, W. Immunogenicity of meningococcal PorA formulations encapsulated in biodegradable microspheres. *Eur J Pharm Sci* **2004**, 21, 131-141.

26. Kath, F.; Kulicke, W. M. Polymer analytical characterization of glucan and mannan from yeast Saccharomyces cerevisiae. *Appl Macromol Chem Phys* **1999**, 268, 69-80.

27. Hrkach, J. S.; Peracchia, M. T.; Domb, A.; Lotan, N.; Langer, R. Nanotechnology for biomaterials engineering: Structural characterization of amphiphilic polymeric nanoparticles by H-1 NMR spectroscopy. *Biomaterials* **1997**, 18, 27-30.

28. Coutinho, P. J. G.; Castanheira, E. M. S.; Rei, M. C.; Oliveira, M. E. C. D. R. Nile red and DCM fluorescence Anisotropy studies in C12E7/DPPC mixed systems. *J Phys Chem B* **2002**, 106, 12841-12846.

29. Kalyanasundaram, K.; Thomas, J. K. Environmental Effects on Vibronic Band Intensities in Pyrene Monomer Fluorescence and Their Application in Studies of Micellar Systems. *J Am Chem Soc* **1977**, 99, 2039-2044.

30. Dong, D. C.; Winnik, M. A. The Py scale of solvent polarities. *Can J Chem* **1984**, 62, 2560-2565.

31. Krauel, K.; Girvan, L.; Hook, S.; Rades, T. Characterisation of colloidal drug delivery systems from the naked eye to Cryo-FESEM. *Micron* **2007**, 38, 796-803.

32. Jones, M. C.; Leroux, J. C. Polymeric micelles - a new generation of colloidal drug carriers. *Eur J Pharm Biopharm* **1999**, 48, 101-111.

33. Smedsrod, B. Clearance function of scavenger endothelial cells. *Comp Hepatol* **2004**, 3 Suppl 1, S22.

34. Liang, Y.; Hilal, N.; Langston, P.; Starov, V. Interaction forces between colloidal particles in liquid: Theory and experiment. *Adv Colloid Interface Sci* **2007**, 134-135, 151-166.

35. Mukerjee, P.; Ray, A. Effect of urea on micelle formation and hydrophobic bonding. *J Phys Chem* **1963**, 67, 190-192.

36. Moore, D. R.; Mathias, L. J. Molecular composites *via* insitu polymerization - poly(phenylene terephthalamide)-nylon 3. *J Appl Polym Sci* **1986**, 32, 6299-6315.

37. Hamidi, M.; Azadi, A.; Rafiei, P. Hydrogel nanoparticles in drug delivery. *Adv Drug Delivery Rev* **2008**, 60, 1638-1649.

38. Oh, J. K.; Lee, D. I.; Park, J. M. Biopolymer-based microgels/nanogels for drug delivery applications. *Prog Polym Sci* **2009**, 34, 1261-1282.

39. Vinogradov, S. V. Nanogels in the race for drug delivery. *Nanomedicine* **2010**, 5, 165-168.

40. Kabanov, A. V.; Vinogradov, S. V. Nanogels as Pharmaceutical Carriers: Finite Networks of Infinite Capabilities. *Angew Chem Int Ed* **2009**, 48, 5418-5429.

41. Lee, K. Y.; Jo, W. H.; Kwon, I. C.; Kim, Y.-H.; Jeong, S. Y. Physicochemical characteristics of self-aggregates of hydrophobically modified chitosans. *Langmuir* **1998**, 14, 2329-2332.

42. Rapoport, N. Physical stimuli-responsive polymeric micelles for anti-cancer drug delivery. *Prog Polym Sci* **2007**, 32, 962-990.

43. Rijcken, C. J. F.; Soga, O.; Hennink, W. E.; van Nostrum, C. F. Triggered destabilisation of polymeric micelles and vesicles by changing polymers polarity: An attractive tool for drug delivery. *J Control Release* **2007**, 120, 131-148.

Chapter 4

Supramolecular assembled nanogel made of mannan

The supramolecular assembly of amphiphilic mannan, synthesized by the Michael addition of hydrophobic 1-hexadecanethiol to vinyl methacrylated mannan, originates in aqueous medium the formation of a nanogel, stabilized by hydrophobic interactions among alkyl chains. The critical aggregation concentration, calculated by fluorescence spectroscopy ranged between 0.002 and 0.01 mg/mL, depending on the polymer degree of substitution. The cryo-field emission scanning electron microscopy showed spherical macromolecular micelles with diameters between 100 and 500 nm. The dynamic light scattering analysis revealed a polydisperse colloidal system, with mean hydrodynamic diameter between 50 and 140 nm, depending on the polymer degree of substitution. The nanogel is negatively charged, stable over a six months storage period, and stable at pH 3–8, salt or urea solutions. Bovine serum albumin and curcumin were spontaneously incorporated in the nanogel, being stabilized by the hydrophobic domains, opening the possibility for future applications as potential delivery systems for therapeutic molecules. *In vitro* assays were carried out to characterize the cytocompatibility of the nanogel. A toxic effect of mannan-C_{16} was observed, specific to mouse macrophage-like cell line J774, not affecting mouse embryo fibroblast cell line 3T3 viability.

Adapted from: *J Colloid Interface Sci* **2011**, 361, 97-108.

Introduction

Amphiphilic polymers, over critical micellar concentration (cmc) or critical aggregation concentration (cac), are capable of self-assembling in water mainly through intra- and/or intermolecular hydrophobic interactions.[1, 2] The resulting nanometer-sized polymeric hydrogels, i.e. nanogels – also called macromolecular micelles – have simultaneously characteristics of nanoparticles and hydrogels, being highly porous and hydrated. They are able to entrap biomolecules and drugs within the polymer matrix and also easily respond to external stimulus.[3-5] These skills triggered a great interest regarding its biomedical applicability, namely as potential delivery systems.[6-8]

Mannan was selected, among other biodegradable and biocompatible polymers, because it is recognized by mannose receptors expressed in the surface of antigen-presenting cells (APC).[9-12] Mannose receptor has been described to be involved in mannose receptor-mediated phagocytosis and also was referred to take part in host defense, providing a linkage between innate and adaptive immunity.[12-15] Therefore, a nanogel made of mannan might not only be a promising vehicle for many pharmaceutical applications, such as the treatment of macrophage associated pathologies[16] but also a helpful adjuvant, suitable to induce a protective and long-lasting immune response to protein-based vaccines.[10, 17]

Yeast mannan, extracted from *Saccharomyces cerevisiae*, is a highly branched polysaccharide with α-(1→2)- and α-(1→3)-linked mono-, di-, and trimannopyranose side chains with phosphodiester-linked side chains (2.6 phosphorus in 100 mannopyranose units) attached to the backbone of α-(1→6)-linked mannopyranoses.[18]

In the present work, new amphiphilic mannan conjugates were designed. The properties of the resulting nanogel were characterized – structure, size, shape, surface charge, stability and the ability to entrap bovine serum albumin (BSA) and curcumin – by using hydrogen nuclear magnetic resonance (^{1}H NMR), fluorescence and ultraviolet-visible (UV-VIS) spectroscopy, cryo-field emission scanning electron microscopy (cryo-FESEM) and dynamic light scattering (DLS). Nanogel cytocompatibility was also tested with MTT cell proliferation assay using two cell lines, mouse embryo fibroblasts 3T3 and mouse macrophage-like J774. Confocal laser scanning microscopy (CLSM) studies were performed using the nanogel labeled with a fluorochrome probe.

Experimental

Materials

Organic and inorganic reagents of laboratory grade were purchased from Sigma and used without any further purification, unless otherwise stated. All cell culture products were of cell culture grade and purchased from Sigma, saving reported exceptions.

Synthesis of amphiphilic mannan

Methacrylated mannan (mannan-VMA) was synthesized by transesterification of mannan (from *S. cerevisiae*), with vinyl methacrylate (VMA), as described by Ferreira et al. (2002)[19] but without enzymes.[20] Briefly, mannan was dissolved in dry dimethyl sulfoxide (DMSO) at a concentration of 1.5% w/v, with different calculated amounts of VMA resulting in 2.5, 3 and 4.5 molar ratios of VMA to mannose residues. After stirring at 50 ºC for 2 days, the resulting mixture was dialyzed in regenerated cellulose tubular membranes (Membrane Filtration Products; molecular weight cut-off (MWCO), 12,000–14,000) for 3 days against frequently changed distilled water, at room temperature (~ 25 ºC). Each sample of modified mannan after being lyophilized resulted as a pallid-yellow and fluffy product. Finally, the amphiphilic molecules mannan-VMA-SC_{16} (mannan-C_{16}) were produced as described elsewhere.[21] In brief, mannan-VMA and C_{16} at 1.2, 2 and 3 molar ratios of 1-hexadecanethiol (C_{16}) to VMA were mixed in dry DMSO (equivalent VMA = 0.03 M). The reaction was catalyzed by triethylamine (TEA) in a 2 molar ratio of TEA to VMA. After stirring for 3.5 days at 50 ºC, the resulting mixture was dialyzed and lyophilized as described above.

Characterization of mannan-C_{16} nanogel

^{1}H NMR spectroscopy

Lyophilized reaction products were dispersed in deuterium oxide (D_2O), in DMSO-d_6 and in 10% D_2O in DMSO-d_6 (5 mg/mL), stirring overnight at 50 ºC. 1D ^{1}H NMR measurements were performed with a Varian Unity Plus 300 spectrometer as previously described.[22]

Fluorescence spectroscopy

The cac of mannan-C_{16} was fluorometrically investigated using hydrophobic guest molecules such as 9-(diethylamino)-5H-benzo[α]phenoxazin-5-one (Nile red, NR) and pyrene (Py). Py was purified by appropriate recrystallization from absolute ethanol. The fluorescence intensity change of these guest molecules was calculated as a function of the mannan-C_{16} concentration using Spex Fluorolog 3 spectrofluorimeter as previously described.[22] The cac was calculated using both the maximum emission intensity of NR (λ_{ex} 570 nm) and the Py fluorescence intensity ratio of the third (384–385 nm) and first vibrational bands (372–374 nm) (I_3/I_1) of the emission spectra (λ_{ex} 339 nm) in the mannan-C_{16}/water system as a function of mannan-C_{16} concentration; in both cases, the cac was estimated as the interception of two trend lines.

Preparation of mannan-C_{16} colloidal dispersion

Each colloidal dispersion of mannan-C_{16} was prepared stirring the lyophilized mannan-C_{16} in ultrapure water (purified with a Milli-Q system, Millipore) for 3–5 days at 50 °C followed by filtration (pore size 0.45 μm), with insignificant material lost, as confirmed with the phenol-sulfuric acid method, using mannose as standard.[23] The viscosity of the resultant nanogel colloidal dispersion is similar to that of the solvent.

Cryo-FESEM

The mannan-C_{16} nanogel concentrated by ultrafiltration (Amicon Ultra-4 Centrifugal Filter Units, MWCO, 1×10^5) was negatively stained with phosphotungstic acid (Riedel-de Haën; 0.01% w/v). Samples were studied using an electronic microscope (SEM/EDS: FESEM JEOL JSM6301F/Oxford Inca Energy 350) as previously described.[22]

DLS

The size distribution and zeta potential measurements were performed in a Malvern Zetasizer NANO ZS (Malvern Instruments Limited, U.K.) as previously described.[22]

Complexation of mannan-C_{16} nanogel with a hydrophobic drug

Curcumin is rather water insoluble and forms yellow aggregates of curcumin powder (negative control) but soluble in absolute ethanol (AppliChem) forming a bright yellow solution (positive control). A volume of 10 μL of a 1 mg/mL curcumin stock solution in absolute ethanol was added to 1 mL of each sample – water, ethanol and mannan-C_{16} colloidal dispersions (1 mg/mL; prepared as describe above) – giving a constant curcumin concentration of 0.01 mg/mL and a final concentration of ethanol equal to 1%. After 24 h of incubation at 25 ºC, the resultant samples were centrifuged at 13,000 rpm (SIGMA 113 centrifuge), for 10 min, to remove the insoluble curcumin, and the UV-Vis absorption spectra of each clear supernatant were recorded on a JASCO V560. Mannan-C_{16} nanogel complexation with curcumin allowed it to be soluble originating a yellowish dispersion with maximum absorbance at 428 nm.

Complexation of mannan-C_{16} nanogel with a water-soluble protein

The mannan-C_{16} nanogel was also evaluated as potential host for BSA, as a model protein readily soluble in water, using an ultrafiltration method (Amicon® Ultra-4 Centrifugal Filter Units; MWCO, 1×10^5). The study was done comparing the results obtained with a BSA water solution (1 mg/mL), mannan water solution (1 mg/mL), mannan-C_{16} colloidal dispersion (1 mg/mL), prepared as described above, alone or mixed with BSA (1 mg/mL) in water after 24 h of incubation at 25 ºC. For all samples fractionated, both in concentrate and in filtrate, the concentration of polysaccharide was determined by the phenol-sulfuric acid method, using mannose as standard,[23] while that of BSA concentration was determined with Pierce® bicinchoninic acid (BCA) Protein assay method.

Cytocompatibility of mannan-C_{16} nanogel

Cell culture

Mouse embryo fibroblast cell line 3T3 (ATCC CCL-164) was grown in Dulbecco's modified Eagle's media (DMEM; 4.5 g/L glucose) supplemented with 10% newborn calf serum (Invitrogen, UK), 100 IU/mL penicillin and 0.1 mg/mL streptomycin at 37 °C in a 95% humidified air containing 5% CO_2. At confluence, 3T3 fibroblasts were harvested with 0.05% (w/v) trypsin-EDTA, adjusted to the required concentration of viable cells – determined by using the trypan blue exclusion assay, indicative of plasma membrane integrity – and were subcultivated in the same medium.

The mouse macrophage-like cell line J774 (ATCC TIB-67) was maintained as an adherent culture at 37 °C in a 95% humidified air containing 5% CO_2 in DMEM (4.5 g/L glucose) supplemented with 10% heat-inactivated fetal bovine serum (Invitrogen, UK), 2 mM L-glutamine, 1 mM sodium pyruvate, 100 IU/mL penicillin and 0.1 mg/mL streptomycin. At confluence, macrophages were detached mechanically, adjusted to the required concentration of viable cells using the trypan blue exclusion assay as above and subcultivated in the same medium.

Cytotoxicity test

The cytotoxicity of mannan-C_{16} nanogel was evaluated *in vitro* using the 3-(4,5-dimethylthiazol-2-yl)-2,5-diphenyltetrazolium bromide (MTT) cell proliferation assay,[24] a colorimetric assay that measures the reduction of a tetrazolium component (MTT) into an insoluble formazan product at the mitochondria of viable cells, by the succinate-tetrazolium reductase. 3T3 fibroblasts (2×10^4 cells/well) and J774 macrophages (5×10^4 cells/well) were plated into 24-well tissue culture plates (Orange) and incubated 5 h at 37 °C in a 95% humidified air containing 5% CO_2. Sterile stock colloidal dispersions of mannan-C_{16} with different DS_{C16}, MVC_{16}-25-11 or MVC_{16}-25-22, were prepared in PBS, as described above, followed by filtration (pore size 0.22 μm). Serial dilutions were prepared in sterile PBS and final sample concentration was adjusted diluting five times with culture medium. Then nanogel, at different concentrations, was incubated with cells, for 24 or 48 h. MTT was added to the culture medium to a final concentration of 0.5 mg/mL. After 3 h of incubation at 37 ºC, the culture medium was carefully removed and the formazan crystals were solubilized with DMSO, and the UV absorbance was measured at 570 and 690 nm in an automated ELISA plate reader. For each sample, the background optical density (690 nm) was subtracted. Cell proliferation and viability was also followed by regular light microscope (LEICA) observations. The results expressed in viability (%) were compared to a control prepared with the same cell culture medium without the addition of nanogel, which viability was normalized to 100%. The results shown are from one experiment, representative of three independent experiments performed in triplicate.

Mannan-C_{16} labeled with SAMSA fluorescein

Synthesis of mannan-C_{16} labeled with 5-((2-(and-3)-*S*-(acetylmercapto)succinoyl)amino) fluorescein (SAMSA fluorescein; Molecular Probes, Invitrogen) was based on the reaction between the thiol group of SAMSA fluorescein with the grafted methacrylate not substituted with C_{16} of mannan-C_{16}. The reaction was performed after optimizing the instructions from the manufacturer. Briefly, SAMSA fluorescein (4 mg) was dissolved in 400 μL of 0.1 M NaOH and incubated at room temperature for 15 min in order to remove acetyl protecting group. Finally the reaction product was neutralized with concentrated HCl, buffered with 0.5 M sodium phosphate, pH 7 and stirred for 10 min. Resulting activated SAMSA fluorescein was conjugated with 2.5 mL of mannan-C_{16} (MVC_{16}-31-20) colloidal dispersion in 0.1 M sodium phosphate buffer, pH 7 (3 mg/mL) prepared as describe above. The conjugation occurred after stirring in the presence of TEA (2 equimolar of VMA) for 48 h at 50 ºC. The unreacted dye was separated from the labeled mannan-C_{16} applying 2.5 mL of reaction medium (after filtration using a membrane with pore size 0.45 µm) on a Sephadex® G-25 gel filtration column (Amersham Biosciences) equilibrated with PBS. Labeled nanogel was eluted with PBS and sterilized by filtration (pore size 0.22 µm) before use. To remove any eventual residual unconjugated fluorescein, labeled mannan-C_{16} was repeatedly washed by ultrafiltration (Amicon® Ultra-4 Centrifugal Filter Units, MWCO, 5×10^3) with sterile pyrogen-free PBS until no fluorescence was detected in the filtrate. The degree of labeling in the concentrate was determined from the absorbance of the labeled mannan-C_{16} at 495 nm. Labeling did not affect the properties of the nanogel, as estimated by DLS.

Confocal studies

For the CLSM 1×10^6 J774 cells were plated in Fluorodish (WPI, UK) in 1 mL of culture medium and incubated overnight at 37 °C in a 95% humidified air containing 5% CO_2. Live cells nuclei were labeled in blue fluorescent with 4'-6-Diamidino-2-phenylindole (DAPI; 0.05 mg/mL) for 3 min at room temperature in culture medium. After washing, cells were incubated for 20 min with 20 µM FM® 4-64 (Molecular Probes, Invitrogen) in culture medium. Membranes are intensely red-fluorescent labeled when FM® 4-64 inserts into the outer leaflet of the surface membrane. FM® 4-64 is frequently used in endocytosis and exocytosis studies in eukaryotic cells because it is water-soluble, nontoxic to cells and virtually nonfluorescent in aqueous media. Propidium iodide (PI; 1 µg/mL) was added to the medium to evaluate the viability of the cells. PI is membrane impermeant commonly used for identifying dead cells by emitting its characteristic red fluorescence in the nuclear region. PI binds to nucleic acids by intercalating between the bases with little or no sequence preference and with a stoichiometry of one dye per 4–5 base pairs of DNA. The plate was then placed on the stage of the confocal microscope (OLYMPUS FluoView CLSM - FV1000) at 37 °C and 5% CO_2. A representative area of the plate was selected at random and zero-time point picture was obtained. Mannan-C_{16} nanogel labeled with SAMSA fluorescein colloidal dispersion was then added into the medium on top of the region containing the selected area. Z-series and time-series in the three filter sequential scanning mode and differential interference contrast (DIC) images were obtained at three lasers 405 nm, 488 nm and 559 nm. All confocal images were obtained under identical scan settings and were analyzed with software OLYMPUS Fluoview1000 (FV viewer v.2.0). The results shown are from one experiment, representative of three independent experiments.

Statistical analysis

Statistical significance of the cell proliferation assay results obtained with each concentration of nanogels in comparison with the control at same incubation period was determined by one-way analysis of variance (ANOVA) with Dunnett's post-test using GraphPad Prism version 4.00 for Windows (GraphPad Software, California, USA).

Results and discussion

Synthesis of amphiphilic mannan-C_{16}

According to the literature and similarly to other reported methacrylates, VMA mainly couples to the ^{6}C of the mannose residues of the mannan side chains.[18, 25] Then by the Michael addition mechanism, the thiol acting as a nucleophile reacts with grafted methacrylate (Scheme 1).

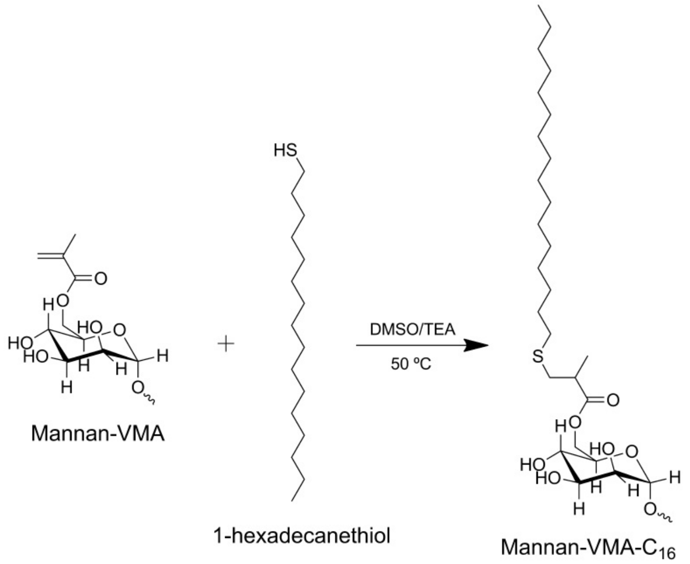

Scheme 1. Synthesis of mannan-C_{16}.

The success of the synthesis, purity, chemical structure and polymer degree of substitution of the reaction products were controlled using ^{1}H NMR spectra in D_2O (Figure 1). The mannan degree of substitution with methacrylate groups (DS_{VMA}, defined as the percentage of grafted VMA relative to the mannose residues), was calculated from the ^{1}H

NMR spectra of mannan-VMA in D_2O, using the equation $(I_a)/(I_{H1})\times100$, in which I_a is the average integral of the protons of the unsaturated carbons of the acrylate groups (detected around 6 ppm) and I_{H1} is the integral of the anomeric proton (4.9–5.5 ppm).[26, 27] The degree of substitution with the hydrophobic alkyl chains (DS_{C16}, defined as the percentage of grafted C_{16} moieties relative to the mannose residues), was calculated from the ^{1}H-NMR spectra of mannan-C_{16}, in D_2O as $(7X)/(37Y)\times100$, in which X is the average integral corresponding to the protons from the alkyl moieties (1.8–0.6 ppm) and Y is the integral of all mannan protons (3.5–5.5 ppm).[21, 27] After washing mannan-C_{16} with *n*-hexane, similar ^{1}H NMR spectra were obtained providing evidence that alkyl chains were covalently bound to the methacrylate groups (data not shown).

Different independent batches of mannan-C_{16} with different DS_{VMA} and DS_{C16} were produced, by varying the molar ratio of VMA to mannose residues and the molar ratio of C_{16} to VMA, proving the versatility, simplicity and reproducibility of the method, as shown in Table 1. In this work, all the batches of mannan-C_{16} were named as MVC_{16}-DS_{VMA}-$DS_{C16.}$

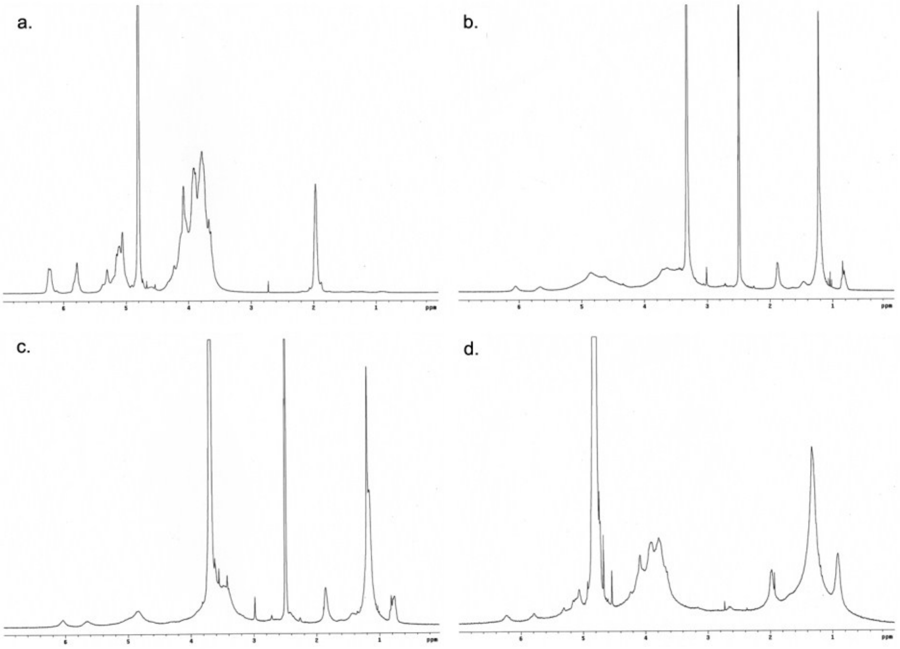

Figure 1. The ^{1}H NMR spectra of mannan-VMA (5 mg/mL) in (*a*) D_2O and of mannan-C_{16} (5 mg/mL) in (*b*) DMSO-d_6, (*c*) 10% D_2O in DMSO-d_6, and (*d*) D_2O for MVC_{16}-29-15 as an example.

Table 1. Characteristics of mannan-C_{16}

$t\mathrm{DS}_{\mathrm{VMA}}$ [a]	$\mathrm{DS}_{\mathrm{VMA}}$ [b]	$t\mathrm{DS}_{\mathrm{C16}}$ [c]	$\mathrm{DS}_{\mathrm{C16}}$ [d]	$\mathrm{DS}_{\mathrm{C16}}/\mathrm{DS}_{\mathrm{VMA}}$ [e]
250	20–26	120	5–12	25–46
		200	8–15	40–58
		300	11–25	55–96
300	20–29	120	8–15	40–52
		200	11–18	55–62
		300	16–28	80–97
450	25–31	120	11–20	44–65
		200	15–26	60–84
		300	22–30	88–97

[a] Theoretical $\mathrm{DS}_{\mathrm{VMA}}$ calculated as the molar ratio of VMA to mannose residue (×100) in the reaction mixture. [b] calculated by ^{1}H NMR of mannan-VMA. [c] theoretical $\mathrm{DS}_{\mathrm{C16}}$ calculated as the molar ratio of C_{16} to VMA (×100) in the reaction mixture. [d] calculated by ^{1}H NMR of mannan-C_{16}. [e] obtained $\mathrm{DS}_{\mathrm{C16}}$ relative to methacrylated groups calculated using the following equation: real $\mathrm{DS}_{\mathrm{C16}}$/real $\mathrm{DS}_{\mathrm{VMA}}$ (×100). The table presents the range of values (%) obtained for different batches using each set of conditions.

Supramolecular assembly of mannan-C_{16}

The supramolecular assembly of amphiphilic mannan-C_{16} in water was studied using ^{1}H NMR and fluorescence spectroscopy.

Analyzing the ^{1}H NMR spectra of mannan-C_{16} (Figure 1), it can be observed that, while the mobility of the polysaccharide skeleton was maintained in environments of different polarity, the shape and width of the proton signals of the methyl (0.8 ppm) and methylene (1.1 ppm) groups of C_{16} depended on the polarity of the solvent used. In DMSO, mannan-C_{16} was soluble, and the C_{16} signals were sharp, as all hydrophobic chains were exposed to the solvent, having the same mobility.[21] The same signals tended to be gradually broadened at the base with an increase in the D_2O content in DMSO-d_6. A large broadening was clear in pure D_2O, which is characteristic of the superposition of peaks representing a collection of chemically identical species, yet possessing various degrees of mobility.[28] These results tip-off that mannan-C_{16} dispersed in water has part of the alkyl chains exposed to hydrophobic domains, while others might have been exposed to the hydrophilic solvent. Differences in the microenvironment and/or mobility of the molecules thus explain the broaden peak observed for the aliphatic protons. Therefore mannan-C_{16} nanogel is obtained upon supramolecular assembly in water as result of the association of the hydrophobic alkyl chains in hydrophobic domains.

The cac of mannan-C_{16} with different DS was studied by fluorescence spectroscopy using hydrophobic dyes, NR[29] and Py.[30, 31] Although weakly soluble and fluorescent in water their solubility and fluorescence boost in hydrophobic environments.

For lower concentrations of amphiphilic mannan-C_{16}, individual molecules exist as premicelles in aqueous environment and the fluorescence intensity of NR remained constant, without any shift in the maximum emission wavelength (Figure 2; zone A). Exceeding cac, fluorescence intensity augmented with a simultaneous blue-shift of the maximum emission wavelength, which was caused by the proximity of NR to the hydrophobic domains of the nanogel. The mannan-C_{16} hydrophobic domains are dissimilar of those present in a typical surfactant system and have two types of hydration levels (Figure 2; zones B and C).

The intensity of Py increased for greater concentrations of mannan-C_{16} and a red shift occurred in the excitation spectra (Figure 3a). The intensity ratio I_3/I_1 rapidly augmented above the cac (Figure 3b). This transition of intensity decode the transference of Py to a less polar and hydrophobic domains, which is coincident with the onset of supramolecular assembly of mannan-C_{16} nanogel. Above cac some bands in the 450 nm region associated to the presence of Py dimers occurred, suggesting themselves the high water penetration into the nanogel, which is in agreement with the ^1H NMR measurements.

As mannan-C_{16} concentration augments above the cac, more hydrophobic domains are formed, solubilizing more NR and Py, which consequently increases the fluorescence detected. The typically observed second plateau was not attained (Figures 2b and 3b) and two hypotheses might be pointed out to explain this result: the highest concentration of mannan-C_{16} used was not enough to enclose all of the hydrophobic dyes available; or the NR or Py molecules, although enclosed in the hydrophobic domains continued to redistribute to those with lower hydration levels, Py forming dimers in the hydrophobic domains with greater hydration level.

The resultant cac values of fluorescence spectroscopy measurements using both dyes, NR and Py, showed dependency on the obtained DS_{C16} relative to methacrylated groups (DS_{C16}/DS_{VMA}), which confirms that C_{16} governs the self-assembly of mannan-C_{16} in water. The cac was 0.002 mg/mL for DS_{C16}/DS_{VMA} values close to 80% (80% for MVC_{16}-20-16 and 88% for MVC_{16}-25-22) but increased to 0.01 mg/mL for lower DS_{C16}/DS_{VMA} (40% for MVC_{16}-20-8, 46% for MVC_{16}-26-12 and 62% for MVC_{16}-29-18).

The low cac values of mannan-C_{16} point out the thermodynamic stability of nanogel in diluted environments, such as when diluted upon intravenous administration (usually about 25-fold dilution at bolus injection or a much higher dilution at infusion) being able to maintain its structure that facilitates prolonged circulation in the bloodstream until attaining its target.[32, 33]

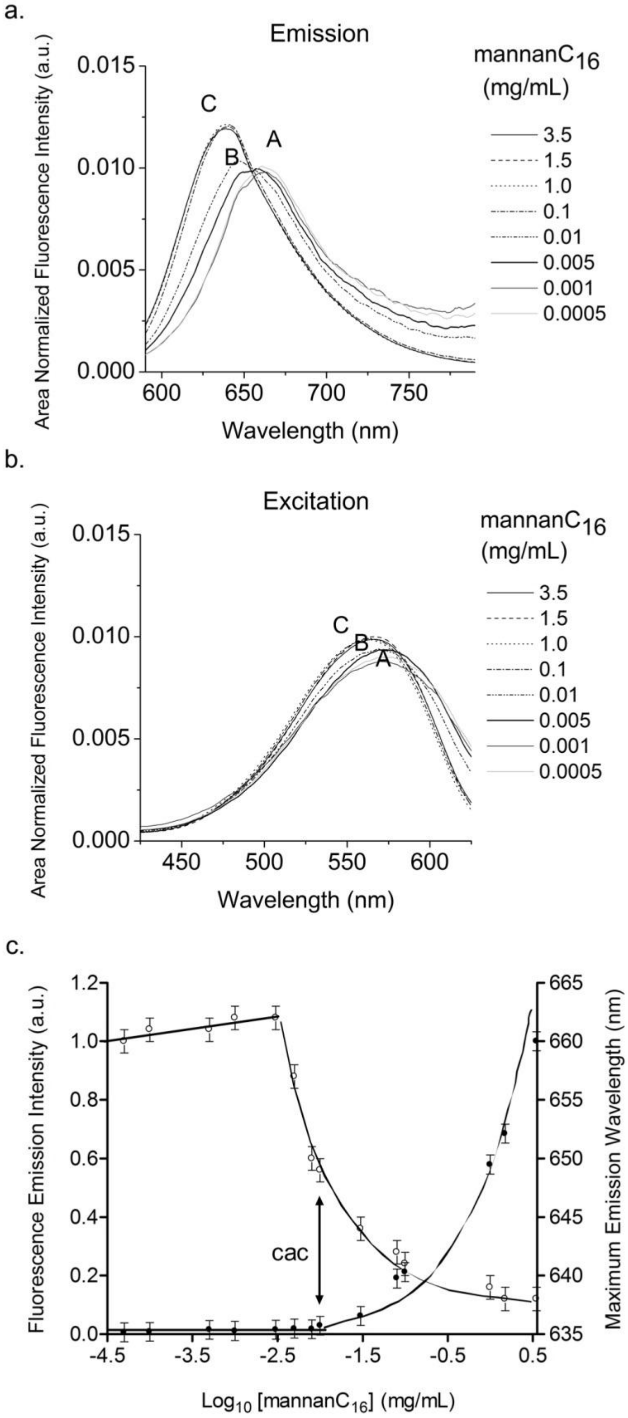

Figure 2. Determination of the cac of mannan-C_{16} using NR fluorescence: area normalized fluorescence (*a*) excitation (λ_{em} 650 nm) and (*b*) emission (λ_{ex} 570 nm) spectra of NR (2×10^{-7} M) in the mannan-C_{16}/water system as a function of mannan-C_{16} concentration; (*c*) area-normalized fluorescence emission intensity (closed circle) and position of maximum emission wavelength (open circle) of NR in the mannan-C_{16}/water system as a function of mannan-C_{16} concentration (λ_{ex} 570 nm), using MVC$_{16}$-20-8 as an example.

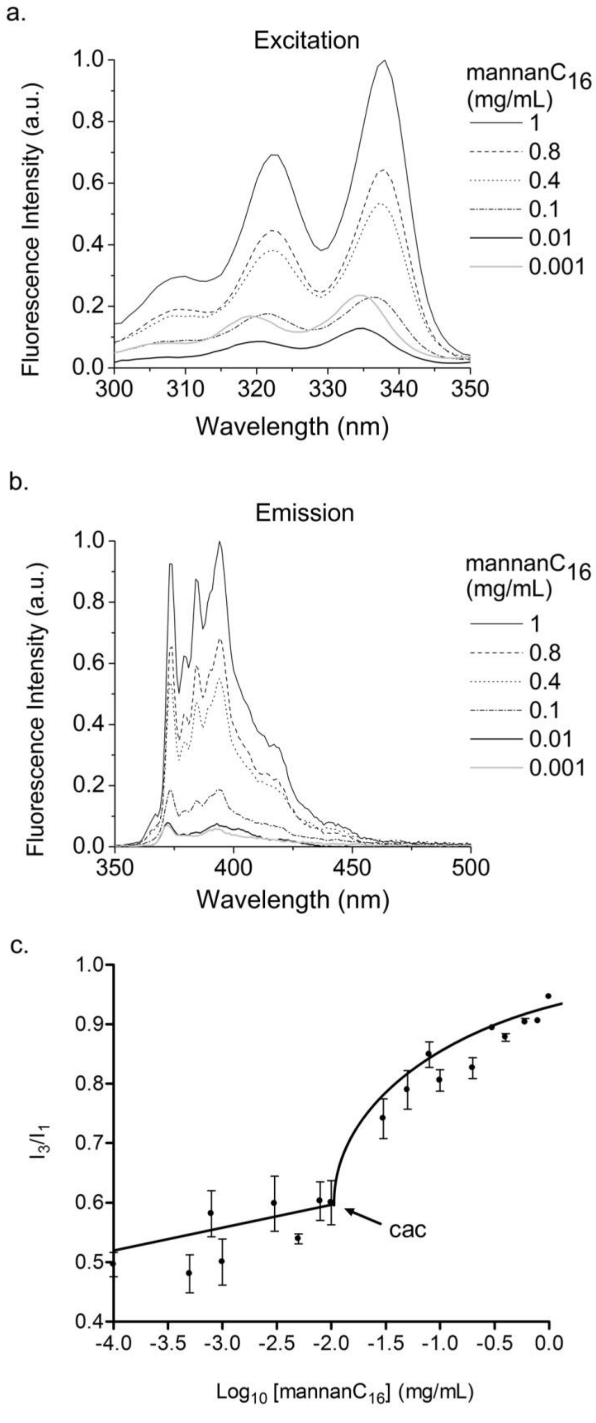

Figure 3. Determination of the cac of mannan-C_{16} using Py fluorescence: (*a*) excitation (λ_{em} 390 nm) and (*b*) emission (λ_{ex} 339 nm) spectra of Py (6×10^{-7} M) in the mannan-C_{16}/water system as a function of mannan-C_{16} concentration; (*c*) fluorescence intensity ratio I_3/I_1 as a function of the mannan-C_{16} concentration (λ_{ex} 339 nm), using MVC_{16}-20-8 as an example.

Characterization of mannan-C_{16} nanogel

Size and shape

The mannan-C_{16} nanogel appeared spherical in cryo-FESEM micrographs, with a fairly large size distribution, in the range of 100–400 nm for MVC_{16}-20-8, 100–500 nm for MVC_{16}-20-11 and 200–500 nm for MVC_{16}-20-16 (Figure 4). These results open the possibility for mannan-C_{16} nanogel being used to address APC, since spherical-shaped is subject to more efficient phagocytosis than ellipsoid or disc-shaped ones, being captured by macrophages;[34] furthermore, the uptake of materials into an ample variety of cells seems to be size dependent, generally considered more effective for materials in the range of 50–200 nm.[35]

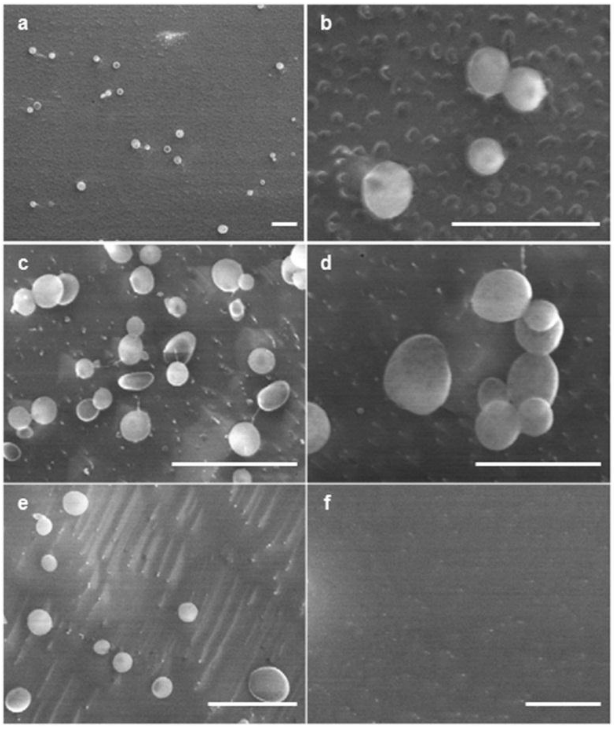

Figure 4. The cryo-FESEM negatively stained micrographs of mannan-C_{16} (scale bar = 1μm): (*a, b*) MVC_{16}-20-8, (*c, d*) MVC_{16}-20-11, (*e*) MVC_{16}-20-16 and (*f*) solvent.

Size stability during storage

The mean hydrodynamic diameter obtained using DLS for mannan-C_{16} colloidal dispersion in ultrapure water was distinct for materials with different DS, in the range of 50–140 nm, but almost constant for each material over a storage period of six months, at room temperature (~ 25 ºC). Materials with DS_{VMA} of 20% are larger than those with DS_{VMA}

above 25%. All samples exhibited fairly high polydispersity, with an average PdI between 0.4 and 0.7, which means that there may be macromolecular micelles with a distribution of sizes and shapes rather than macromolecular micelles of a single size and shape, as also revealed by the cryo-FESEM micrographs. No aggregation followed by sedimentation was observed during storage and changes in nanogel size were minimal. These results evidence the stability of nanogel produced (Figures 5, 6).

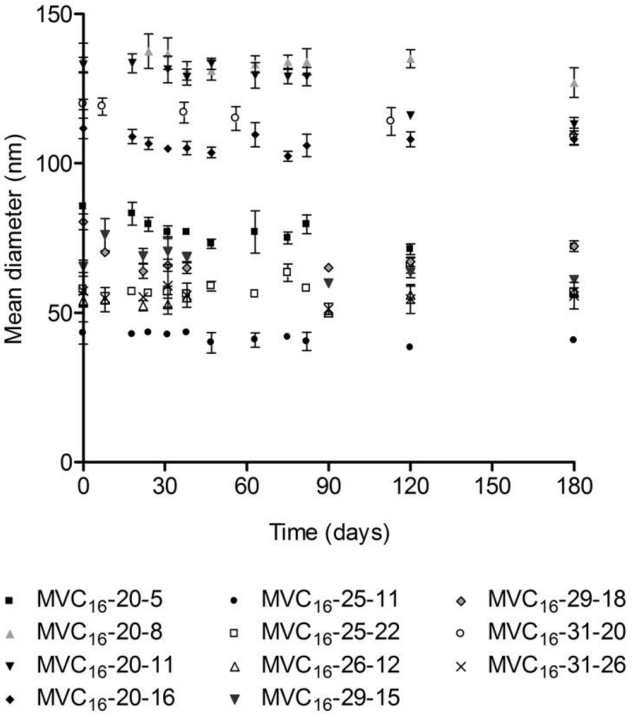

Figure 5. The size of mannan-C_{16} water dispersions (1 mg/mL) over a six months storage period, at room temperature (25 °C), measured periodically by DLS (mean ± S.D., *n* = 10).

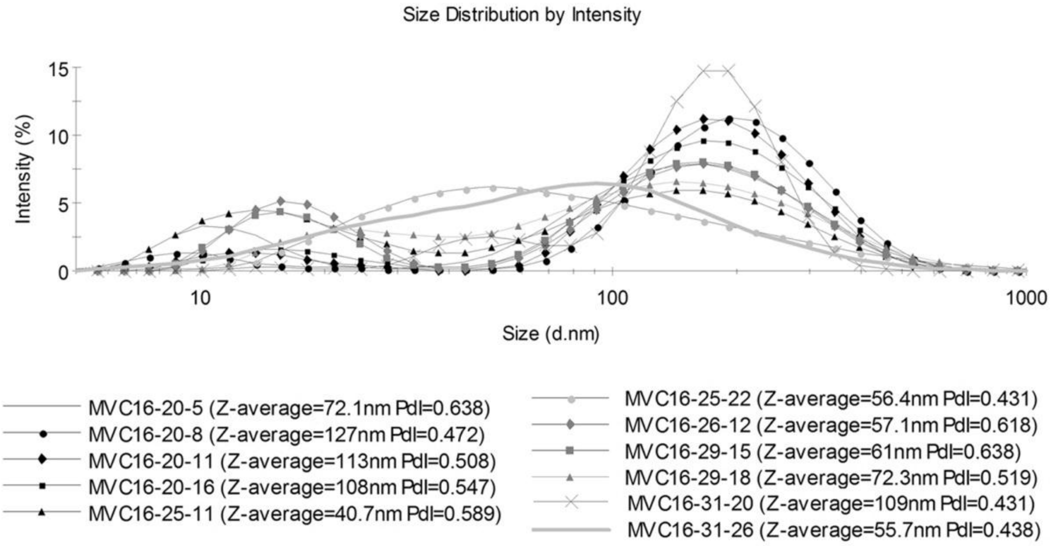

Figure 6. The size distribution by intensity, z-average and PdI of the mannan-C_{16} water dispersions (1 mg/mL) measured by DLS (mean ± S.D., *n* = 10) after a six months storage period, at room temperature (25 ºC).

Size and surface charge in different environments

The properties of the dispersion medium, such as concentration, pH, temperature, ionic strength, urea and solvent can control the size, surface charge and shape of colloidal dispersions, being decisive in their propensity either to be stable or to aggregate and precipitate. The micellar size is mainly determined by the hydrophobic forces that sequester the hydrophobic chains in the core and by the excluded volume repulsion between the chains that limits their size. The amphiphilic material obtained consists of mannan randomly substituted with hydrophobic alkyl chains. In randomly modified polymers, hydrophobic and hydrophilic parts are entangled together, which permits interaction between the core and the aqueous media. Exposed hydrophobic domains within a less mobile shell formed by hydrophilic chains, may result in secondary aggregation of polymeric micelles.[36] Using DLS, mean hydrodynamic diameter and zeta potential of mannan-C_{16} colloidal dispersions with different DS in different environments were studied (Figure 7).

Varying the concentration of mannan-C_{16} in a range 0.05–2 mg/mL, mean hydrodynamic diameter revealed to be smaller for higher concentrations. It appears that, for higher concentration of the polymer, the remaining solvent is gradually released from the hydrophobic domains, resulting in a decrease in micellar size.[36] These results are in agreement with the two types of hydrophobic environments with different hydration levels observed with NR and Py fluorescence. In the same range of concentrations, no major differences were observed in terms of surface charge, since zeta potential values were always negative and close to zero. Once zeta potential approaches zero, electrostatic repulsion becomes small compared to the ever-present van der Waals attraction. In these conditions, eventually, instability may arise, leading to aggregation followed by sedimentation and phase separation. In the current case, the macromolecular micelles conserved their nanosize, only MVC_{16}-20-16 batch at 0.05 mg/mL reaching a size larger than 1000 nm (Figure 7a). As, according to the zeta potential, the electrostatic repulsions should not be very high, the stability of the nanogel must be related to the hydration forces, and to the steric effects, which play a role whenever a reduction in the degree of freedom of the molecules in interacting colloids contributing to the stabilization of those colloids.

Colloidal stability might be compromised when the electrostatic barrier is removed, for instance by changing the pH or by the addition of enough quantity of salt to neutralize the surface charge of the macromolecular micelles in dispersion. Without the repulsive forces that keep colloidal macromolecular micelles separate, coagulation might occur due to attractive van der Waals forces. In presence of different concentrations on NaCl (0–0.6 M) mannan-C_{16} colloidal dispersions were stable, although a trend towards increased size may be noticed, as the ionic strength increased (Figure 7b). Moreover, macromolecular micelles equilibrated at different pH values showed minimal changes in their size and zeta potential (Figure 7c). In all cases, the zeta potential values were always negative and close to zero, never lower than −20 mV, the lowest value was obtained in ultrapure water. However those small values translate little repulsion, macromolecular micelles showed to be stable in nanoscale. The nearly neutral charge is precious for *in vivo* use, as large positive or negative charges may be rapidly cleared from the blood. Positively charged materials cause non-specific cell sticking, while those negatively charged are efficiently taken up by scavenger endothelial cells or “professional pinocytes” found in liver.[37]

The size stability of nanogels was also evaluated in presence of different concentrations of urea (0–7 M), which is known for its ability to break intramolecular hydrogen bonds and to destabilize hydrophobic domains.[38, 39] Experimental results suggest that urea neither affected the self-assembly of the studied amphiphilic system in water nor avoided nanogel formation (Figure 7d).

This nanogel is an upgrade version of mannan-C_{16} described in Ferreira et al. 2010.[22] Its synthesis is much easier, cheaper and less time consuming since VMA but not CDI-activated hydroxyethyl methacrylate (HEMA-CI) is commercially available to produce methacrylated mannan. Resultant self-assembled nanogel cac is smaller and the spherical macromolecular micelles size is smaller, less polydisperse, more stable and for consequence more adequate for biological applications.

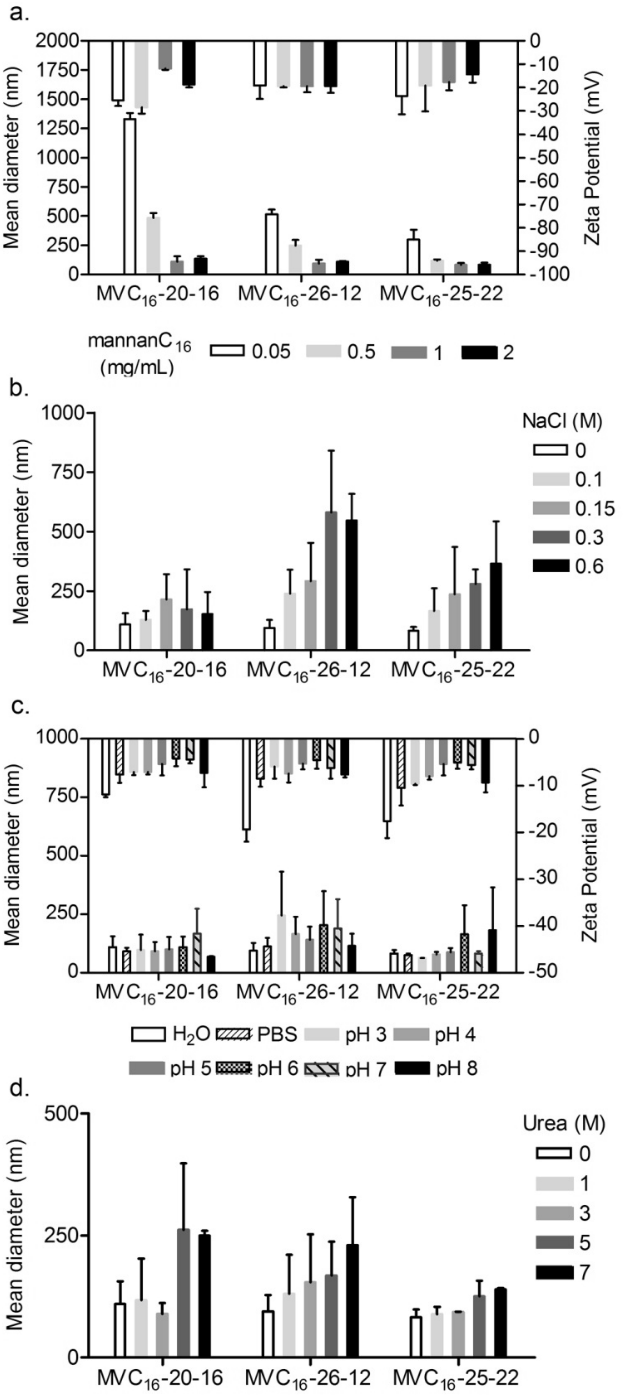

Figure 7. The size and zeta potential of mannan-C_{16} colloidal dispersions (*a*) (0.05–2 mg/mL) in water; (*b*) (1 mg/mL) in solutions of NaCl (0–0.6 M); (*c*) (1 mg/mL) in water, PBS, and phosphate-citrate buffer (pH 3–8.0); and (*d*) (1 mg/mL) in solutions of urea (0–7 M). Mean diameter and zeta potential were calculated by DLS at 37 ºC (mean ± S.D. *n* = 10).

Mannan-C_{16} nanogel as a host

Curcumin, a lipid soluble drug with wide spectrum of biological and pharmacological activities, exhibits solvent and medium sensitive absorption and fluorescence properties. Curcumin is poorly soluble in water at acidic and physiological pH, rapidly hydrolyzes in alkaline media[40] and is vulnerable to photochemical degradation in organic solvents.[41-44] Curcumin is soluble in ethanol (positive control) and exhibits a high absorbance at 428 nm. In water (negative control), curcumin forms insoluble aggregates and precipitates resulting in a very low absorbance detected in supernatant. As a hydrophobic molecule, one possible way to improve its aqueous solubility and stability is through the formation of inclusion complexes, in order to be encapsulated or entrapped as a guest within the internal cavity of a water-soluble host. Above cac the amphiphilic polymer self-assembles in water, originating nanostructures containing hydrophobic domains. The physical entrapment of hydrophobic curcumin in the nanogels was performed following the nanogels formation. After 24 h of incubation of the curcumin with the mannan-C_{16} nanogel, at room temperature (~25 °C), high stability of the colloidal dispersion was observed, no aggregation was detected by visual inspection. The addition of curcumin to aqueous dispersion of mannan-C_{16} nanogels results in a bright yellow solution after incubation. The unentrapped curcumin precipitates after centrifugation, only the entrapped curcumin being quantified. The UV-Vis spectra reveal an intense absorption at 428 nm, confirming the curcumin dissolution, and suggesting the physical entrapment of the curcumin, presumably into the hydrophobic domains within the mannan-C_{16} nanogel. Curcumin is less soluble in mannan-C_{16} nanogels than in absolute ethanol as evidenced by UV-Vis absorption value at 428 nm (Figure 8).

All batches tested with different DS_{VMA} and DS_{C16} were able to entrap reasonable amount of curcumin. The more substituted polymer forms more densely packed hydrophobic domains, such that the colloidal stability of nanogel is increased. Consequently the solubility of the curcumin among the hydrophobic domains tends to increase. Although stability of the nanosystem and consequently the drug load and release capacity is affected by the hydrophobic interactions among hydrophobic alkyl chains, several environmental conditions might eventually disturb the equilibrium of the nanosystem.

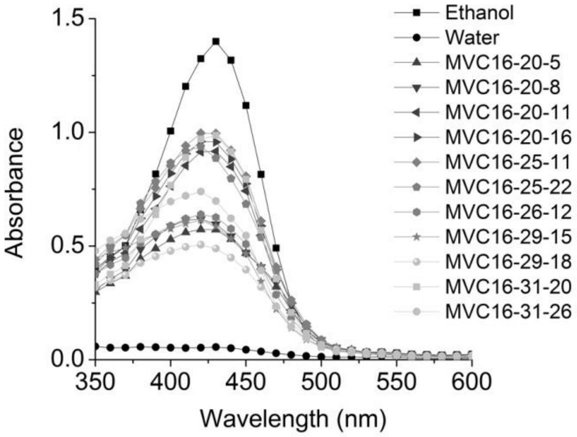

Figure 8. The mannan-C_{16} nanogel as potential host for curcumin. UV-Vis spectra of curcumin (0.1 mg/mL) incubated 24 h at 25 ºC in water (negative control), ethanol (positive control) and mannan-C_{16} colloidal dispersions in water.

The interior of the nanogel is not fully hydrophobic. In the interior of the nanogel – as proposed by several authors,[3, 5] including ourselves – there are multiple hydrophobic domains. The proteins are not expected to get fully buried in these hydrophobic domains. Instead, they are likely to position by these domains establishing interactions through more hydrophobic parts. These interactions are responsible for the stabilization of proteins when encapsulated in these nanogels (as demonstrated by circular dichroism using as case study the dextrin nanogel and interleukin (IL)-10).[45] In the same work, the encapsulation of IL-10 was demonstrated using ELISA method. After mixing IL-10 with the nanogel, the ELISA no longer detects the IL-10, presumably because it is encapsulated. The same is expected to occur in the present case of the mannan nanogel and BSA. The complexation between BSA and the mannan-C_{16} nanogel, in water, was studied by an ultra-filtration method. Ultra-filtration of BSA and mannan through the 1×10^5 Da cut-off membrane demonstrated that both macromolecules freely cross the membrane, as expected. In turn, mannan-C_{16} nanogel (1 mg/mL) accumulated in the concentrate (data not shown). After incubation 24 h at 25 ºC of BSA (1 mg/mL) with mannan-C_{16} nanogel (1 mg/mL) the majority of BSA, similar to 80% of initial amount calculated by Pierce BCA Protein assay method was found in the concentrate, where there were also 75% of the initial amount of the mannan-C_{16} nanogel, calculated by phenol-sulfuric acid method. Therefore a complex is formed in water between nanogel and the protein, resulting as a clear dispersion without any aggregation observed during the period of the assay (24 h). The stabilization of BSA by complexation could be due to the formation of multiple noncovalent interactions, namely hydrophobic and H-bonding between BSA and the nanogel. Thus amphiphilic property of mannan-C_{16} nanogel plays an important role in the complexation of soluble proteins that have both hydrophobic and hydrophilic patches on their surface.

The self-assembled mannan-C_{16} nanogel is therefore a suitable host for hydrophobic and for macromolecular water-soluble guests. These results open the possibility for new studies of mannan-C_{16} nanogel as a vehicle for multiple molecules acting like a perfect mix to modulate efficient and safe therapeutic responses.

Cytocompatibility of mannan-C_{16} nanogel

MTT cell proliferation assay offers a quantitative and convenient method for evaluating a cell population's response to external factors, whether it may be an increase in cell growth, no effect, or a decrease in growth due to necrosis or apoptosis.

Cytotoxicity of mannan-C_{16} nanogel with different DS_{C16}, MVC_{16}-25-11 and MVC_{16}-25-22 was evaluated on two mouse cell lines, J774 macrophages as a model for professional phagocytes and 3T3 fibroblasts as a non-phagocytic and recommended reference cell line (Figure 9). For each cell type a linear relationship between viable cell number and absorbance is established, enabling accurate, straightforward quantification of changes in proliferation. The results of the MTT assay clearly show that nanogels were cytotoxic for macrophages in contrast to what was observed for fibroblasts. Fibroblasts proliferated normally and had the typical flattened and spread fibroblast morphology. Neither cell death nor growth disorders – statistically significant – were noticed at any concentration of nanogel used. In contrast, dose dependent nanogel toxicity to J774 macrophages was observed, death cells being clearly noticed by optical microscopy. After 24 and 48 h of incubation, MVC_{16}-25-11 seems to be more toxic than MVC_{16}-25-22. Thus, nanogels significantly affected the morphology, viability and proliferation of J774 macrophages, the toxic effect being dose and time dependent and more intense in the batch with lower percentage of grafted hydrophobic alkyl chains.

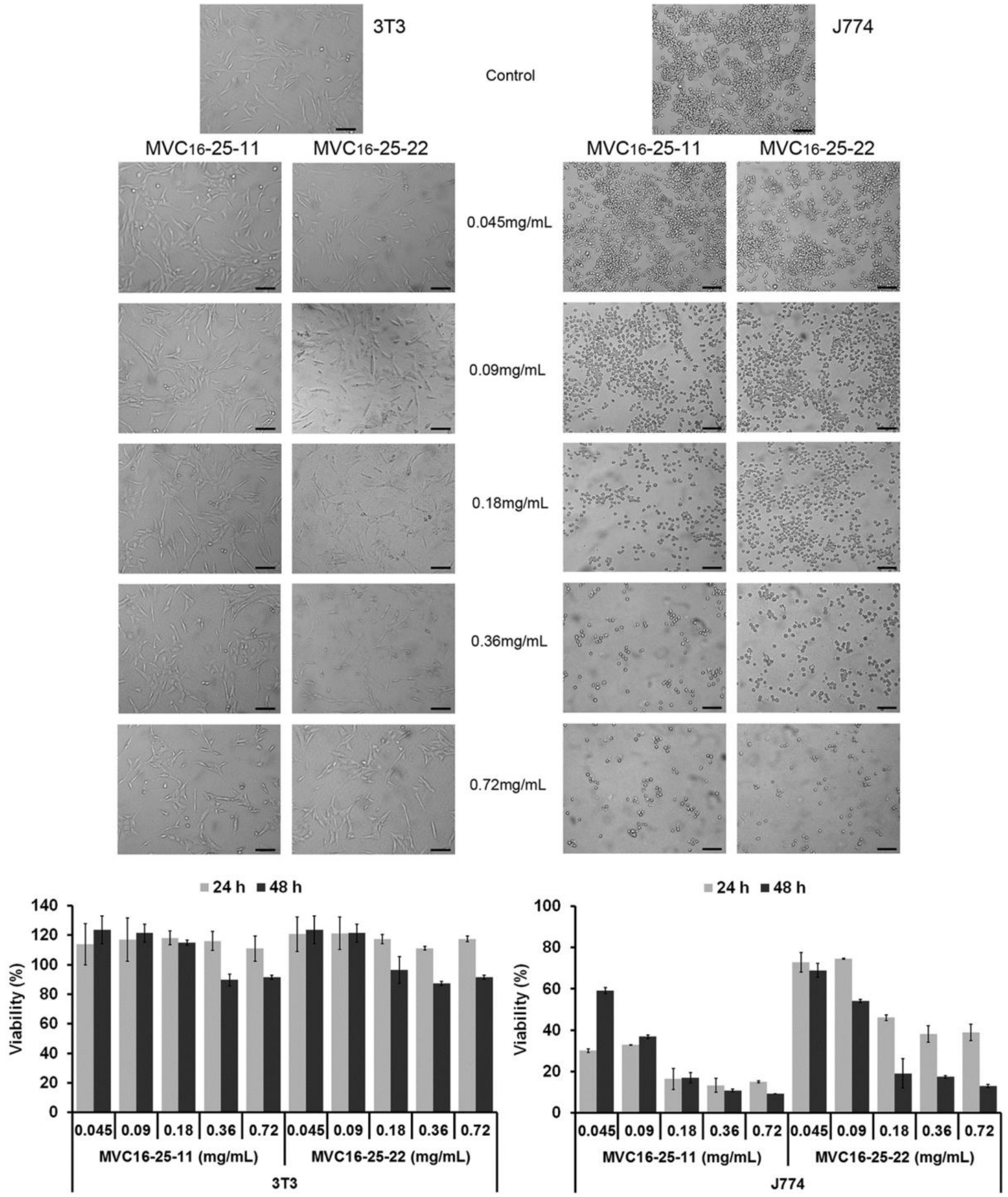

Figure 9. Effect of mannan-C_{16} nanogel on cell viability and cell growth. Images of mouse embryo fibroblast 3T3 and mouse macrophage-like J774 growth, after 48 h of incubation, in absence (control) or presence of mannan-C_{16} nanogel obtained by optical microscopy (scale bar = 100 µm). MTT cell proliferation assay results, using both cell lines (mean ± S.D.), after 24 and 48 h of incubation with nanogel at different concentrations (0.045–0.72 mg/mL). No statistical significant differences were obtained with fibroblast 3T3 viability. Statistical significant differences ($p < 0.01$) were obtained with all J774 viability results in all tested conditions.

According to the literature, some nanosystems including polymer-based nanoparticles also revealed cytotoxicity specific to this mouse phagocytic cell line, which seems to be quite sensitive to the presence of nanoparticles.[16, 46-48] The amphiphilic carboxymethylpullulan solutions reduced the number of viable J774.A1 cells in a time and dose-dependent manner but did not affect MCF-7 (human breast adenocarcinoma cell line) cell growth at all concentrations tested.[47] The poly(ε-caprolactone) nanoparticles specifically inhibited J774 cell proliferation by 80% after 24 h of incubation but no cytotoxicity on THP-1 cells (human acute monocytic leukemia cell line), MCF-7 and HeLa cells (human epithelial carcinoma cell line) has been reported.[46] Indeed, mannan-C_{16} interact with primary phagocytic cell culture of mouse bone-morrow derived macrophages (BMDM) showing almost no toxicity.[49] Dextrin nanoparticles – recently developed in our laboratory – are not toxic to BMDM.[50] So, depending on the cells used, the effect of the nanogel on the proliferation rate and the cell morphology is different: the cytotoxicity of a nanomaterial is cell-specific. Different cell types present different uptake, intracellular localization, processing and removal of the nanomaterials.[51] The toxicity of the nanomaterial can be related not only to cell necrosis or apoptosis but also to effects on cell signaling, membrane perturbations, influence on the cellular electron transfer cascades, production of cytokines, chemokines and reactive oxygen species, transcytosis and inter-cellular transport or gene regulation.[48, 51]

With the purpose of better understanding the toxicity of the mannan-C_{16} nanogel to J774 macrophages CLSM studies were performed. Mannan-C_{16} nanogel labeled with SAMSA fluorescein was used. The size and surface charge of the nanogel were not affected by the labeling with SAMSA Fluorescein. Furthermore, the effective covalent binding of fluorescein to the nanogel was confirmed by analysis of the UV-Vis spectra (a sharp single peak with maximum absorbance of 0.45 ± 0.05 at 495 nm was detected). Several studies reported that the cytotoxicity of nanomaterials to macrophages cytotoxicity is related to their phagocytic properties.[46, 52] Indeed, Z-series and time-series confocal images with phagocytic J774 macrophages revealed toxicity of mannan-C_{16} nanogel at various concentrations (0.1–0.6 mg/mL). For all tested concentrations, the viable cells were the ones that did not internalize the nanogel. Nanogel caused the cell death at the tested concentrations to similar extent. Images obtained with nanogel at 0.6 mg/mL are shown in Figure 10, as an example. Nanogel was observed inside dead cell (detected on the green channel on Figure 10) distributed uniformly in the cytoplasm. Cell death increased over time due to their higher internalization activity. All confocal conditions and parameters, such as lasers intensity, temperature, CO_2 and fluoroprobes at similar time of incubation were tested with same number of z-series and time-series and ensured the cell viability.

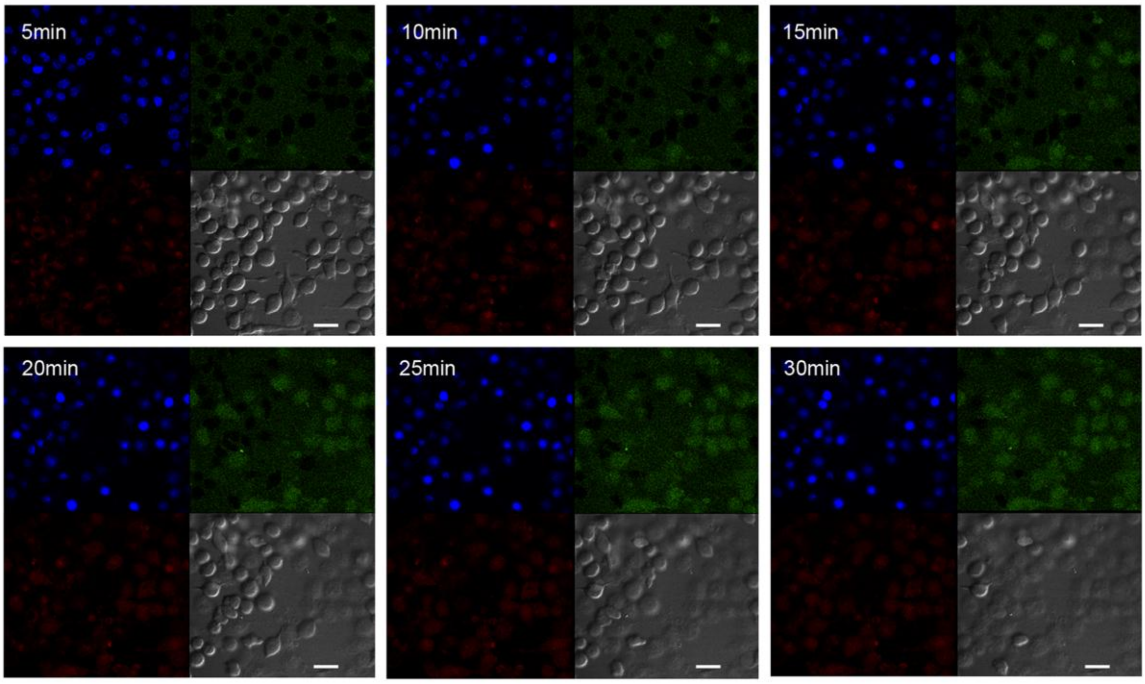

Figure 10. Time-series confocal images of mouse macrophage-like J774 cells incubated with mannan-C_{16} nanogel. Cells were initially labeled with DAPI (blue fluorescence), FM 4-64 (red fluorescence). PI was used to screen the viability of the cells. The nanogel at 0.6 mg/mL (green fluorescence) effect was followed by a series of time scans at a certain Z-stack. DIC images (in grey) illustrate the cell morphology changes (scale bar = 20 μm).

These results suggest that it was the internalization of the nanogel that caused cytotoxicity since the non-phagocytic cell line was not affected and internalization was confirmed with J774. The mannose receptor binds ligands at the cell surface and these receptor-ligand complexes are internalized *via* the endocytic pathway. The adenosine triphosphate (ATP)-dependent acidification of the endosome vesicle results in receptor-ligand dissociation with the released receptor recycling back to the cell surface.[53] If somehow this dissociation does not occur and the cell continues to internalize the nanogel it probably would induce cell death. In contrast to cell line J774, bone marrow-derived cells seem to be less sensitive to this nanogel, upon confirmation of nanogel internalization; these results indicate that the primary culture is able to efficiently process the nanogel.[49] The high nanogel toxicity observed with the macrophage cell line indicates that the cell line J774 is not suitable for studies with mannan-C_{16} nanogel and primary cultures of macrophages that do not exhibit cytotoxicity should be used instead.

Conclusions

The supramolecular assembled amphiphilic mannan-C_{16} nanogel was designed with a versatile, easy, reproducible and low-cost method. Above the cac, spherical polydisperse macromolecular micelles revealed long-term stability in aqueous environment, with mean hydrodynamic diameter ranging between 50 and 140 nm and nearly neutral negative surface charge. Colloidal stability was maintained when nanogel was exposed to potential destabilizing conditions of pH, ionic strength or in presence of urea. The mannan-C_{16} nanogel was able to entrap BSA and a hydrophobic drug, curcumin, thus having potential to perform as a carrier of different kinds of pharmaceuticals. The nanogel is non-toxic to mouse embryo fibroblast 3T3. This study also confirms that, as suggested in the literature, mouse macrophage-like J774 are highly sensitive to the presence of mannan-C_{16} nanogel, and internalization studies should be performed with other phagocytic cell, like the bone marrow-derived cells.

References

1. Huie, J. C. Guided molecular self-assembly: a review of recent efforts. *Smar Mat St* **2003**, 12, 264-271.

2. Rinaudo, M. Non-covalent interactions in polysaccharide systems. *Macromol Biosci* **2006**, 6, 590-610.

3. Nishikawa, T.; Akiyoshi, K.; Sunamoto, J. Macromolecular complexation between bovine serum albumin and the self-assembled hydrogel nanoparticle of hydrophobized polysaccharides. *J Am Chem Soc* **1996**, 118, 6110-6115.

4. Morimoto, N.; Endo, T.; Iwasaki, Y.; Akiyoshi, K. Design of hybrid hydrogels with self-assembled nanogels as cross-linkers: Interaction with proteins and chaperone-like activity. *Biomacromolecules* **2005**, 6, 1829-1834.

5. Akiyama, E.; Morimoto, N.; Kujawa, P.; Ozawa, Y.; Winnik, F. M.; Akiyoshi, K. Self-assembled nanogels of cholesteryl-modified polysaccharides: Effect of the polysaccharide structure on their association characteristics in the dilute and semidilute regimes. *Biomacromolecules* **2007**, 8, 2366-2373.

6. Janes, K. A.; Calvo, P.; Alonso, M. J. Polysaccharide colloidal particles as delivery systems for macromolecules. *Adv Drug Deliv Rev* **2001**, 47, 83-97.

7. Pillai, O.; Panchagnula, R. Polymers in drug delivery. *Curr Opin Chem Biol* **2001**, 5, 447-451.

8. Torchilin, V. P. Multifunctional nanocarriers. *Adv Drug Deliv Rev* **2006**, 58, 1532-1555.

9. Apostolopoulos, V.; Pietersz, G. A.; Loveland, B. E.; Sandrin, M. S.; McKenzie, I. F. Oxidative/reductive conjugation of mannan to antigen selects for T1 or T2 immune responses. *Proc Natl Acad Sci USA* **1995**, 92, 10128-10132.

10. Gu, X. G.; Schmitt, M.; Hiasa, A.; Nagata, Y.; Ikeda, H.; Sasaki, Y.; Akiyoshi, K.; Sunamoto, J.; Nakamura, H.; Kuribayashi, K*., et al.* A novel hydrophobized polysaccharide/oncoprotein complex vaccine induces in vitro and in vivo cellular and humoral immune responses against HER2-expressing murine sarcomas. *Cancer Res* **1998**, 58, 3385-3390.

11. Sihorkar, V.; Vyas, S. P. Potential of polysaccharide anchored liposomes in drug delivery, targeting and immunization. *J Pharm Pharm Sci* **2001**, 4, 138-158.

12. Gupta, A.; Gupta, R. K.; Gupta, G. S. Targeting cells for drug and gene delivery: Emerging applications of mannans and mannan binding lectins. *J Sci Ind Res* **2009**, 68, 465-483.

13. Avrameas, A.; McIlroy, D.; Hosmalin, A.; Autran, B.; Debre, P.; Monsigny, M.; Roche, A. C.; Midoux, P. Expression of a mannose/fucose membrane lectin on human dendritic cells. *Eur J Immunol* **1996**, 26, 394-400.

14. Fukasawa, M.; Shimizu, Y.; Shikata, K.; Nakata, M.; Sakakibara, R.; Yamamoto, N.; Hatanaka, M.; Mizuochi, T. Liposome oligomannose-coated with neoglycolipid, a new candidate for a safe adjuvant for induction of CD8+ cytotoxic T lymphocytes. *FEBS Lett* **1998**, 441, 353-356.

15. Apostolopoulos, V.; McKenzie, I. F. Role of the mannose receptor in the immune response. *Curr Mol Med* **2001**, 1, 469-474.

16. Chellat, F.; Merhi, Y.; Moreau, A.; Yahia, L. H. Therapeutic potential of nanoparticulate systems for macrophage targeting. *Biomaterials* **2005**, 26, 7260-7275.

17. Tang, C. K.; Lodding, J.; Minigo, G.; Pouniotis, D. S.; Plebanski, M.; Scholzen, A.; McKenzie, I. F.; Pietersz, G. A.; Apostolopoulos, V. Mannan-mediated gene delivery for cancer immunotherapy. *Immunology* **2007**, 120, 325-335.

18. Nakajima, T.; Ballou, C. E. Structure of the linkage region between the polysaccharide and protein parts of Saccharomyces cerevisiae mannan. *J Biol Chem* **1974**, 249, 7685-7694.

19. Ferreira, L.; Gil, M. H.; Dordick, J. S. Enzymatic synthesis of dextran-containing hydrogels. *Biomaterials* **2002**, 23, 3957-3967.

20. Carvalho, J.; Goncalves, C.; Gil, A. M.; Gama, F. M. Production and characterization of a new dextrin based hydrogel. *Eur Polym J* **2007**, 43, 3050-3059.

21. Goncalves, C.; Martins, J. A.; Gama, F. M. Self-assembled nanoparticles of dextrin substituted with hexadecanethiol. *Biomacromolecules* **2007**, 8, 392-398.

22. Ferreira, S. A.; Coutinho, P. J. G.; Gama, F. M. Self-assembled nanogel made of mannan: synthesis and characterization. *Langmuir* **2010**, 26, 11413-11420.

23. Dubois, M.; Gilles, K. A.; Hamilton, J. K.; Rebers, P. A.; Smith, F. Colorimetric method for determination of sugars and related substances. *Anal Chem* **1956**, 28, 350-356.

24. Mosmann, T. Rapid colorimetric assay for cellular growth and survival: application to proliferation and cytotoxicity assays. *J. Immunol. Methods* **1983**, 65, 55-63.

25. Arigita, C.; van den Berg, J.; Wensink, K.; van Steenbergen, M.; Hennink, W. E.; Crommelin, D. J. A.; Kersten, G. F. A.; Jiskoot, W. Immunogenicity of meningococcal PorA formulations encapsulated in biodegradable microspheres. *Eur J Pharm Sci* **2004**, 21, 131-141.

26. van Dijk-Wolthuis, W. N. E.; Tsang, S. K. Y.; Kettenes-van den Bosch, J. J.; Hennink, W. E. A new class of polymerizable dextrans with hydrolyzable groups: hydroxyethyl methacrylated dextran with and without oligolactate spacer. *Polymer* **1997**, 38, 6235-6242.

27. Kath, F.; Kulicke, W. M. Polymer analytical characterization of glucan and mannan from yeast Saccharomyces cerevisiae. *Appl Macromol Chem Phys* **1999**, 268, 69-80.

28. Hrkach, J. S.; Peracchia, M. T.; Domb, A.; Lotan, N.; Langer, R. Nanotechnology for biomaterials engineering: Structural characterization of amphiphilic polymeric nanoparticles by H-1 NMR spectroscopy. *Biomaterials* **1997**, 18, 27-30.

29. Coutinho, P. J. G.; Castanheira, E. M. S.; Rei, M. C.; Oliveira, M. E. C. D. R. Nile red and DCM fluorescence anisotropy studies in C12E7/DPPC mixed systems. *J Phys Chem B* **2002**, 106, 12841-12846.

30. Kalyanasundaram, K.; Thomas, J. K. Environmental effects on vibronic band intensities in pyrene monomer fluorescence and their application in studies of micellar systems. *J Am Chem Soc* **1977**, 99, 2039-2044.

31. Dong, D. C.; Winnik, M. A. The Py scale of solvent polarities. *Can J Chem* **1984**, 62, 2560-2565.

32. Rapoport, N. Physical stimuli-responsive polymeric micelles for anti-cancer drug delivery. *Prog Polym Sci* **2007**, 32, 962-990.

33. Lee, K. Y.; Jo, W. H.; Kwon, I. C.; Kim, Y.-H.; Jeong, S. Y. Physicochemical characteristics of self-aggregates of hydrophobically modified chitosans. *Langmuir* **1998**, 14, 2329-2332.

34. Oh, J. K.; Lee, D. I.; Park, J. M. Biopolymer-based microgels/nanogels for drug delivery applications. *Prog Polym Sci* **2009**, 34, 1261-1282.

35. Mailander, V.; Landfester, K. Interaction of nanoparticles with cells. *Biomacromolecules* **2009**, 10, 2379-2400.

36. Jones, M. C.; Leroux, J. C. Polymeric micelles - a new generation of colloidal drug carriers. *Eur J Pharm Biopharm* **1999**, 48, 101-111.

37. Smedsrod, B. Clearance function of scavenger endothelial cells. *Comp Hepatol* **2004**, 3 Suppl 1, S22.

38. Mukerjee, P.; Ray, A. Effect of urea on micelle formation and hydrophobic bonding. *J Phys Chem* **1963**, 67, 190-193.

39. Moore, D. R.; Mathias, L. J. Molecular composites *via* insitu polymerization - poly(phenylene terephthalamide)-nylon 3. *J Appl Polym Sci* **1986**, 32, 6299-6315.

40. Tonnesen, H. H.; Karlsen, J. Studies on curcumin and curcuminoids .6. Kinetics of curcumin degradation in aqueous-solution. *Eur Food Res Technol* **1985**, 180, 402-404.

41. Tonnesen, H. H.; Karlsen, J.; Vanhenegouwen, G. B. Studies on curcumin and curcuminoids .8. Photochemical stability of curcumin. *Eur Food Res Technol* **1986**, 183, 116-122.

42. Bong, P. H. Spectral and photophysical behaviors of curcumin and curcuminoids. *Bulletin Korean Chem Soc* **2000**, 21, 81-86.

43. Chignell, C. F.; Bilski, P.; Reszka, K. J.; Motten, A. G.; Sik, R. H.; Dahl, T. A. Spectral and photochemical properties of curcumin. *Photochem Photobiol* **1994**, 59, 295-302.

44. Khopde, S. M.; Priyadarsini, K.; Palit, D. K.; Mukherjee, T. Effect of solvent on the excited-state photophysical properties of curcumin. *Photochem Photobio* **2000**, 72, 625-631.

45. Carvalho, V.; Castanheira, P.; Faria, T. Q.; Gonçalves, C.; Madureira, P.; Faro, C.; Domingues, L.; Brito, R. M.; Vilanova, M.; Gama, M. Biological activity of heterologous murine interleukin-10 and preliminary studies on the use of a dextrin nanogel as a delivery system. *Int J Pharm* **2010**, 400, 234-242.

46. Lemarchand, C.; Gref, R.; Passirani, C.; Garcion, E.; Petri, B.; Müller, R.; Costantini, D.; Couvreur, P. Influence of polysaccharide coating on the interactions of nanoparticles with biological systems. *Biomaterials* **2006**, 27, 108-118.

47. Henni-Silhadi, W.; Deyme, M.; Boissonnade, M.-M.; Appel, M.; Le Cerf, D.; Picton, L.; Rosilio, V. Enhancement of the Solubility and Efficacy of Poorly Water-Soluble Drugs by Hydrophobically-Modified Polysaccharide Derivatives. *Pharm Res* **2007**, 24, 2317-2326.

48. Jones, C. F.; Grainger, D. W. In vitro assessments of nanomaterial toxicity. *Adv Drug Delivery Rev* **2009**, 61, 438-456.

49. Ferreira, S. A.; Carvalho, V.; Costa, C.; Teixeira, J. P.; Vilanova, M.; Gama, F. M. Self-assembled mannan nanogel: cytocompatibility and cell localization. *J Biomed Nanotech* **2012**, 8, 1-9.

50. Gonçalves, C.; Torrado, E.; Martins, T.; Pereira, P.; Pedrosa, J.; Gama, M. Dextrin nanoparticles: studies on the interaction with murine macrophages and blood clearance. *Colloid Surface B* **2010**, 75, 483-489.

51. Park, M. V.; Lankveld, D. P.; van Loveren, H.; de Jong, W. H. The status of in vitro toxicity studies in the risk assessment of nanomaterials. *Nanomedicine (Lond)* **2009**, 4, 669-685.

52. Cruz, T.; Gaspar, R.; Donato, A.; Lopes, C. Interaction between polyalkylcyanoacrylate nanoparticles and peritoneal macrophages: MTT metabolism, NET reduction, and NO production. *Pharm Res* **1997**, 14, 73-79.

53. Wileman, T.; Boshans, R.; Stahl, P. Uptake and transport of mannosylated ligands by alveolar macrophages. Studies on ATP-dependent receptor-ligand dissociation. *J Biol Chem* **1985**, 260, 7387-7393.

Chapter 5

Self-assembled mannan nanogel: cytocompatibility and cell localization

Amphiphilic mannan, produced by the Michael addition of hydrophobic 1-hexadecanethiol to vinyl methacrylated mannan, self-assembles in aqueous medium through hydrophobic interactions among alkyl chains. Resultant nanogel is stable, spherical, polydisperse, with 50–140 nm mean hydrodynamic diameter depending on the polymer degree of substitution, and nearly neutral negative surface charge. No cytotoxicity of mannan nanogel is detected up to about 0.4 mg/mL in mouse embryo fibroblast cell line 3T3 and mouse bone marrow-derived macrophages (BMDM) using cell proliferation, lactate dehydrogenase and Live/Dead assays. Comet assay, under the tested conditions, reveals no DNA damage in fibroblasts but possible in BMDM. BMDM internalize the mannan nanogel, which is observed in vesicles in the cytoplasm by confocal laser scanning microscopy. Confocal colocalization image analysis denotes that the entrance and exit of nanogel and FM 4-64 might occur by the same processes – endocytosis and exocytosis – in BMDM. Physicochemical characteristics, *in vitro* cytocompatibility and uptake of self-assembled mannan nanogel by mouse BMDM are great signals of the potential applicability of this nanosystem for macrophages targeted delivery of vaccines or drugs, acting as potential nanomedicines, always with the key goal of preventing and/or treating diseases.

Adapted from: *J Biomed Nanotechnol* **2012** (accepted)

Introduction

The performance of nanogels as carriers intended to deliver biologically active agents to specific targets are mainly regulated by their physicochemical properties. These properties include hydrophilicity, surface charge, size, shape, composition, concentration, and presence of various ligands, which ultimately govern their interaction with proteins, perturbation of the cell membranes, cell activation, cellular uptake, intracellular localization and removal of nanomaterials by cells, cell necrosis or apoptosis, gene regulation, effects on cell signaling, influence on the cellular electron transfer cascades, production of cytokines, chemokines and reactive oxygen species.[1-3]

Amphiphilic mannan, self-assembled in nanometer-sized supramolecular hydrogels – i.e. hydrogel nanoparticles or nanogels – were developed in previous work,[4] aiming the drug targeted delivery to mannose receptors expressed in the surface of antigen-presenting cells (APC).[5-8] Similarly, mannan-coated gelatin nanoparticles targeted didanosine, an anti-HIV drug, to macrophages both *in vitro* and *in vivo*.[9] Moreover, mannosylated chitosan nanoparticle-based murine interleukin(IL)-12 gene therapy suppressed cancer growth and angiogenesis, and significantly induced cell cycle arrest and apoptosis in BALB/c mice bearing CT-26 carcinoma cells.[10] Mannose receptor participates in mannose receptor-mediated endocytosis contributing to the host defense, providing a linkage between innate and adaptive immunity.[8, 11-13] Plasmid DNA encoding β-galactosidase, used as a model antigen, coated on the surface of mannan coated-nanoparticles resulted in a significant enhancement in both antigen-specific immunoglobulin (Ig)G titers and splenocyte proliferation over “naked” plasmid DNA alone upon topical application in mice.[14] Cholesterol-bearing mannan (CHM) complexed with human epidermal growth factor receptor 2 (HER2) oncoprotein, encoded by the HER2/neu/c-erbB2 oncogene, containing the 147 N-terminal amino acids were able to induce $CD8^+$ cytotoxic T-cells against $HER2^+$ tumors and to strongly enhance the production of IgG antibodies against HER2 in mice immunized subcutaneously. Mice immunized with CHM-HER2 before or early after tumor challenge successfully rejected HER2-transfected tumors.[6, 15]

The particles of the mannan nanogel are stable, spherical, polydisperse, with mean hydrodynamic diameter or z-average ranging between 50 and 140 nm depending on the polymer degree of substitution, and with nearly neutral negative surface charge or zeta potential, as previously studied.[4] Mannan nanogel spontaneously incorporated bovine serum albumin and curcumin indicating its potential as delivery systems for therapeutic molecules.[4] In the present work, the essential focus was to assess nanomaterial cytocompatibility and to analyze the internalization by macrophages. The mannan nanogel cytocompatibility was tested in mouse embryo fibroblast cell line 3T3 and mouse bone marrow-derived macrophages (BMDM), using the CellTiter 96® AQ$_{ueous}$ one-solution cell proliferation assay, lactate dehydrogenase (LDH) cytotoxicity detection kit^{PLUS} and Live/Dead® viability/cytotoxicity kit for mammalian cells. Genotoxicity was evaluated with comet assay. Uptake of mannan nanogel labeled with a fluorochrome probe by the BMDM was studied by confocal laser scanning microscopy (CLSM).

Experimental

Materials

Mannan-VMA-SC$_{16}$ (VMA: vinyl methacrylate, SC$_{16}$: hydrophobic alkyl chain) was synthesized as described previously.[4] According to the polymer degree of substitution (DS), defined as the percentage of grafted acrylate groups (DS$_{VMA}$) or alkyl chains (DS$_{C16}$) relative to the mannose residues, samples of mannan-C$_{16}$ nanogel were named as MVC$_{16}$-DS$_{VMA}$-DS$_{C16.}$ Three batches were studied: MVC$_{16}$-25-11, MVC$_{16}$-25-22 and MVC$_{16}$-31-20. Organic and inorganic reagents of laboratory grade were purchased from Sigma and used without any further purification. All cell culture products were of cell culture grade and purchased from Sigma, saving reported exceptions.

Preparation of self-assembled mannan nanogel

Each sterile stock colloidal dispersion of mannan-C$_{16}$ was prepared stirring the lyophilized mannan-C$_{16}$ in phosphate buffered saline, pH 7.4 (PBS), for 3–5 days at 50 °C, followed by sterilized filtration (Orange; pore size 0.22 µm). The nanogel formation was confirmed by dynamic light scattering (DLS). The size distribution and zeta potential measurements were performed in a Malvern Zetasizer NANO ZS (Malvern Instruments Limited, UK) as previously described.[4] Serial dilutions were prepared in sterile apyrogenic PBS and final sample concentration was adjusted diluting five times with culture medium.

Cell culture

Fibroblast cell line 3T3

Mouse embryo fibroblast cell line 3T3 (ATCC CCL-164) was grown in Dulbecco's modified Eagle's media (DMEM; 4.5 g/L glucose) supplemented with 10% newborn calf serum (Invitrogen, UK), 100 IU/mL penicillin and 0.1 mg/mL streptomycin at 37 °C in a 95% humidified air containing 5% CO_2. At confluence, fibroblasts were harvested with 0.05% (w/v) trypsin-EDTA, adjusted to the required concentration of viable cells – determined using the trypan blue exclusion assay, indicative of plasma membrane integrity – and were subcultivated in the same medium. Fibroblasts were plated at 4×10^3 cells/200 µL/well for cell proliferation assay, 1×10^4 cells/200 µL/well for LDH assay or 4×10^5 cells/200 µL/well for comet assay in 96-well plates (Sarstedt, Canada) and 1×10^5 cells/2 mL/well for Live/Dead assay in 6-well plates (Sarstedt, Canada). Then fibroblasts were incubated 5 h at 37 °C in a 95% humidified air containing 5% CO_2.

Mouse BMDM

Female BALB/c mice (6–8 weeks old) were purchased from Charles River (Barcelona, Spain). Animals were kept at the animal facilities of the Institute Abel Salazar during the experiments. Hiding and nesting materials were provided as enrichment. Procedures involving mice were performed according to the European Convention for the Protection of Vertebrate Animals used for Experimental and Other Scientific Purposes (ETS 123) and 86/609/EEC Directive and Portuguese rules (DL 129/92). In order to obtain mouse BMDM, femurs and tibias were collected under aseptic conditions and flushed with Hanks' balanced salt solution. The resulting cell suspension was centrifuged at 500 g and resuspended in RPMI 1640 medium supplemented with 10 mM HEPES, 10% heat-inactivated fetal bovine serum (FBS), 60 IU/mL penicillin, 60 µg/mL streptomycin, 0.5 mM β-mercaptoethanol (complete RPMI [cRPMI]), and 10% L929 cell conditioned medium (LCCM). To remove fibroblasts or differentiated macrophages, cells were cultured, on cell culture dishes (Sarstedt, Canada), overnight at 37 ºC in a 95% humidified air containing 5% CO_2. Then, nonadherent cells were collected with warm cRPMI, centrifuged at 500 g, resuspended in cRPMI and distributed 2×10^4 cells/200 µL/well in 96-well plates for cell proliferation and LDH assays, 1×10^5 cells/1 mL/well in 24-well plates (Sarstedt, Canada) for comet assay, 2×10^5 cells/2 mL/well in 6-well plates for Live/Dead assay, and 5×10^5 cells/1 mL/well in 24-well plates or 1×10^6 cells/2 mL/fluorodish (WPI, UK) for confocal studies. Cells were then incubated at 37 °C in a 95% humidified air containing 5% CO_2.

Four days after seeding, 10% of LCCM was added, and the medium was renewed on the seventh day. After 10 days in culture, cells were completely differentiated into macrophages. This method allows for the differentiation of a homogenous primary culture of macrophages that retain the morphological, physiological and surface markers characteristics of these phagocytic cells.[16-18]

Effect of mannan nanogel on cell viability and cell proliferation

Cell proliferation assay

The cell viability was determined by CellTiter 96® AQ$_{ueous}$ one-solution non-radioactive cell proliferation assay (Promega, USA) composed by 3-(4,5-dimethylthiazol-2-yl)-5-(3-carboxymethoxyphenyl)-2-(4-sulfophenyl)-2H-tetrazolium (MTS) and an electron coupling reagent (phenazine methosulfate; PMS). Nanogel at different concentrations was incubated with mouse fibroblast 3T3 cells and mouse BMDM, for 24 or 48 h at 37 °C, in a 95% humidified air containing 5% CO_2. Then, each well was washed with 100 µL of fresh cell culture medium and MTS (20 µL) was added. After 1 h of incubation in same conditions, MTS is bioreduced by dehydrogenase enzymes found in metabolically active cells into a formazan product that is soluble in culture medium. The UV absorbance of the formazan was measured at 490 nm in an automated ELISA plate reader, which is directly proportional to the number of living cells in culture. The results were compared to a control prepared with the same cell culture medium without the addition of nanogel. The results are expressed as cell proliferation index (CPI) after normalizing the viability of untreated cells to 100%.

LDH assay

The cytotoxicity/cytolysis of mannan nanogel to mouse fibroblast 3T3 cells and mouse BMDM, after 3 and 20 h of incubation at 37 °C, in a 95% humidified air containing 5% CO_2 was evaluated using LDH Cytotoxicity Detection Kit^{PLUS} (Roche, Germany), following the manufacturer instructions. Preliminary assays were carried out to determine the optimal cell concentration and confirm that nanogel did not interfere with the assay, using culture medium with 1% of serum and without sodium pyruvate. The results are expressed in absorbance values, after subtracting the background control to the average of the triplicate samples and controls absorbance values, measured at 490 nm in an automated ELISA, using as reference the absorbance obtained at 620 nm.

Live/Dead assay

The Live/Dead® viability/cytotoxicity kit for mammalian cells (Invitrogen, UK) was used to determine mouse fibroblast 3T3 cells and mouse BMDM viability in presence of nanogel incubated with cells at different concentrations, for 24 h at 37 °C, in a 95% humidified air containing 5% CO_2. At the end, 100 µL of a solution with 2 µM calcein acetoxymethylester and 4 µM ethidium homodimer-1 in sterile PBS was added to each well. After incubation for 30–45 min in the same conditions as above, cells were visualized in a fluorescence microscope Olympus BX-61 Fluorescence Microscope (Olympus, Germany) coupled with a DP70 digital camera (Melville, NY) using objective 10×. Images were analyzed with Cell-P software (Olympus, Germany).

Comet assay

Nanogel at different concentrations was incubated with mouse fibroblast 3T3 cells and mouse BMDM, for 24 or 48 h at 37 °C, in a 95% humidified air containing 5% CO_2. After the period of incubation, fibroblasts were harvested with 0.05% (w/v) trypsin-EDTA and macrophages were mechanically harvested, and washed three times with ice cold PBS, pH 7.4. Cell viability, determined by trypan blue exclusion, was higher than 80% in all cases. The alkaline version of the comet assay was performed as described by Singh *et al.*[19] with minor modifications. Briefly, cells collected by centrifugation (7500 g for 3 min) and suspended in 120 µL of 0.6% low melting point agarose in PBS were dropped onto a frosted slide precoated with a layer of 1% normal melting point agarose. Slides were placed on ice for 4 min and allowed to solidify. Coverslips were then removed and slides were immersed in freshly prepared lysing solution (2.5 M NaCl, 100 mM Na_2EDTA, 10 mM TrisBase, 10 M NaOH, pH 10) for 1 h at 4 ºC, in the dark. After lysis, slides were washed with ice water and placed on a horizontal electrophoresis tank in an ice bath. The tank was filled with freshly made alkaline electrophoresis solution (1 mM Na_2EDTA, 300 mM NaOH, pH 13) to cover the slides that were left for 20 min in the dark to allow DNA unwinding and alkali-labile site expression. Electrophoresis was carried out for 20 min at 30 V and 300 mA (1 V/cm). The slides were then washed for 10 min with 1 mL of neutralizing solution (0.4 M TrisBase, pH 7.5). After neutralization, gels were dried overnight in the dark. Then in the dark the gels were rehydrated with ice cold water and stained with ethidium bromide solution (20 µg/mL) for 20 min. After staining the slides were washed twice with ice cold bidistilled water for 20 min and dried. Before observation with the fluorescence microscope the dried slide was rehydrated and covered with a coverslip. Two slides were prepared for each treatment with nanogel and a "blind" scorer examined 100 randomly selected cells per replicate using a magnification of 400×. Image capture by an on-line CCD camera and analysis were performed with Comet Assay IV software (Perceptive Instruments).

Uptake of mannan nanogel by the BMDM

Mannan nanogel labeled with SAMSA fluorescein

Synthesis of mannan-C_{16} labeled with 5-((2-(and-3)-*S*-(acetylmercapto)succinoyl)amino) fluorescein (SAMSA fluorescein; Molecular Probes, Invitrogen) was based on the reaction between the thiol group of SAMSA fluorescein with the grafted methacrylate not substituted with C_{16} of MVC_{16}-31-20, as previously described.[4] Labeling did not affect the properties of the nanogel, as estimated by DLS.

Confocal studies

In order to evaluate the phagocytic activity, mouse BMDM (5×10^5 cells/well) were seeded on coverslips (Sarstedt, Canada) and stimulated with and without lipopolysaccharide (LPS from *E. coli*; 100 ng/mL) and interferon-γ (IFN-γ; 1 ng/mL; R&D systems). Then, the macrophages were incubated with or without mannan nanogel labeled with SAMSA fluorescein (0.1 mg/mL; λ_{em} 519 nm) for 6 h. The coverslips were washed twice with PBS and cells were fixed with methanol absolute (−20 ºC) for 10 min. Following PBS washing (twice), nuclei were stained with 4'-6-diamidino-2-phenylindole (DAPI; λ_{em} 461 nm) using vectashield mounting medium (Vector Laboratories) as an anti-fading. Z-series of cells with 284.90 nm Z spacing between image planes, with 5× optical zoom and 512×512 pixel size were obtained using confocal laser scanning microscope Leica SP2 AOBS SE (Leica Microsystems, Germany), an inverted microscope Leica DMIRE2 equipped with objective HC PL APO Lbl. Blue 63× with a numerical aperture of 1.40 Oil LEICA, and confocal software LCS 2.61 (Leica Microsystems, Germany).

The internalization of nanogel by BMDM plated in fluorodish (WPI, UK) was followed by the CLSM. Live cells nuclei' were labeled with DAPI (0.05 mg/mL) for 3 min at room temperature in cRPMI. After washing, cells were incubated for 20 min with 20 µM FM 4-64® (Molecular Probes, Invitrogen, λ_{em} 618 nm) in cRPMI. Membranes are intensely red-fluorescent labeled when FM 4-64 inserts into the outer leaflet of the surface membrane. FM 4-64 is frequently used in endocytosis and exocytosis studies in eukaryotic cells because it is water-soluble, nontoxic to cells and virtually nonfluorescent in aqueous media. Propidium iodide (PI, 1 µg/mL) was added to the medium to evaluate the viability of the cells. The plate was then placed on the stage of the confocal laser scanning microscope (OLYMPUS FluoView^{TM} - FV1000) at 37 °C and 5% CO_2. A representative area of the fluorodish was selected at random and control picture was obtained. Labeled nanogel was then added into the medium (0.1 mg/mL). Five z-series with 0.98 µm Z spacing between image planes and time-series with 15 min interval were obtained using 3 lasers (405 nm, 488 nm and 559 nm) in the three narrow bandwidth emission filter, sequential acquisition and Kalman filter mode, 40× objective with a numerical aperture of 0.9, 2× optical zoom, and 640×640 pixel size with four detectors. To follow the exocytosis of the nanogel, the incubating medium was carefully removed from the fluorodish, washed three times with PBS and then filled with fresh medium with PI. Another series of time scans were obtained as described before. All confocal images were obtained under identical scan settings. Control specimens were prepared with each fluorochrome separately and in the absence of staining for excitation cross-talk and emission bleed-through analysis, and autofluorescence characterization, respectively. In time lapses, threshold-based analysis (annotation) measurements were performed with software Olympus FluoView1000 (FV viewer v.2.0), after removing unspecific events generated by noise and background, using a two-dimensional scatterplot of intensity ranges of red channel versus green channel, where thresholds were defined using the controls results. Colocalization coefficient in total pixels area (C_T, correspondent to the ratio between colocalized pixels and total number of pixels) was calculated in two-color – red and green corresponding to FM 4-64 and labeled nanogel – two-dimensional microscopic images. Reported values of C_T for each time correspond to mean obtained using “regions of interest” (ROIs) corresponding to cytoplasm of 45 cells.

Statistical analysis

Statistical significance of the cytotoxicity and genotoxicity results was determined by one-way analysis of variance (ANOVA) with Dunnett's post-test using GraphPad Prism version 4.00 for Windows (GraphPad Software, CA, USA). Statistical significant differences within results obtained with each concentration of nanogels in comparison with the control at same incubation period were labeled with a single asterisk ($p < 0.05$) and with two asterisks ($p < 0.01$).

Results and discussion

Cytocompatibility of mannan nanogel

Self-assembled amphiphilic mannan nanogel, with different DS_{C16} – MVC_{16}-25-11 and MVC_{16}-25-22 – and different DS_{VMA} – MVC_{16}-25-22 and MVC_{16}-31-20, corresponding to different nanogel size (Table 1), were selected to study the cytocompatibility of the nanogel using cell proliferation, LDH and Live/Dead assays.

Table 1. Size and zeta potential measurements obtained in DLS for mannan nanogel at 1 mg/mL in PBS

	MVC_{16}-25-11	MVC_{16}-25-22	MVC_{16}-31-20
Z-average (nm)	50.7 ± 0.9	56.4 ± 1.5	109.0 ± 2.9
Polydispersity Index (PdI)	0.589 ± 0.010	0.431 ± 0.010	0.431 ± 0.056
Zeta potential (mV)	−8.49 ± 1.71	−10.49 ± 3.76	−7.29 ± 0.37

(mean ± S.D., *n* = 10)

Cell proliferation assay using MTS is a colorimetric, easy, fast and safe assay that measures the mitochondrial metabolic activity.[20, 21] MTS assay (Figure 1) showed that, after 24 h of incubation, the viability of mouse embryo fibroblast 3T3 was not significantly affected by any of the concentrations of the three batches of mannan nanogel used. After 48 h of incubation, the toxicity of the nanogel was dose dependent and significant for the higher concentrations of each batch. Fibroblasts proliferated normally. The viability of mouse BMDM after 24 h of incubation was overall not affected by the nanogel, being significantly reduced only for MVC_{16}-25-11 at 0.05 mg/mL, where the CPI was close to 75%. After 48 h of incubation, the viability in the majority of treatments was similar to the control, with the CPI close to 100%, except for MVC_{16}-31-20 at 0.4 mg/mL, where it was close to 75%. Fibroblasts and macrophages had the typical flattened and spread morphology and no cell death was noticed at any concentration of nanogel used.

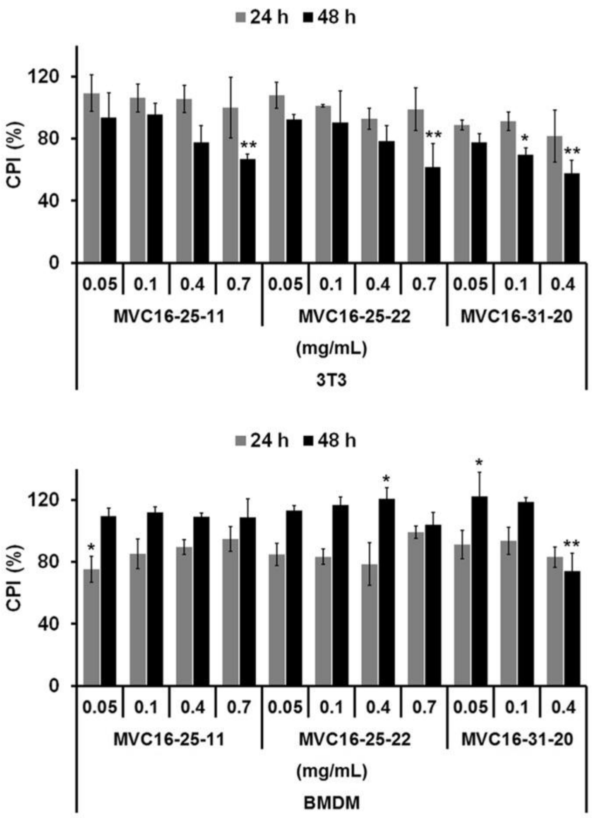

Figure 1. Effect of mannan nanogel, at the indicated concentrations, in mouse embryo fibroblast 3T3 cells and BMDM, assessed with the MTS assay. Results correspond to the mean ± S.D. of the cell proliferation index (CPI, * $p < 0.05$ and ** $p < 0.01$), obtained for the different groups at 24 and 48 h of incubation with mannan nanogel at the indicated concentrations. The results shown are from one experiment, representative of three independent experiments performed in triplicate.

LDH assay is a non-radioactive, precise, fast and simple colorimetric assay suitable for high-throughput quantification of cell death and lysis, based on measurement of LDH activity released from the cytosol of cells with damaged plasma membranes. LDH assay (Figure 2) was used to evaluate the cytotoxicity of mannan nanogel in smaller periods of incubation. All treatments originated values of absorbance similar to low control, which determines the LDH activity released from the untreated healthy cells and corresponds to the spontaneous LDH release. Results were significantly ($p < 0.01$) lower than the high control, which determines the maximum releasable LDH activity in the cells and corresponds to the maximum LDH release.

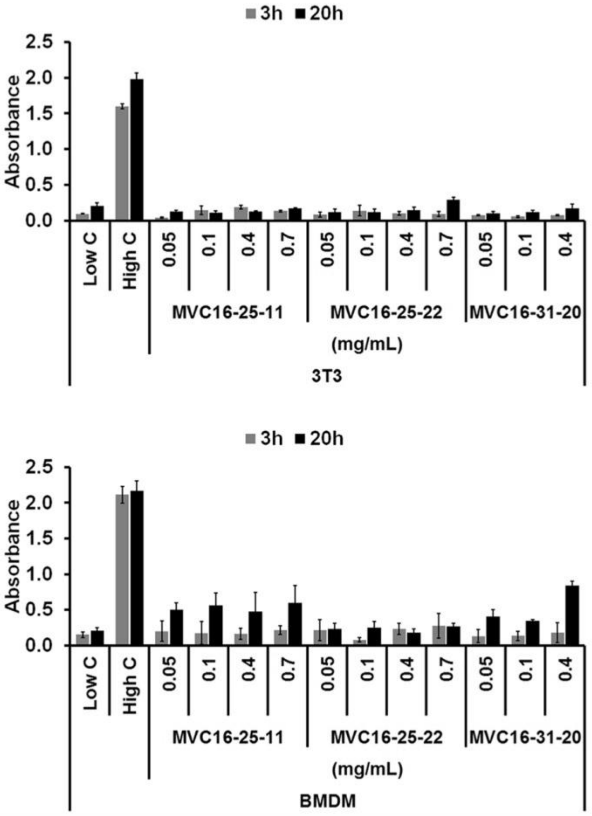

Figure 2. Cytotoxic effect of mannan nanogel, at the indicated concentrations, in mouse embryo fibroblast 3T3 cells and BMDM, assessed with the LDH assay. Results represent the mean ± S.D. of the obtained absorbance measurements at 3 and 20 h of incubation of the different nanogel samples, low control (Low C) and high control (High C), as indicated. Statistical significant differences ($p < 0.01$) within results were obtained with all tested concentrations of different nanogel samples in comparison with the High C, at same incubation period, for both fibroblasts and macrophages. The results shown are from one experiment, representative of two independent experiments.

The nontoxicity of mannan nanogel to mouse embryo fibroblast 3T3 cells and mouse BMDM, after 24 h of incubation, was further confirmed by Live/Dead assay (Figure 3).

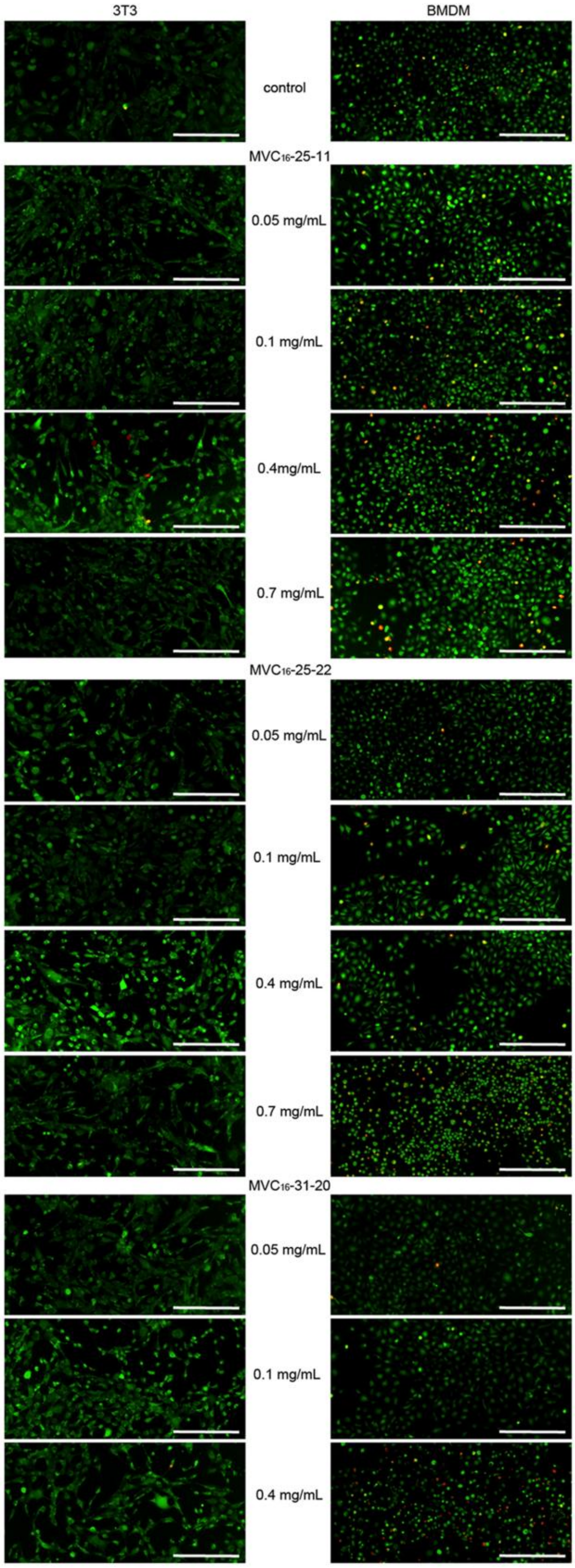

Figure 3. Fluorescence images of mouse embryo fibroblast 3T3 cells (left) and BMDM (right) stained using a Live/Dead® viability/cytotoxicity kit at 24 h of incubation in absence (control) or presence of mannan nanogel. Live cells are stained in green and dead cells are stained in red (scale bar = 200 μm).

The Live/Dead assay is a two-color fluorescence cell viability assay, that measures intracellular esterase activity and plasma membrane integrity, based on the simultaneous determination of live (green fluorescence) and dead cells (red fluorescence) with two probes, which are calcein, a polyanionic dye retained within living cells, and an ethidium homodimer-1 dye that enters the cells through damaged membranes, binding to nucleic acids, but is excluded by the intact plasma membrane of living cells. Only morphological changes were detected in life mouse BMDM for MVC_{16}-25-22 at 0.7 mg/mL and MVC_{16}-31-20 at 0.4 mg/mL, where the number of dead cells was slightly bigger when compared with the control.

The alkaline comet assay (or single cell gel electrophoresis assay) is a useful technique for the evaluation of DNA damage at the single cell level and is a sensitive biological indicator in the evaluation of the genotoxicity in cell lines or primary cells.[22-25] The comet assay is based on the ability of negatively charged loops/fragments of DNA to be drawn through an agarose gel under the force of an electric field. The extent of DNA migration is dependent on the DNA damage within cells.[25, 26] The advantages of using the comet assay, comparatively to other genotoxicity tests, include its high sensitivity for detecting low levels of both single and double stranded breaks in damaged DNA, the requirement for small numbers of eukaryotic cells per sample, flexibility, low cost, and ease and rapid of application.[25-27]

Comet assay has been described as a reproducible assay to evaluate nanoparticles genotoxicity.[28-33] Upon fluorescent staining, a “comet”-like structure is visualized with a circular head and a tail extending toward the anode due to the overall negative charge of DNA damaged. The genotoxicity caused by mannan nanogel at 0.1 and 0.4 mg/mL was evaluated in comparison to control (untreated cells) after 24 and 48 h of incubation, attending the tail intensity (%), which is expected to be proportional to the level of single strand breaks, crosslinks and alkalilabile sites (Table 2). The nanogel does not induce DNA damage in mouse embryo fibroblast 3T3 cells under the concentrations tested, as the negative control and samples with nanogel presented similar results. A statistically significant ($p < 0.01$) induction of DNA damage was observed in mouse BMDM after 24 h of exposure to 0.4 mg/mL and after 48 h of exposure to 0.1 mg/mL of mannan nanogel as compared to the respective control cells.

Table 2. DNA damage in mouse embryo fibroblast 3T3 cells and BMDM caused by mannan nanogel at 0.1 and 0.4 mg/mL in comparison with control (untreated cells) after 24 and 48 h of incubation, expressed in tail DNA intensity (%). The results shown are from one representative experiment preformed in duplicate

Tail DNA Intensity (%)			
		MVC_{16}-31-20	
	control	0.1 mg/mL	0.4 mg/mL
		3T3	
24 h	3.03 ± 3.86	2.04 ± 2.34	2.51 ± 2.82
48 h	2.37 ± 4.36	5.05 ± 4.48	4.83 ± 5.49
		BMDM	
24 h	9.76 ± 9.84	13.77 ± 11.63	26.48 ± 19.45**
48 h	7.39 ± 12.80	16.00 ± 13.07**	8.78 ± 9.23

(mean ± S.D., ** $p < 0.01$)

Uptake of mannan nanogel by the BMDM

The full viability of cells was ensured for the experimental concentration of 0.1 mg/mL used throughout confocal studies. Z-series confocal images of fixed phagocytic BMDM revealed that mannan nanogel is internalized in presence of LPS/IFN-γ. Upon internalization mannan nanogel labeled with SAMSA fluorescein (in green) is apparently present in vesicles, as could be inferred from the non-even distribution over the cytoplasm, and concentration of the fluorescence in internalized structures (Figure 4). Similar internalization results were obtained in the absence of LPS/IFN-γ (data not shown).

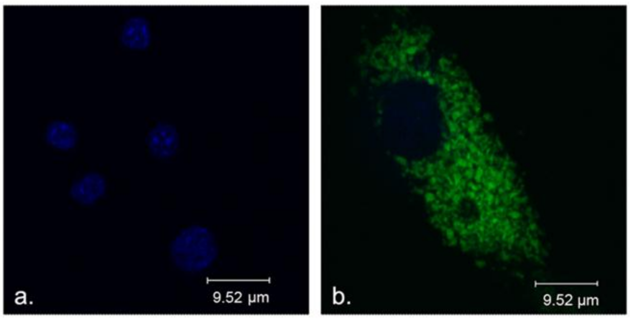

Figure 4. Confocal images of mouse BMDM incubated 6 h (*a*) without and (*b*) with mannan nanogel labeled with SAMSA fluorescein at 0.1 mg/mL (green fluorescence). Nuclei of fixed cells are stained with DAPI (blue fluorescence). Images correspond to a central Z-stack of a representative experiment preformed in duplicate.

In live cells studies, cell viability was guaranteed at all confocal conditions and parameters, such as lasers intensity, temperature, CO_2, fluoroprobes concentration, time of incubation, number z-series and time-series. In the absence of nanogel (control) cells labeled with DAPI, FM 4-64 and PI showed residual cell death randomly distributed in all fluorodish over time analysis (data not shown).

The visual-based evaluation of the extent of colocalization is prone to error and bias, as the “amount of yellow” resultant from the superposition of one fluorescence image, pseudo-colored “green”, on image two, colored “red” depends on the brightness of the merged images, the monitor settings, as well as the viewer’s perception. Qualitative colocalization based on an image-overlay method was not possible due to the lower resultant green signal from the labeled nanogel when compared with the red signal intensity of FM 4-64. Therefore the colocalization was quantified in cytoplasm by image analysis. Colocalization can be explained as an existence of the signal generated by two or more different fluorochromes at the same three-dimensional volume, voxel, when examining multichannel fluorescence microscopy images of a sample region. The colocalization of two or more markers within cellular structures gives information about structural and functional characteristics of the molecular populations[34] but not necessarily means molecular interaction or functional relationship. Colocalization coefficient in total pixels area (C_T) obtained by threshold-based analysis (annotation) increased over time when cells were incubated with nanogel and FM 4-64 in culture medium showing the entrance of labeled nanogel and of FM 4-64 to the cytoplasm of the viable cells. When nanogel and FM 4-64 were removed and cells were incubated in fresh medium, C_T reduced over time of incubation denoting the exit of both FM 4-64 and labeled nanogel from the cells. One hour was not enough for cells to release all previously internalized nanogel and FM 4-64 (Figure 5 and Table 3). According to the C_T values the entrance and exit of nanogel and FM 4-64 in BMDM are associated. As FM 4-64 is a marker of endocytosis and exocytosis in eukaryotic cells, it is plausible that mannan nanogel entrance and exit in BMDM occurs by the same processes. More studies are necessary to better understand the macrophage uptake mechanism of mannan nanogel.

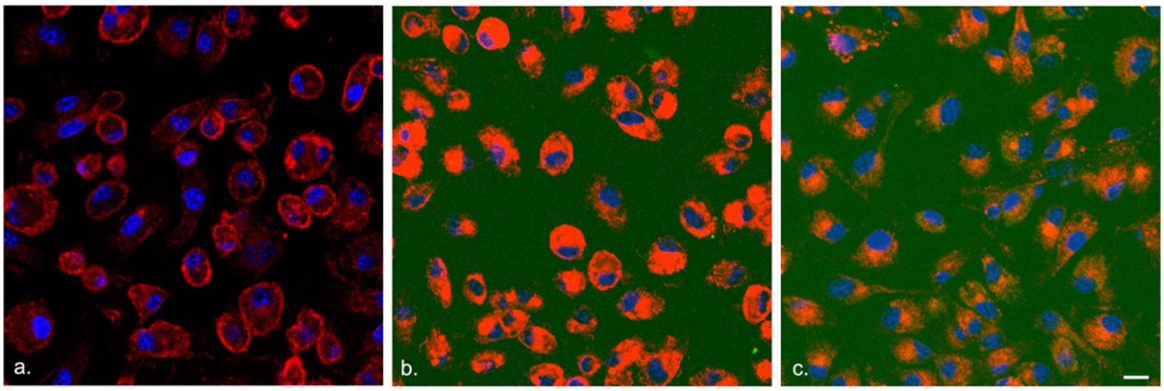

Figure 5. Confocal microscopy analysis of entrance and exit of mannan nanogel using live mouse BMDM. Confocal images at a certain Z-stack (scale bar = 10 μm) of a representative experiment of three independent experiments: (*a*) control cells labeled with DAPI (blue fluorescence) and FM 4-64 (red fluorescence); (*b*) cells after 3 h of incubation with the nanogel at 0.1 mg/mL (green fluorescence) and FM 4-64 present in culture medium; (*c*) cells after 1 h of incubation in fresh culture medium. PI was used to screen the viability of the cells.

Table 3. Colocalization coefficient C_T calculated by confocal image analysis throughout the entrance and exit of mannan nanogel and FM 4-64 in cytoplasm of mouse BMDM

Entrance		Exit	
time (h)	C_T	time (h)	C_T
Control	0.00	0	0.50
0.5	0.19	0.25	0.46
0.75	0.39	0.5	0.42
1	0.34	0.75	0.43
1.25	0.28	1	0.43
1.5	0.38		
1.75	0.40		
2	0.43		
2.25	0.46		
2.5	0.41		
2.75	0.45		
3	0.51		

Conclusions

The mannan nanogel is biocompatible to mouse embryo fibroblast 3T3 cells and mouse BMDM. Essentially, no cytotoxic effect was observed with mannan nanogel up to about 0.4 mg/mL in *in vitro* experiments using MTS, LDH, Live/Dead assays, and no significant differences were caused by differences in the DS of batches. Cell survival rate only dropped significantly at higher tested concentration after 48 h of incubation. Comet assay, under tested conditions, revealed no DNA damage in mouse embryo fibroblast 3T3 cells but possible DNA damage in mouse BMDM. Upon internalization by mouse BMDM mannan nanogel is localized in vesicles, as judged by the non-even distribution over the cytoplasm, and concentration of the fluorescence in internalized structures. Exit of nanogel from the mouse BMDM was observed when cells were incubated in fresh medium. Confocal colocalization image analysis denotes that the entrance and exit of nanogel and FM 4-64 might occur by the same processes – endocytosis and exocytosis – in BMDM.

References

1. Ahsan, F.; Rivas, I. P.; Khan, M. A.; Torres Suárez, A. I. Targeting to macrophages: role of physicochemical properties of particulate carriers - liposomes and microspheres - on the phagocytosis by macrophages. *J Control Release* **2002**, 79, 29-40.

2. Park, M. V.; Lankveld, D. P.; van Loveren, H.; de Jong, W. H. The status of in vitro toxicity studies in the risk assessment of nanomaterials. *Nanomedicine (Lond)* **2009**, 4, 669-685.

3. Jones, C. F.; Grainger, D. W. In vitro assessments of nanomaterial toxicity. *Adv Drug Deliv Rev* **2009**, 61, 438-456.

4. Ferreira, S. A.; Pereira, P.; Sampaio, P.; Coutinho, P. J. G.; Gama, F. M. Supramolecular assembled nanogel made of mannan. *J Colloid Interface Sci* **2011**, 361, 97-108.

5. Apostolopoulos, V.; Pietersz, G. A.; Loveland, B. E.; Sandrin, M. S.; McKenzie, I. F. Oxidative/reductive conjugation of mannan to antigen selects for T1 or T2 immune responses. *Proc Natl Acad Sci USA* **1995**, 92, 10128-10132.

6. Gu, X. G.; Schmitt, M.; Hiasa, A.; Nagata, Y.; Ikeda, H.; Sasaki, Y.; Akiyoshi, K.; Sunamoto, J.; Nakamura, H.; Kuribayashi, K.*, et al.* A novel hydrophobized polysaccharide/oncoprotein complex vaccine induces in vitro and in vivo cellular and humoral immune responses against HER2-expressing murine sarcomas. *Cancer Res* **1998**, 58, 3385-3390.

7. Sihorkar, V.; Vyas, S. P. Potential of polysaccharide anchored liposomes in drug delivery, targeting and immunization. *J Pharm Pharm Sci* **2001**, 4, 138-158.

8. Gupta, A.; Gupta, R. K.; Gupta, G. S. Targeting cells for drug and gene delivery: Emerging applications of mannans and mannan binding lectins. *J Sci Ind Res* **2009**, 68, 465-483.

9. Kaur, A.; Jain, S.; Tiwary, A. K. Mannan-coated gelatin nanoparticles for sustained and targeted delivery of didanosine: in vitro and in vivo evaluation. *Acta Pharm* **2008**, 58, 61-74.

10. Kim, T. H.; Jin, H.; Kim, H. W.; Cho, M.-H.; Cho, C. S. Mannosylated chitosan nanoparticle-based cytokine gene therapy suppressed cancer growth in BALB/c mice bearing CT-26 carcinoma cells. *Mol Cancer Ther* **2006**, 5, 1723-1732.

11. Avrameas, A.; McIlroy, D.; Hosmalin, A.; Autran, B.; Debre, P.; Monsigny, M.; Roche, A. C.; Midoux, P. Expression of a mannose/fucose membrane lectin on human dendritic cells. *Eur J Immunol* **1996**, 26, 394-400.

12. Fukasawa, M.; Shimizu, Y.; Shikata, K.; Nakata, M.; Sakakibara, R.; Yamamoto, N.; Hatanaka, M.; Mizuochi, T. Liposome oligomannose-coated with neoglycolipid, a new candidate for a safe adjuvant for induction of CD8+ cytotoxic T lymphocytes. *FEBS Lett* **1998**, 441, 353-356.

13. Apostolopoulos, V.; McKenzie, I. F. Role of the mannose receptor in the immune response. *Curr Mol Med* **2001**, 1, 469-474.

14. Cui, Z.; Mumper, R. J. Topical immunization using nanoengineered genetic vaccines. *J Control Release* **2002**, 81, 173-184.

15. Shiku, H.; Wang, L.; Ikuta, Y.; Okugawa, T.; Schmitt, M.; Gu, X.; Akiyoshi, K.; Sunamoto, J.; Nakamura, H. Development of a cancer vaccine: peptides, proteins, and DNA. *Cancer Chemother Pharmacol* **2000**, 46 Suppl, S77-82.

16. Tushinski, R. J.; Oliver, I. T.; Guilbert, L. J.; Tynan, P. W.; Warner, J. R.; Stanley, E. R. Survival of mononuclear phagocytes depends on a lineage-specific growth factor that the differentiated cells selectively destroy. *Cell* **1982**, 28, 71-81.

17. Warren, M. K.; Vogel, S. N. Bone marrow-derived macrophages: development and regulation of differentiation markers by colony-stimulating factor and interferons. *J Immunol* **1985**, 134, 982-989.

18. Zhang, X.; Goncalves, R.; Mosser, D. M. The isolation and characterization of murine macrophages. *Curr Protoc Immunol* **2008**, Chapter 14, Unit 14.11.

19. Singh, N. P.; McCoy, M. T.; Tice, R. R.; Schneider, E. L. A simple technique for quantitation of low levels of DNA damage in individual cells. *Exp Cell Res* **1988**, 175, 184-191.

20. Mosmann, T. Rapid colorimetric assay for cellular growth and survival: application to proliferation and cytotoxicity assays. *J Immunol Methods* **1983**, 65, 55-63.

21. Barltrop, J. A.; Owen, T. C.; Cory, A. H.; Cory, J. G. 5-(3-carboxymethoxyphenyl)-2-(4,5-dimethylthiazolyl)-3-(4-sulfophenyl)tetrazolium, inner salt (MTS) and related analogs of 3-(4,5-dimethylthiazolyl)-2,5-diphenyltetrazolium bromide (MTT) reducing to purple water-soluble formazans As cell-viability indicators. *Bioorg Medicinal Chem Lett* **1991**, 1, 611-614.

22. Anderson, D.; Plewa, M. J. The international comet assay workshop. *Mutagenesis* **1998**, 13, 67-73.

23. Anderson, D.; Yu, T.-W.; McGregor, D. B. Comet assay responses as indicators of carcinogen exposure. *Mutagenesis* **1998**, 13, 539-555.

24. Collins, A. The comet assay for DNA damage and repair: principles, applications, and limitations. *Mol Biotechnol* **2004**, 26, 249-261.

25. Tice, R. R.; Agurell, E.; Anderson, D.; Burlinson, B.; Hartmann, A.; Kobayashi, H.; Miyamae, Y.; Rojas, E.; Ryu, J. C.; Sasaki, Y. F. Single cell gel/comet assay: Guidelines for in vitro and in vivo genetic toxicology testing. *Environ Mol Mutagen* **2000**, 35, 206-221.

26. Collins, A. R.; Oscoz, A. A.; Brunborg, G.; Gaivão, I.; Giovannelli, L.; Kruszewski, M.; Smith, C. C.; Stetina, R. The comet assay: topical issues. *Mutagenesis* **2008**, 23, 143-151.

27. Collins, A. R.; Dobson, V. L.; Duinská, M.; Kennedy, G.; Stetina, R. The comet assay: what can it really tell us? *Mutat Res* **1997**, 375, 183-193.

28. Dandekar, P. P.; Jain, R.; Patil, S.; Dhumal, R.; Tiwari, D.; Sharma, S.; Vanage, G.; Patravale, V. Curcumin-loaded hydrogel nanoparticles: Application in anti-malarial therapy and toxicological evaluation. *J Pharm Sci* **2010**, 99, 4992-5010.

29. Vevers, W.; Jha, A. Genotoxic and cytotoxic potential of titanium dioxide (TiO_2) nanoparticles on fish cells in vitro. *Ecotoxicology* **2008**, 17, 410-420.

30. Barnes, C. A.; Elsaesser, A.; Arkusz, J.; Smok, A.; Palus, J.; Lesniak, A.; Salvati, A.; Hanrahan, J. P.; Jong, W. H. d.; Dziubałtowska, E.*, et al.* Reproducible comet assay of amorphous silica nanoparticles detects no genotoxicity. *Nano Lett* **2008**, 8, 3069-3074.

31. Barillet, S.; Jugan, M. L.; Laye, M.; Leconte, Y.; Herlin-Boime, N.; Reynaud, C.; Carrière, M. In vitro evaluation of SiC nanoparticles impact on A549 pulmonary cells: Cyto-, genotoxicity and oxidative stress. *Toxicol Lett* **2010**, 198, 324-330.

32. Sathya, T. N.; Vardhini, N. V.; Balakrishnamurthy, P. Revolution of ‘nano’ in in-vitro genetic toxicology. *J Cell Tissue Res* **2010**, 10, 2389-2396.

33. Ng, C. T.; Li, J. J.; Bay, B. H.; Yung, L. Y. Current studies into the genotoxic effects of nanomaterials. *J Nucleic Acids* **2010**, 2010,

34. Zinchuk, V.; Zinchuk, O.; Okada, T. Quantitative colocalization analysis of multicolor confocal immunofluorescence microscopy images: pushing pixels to explore biological phenomena. *Acta Histochem Cytochem* **2007**, 40, 101-111.

Chapter 6

Unraveling the uptake mechanism of mannan nanogel in bone marrow-derived macrophages

Characterizing the cellular entry of nanomedicines has become central to the field of drug and vaccine delivery because, depending on the route of uptake and intracellular trafficking, their cellular fate and the resultant responses might be different. A self-assembled mannan nanogel has been developed as a vaccination platform for antigen and adjuvant delivery. Mannan nanogel uptake profile by mouse bone marrow-derived macrophages is found to be time-, concentration- and energy-dependent, involving mannose receptor-mediated phagocytosis and clathrin-mediated endocytosis. The nanogel is also visualized in the cytosol suggesting endolysosomal escape. These results indicate that mannan nanogel is a promising versatile carrier for intracellular delivery of vaccines or therapeutic agents.

Introduction

Nanoparticles (NPs) are suitable systems for intracellular delivery of vaccines or therapeutic agents, such as proteins or genes. Nanosystems physicochemical properties, such as size, shape, chemical composition and functionality, hydrophilicity/hydrophobicity, surface chemistry and charge,[1-8] by affecting protein adsorption on the colloids, influence mechanisms involved in nanomaterial-cell interactions, endocytosis, intracellular trafficking and, therefore, resultant cellular responses.[7, 9-11] Minor variations in NPs size and surface charge, or the usage of different cell lines, modified their uptake process as exemplified by NPs made of chitosan with high surface charge and large particle size, which were phagocytozed more efficiently by murine macrophages.[12] In another example, the uptake rate, the mechanism of internalization and the concentration of internalized hydrogel NPs by RAW 264.7 murine macrophage cells was shown to be correlated with the NPs mechanical properties.[13] Therefore, full characterization of the relationship between NPs features and their internalization mechanisms is necessary for controlled delivery.

The cell uptake of nanomaterials can occur by phagocytosis and/or pinocytosis and their intracellular fate may vary with the cell type and/or cell phenotype and growing conditions.[5, 6, 8, 14] Phagocytosis is a dynamin-dependent actin-based mechanism characteristic of specialized professional phagocytes, such as macrophages, neutrophils, monocytes and dendritic cells. Particles to be phagocytozed may bind the phagocyte surface through specific receptors, such as Fc, complement, mannose and scavenger receptors. The resultant phagosome and its contents undergo maturation through a series of fusion and fission events, which lead to the transfer of the cargo to the late phagosomes and ultimately lysosomes to form a phagolysosome.[8, 11] In contrast, pinocytosis exists in almost all cell types, though each cell will have a distinct profile of endocytic uptake routes, such as macropinocytosis, clathrin-mediated endocytosis, caveolae-mediated endocytosis, or clathrin/caveolae independent endocytosis. In these endocytic routes, vesicles differ in their coat composition and size as well as in the fate of the internalized material.[15] In clathrin-mediated endocytosis ligand-bound receptors are internalized into clathrin-coated vesicles and their final scission from the plasma membrane involves the GTPase dynamin. Once invaginated the clathrin coat is shed and the vesicle then fuses with an early or sorting endosome. The cell cytoskeleton in many cases then defines spatial regulation and movement of the endocytic vesicle towards the interior of the cells. Receptor-ligand complexes are separated by low pH, generated by vacuolar proton ATPases. The fate of the ligand and receptor is then varied as some are transferred to trans-Golgi network, trafficked together to late endosomes and lysosomes for degradation, or the ligand and receptor are recycled in early and recycling endosomes.[8, 16, 17] Caveolae consist of plasma membrane microdomains enriched in caveolins, cavins, cholesterol and sphingolipids.[18, 19] The uptake kinetics of caveolae-mediated endocytosis occurs at a much slower rate than that of clathrin-mediated endocytosis.[20, 21] There is data to suggest that caveolae vesicles can translocate to the endoplasmic reticulum or to the Golgi complex,[18, 22] enter the endosomal pathway[19] or in some cases, bypass lysosomes.[8] Caveolae-mediated endocytosis is the most prominent transendothelial pathway.[8]

NPs may be internalized by multiple or single pathways. Cellular uptake profile of hydrophobically modified glycol chitosan NPs in human epithelial carcinoma (HeLa) cells is time- and dose-dependent, with several distinct uptake pathways involved, such as macropinocytosis, clathrin- and caveolae-mediated endocytosis.[23] On the other hand, the uptake of poly(-D,L-lactide-co-glycolide) (PLGA) NPs in human arterial smooth muscle cells (HASMCs) is an energy dependent process, mediated by clathrin- but not by caveolae-mediated endocytosis.[24] In another example, the uptake of non- and chitosan-modified PLGA nanospheres by human lung adenocarcinoma (A549) cells is a time-, temperature-, concentration-dependent and saturable event mediated by clathrin-mediated endocytosis.[25]

We recently showed that the self-assembled amphiphilic mannan – mannan nanogel – has long-term stability, spherical shape, polydisperse size distribution, near neutral surface charge and mean hydrodynamic diameter of 50–140 nm.[26] Mannan nanogel is being developed in our laboratory as a vaccination platform. Therefore, in this work, the phagocytic cell internalization kinetics and uptake mechanism(s) of fluorescein-labeled mannan nanogel were evaluated by flow cytometric (FACS) analysis and confocal laser scanning microscopy (CLSM) using several endocytic inhibitors. Intracellular trafficking pathway(s) were also studied by CLSM.

Experimental

Materials

Mannan-VMA-SC_{16} (VMA: vinyl methacrylate, SC_{16}: hydrophobic alkyl chain) was synthesized as described previously[26] with 31 acrylate groups (DS_{VMA} 31%) and 20 alkyl chains (DS_{C16} 20%) per 100 mannose residues. Resultant amphiphilic mannan is named MVC_{16}-31-20. Organic and inorganic reagents of laboratory grade were purchased from Sigma (St Louis, Missouri, USA) and used without any further purification. All cell culture products were purchased from Sigma, unless otherwise specified.

Preparation of self-assembled SAMSA fluorescein-labeled mannan nanogel

Mannan nanogel covalently labeled with 5-((2-(and-3)-S-(acetylmercapto)succinoyl) amino)fluorescein (SAMSA fluorescein; Molecular Probes, Invitrogen, Carlsbad, California, USA) resulted from the reaction between the thiol group of SAMSA fluorescein with the grafted methacrylate not substituted with SC_{16} of MVC_{16}-31-20, as previously described.[26] To remove any residual unconjugated fluorescein, obtained sterile stock colloidal dispersion of labeled MVC_{16}-31-20 (2 mg/mL) was repeatedly washed by ultrafiltration (Amicon® Ultra-4 Centrifugal Filter Units, molecular weight cut-off, 5×10^3; Millipore, Billerica, Massachusetts, USA) with sterile pyrogen-free phosphate buffered saline (PBS) until no fluorescence was detected in the filtrate. The degree of labeling was determined from the absorbance of the labeled nanogel at 495 nm recorded in V560 spectrophotometer (JASCO, UK) and the nanogel formation was confirmed by dynamic light scattering (DLS; Malvern Zetasizer NANO ZS - Malvern Instruments Limited, UK), as was previously described.[26] Fluorescence emission spectra were recorded in a Spex Fluorolog 3 spectrofluorimeter (Horiba Jobin Yvon IBH Ltd).

Cell culture

Female BALB/c mice (6–8 weeks old) were purchased from Charles River (Barcelona, Spain). Animals were kept at the animal facilities of the Institute Abel Salazar during the experiments. Hiding and nesting materials were provided as enrichment. Procedures involving mice were performed according to the European Convention for the Protection of Vertebrate Animals used for Experimental and Other Scientific Purposes (ETS 123) and 86/609/EEC Directive and Portuguese rules (DL 129/92). In order to obtain bone marrow-derived macrophages (BMDM), femurs and tibias were collected under aseptic conditions and flushed with Hanks' balanced salt solution. The resulting cell suspension was centrifuged at 500 g and resuspended in RPMI 1640 medium supplemented with 4-(2-hydroxyethyl)-1-piperazineethanesulfonic acid (HEPES; 10 mM), 10% heat-inactivated fetal bovine serum (FBS), penicillin (60 IU/mL), streptomycin (60 µg/mL), β-mercaptoethanol (0.5 mM) (complete RPMI [cRPMI]), and 10% L929 cell conditioned medium (LCCM). To remove fibroblasts or differentiated macrophages, cells were cultured, on cell culture dishes (Sarstedt, Canada), overnight at 37 ºC in a 5% CO_2 atmosphere. Then, nonadherent cells were collected with warm cRPMI, centrifuged at 500 g, resuspended in cRPMI at a density of 5×10^5 cells/mL and distributed 1×10^6 cells/fluorodish (WPI, UK) or 5×10^5 cells/well in 24-well plates (Sarstedt). Cells were incubated at 37 °C in a 95% humidified atmosphere containing 5% CO_2. Four days after seeding, 10% of LCCM was added, and the medium was renewed on the seventh day. After ten days in culture, cells were completely differentiated into macrophages. This method allows for the differentiation of a homogenous primary culture of macrophages that retain the morphological, physiological and surface markers characteristics of these phagocytic cells.[27-29]

Kinetics of mannan nanogel internalization by BMDM

The BMDM seeded in 24-well plates (Sarstedt) were incubated at 37 °C in a 95% humidified atmosphere containing 5% CO_2 for 0, 0.5, 1, 2, 6 and 16 h, with SAMSA fluorescein-labeled nanogel in cRPMI (0.01, 0.05 and 0.1 mg/mL) or only with cRPMI (negative control). Then, cells were washed twice with PBS and detached mechanically in 400 µL of PBS with 10 mM of sodium azide and 1% of bovine serum albumin (FACS buffer). The cell suspension of each well was divided in two aliquots and transferred into polystyrene tubes for FACS analysis in a FACScan flow cytometer (Becton Dickinson, San Jose, California, USA) using the CellQuest software (Becton Dickinson) before and after adding 1 µL of propidium iodide (PI; 500 ng/mL) or 40 µL of trypan blue (2.5 mg/mL) to different aliquots. Data were collected for 20,000 live cells per sample. Before FACS analysis samples were kept at 4 ºC and protected from light. Dead cells were excluded from the analysis by PI incorporation.

Mechanism of mannan nanogel uptake by BMDM

Inhibitors

Uptake mechanism and intracellular fate of the labeled mannan nanogel in BMDM was studied by using inhibitors at the following concentrations and pre-incubation periods for internalization pathway analysis: sodium azide (NaN_3; 0.1% w/v) and 6-deoxyglucose (50 mM) for 30 min;[7, 24] cytochalasin D (20 µM) for 1 h;[6, 30] mannan (200 µg/mL) for 30 min;[31] monodansylcadaverine (300 µM) for 1 h;[32] sucrose (450 mM) for 1 h;[24, 25] filipin (1 µg/mL) for 30 min;[7, 24, 25] brefeldin A (5 µM) for 1 h;[24] and nocodazole (33 µM) for 1 h.[6, 9] Control cells were incubated in the corresponding volume of drug diluent.

FACS analysis

To study the effect of the different inhibitors on the nanogel uptake, BMDM seeded in 24-well plates were pre-incubated with each inhibitor in cRPMI, at the conditions described above, at 37 °C in a 95% humidified atmosphere containing 5% CO_2. Cells were coincubated with each inhibitor, at the same concentration used for pre-incubation, together with SAMSA fluorescein-labeled nanogel (0.1 mg/mL) in cRPMI, for 1 h at 37˚C. BMDM were incubated with cRPMI (negative control), with labeled nanogel in cRPMI (positive control), or with the inhibitor in cRPMI. Then, cells were washed twice with PBS and mechanically detached in 600 µL PBS. The cell suspension of each well was divided in two aliquots that were transferred into polystyrene tubes for FACS analysis. Cells of one aliquot were washed in FACS buffer and immediately FACS analyzed. Cell autofluorescence was determined by the negative control. Dead cells were excluded by PI incorporation. A cell viability of 85% was arbitrarily chosen as the minimum allowable for use in uptake assays. Data were collected for 20,000 cells per sample. Cells of the other aliquot were fixed with 2% formaldehyde for 25 min at room temperature, protected from light. Then, cells were sequentially washed with PBS and with FACS buffer and analyzed. Cell autofluorescence was determined by using the negative control and data from 50,000 cells were collected per sample. Fluorescence of cells incubated with the inhibitors was compared to the positive control and the extent of inhibition was calculated as follows: inhibitory effect (%) = 100 – mean fluorescence intensity (MFI) inhibitor sample/MFI of positive control × 100.

Confocal Studies

For CLSM, BMDM plated in 24-well plates were mechanically detached in cRPMI and seeded (5×10^5 cells/well) on coverslips (Sarstedt). To study the effect of different inhibitors on the intracellular distribution of the labeled nanogel, cells were first pretreated with inhibitors as described above, together with Texas Red® transferrin (100 µg/mL; Molecular Probes, Invitrogen) or LysoTracker® Red DND-99 (2.5 µM; Molecular Probes, Invitrogen) – λ_{em} 612 nm – in cRPMI for 1 h. Texas Red transferrin labels early and recycling endosomes and LysoTracker, a live-cell acid sensitive probe, colorless at physiological pH, labels late endosomes and lysosomes. The early endocytic vesicles have physiological pH, early endosomes pH 5.9–6 and late endosomes and lysosomes pH 4.5–5.5.[33] Then the labeled nanogel was added (0.1 mg/mL) and cells were incubated for another hour at 37 °C in a 95% humidified atmosphere containing 5% CO_2. At that point, cells were washed twice with PBS, fixed with 2% formaldehyde for 25 min at room temperature, permeabilized with 0.1% Triton-100 in PBS for 5 min and incubated overnight at 4 ºC with 1:100 Alexa Fluor® 488 labeled anti-fluorescein/Oregon Green rabbit polyclonal IgG antibody (Molecular Probes, Invitrogen; λ_{em} 520 nm). This labeled anti-fluorescein antibody was used to amplify the detectable signal of the SAMSA fluorescein-labeled nanogel above the detector noise level. Cell nuclei were finally labeled with 4'-6-diamidino-2-phenylindole (DAPI; 120 ng/mL; λ_{em} 461 nm) for 5 min at room temperature. Each of the last four steps was followed by three washes with PBS. Results were compared with a positive control prepared as described before but without using any inhibitor. Control samples were prepared by using the same experimental conditions with each fluorophore separately for excitation cross-talk and bleed-through analysis or in the absence of staining to determine autofluorescence. Samples were observed with a confocal laser scanning microscope (Olympus BX61/FluoView™ - FV1000). Five Z-series with 0.75 µm Z spacing were obtained for each treatment by using the following microscope settings: 3 lasers (405 nm, 488 nm and 559 nm) in the three narrow bandwidth emission filter, sequential acquisition and Kalman filter mode, 60× oil objective with numerical aperture of 1.42, 2× optical zoom, and 800×800 pixel size with four detectors. Detector gains were set to be constant between samples to facilitate sample comparison.

Confocal image analysis

The experimental design, image acquisition (as detailed above), qualitative and quantitative evaluation were performed following guidelines previously described for colocalization purposes.[34-40] Fluorescence intensity measurements, qualitative evaluation of overlapping pixels by dye-overlay and threshold-overlap, and quantitative threshold-based analysis – annotation and statistics – were obtained with Olympus FluoView1000 (FV viewer v.2.0) software after removing unspecific events generated by noise and background. The annotation analysis provides the number of total (T), green (G), red (R), and colocalized (C) pixels and colocalization coefficients, such as colocalization coefficient in green (C_G, corresponding to the ratio between C and G), colocalization coefficient in red (C_R, corresponding to the ratio between C and R), colocalization coefficient in total pixels (C_T, corresponding to the ratio between C and T). The statistical analysis of the software provides the Pearson's correlation coefficient *rp,*[41, 42] the overlap coefficient *r,*[42] and colocalization coefficients M_1 (or M_{green}) and M_2 (or M_{red}).[36, 42] To calculate the relative extent of spatial overlap of SAMSA fluorescein-labeled nanogel and Texas Red transferrin or LysoTracker, the correlation, overlap and colocalization coefficients were tested because there is not a single colocalization coefficient that fully describes a particular situation. Pearson's correlation coefficient *rp*[41, 42] uses the information of all pixels and calculates the degree of correlation between the intensity grey values of the pixels in a dual-color image and only indirectly reflect probe colocalization. The *rp* values range from 1 for two images whose fluorescence intensities are perfectly, linearly related, to -1 for two images whose fluorescence intensities are perfectly, but inversely related to one another. Low (close to zero) and negative values of *rp* for fluorescent images can be difficult to interpret and might not necessarily mean random localization. Even if two probes colocalize on the same cellular structures, there may be no reason that they should colocalize in fixed proportion to one another. Unlike *rp*, the overlap coefficient *r* is almost independent of signal proportionality; instead it is primarily sensitive to colocalization.[42] Overlap coefficient *r* provides useful information only when the number of objects (pixels) in the red and green components are equal.[42] If not, colocalization coefficients M_1 and M_2 should be used.[42] They are proportional to the amount of fluorescence of the colocalizing objects in each component image, relative to the total fluorescence in that component;[42] instead of the overlapping pixel area alone, M_1 and M_2 weigh the area with the colocalized pixel intensity being in some way a hybrid between a pixel-based and an object-based measurement.[36] The degree of colocalization is defined as the ratio of the integral of the intensity distribution of colocalizing pixels and the total intensity in the component image studied.[36]

Colocalization measurements were obtained using a two-dimensional scatterplot of intensity ranges of red channel versus green channel where thresholds were defined using the controls results. The colocalization with SAMSA fluorescein-labeled nanogel was evaluated in "regions of interest" (ROIs) corresponding to early and recycling endosomes (labeled with Texas Red transferrin) or late endosomes and lysosomes (labeled with LysoTracker) with area greater than 12 $pixels^2$ randomly selected in 10 cells per experimental condition. The fluorescence intensity measurements were performed in two color three-dimensional microscopic images using ROIs corresponding to cytoplasm of 20 cells per experimental condition. The reported values represent the mean ± standard deviation (S.D.) of inhibitory effect (%) = 100 - MFI for the inhibitor sample/MFI of positive control × 100.

Statistical analysis

Statistical significance of the mean values of inhibitory effects (%) caused by different inhibitors, as evaluated by FACS analysis and CLSM image analysis was determined by Student's two-tailed unpaired t-test (at the 95% confidence interval) using GraphPad Prism version 4.00 for Windows (GraphPad Software, San Diego, California, USA). Statistical significant differences were labeled with a single asterisk ($p < 0.05$), two asterisks ($p < 0.01$), and three asterisks ($p < 0.001$).

Results and discussion

Physical properties of SAMSA fluorescein-labeled mannan nanogel

We initially determined if labeling with the SAMSA fluorescein had any effects on the physical properties of the nanogel. Using DLS colloidal dispersion of labeled nanogel in PBS (2 mg/mL) showed z-average equal to 168.0 ± 3.2 nm with polydispersity index (PdI) of 0.270 ± 0.008 and zeta potential of -11.8 ± 1.4 mV. These characteristics were similar to those observed for colloidal dispersion of non-labeled nanogel in PBS (2 mg/mL): z-average equal to 154.1 ± 5.6 nm with PdI of 0.229 ± 0.007 and zeta potential of -10.9 ± 1.4 mV. The colloidal dispersion of labeled nanogel in cRPMI (0.1 mg/mL) showed z-average equal to 163.8 ± 2.8 nm with PdI of 0.576 ± 0.084 and zeta potential of -11.5 ± 2.1 mV. The labeled nanogel formation was not affected by the presence of inhibitors as confirmed by DLS (Figure 1a).

The UV-Vis spectrum of labeled nanogel was defined with a sharp single peak with maximum absorbance at 495 nm of 0.9 ± 0.05 when at 2 mg/mL in PBS and of 0.03 ± 0.05 when at 0.1 mg/mL in cRPMI, characteristic of covalently linked fluorescein (according to the manufacturer). As previously reported,[26] size, zeta potential and UV-Vis spectrum of the colloidal dispersion in PBS was stable, if stored at 4 ºC in the dark. SAMSA fluorescein-labeled nanogel fluorescence emission spectrum in cRPMI was not affected by any of the inhibitors at the concentration used in uptake inhibition analysis (Figure 1b).

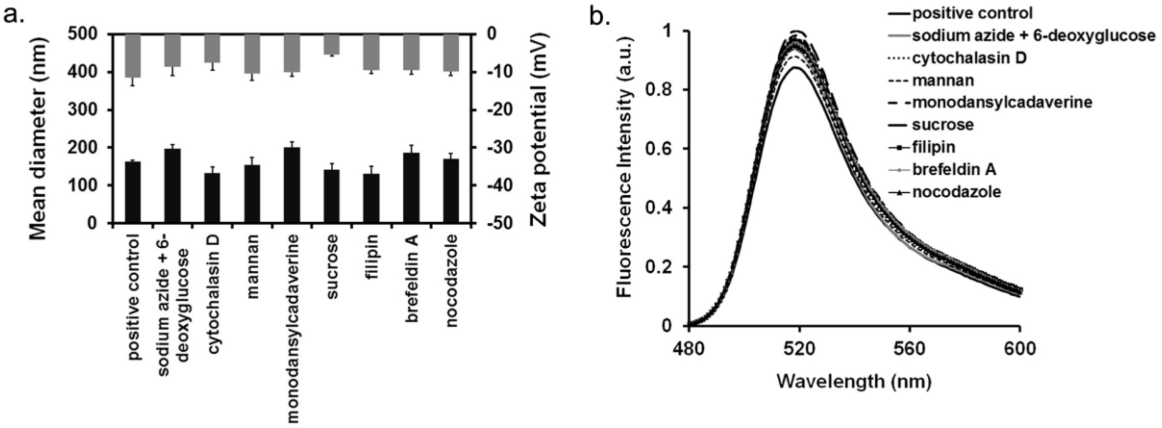

Figure 1. Physical properties of SAMSA fluorescein-labeled mannan nanogel: (*a*) the size and zeta potential calculated by DLS at 37 °C (mean ± S.D., *n* = 5) and (*b*) the fluorescence emission spectra of SAMSA fluorescein-labeled mannan nanogel in cRPMI (0.1 mg/mL) in absence (positive control) or in presence of different inhibitors at the concentration used in *in vitro* uptake inhibition analysis. The negative control (cRPMI only) emission spectrum was subtracted from the spectrum obtained in each condition.

Kinetics of mannan nanogel internalization by BMDM

In order to discriminate between internalized and surface-adherent SAMSA fluorescein-labeled mannan nanogel, samples were analyzed by FACS before and after the addition of trypan blue. Trypan blue is a vital dye incapable of penetrating intact cell membranes which is known to quench extracellular and surface-bound fluorescein fluorescence.[7, 14, 43] The MFI of BMDM incubated with labeled nanogel was not significantly different before and upon trypan blue addition (Table 1), indicating that the detected fluorescence was due to nanogel internalized by macrophages.

Mannan nanogel uptake by BMDM was found to be time- and concentration-dependent (Figure 2). After an initial linear stage during the first 4 h of incubation, a trend towards saturation in the internalization process was observed; this is typical of endocytosis of many probes [7, 13, 24, 25, 44] but gives no information on the fate of the nanogel.

Table 1. FACS analysis of mouse BMDM internalization of SAMSA fluorescein-labeled mannan nanogel at three different concentrations, before and after trypan blue addition. Results represent the MFI ± S.D. of duplicate samples of one experiment, representative of two independent experiments

Time (h)	0.01 mg/mL	0.05 mg/mL	0.1 mg/mL
0	15.63 ± 1.17	15.52 ± 1.07	15.53 ± 1.17
0.5	31.01 ± 1.03	85.40 ± 6.60	131.92 ± 14.04
1	43.98 ± 1.61	134.14 ± 23.99	212.74 ± 3.86
2	82.33 ± 14.18	319.69 ± 55.45	507.15 ± 22.89
6	158.35 ± 1.53	609.42 ± 73.72	1418.32 ± 161.15
16	298.79 ± 0.20	945.29 ± 53.38	1905.9 ± 220.4
		after trypan blue addition	
0	14.76 ± 1.16	14.76 ± 1.01	14.65 ± 1.01
0.5	26.42 ± 1.09	79.86 ± 8.02	132.85 ± 13.93
1	38.08 ± 1.92	130.78 ± 22.87	210.32 ± 3.23
2	77.18 ± 11.32	307.7 ± 34.92	449.99 ± 31.06
6	158.90 ± 1.33	667.5 ± 82.32	1412.41 ± 157.32
16	284.24 ± 0.60	1101.06 ± 134.15	1755.96 ± 243.92

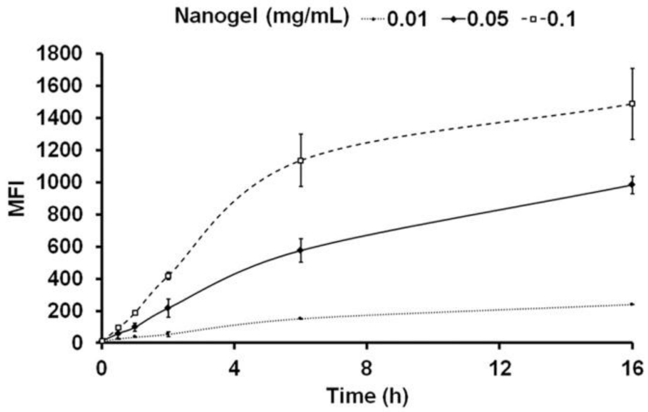

Figure 2. FACS analysis of mouse BMDM internalization of SAMSA fluorescein-labeled mannan nanogel at three different concentrations. Each point represents the MFI ± S.D. of duplicate samples of one experiment, representative of two independent experiments.

Uptake mechanism and intracellular fate of the mannan nanogel in BMDM

Eight inhibitory conditions were selected to examine the pathways of cellular uptake and intracellular trafficking of the mannan nanogel by using FACS and CSLM analysis.

In energy depletion conditions, due to a metabolic inhibitors mixture of NaN_3 and 6-deoxyglucose,[7] a 54 ± 5% reduction in the uptake of mannan nanogel detected by FACS analysis (Figure 3) suggests an active process of internalization. NaN_3 prevents the production of ATP by interfering with the glycolytic and oxidative metabolic pathways;[13] in the inhibitory conditions used in the assay, the mannan nanogel internalization was not fully blocked, as it has been observed in other cases reported in the literature.[13, 45, 46] A possible explanation for the partial blockade could lie on the presence of exogenous ATP and glucose in the culture medium.[12, 47] The inhibitory effect of energy depletion conditions was confirmed by using CLSM, as a reduction of nanogel internalization was also observed (Figures 4 and 5). A lower inhibitory effect was nevertheless observed in the assay carried out in the presence of Texas Red transferrin (Figure 4).

Cytochalasin D, a drug that disrupts F-actin filaments via actin depolymerization,[6] inhibited nanogel uptake by 43 ± 13%, as assessed by FACS analysis (Figure 3). F-actin has been shown to be involved in phagocytosis, macropinocytosis, and clathrin- and caveolae- mediated endocytosis.[48] A similar inhibitory effect of cytochalasin D was confirmed by confocal microscopy (Figures 4 and 5).

The mannose receptor (MR) is a cell surface receptor primarily expressed on antigen-presenting cells (APC), namely, macrophages and dendritic cells. MR-mediated phagocytosis[49] is an important pathway in antigen uptake for presentation in the context of major histocompatibility complex (MHC) class II molecules[50, 51] and MHC class I molecules,[52, 53] playing a key role in host defense and providing a link between innate and adaptive immunity.[54] As MR is a key molecule in antigen recognition, this receptor is a privileged target for vaccine and drug delivery to macrophages.[52, 55] Mannan nanogel endocytosis was significantly inhibited by competition with soluble mannan (inhibitory effect: 52 ± 1%, Figure 3). A similar effect was observed for soluble mannan inhibition by using confocal microscopy analysis (Figures 4 and 5). These results indicate that nanogel made of mannan targets the MR and that this receptor is involved in uptake of the nanogel.

The effect of clathrin-mediated endocytosis inhibition on nanogel uptake was tested by using monodansylcadaverin, which blocks the formation of clathrin-coated pits.[56] Inhibition of energy-dependent clathrin-mediated endocytosis was further tested via sucrose-induced hypertonicity, which prevents the assembly of clathrin-coated pits.[24, 25, 57] The uptake of the mannan nanogel in monodansylcadaverine-treated and sucrose-treated cells was markedly reduced, with an inhibitory effect of 75 ± 2% and 85 ± 2%, respectively, as determined by FACS analysis (Figure 3). A marked inhibition, however to a lesser extent, was also observed by using confocal microscopy (Figures 4 and 5). Transferrin is generally accepted as a ligand exclusively internalized via the clathrin-coated-pit pathway[9] and monodansylcadaverin and sucrose treatment similarly reduced, as expected, the uptake of the Texas Red conjugated probe by 70–80% (Figure 4). Altogether, these results indicate that clathrin-mediated endocytosis is also an internalization mechanism of mannan nanogel.

To examine clathrin-independent endocytosis, which includes caveolae-mediated endocytosis, cells were incubated with filipin, a cholesterol-binding drug that perturbs cholesterol function.[24, 58, 59] Filipin did not reduce the uptake of nanogel, as could be detected by FACS analysis (inhibitory effect: 8 ± 3%, Figure 3). A slight inhibitory effect of filipin in mannan nanogel uptake was however detected by CLSM (Figures 4 and 5). Although we cannot exclude that mannan nanogel uptake could also occur by caveolae-mediated endocytosis, this pathway would be a minor route of uptake for this nanogel.

Brefeldin A interferes with intracellular vesicular transport inducing tubulation of Golgi complex, endosomes and lysosomes.[60] Brefeldin A reduced the mannan nanogel uptake and intracellular trafficking in mouse BMDM. The inhibitory effect measured by FACS analysis corresponded to 43% (Figure 3), while it was less marked when evaluated by confocal image analysis (Figures 4 and 5).

Nocodazole inhibits endosome-lysosome trafficking by interfering with the microtubule network causing depolymerization of microtubules.[6, 61, 62] Nocadozole reduced the uptake of nanogel by 31 ± 3%, as measured by FACS analysis (Figure 3). A similar effect was observed by using CLSM (Figures 4 and 5) indicating that a dynamic microtubule network, which is important for vesicular transport, is necessary for mannan nanogel uptake.

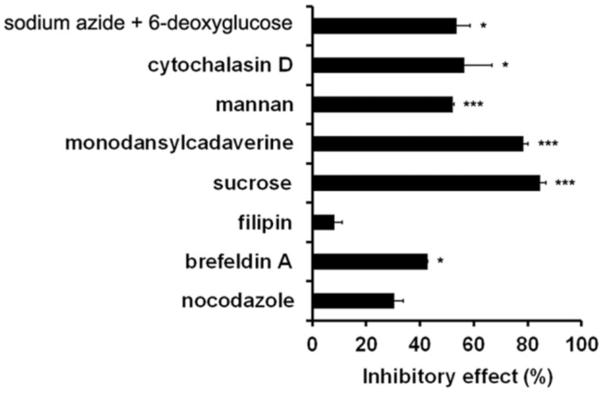

Figure 3. Uptake mechanism inhibition analysis of mannan nanogel by mouse BMDM. Results represent the mean of % inhibitory effect ± S.D. obtained by FACS analysis in a representative experiment performed in triplicate (* $p < 0.05$, ** $p < 0.01$ and *** $p < 0.001$).

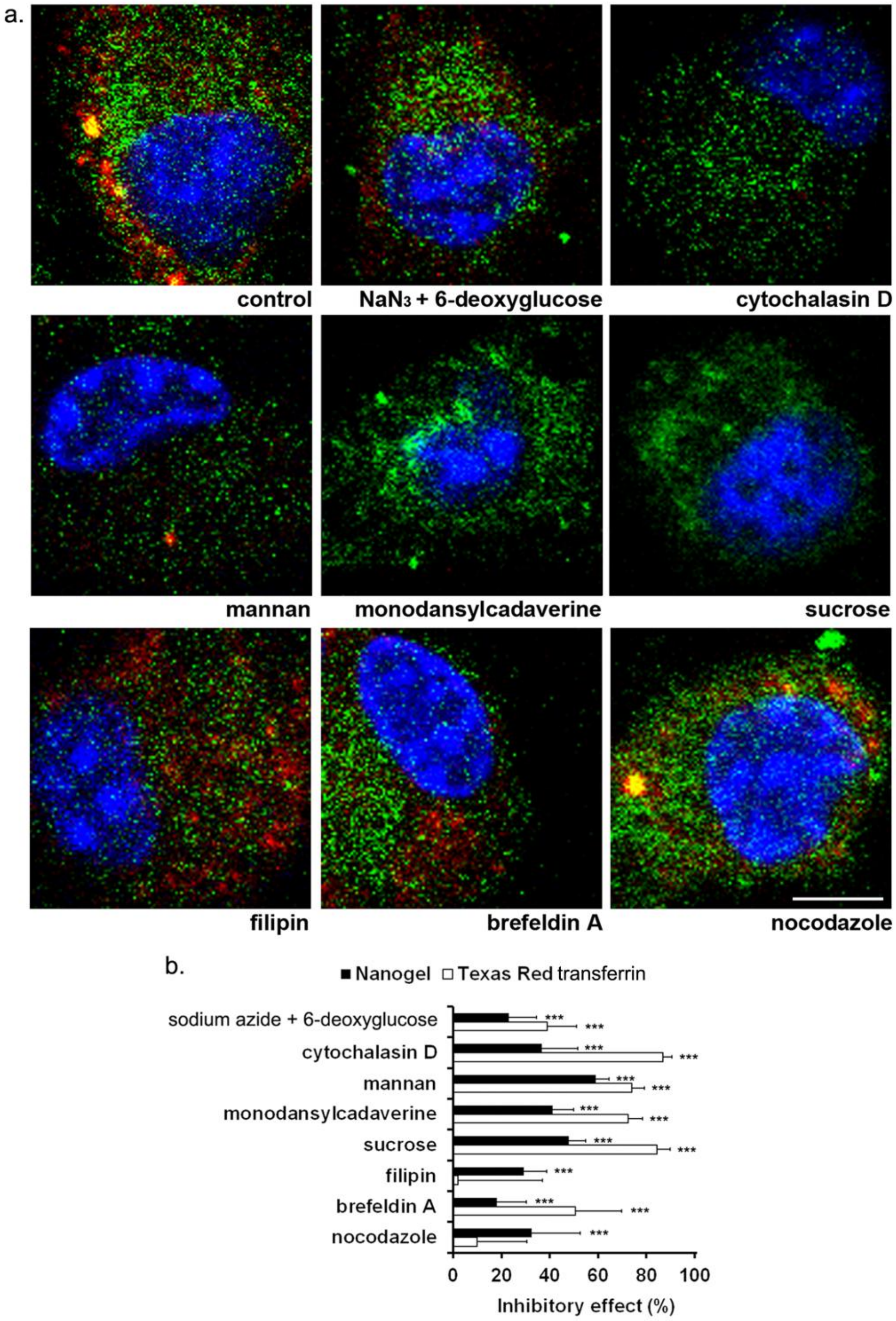

Figure 4. Confocal microscopy uptake and intracellular trafficking inhibition analysis of mannan nanogel in mouse BMDM. (*a*) Confocal images of a representative cell at a certain Z-stack (scale bar = 5 µm). Blue indicates DAPI-stained nuclei. (*b*) Fluorescence intensity measurements of Texas Red transferrin and SAMSA fluorescein-labeled nanogel present in the cytoplasm (mean of % inhibitory effect ± S. D.; *n* = 20; * $p < 0.05$, **$p < 0.01$ and ***$p < 0.001$) obtained by image analysis. Results are from one experiment representative of two independent experiments.

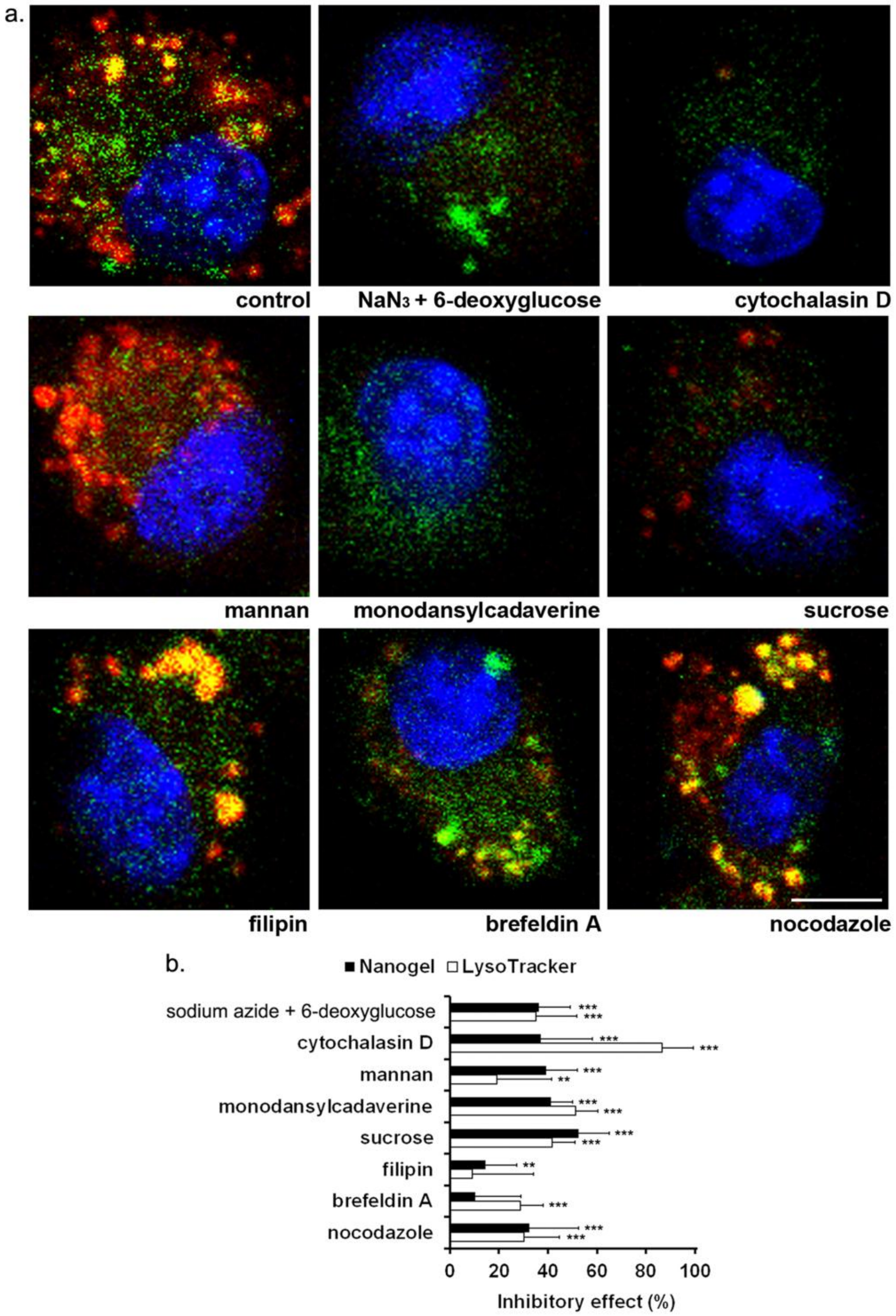

Figure 5. Confocal microscopy uptake and intracellular trafficking inhibition analysis of mannan nanogel by mouse BMDM. (*a*) Confocal images of a representative cell at a certain Z-stack (scale bar = 5 μm). Blue indicates DAPI-stained nuclei. (*b*) Fluorescence intensity measurements of LysoTracker and SAMSA fluorescein-labeled nanogel present in the cytoplasm (mean of % inhibitory effect ± S. D.; *n* = 20; * p < 0.05, **p < 0.01 and ***p < 0.001) obtained by image analysis. Results are from one experiment representative of two independent experiments.

The visual-based evaluation of colocalization is prone to error and bias, as the “amount of yellow” resulting from the superposition of one fluorescence image, pseudo-colored “green”, on image two, colored “red”, depends on the brightness of the merged images, the monitor settings, as well as the viewer’s perception. Therefore the fluorescence intensity was quantified by image analysis in ROIs corresponding to the cytoplasm, where the acquired intensity better reflects the concentration of fluoroprobes (Figures 4 and 5). Moreover, the colocalization was quantified by image analysis in ROIs corresponding to endosomes or lysosomes with area superior to 12 pixels^2 randomly selected in 10 cells per experimental condition. This design is very important because the inclusion of irrelevant pixels not corresponding to the cellular structures in study may lead to significant mistakes in the colocalization coefficients calculated.[40]

The inhibitory effect was evaluated by confocal image analysis in terms of fluorescence intensity of Texas Red transferrin and LysoTracker. The fluorescence intensity of Texas Red transferrin was drastically reduced in the presence of cytochalasin D, mannan, monodansylcadaverine, and sucrose and consequently early and recycling endosomes were impossible to isolate for colocalization evaluation (Figure 4). For the other used inhibitors and for the positive control, the degree of colocalization is shown in Table 2. The colocalization coefficients C_G, C_R, C_T, M_1 and M_2 were the most suitable choices in this study, because the number of objects (pixels) in the red and green components was different. When the number of pixels carrying an intensity above the threshold t is very different, overlap coefficient r does not provide useful information, and colocalization coefficients M_1 and M_2 are a proper choice because they are not dependent on the intensity of the signals.[42] Also, *rp* values obtained were close to zero, which might not necessarily mean random localization and are difficult to interpret. LysoTracker fluorescence was drastically reduced in the presence of cytochalasin D. Although the fluorescence observed in monodansylcadaverine-treated cells was not that affected, late endosomes and lysosomes were impossible to isolate for colocalization evaluation in both inhibitory conditions (Figure 5). The colocalization coefficients C_G, C_R, C_T, M_1 and M_2 indicated colocalization between green and red dyes in the positive control and in cells treated with each of the tested inhibitors, with the exception of sucrose (Table 2).

Colocalization assays with endosomal and lysosomal markers (red fluorescence) allowed the identification of the intracellular pathways followed by the labeled nanogel (green fluorescence) after internalization. Nanogel was found in the early and recycling endosomes, in the late endosomes and lysosomes, and in the cytosol but was not observed in the nucleus. We hypothesize that nanogel in early endosomes, may be either recycled to the surface or transported to the late endosomes, from which it may escape into the cytosol or end up in lysosomes. As scattered cytosolic green fluorescence could be observed; this might indicate endolysosomal escape. The high degree of colocalization of the labeled nanogel with the fluorescent endosome and lysosome markers, Texas Red transferrin and LysoTracker, confirms the expected transport of these particles in vesicles of the endolysosomal pathway.

Table 2. Colocalization coefficients calculated by confocal image analysis, after mouse BMDM internalization of SAMSA fluorescein-labeled mannan nanogel (green), within early and recycling endosomes, labeled with Texas Red transferrin, or within late endosomes and lysosomes, labeled with LysoTracker Red (mean ± S. D., *n* = 10)

	C_G[a]	C_R[b]	C_T[c]	M_1 or M_{green}[d]	M_2 or M_{red}[e]
		early and recycling endosomes			
positive control	0.83 ± 0.10	0.47 ± 0.14	0.40 ± 0.10	0.79 ± 0.10	0.46 ± 0.20
sodium azide + 6-deoxyglucose	0.63 ± 0.18	0.77 ± 0.10	0.47 ± 0.01	0.53 ± 0.28	0.46 ± 0.34
filipin	0.55 ± 0.13	0.83 ± 0.21	0.56 ± 0.21	0.51 ± 0.17	0.58 ± 0.24
brefeldin A	0.54 ± 0.17	0.54 ± 0.04	0.30 ± 0.09	0.68 ± 0.23	0.60 ± 0.22
nocodazole	0.82 ± 0.10	0.68 ± 0.14	0.54 ± 0.15	0.74 ± 0.16	0.68 ± 0.14
		late endosomes and lysosomes			
positive control	0.84 ± 0.13	0.65 ± 0.30	0.50 ± 0.25	0.78 ± 0.12	0.58 ± 0.29
sodium azide + 6-deoxyglucose	0.80 ± 0.02	0.69 ± 0.22	0.47 ± 0.16	0.74 ± 0.20	0.63 ± 0.24
mannan	0.86 ± 0.14	0.49 ± 0.18	0.44 ± 0.21	0.75 ± 0.21	0.41 ± 0.22
sucrose	0.63 ± 0.12	0.38 ± 0.19	0.11 ± 0.05	0.10 ± 0.12	0.04 ± 0.08
filipin	0.88 ± 0.11	0.51 ± 0.26	0.51 ± 0.20	0.77 ± 0.20	0.38 ± 0.20
brefeldin A	0.65 ± 0.16	0.82 ± 0.12	0.47 ± 0.19	0.70 ± 0.08	0.77 ± 0.13
nocodazole	0.95 ± 0.03	0.75 ± 0.16	0.75 ± 0.13	0.86 ± 0.22	0.66 ± 0.27

[a] colocalization coefficient in green pixels, corresponding to the ratio between the number of colocalized and green pixels, obtained by confocal image analysis (annotation). [b] colocalization coefficient in red pixels, corresponding to the ratio between the number of colocalized and red pixels, obtained by confocal image analysis (annotation). [c] colocalization coefficient in total pixels, corresponding to the ratio between the number of colocalized and total pixels, obtained by confocal image analysis (annotation). [d] colocalization coefficient M_1 or M_{green}, calculated as described previously,[42] obtained by confocal image analysis (statistics). [e] colocalization coefficient M_2 or M_{red}, calculated as described previously,[42] obtained by confocal image analysis (statistics).

Our study was performed using cell culture medium supplemented with heat-inactivated FBS. In this medium, the protein adsorption pattern on the nanogel might be different than the one encountered in a more physiological situation where, for example, the complement system could be activated and promote foreign particle recognition by phagocytic cells.

Taken together, the results obtained in the inhibition study reported here, suggest that the internalization of the used mannan nanogel is mediated by multiple cellular uptake mechanisms. This has significant implications for drug and vaccine delivery, as intracellular trafficking is largely dependent on initial pathway of cell entry. It might be expected that part of nanogel uptaken by macrophages will be trafficked to the lysosomes by MR-mediated phagocytosis and clathrin-mediated endocytosis while part of the nanogel may end up in the cell cytosol. As one of the envisaged applications of this nanomaterial concern its usage as antigen-delivery system, the cytosolic and endolysosomal location, might allow delivered antigens to be presented on both MHC class I and class II molecules.

Conclusions

Cellular uptake profile of mannan nanogel is saturable and time-, concentration- and energy-dependent. *In vitro* experiments with endocytic inhibitors suggested that distinct uptake pathways, such as MR-mediated phagocytosis and clathrin-mediated endocytosis are involved in internalization. Mannan nanogel was also visualized in the cytosol, which suggests a fraction of the uptaken material was able to escape from the endolysosomal compartments. We have previously reported that this mannan nanogel possesses tunable physicochemical properties and low toxicity. Altogether, this makes mannan nanogel a promising macromolecular carrier to be used as a vaccination platform.

References

1. Chellat, F.; Merhi, Y.; Moreau, A.; Yahia, L. H. Therapeutic potential of nanoparticulate systems for macrophage targeting. *Biomaterials* **2005**, 26, 7260-7275.

2. Chavanpatil, M. D.; Khdair, A.; Panyam, J. Nanoparticles for cellular drug delivery: mechanisms and factors influencing delivery. *J Nanosci Nanotechnol* **2006**, 6, 2651-2663.

3. Dausend, J.; Musyanovych, A.; Dass, M.; Walther, P.; Schrezenmeier, H.; Landfester, K.; Mailander, V. Uptake mechanism of oppositely charged fluorescent nanoparticles in HeLa cells. *Macromol Biosci* **2008**, 8, 1135-1143.

4. Jiang, W.; KimBetty, Y. S.; Rutka, J. T.; ChanWarren, C. W. Nanoparticle-mediated cellular response is size-dependent. *Nat Nanotechnol* **2008**, 3, 145-150.

5. Mailander, V.; Landfester, K. Interaction of nanoparticles with cells. *Biomacromolecules* **2009**, 10, 2379-2400.

6. Zhang, L. W.; Monteiro-Riviere, N. A. Mechanism of quantum dot nanoparticle cellular uptake. *Toxicol Sci* **2009**, 110, 138-155.

7. Missirlis, D.; Hubbell, J. A. In vitro uptake of amphiphilic, hydrogel nanoparticles by J774A.1 cells. *J Biomed Mater Res, Part A* **2009**, 93A, 1557-1565.

8. Sahay, G.; Alakhova, D. Y.; Kabanov, A. V. Endocytosis of nanomedicines. *J Control Release* **2010**, 145, 182-195.

9. Rejman, J.; Oberle, V.; Zuhorn, I. S.; Hoekstra, D. Size-dependent internalization of particles via the pathways of clathrin- and caveolae-mediated endocytosis. *Biochem J* **2004**, 377, 159-169.

10. Tabata, Y.; Ikada, Y. Effect of the size and surface charge of polymer microspheres on their phagocytosis by macrophage. *Biomaterials* **1988**, 9, 356-362.

11. Hillaireau, H.; Couvreur, P. Nanocarriers' entry into the cell: relevance to drug delivery. *Cell Mol Life Sci* **2009**, 66, 2873-2896.

12. He, C.; Hu, Y.; Yin, L.; Tang, C.; Yin, C. Effects of particle size and surface charge on cellular uptake and biodistribution of polymeric nanoparticles. *Biomaterials* **2010**, 31, 3657-3666.

13. Banquy, X.; Suarez, F.; Argaw, A.; Rabanel, J.-M.; Grutter, P.; Bouchard, J.-F.; Hildgen, P.; Giasson, S. Effect of mechanical properties of hydrogel nanoparticles on macrophage cell uptake. *Soft Matter* **2009**, 5, 3984-3991.

14. Douglas, K. L.; Piccirillo, C. A.; Tabrizian, M. Cell line-dependent internalization pathways and intracellular trafficking determine transfection efficiency of nanoparticle vectors. *Eur J Pharm Biopharm* **2008**, 68, 676-687.

15. Kumari, S.; Mg, S.; Mayor, S. Endocytosis unplugged: multiple ways to enter the cell. *Cell Res* **2010**, 20, 256-275.

16. Takei, K.; Haucke, V. Clathrin-mediated endocytosis: membrane factors pull the trigger. *Trends Cell Biol* **2001**, 11, 385-391.

17. Rappoport, J. Z. Focusing on clathrin-mediated endocytosis. *Biochem J* **2008**, 412, 415-423.

18. Parton, R. G.; Simons, K. The multiple faces of caveolae. *Nat Rev Mol Cell Biol* **2007**, 8, 185-194.

19. Hayer, A.; Stoeber, M.; Ritz, D.; Engel, S.; Meyer, H. H.; Helenius, A. Caveolin-1 is ubiquitinated and targeted to intralumenal vesicles in endolysosomes for degradation. *J Cell Biol* **2010**, 191, 615-629.

20. Rejman, J.; Bragonzi, A.; Conese, M. Role of clathrin- and caveolae-mediated endocytosis in gene transfer mediated by lipo- and polyplexes. *Mol Ther* **2005**, 12, 468-474.

21. Gabrielson, N. P.; Pack, D. W. Efficient polyethylenimine-mediated gene delivery proceeds via a caveolar pathway in HeLa cells. *J Control Release* **2009**, 136, 54-61.

22. Pelkmans, L.; Helenius, A. Endocytosis via caveolae. *Traffic* **2002**, 3, 311-320.

23. Nam, H. Y.; Kwon, S. M.; Chung, H.; Lee, S.-Y.; Kwon, S.-H.; Jeon, H.; Kim, Y.; Park, J. H.; Kim, J.; Her, S.*, et al.* Cellular uptake mechanism and intracellular fate of hydrophobically modified glycol chitosan nanoparticles. *J Control Release* **2009**, 135, 259-267.

24. Panyam, J.; Zhou, W. Z.; Prabha, S.; Sahoo, S. K.; Labhasetwar, V. Rapid endo-lysosomal escape of poly(DL-lactide-co-glycolide) nanoparticles: implications for drug and gene delivery. *FASEB J* **2002**, 16, 1217-1226.

25. Tahara, K.; Sakai, T.; Yamamoto, H.; Takeuchi, H.; Hirashima, N.; Kawashima, Y. Improved cellular uptake of chitosan-modified PLGA nanospheres by A549 cells. *Int J Pharm* **2009**, 382, 198-204.

26. Ferreira, S. A.; Pereira, P.; Sampaio, P.; Coutinho, P. J. G.; Gama, F. M. Supramolecular assembled nanogel made of mannan. *J Colloid Interface Sci* **2011**, 361, 97-108.

27. Tushinski, R. J.; Oliver, I. T.; Guilbert, L. J.; Tynan, P. W.; Warner, J. R.; Stanley, E. R. Survival of mononuclear phagocytes depends on a lineage-specific growth factor that the differentiated cells selectively destroy. *Cell* **1982**, 28, 71-81.

28. Warren, M. K.; Vogel, S. N. Bone marrow-derived macrophages: development and regulation of differentiation markers by colony-stimulating factor and interferons. *J Immunol* **1985**, 134, 982-989.

29. Zhang, X.; Goncalves, R.; Mosser, D. M. The isolation and characterization of murine macrophages. *Curr Protoc Immunol* **2008**, Chapter 14, Unit 14.11.

30. Chiu, Y. L.; Ho, Y. C.; Chen, Y. M.; Peng, S. F.; Ke, C. J.; Chen, K. J.; Mi, F. L.; Sung, H. W. The characteristics, cellular uptake and intracellular trafficking of nanoparticles made of hydrophobically-modified chitosan. *J Control Release* **2010**, 146, 152-159.

31. Hiltbold, E. M.; Vlad, A. M.; Ciborowski, P.; Watkins, S. C.; Finn, O. J. The mechanism of unresponsiveness to circulating tumor antigen MUC1 Is a block in intracellular sorting and processing by dendritic cells. *J Immunol* **2000**, 165, 3730-3741.

32. Kapur, N.; Thakral, D.; Durgapal, H.; Panda, S. K. Hepatitis E virus enters liver cells through receptor-dependent clathrin-mediated endocytosis. *J Viral Hepatitis* **2011**, no-no.

33. Mukherjee, S.; Ghosh, R. N.; Maxfield, F. R. Endocytosis. *Physiol Rev* **1997**, 77, 759-803.

34. Costes, S. V.; Daelemans, D.; Cho, E. H.; Dobbin, Z.; Pavlakis, G.; Lockett, S. Automatic and quantitative measurement of protein-protein colocalization in live cells. *Biophys J* **2004**, 86, 3993-4003.

35. Bolte, S.; Cordelieres, F. P. A guided tour into subcellular colocalization analysis in light microscopy. *J Microsc* **2006**, 224, 213-232.

36. Oheim, M.; Li, D., Quantitative colocalisation imaging: concepts, measurements, and pitfalls. In *Imaging Cellular and Molecular Biological Functions*, Shorte, S. L.; Frischknecht, F., Eds. Springer Berlin Heidelberg, 2007; pp 117-155.

37. Zinchuk, V.; Zinchuk, O.; Okada, T. Quantitative colocalization analysis of multicolor confocal immunofluorescence microscopy images: pushing pixels to explore biological phenomena. *Acta Histochem Cytochem* **2007**, 40, 101-111.

38. Scriven, D. R. L.; Lynch, R. M.; Moore, E. D. W. Image acquisition for colocalization using optical microscopy. *Am J Physiol - Cell Physiol* **2008**, 294, C1119-C1122.

39. Zinchuk, V.; Zinchuk, O. Quantitative colocalization analysis of confocal fluorescence microscopy images. *Curr Protoc Cell Biol* **2008**, Ch. 4, Unit 4.19.

40. Dunn, K. W.; Kamocka, M. M.; McDonald, J. H. A practical guide to evaluating colocalization in biological microscopy. *Am J Physiol - Cell Physiol* **2011**, 300, C723-742.

41. Manders, E. M.; Stap, J.; Brakenhoff, G. J.; van Driel, R.; Aten, J. A. Dynamics of three-dimensional replication patterns during the S-phase, analysed by double labelling of DNA and confocal microscopy. *J Cell Sci* **1992**, 103, 857-862.

42. Manders, E. M.; Verbeek, F. J.; Aten, J. A. Measurement of co-localization of objects in dual-colour confocal images. *J Microsc* **1993**, 169, 375–382.

43. Huang, M.; Khor, E.; Lim, L.-Y. Uptake and cytotoxicity of chitosan molecules and nanoparticles: effects of molecular weight and degree of deacetylation. *Pharm Res* **2004**, 21, 344-353.

44. Lunov, O.; Zablotskii, V.; Syrovets, T.; Rocker, C.; Tron, K.; Nienhaus, G. U.; Simmet, T. Modeling receptor-mediated endocytosis of polymer-functionalized iron oxide nanoparticles by human macrophages. *Biomaterials* **2010**, 32, 547-555.

45. Kakizawa, Y.; Furukawa, S.; Kataoka, K. Block copolymer-coated calcium phosphate nanoparticles sensing intracellular environment for oligodeoxynucleotide and siRNA delivery. *J Control Release* **2004**, 97, 345-356.

46. Liu, Y.; Sun, J.; Cao, W.; Yang, J.; Lian, H.; Li, X.; Sun, Y.; Wang, Y.; Wang, S.; He, Z. Dual targeting folate-conjugated hyaluronic acid polymeric micelles for paclitaxel delivery. *Int J Pharm* **2011**, 421, 160-169.

47. Gratton, S. E. A.; Ropp, P. A.; Pohlhaus, P. D.; Luft, J. C.; Madden, V. J.; Napier, M. E.; DeSimone, J. M. The effect of particle design on cellular internalization pathways. *Proc Natl Acad Sci* **2008**, 105, 11613-11618.

48. Engqvist-Goldstein, A. E.; Drubin, D. G. Actin assembly and endocytosis: from yeast to mammals. *Annu Rev Cell Dev Biol* **2003**, 19, 287-332.

49. Ezekowitz, R. A.; Sastry, K.; Bailly, P.; Warner, A. Molecular characterization of the human macrophage mannose receptor: demonstration of multiple carbohydrate recognition-like domains and phagocytosis of yeasts in Cos-1 cells. *J Exp Med* **1990**, 172, 1785-1794.

50. Engering, A. J.; Cella, M.; Fluitsma, D.; Brockhaus, M.; Hoefsmit, E. C. M.; Lanzavecchia, A.; Pieters, J. The mannose receptor functions as a high capacity and broad specificity antigen receptor in human dendritic cells. *Eur J Immunol* **1997**, 27, 2417-2425.

51. Tan, M. C. A. A.; Mommaas, A. M.; Drijfhout, J. W.; Jordens, R.; Onderwater, J. J. M.; Verwoerd, D.; Mulder, A. A.; van der Heiden, A. N.; Scheidegger, D.; Oomen, L. C. J. M.*, et al.* Mannose receptor-mediated uptake of antigens strongly enhances HLA class II-restricted antigen presentation by cultured dendritic cells. *Eur J Immunol* **1997**, 27, 2426-2435.

52. Apostolopoulos, V.; Barnes, N.; Pietersz, G. A.; McKenzie, I. F. C. Ex vivo targeting of the macrophage mannose receptor generates anti-tumor CTL responses. *Vaccine* **2000**, 18, 3174-3184.

53. Apostolopoulos, V.; Pietersz, G. A.; Gordon, S.; Martinez-Pomares, L.; McKenzie, I. F. C. Aldehyde-mannan antigen complexes target the MHC class I antigen-presentation pathway. *Eur J Immunol* **2000**, 30, 1714-1723.

54. Apostolopoulos, V.; McKenzie, I. F. Role of the mannose receptor in the immune response. *Curr Mol Med* **2001**, 1, 469-474.

55. Avrameas, A.; McIlroy, D.; Hosmalin, A.; Autran, B.; Debre, P.; Monsigny, M.; Roche, A. C.; Midoux, P. Expression of a mannose/fucose membrane lectin on human dendritic cells. *Eur J Immunol* **1996**, 26, 394-400.

56. Goldberg, D. S.; Ghandehari, H.; Swaan, P. W. Cellular entry of G3.5 poly (amido amine) dendrimers by clathrin- and dynamin-dependent endocytosis promotes tight junctional opening in intestinal epithelia. *Pharm Res* **2010**, 27, 1547-1557.

57. Heuser, J. E.; Anderson, R. G. Hypertonic media inhibit receptor-mediated endocytosis by blocking clathrin-coated pit formation. *J Cell Biol* **1989**, 108, 389-400.

58. Schnitzer, J. E.; Oh, P.; Pinney, E.; Allard, J. Filipin-sensitive caveolae-mediated transport in endothelium: reduced transcytosis, scavenger endocytosis, and capillary permeability of select macromolecules. *J Cell Biol* **1994**, 127, 1217-1232.

59. Sandvig, K.; Torgersen, M. L.; Raa, H. A.; van Deurs, B. Clathrin-independent endocytosis: from nonexisting to an extreme degree of complexity. *Histochem Cell Biol* **2008**, 129, 267-276.

60. Wagner, M.; Rajasekaran, A. K.; Hanzel, D. K.; Mayor, S.; Rodriguez-Boulan, E. Brefeldin A causes structural and functional alterations of the trans-Golgi network of MDCK cells. *J Cell Sci* **1994**, 107 (Pt 4), 933-943.

61. Peterson, J. R.; Mitchison, T. J. Small molecules, big impact: a history of chemical inhibitors and the cytoskeleton. *Chem Biol* **2002**, 9, 1275-1285.

62. Watson, P.; Jones, A. T.; Stephens, D. J. Intracellular trafficking pathways and drug delivery: fluorescence imaging of living and fixed cells. *Adv Drug Delivery Rev* **2005**, 57, 43-61.

Chapter 7

Biocompatibility of mannan nanogel – safe interaction with plasma proteins

Self-assembled mannan nanogels are designed to provide a therapeutic or vaccine delivery platform based on the bioactive properties of mannan to target mannose receptor expressed on the surface of antigen-presenting cells, combined with the performance of nanogels as carriers of biologically active agents.

Proteins in the corona around mannan nanogel formed in human plasma were identified by mass spectrometry after size exclusion chromatography or centrifugation followed by sodium dodecyl sulphate polyacrylamide gel electrophoresis. Structural changes and time dependent binding of human apolipoprotein A-I (apoA-I) and human serum albumin (HSA) to mannan nanogel were studied using intrinsic tryptophan fluorescence and circular dichroism spectroscopy. The mannan nanogel effect on blood coagulation and fibrillation of Alzheimer's disease-associated amyloid β peptide and haemodialysis-associated amyloidosis β2 microglobulin was evaluated using thrombin generation assay or thioflavin T fluorescence assay, respectively.

The protein corona around mannan nanogel is formed through a slow process, is quite specific comprising apolipoproteins B-100, A-I and E and HSA, evolves over time and the equilibrium is reached after hours to days. Structural changes and time dependent binding of apoA-I and HSA to mannan nanogel are minor. The mannan nanogel does not affect blood coagulation and retards the fibril formation.

Mannan nanogel has a high biosafety and biocompatibility, which is mandatory for nanomaterials to be used in biomedical applications. Our research provides a molecular approach to evaluate the safety aspects of nanomaterials, which is of general concern in society and science.

Adapted from: *Biochim Biophys Acta* **2012** (accepted)

Introduction

Nanometer-sized polymeric hydrogels, i.e., nanogels combine favorable and exceptional properties, such as flexible size in the nanometer range, tunable chemical and physical structures, large surface areas for multivalent conjugation, high water content, and biocompatibility.[1, 2] Nanogels represent a promising class of delivery devices for biologically active agents because of their loading capacity, their stability, as well as their responsiveness to environmental factors.[1]

A self-assembled mannan nanogel has been designed and characterized in our group as a potential multifunctional nanosized device for biomedical applications.[3] The mannan nanogel is spherical and polydisperse with a mean hydrodynamic diameter between 50–140 nm and has a slightly negative surface charge.[3]

Mannose receptor, expressed in the surface of antigen-presenting cells,[4-7] was previously shown to take part in host defense, providing a linkage between innate and adaptive immunity.[7-10] The choice of mannan as the main component of the nanogel aims to take advantage of the association of the bioactive properties of mannan with the performance of nanogels as carriers of biologically active agents. The mannan nanogel is thus suggested as a possible tool for vaccine formulations, acting as an adjuvant suitable to induce a protective and long-lasting immune response, or as a targeted therapeutic delivery system to be used for the treatment of macrophage associated pathologies.

Nanoparticles, including nanogels, will interact with proteins in a biological environment creating an outer layer around the particle known as the protein corona.[11, 12] The proteins are the most studied substances in the corona but it can include other biomolecules, for example lipids.[13] The composition and surface chemistry of a specific nanoparticle will dictate the extent and specificity of protein binding.[12] Surface charge, hydrophobicity, particle size, morphology, shape and surface curvature of nanoparticles affect what proteins bind to the nanoparticle.[11, 12, 14-20] The composition of the protein corona on a given nanoparticle, at a given time, will depend on the protein concentrations in the physiological fluid and the on- and off-rates for each protein.[14] Thus the protein corona, the biological identity of the nanoparticle, will change with time[20-24] and with environmental changes;[24, 25] for example, when nanoparticles travel from blood to inside cells.[25] The protein corona will be important for the biocompatibility and biosafety. Proteins on the nanoparticle surface can interact with blood proteins and cell receptors, and consequently affect uptake and intracellular fate,[24, 26-32] biodistribution of the nanomaterials throughout the body, toxicity and/or efficacy.[14, 15, 33-35]

When proteins bind to nanoparticles a structural change in the protein often occurs.[16, 36] It has been proposed that these structural changes, in addition to the protein composition in the corona, may lead to changed biological functions and consequently be important for evaluating the biosafety of nanoparticles.[14, 30, 36] Recent reports describe how changes in the corona can mediate the biological impact of the nanoparticles. Fibrinogen bound to poly(acrylic acid)-coated gold nanoparticles undergo a structural change that can facilitate interaction and activation of MAC-1 receptor pathway on macrophage-like cells and subsequent inflammation response.[37] Enzyme activity can be enhanced and stabilized over time when bound to nanoparticles.[38] The opposite is also true as trypsin immobilized on silica and polystyrene nanospheres,[39] or lysozyme and α-chymotrypsin[40] bound to gold nanoparticles experienced a large structural change and the enzymes lost their activity. On most studied spherical particles, apolipoproteins are identified in the corona formed in human blood plasma.[11] They suffered a structural change after binding to polystyrene particles.[41] Apolipoproteins are central in the fat metabolism and uptake of apolipoprotein binding polystyrene particles through a feeding web could cause severe metabolic and behavioral disturbances in fish.[42]

Proteins important for the initiation and regulation in the coagulation cascade have been identified in the corona from polystyrene,[20] citrate-capped gold,[24] and silica nanoparticles.[25] Recent results in our laboratory have shown that amine-modified polystyrene nanoparticles inhibited coagulation by specific interactions with two coagulation factors and that in opposite carboxyl-modified polystyrene nanoparticles activated the coagulation.[43] It is highly relevant to test particle destined to circulate in the body for its effect on the coagulation cascade because disorders of coagulation can lead to an increased risk of bleeding (hemorrhage) or obstructive clotting (thrombosis). The fluorometric thrombin generation assay is proposed as a good method to evaluate the procoagulant activity of nanomaterials in human plasma and has been used to study the procoagulation effects caused by several nanoparticles.[44]

Protein aggregation can lead to major disturbances of cellular processes and is associated with several diseases. Proteins may under certain conditions and as a function of time give up their natively folded state and form amyloid fibrils.[45, 46] Human amyloid diseases involve self-assembly of soluble proteins into large insoluble fibrils through nucleation-dependent assembly, often *via* the formation of oligomeric structures that possess toxic properties.[47, 48] The fibrillation of amyloid proteins and peptides as Alzheimer's disease-associated amyloid β peptide (Aβ(M1-40)) found in brain lesions and haemodialysis-associated amyloidosis β2 microglobulin (β2m), are well studied.

Nanomaterials,[46] such as nanogel formed by self-aggregation of cholesterol-bearing pullulan with molecular chaperone-like activity,[49] and *N*-isopropylacrylamide:*N-tert*-butylacrylacrylamide (NIPAM:BAM) nanoparticles,[50] have been linked to Aβ fibrillation retardation. In contrast, NIPAM:BAM nanoparticles caused acceleration of β2m fibrillation.[51] Also, at constant Aβ(M1-40) concentration, the fibrillation process was accelerated by amine-modified polystyrene nanoparticles at low concentration, while at high nanoparticle concentration, the fibrillation process was retarded.[52]

In the present work, the protein corona around mannan nanogel in human plasma was characterized to evaluate its biosafety and biocompatibility from a molecular perspective. Proteins in the corona were identified by mass spectrometry after gel filtration using size exclusion chromatography (SEC) or centrifugation followed by sodium dodecyl sulphate polyacrylamide gel electrophoresis (SDS-PAGE). Time dependence and structural changes of human apolipoprotein A-I (apoA-I) and human serum albumin (HSA) binding to mannan nanogel were studied using intrinsic tryptophan fluorescence and circular dichroism (CD) spectroscopy. The mannan nanogel effect on blood coagulation was evaluated by fluorometric thrombin generation assay. The role of mannan nanogel in protein fibrillation was evaluated by continuous thioflavin T (ThT) fluorescence assay using both Aβ(M1-40) and β2m.

Experimental

Materials

Mannan-VMA-SC_{16} (VMA: vinyl methacrylate, SC_{16}: hydrophobic alkyl chain) was synthesized as described previously[3] with 31 acrylate groups (DS_{VMA} 31%) and 20 alkyl chains (DS_{C16} 20%) per 100 mannose residues. Resultant amphiphilic mannan is named as MVC_{16}-31-20. With DS_{C16}/DS_{VMA} equal to 65%, it has critical aggregation concentration (cac) or critical micelle concentration (cmc) equal to 0.01 mg/mL.[3] Human donors plasma from lipidemic patients was obtained from the local hospital blood bank and preserved in aliquots at −80 °C. Before each experiment aliquots were defrosted and centrifuged for 2 min at 14927 g (Biofuge 13, Heraeus) and immediately used after rejecting the top lipid layer. ApoA-I was purified from human plasma as previously described.[53] HSA (Sigma, A3782, fatty acid free, 99% pure) was purified from dimer and contaminating proteins using gel filtration on a 200 × 3.4 cm Sephadex G50 column in 50 mM ammonium acetate buffer, pH 6.5. Fractions containing HSA monomer were pooled, lyophilized and desalted by gel filtration on a G25 Sephadex superfine column in Millipore water. ApoA-I and HSA stock solutions (10 mg/mL) were dialyzed for 5 days against frequently changed phosphate buffered saline, pH 7.5 (PBS) at 4 ºC using twice boiled in distilled water regenerated cellulose tubular membranes, with 6,000–8,000 nominal molecular weight cut-off (Membrane Filtration Products). Phospholipids were obtained from Avanti Polar Lipids, Inc. (Alabaster, AL, USA). Recombinant tissue factor was obtained from Dade Innovin (Marburg, Germany). The thrombin fluorogenic substrate I-1140 (Z-Gly-Gly-Arg-7-amino-4-methylcoumarin·HCl) was purchased from Bachem (Bubendorf, Switzerland). Aβ(M1-40) was expressed in *E. coli* and purified as previously described.[54] β2m was expressed in *E. coli* and purified as previously described.[51] Organic and inorganic reagents of laboratory grade were purchased from Sigma-Aldrich and used without any further purification, unless otherwise stated. Water was purified with a Milli-Q system (Millipore Corporation). The NIPAM coated gold particles was a kind gift from Colloidal Chemistry Group from Vigo University, Spain.

Mannan nanogel preparation

Colloidal dispersions of amphiphilic mannan were prepared stirring the lyophilized MVC_{16}-31-20 in PBS, for 3–5 days at 50 °C, followed by filtration (Orange; pore size 0.22 µm). The nanogel formation was confirmed by dynamic light scattering (DLS; Malvern Zetasizer NANO ZS – Malvern Instruments Limited, UK) as previously described.[3] The colloidal dispersion of nanogel (2 mg/mL) showed z-average equal to 154.1 ± 5.625 nm and polydispersity index (PdI) of 0.229 ± 0.007.

Gel filtration of mannan nanogel and plasma proteins

Plasma (250 µL) was incubated with mannan nanogel (800 µL at 2 mg/mL) or with PBS (800 µL; control) stirring for 24 h at 37 °C. Samples were separated by SEC on a 100 × 1 cm Sephacryl 1000 column. The absorbance of all fractions was recorded at 280 nm in UV-1800 spectrophotometer (SHIMADZU UV). All fractions resultant of SEC separation of nanogel alone had similar absorbance to that obtained with the PBS at 280 nm. Individual fractions from 22 to 37 pooled from four different experiments were precipitated with trichloroacetic acid 10% and froze at −20 °C. Samples were centrifuged 15 min at 14927 g (Heraeus Kendro Biofuge 13) and the pellet was washed with ice cold acetone. Pellets were resuspended in 5 µL of PBS and proteins were desorbed from the nanogel by adding 10 µL of sodium dodecyl sulfate (SDS) loading buffer and incubated for 5 min at 95

°C. Samples were separated by SDS-PAGE, with resolving gel 15% and stacking gel 4%. As a control human plasma used in this study was also directly separated by SDS-PAGE, with resolving gel 12% and stacking gel 4%. Each gel run included one lane of a molecular weight ladder standard, PageRuler Prestained Protein Ladder (Fermentas). Gels were coomassie stained.

Identification of corona proteins using centrifugation and mass spectrometry

Colloidal dispersions of mannan nanogel in PBS (100 µL; 0, 0.1, 0.25, 0.5, 0.75, 1 or 2 mg/mL) were incubated stirring with plasma or PBS (100 µL) for 1 and 24 hours at 37 °C. Colloidal dispersions of mannan nanogel in PBS (100 µL; 2 mg/mL) were incubated stirring with increasing amount of plasma (50 µL, 100 µL, 200 µL, 400 µL or 800 µL; in a fixed final volume), for 1 and 24 h at 37 °C. Samples were centrifuged 15 min at 19873 g (Heraeus Kendro Biofuge 15) and the pellet was washed twice with 500 µL PBS changing the vial after each washing step. Samples were separated by SDS-PAGE and coomassie blue stained as described above. Each experiment was performed twice. Gels were preserved in 1% acetic acid in water at 4 °C for mass spectrometry. Bands were excised from the gel, reduced, alkylated, and digested with trypsin (Sequencing Grade Promega, Madison, Wisconsin), and the resulting peptide mixtures were analyzed by MALDI-TOF mass spectrometry using a 4700 Proteomics Analyzer (Applied Biosystems, Massachusets, USA) mass spectrometer in positive reflector mode. Both MS and tandem MS (MS/MS) spectra were analyzed by Matrix science Mascot software to identify tryptic peptide sequences.

Circular dichroism spectroscopy

ApoA-I or HSA were incubated stirring at 37 °C in the absence and in the presence of the mannan nanogel at various concentrations in PBS. CD measurements were carried out using a JASCO J-815 spectropolarimeter (JASCO, Easton, Maryland, USA) with a Peltier type thermostated cell holder. Far-UV CD spectra (190–260 nm) were recorded at 37 °C in continuous mode with a scan rate of 50 nm/min and a digital integration time of 8 s using 0.1 cm quartz cuvettes with a Teflon stopper. Three spectra were accumulated and averaged for each sample. The average spectra for a blank (colloidal dispersion of mannan nanogel or buffer) were subtracted from the spectrum of each protein sample. The conformation of protein in the absence and in the presence of the nanogel was estimated from CD spectra. This experiment was performed at least twice.

Intrinsic tryptophan fluorescence

ApoA-I or HSA were incubated stirring at 37 °C in the absence and the presence of the mannan nanogel at various concentrations in PBS. Fluorescence measurements were performed on a luminescence spectrometer LS 50B (PerkinElmer) with a cuvette holder thermostated at 37 °C. Fluorescence emission spectra (310–460 nm) were recorded at an excitation wavelength of 290 nm with a scan rate of 100 nm/min. Three spectra were accumulated and averaged for each sample. Reported average spectra are those after the subtraction of the spectrum for a blank (colloidal dispersion of mannan nanogel or buffer) from the spectrum of each protein sample. Also fluorescence emission spectra of a colloidal dispersion of mannan nanogel (0.6 mg/mL) with ApoA-I or HSA (0.1 mg/mL) were recorded over time at 37 °C. These experiments were performed at least twice.

Isothermal titration calorimetry

Isothermal titration calorimetry (ITC) experiments were performed using a VP-ITC MicroCalorimeter (Microcal, Northhampton, Massachusets, USA). HSA was titrated at 37 °C from a 5 mg/mL (75.76 μM) or 10 mg/mL (151.52 μM) stock solutions, in the syringe, into the nanogel colloidal dispersion at 2 mg/mL (2.31 μM), in the reaction cell (1.4 mL). The molar concentration of nanogel is calculated by assuming a density close to 1 g/mL when nanoparticles are swollen and spherical. Before the measurements were performed, the nanogel colloidal dispersion and HSA solution were dialyzed against the same solvent – 10 mM (4-(2-hydroxyethyl)-1-piperazineethanesulfonic acid (HEPES)/NaOH buffer, pH 7.5 with 150 mM NaCl – in order to have the same pH in both samples. Different combinations of HSA concentration and injection sizes were tested in separate experiments. To exclude background, HSA was injected in buffer and nanogel was injected in buffer as control experiments. The nanogel formation was confirmed by DLS. A colloidal dispersion of nanogel (2 mg/mL) in 10 mM HEPES/NaOH buffer, pH 7.5 with 150 mM NaCl showed z-average equal to 145.1 ± 2.057 nm and PdI of 0.207 ± 0.011.

Thrombin generation assay

The amount of thrombin formed in plasma/mannan nanogel samples were monitored using the thrombin generation assay as previously described[55] with the following modifications. Natural phospholipids, 20-20-60 phosphatidylserine-phosphatidylethanolamine-phosphatidylcholine (PS-PE-PC), were mixed and prepared. Citrate platelet poor plasma (40 μL) was preincubated with 40 μL of HEPES buffered saline (HBS, 10 mM HEPES, 150 mM NaCl, pH 7.4) or mannan nanogel (final concentration of 1 mg/mL) at 37 °C for 15 min. Fluorogenic substrate (Z-Gly-Gly-Arg-7-amino-4-methylcoumarin·HCl; 20 µL) was added to samples and coagulation was initiated with 20 µL of phospholipids/tissue factor/$CaCl_2$ mixture in a final volume of 120 µL. All reagents were diluted in HBSBSA (HBS buffer supplemented with 5 mg/mL of bovine serum albumin (BSA)) and final concentrations were approximately 1.17 pM tissue factor, 4.2 µM phospholipids, 300 µM fluorogenic substrate and 16 mM $CaCl_2$. Fluorescence measurements over time were taken in black flat bottom 96-well plates (Nalge Nunc International, Rochester, New York, USA) in a plate Tecan infinite 200 fluorometer equipped with a 360 nm excitation/460 nm emission filter set (Mölndal, Sweden) and Magellan software (Gröedig, Austria).

Thioflavin T fluorescence assay

Peptide Aβ(M1-40) samples in 20 mM sodium phosphate buffer pH 7.4, 200 µM ethylenediaminetetraacetic acid (EDTA), 0.02% NaN_3 or protein β2m samples in 20 mM sodium phosphate buffer pH 2.5, 50 mM NaCl, 0.02% NaN_3, were pipetted into wells of a 96-well half-area plate of black polystyrene with a clear bottom and polyethylene glycol coating (Corning 3881), 50 µL per well, which contained either 50 µL of respective buffer or 50 µL of mannan nanogel in respective buffer, resulting in final 10 µM Aβ(M1-40) or 40 µM β2m concentrations and final nanogel concentrations between 0.001 mg/mL and 0.9 mg/mL. The nanogel size was not affected in the buffers used as confirmed by DLS. All samples were supplemented with 20 µM ThT. Plate was sealed with a plastic film (Corning 3095). Fibrillation of Aβ(M1-40) and of β2m at 37 °C was monitored by the temporal development of ThT binding in the absence and in the presence of mannan nanogel at 0.001–0.9 mg/mL. The experiment was initiated by placing the 96-well plate at 37 °C and shaking at 100 rpm in a plate reader (Fluostar Omega, BMGLabtech, Offenburg, Germany). The ThT fluorescence was measured through the bottom of the plate every 6 min (with excitation filter 440 nm and emission filter 480 nm) with continuous shaking at 100 rpm between reads. The ThT fluorescence was followed for two different 96-well plates (one plate with 8 samples for Aβ(M1-40) and β2m in pentaplicate; and another plate with 8 samples for Aβ(M1-40) and β2m in hexaplicate) yielding in total 11 kinetic traces per sample. Controls ran with only nanogel with ThT showed that the nanogel did not interfere with the assay. The dye selectively binds to amyloid fibrils with an accompanying increase in fluorescence intensity.[56, 57] Interaction of amyloid fibrils and protofibrils with ThT causes a red shift in its excitation spectrum,[58] and ThT fluorescence is therefore a measure of fibrillogenesis. The kinetics aggregation data have a sigmoidal appearance and exhibits characteristics of a typical nucleation-dependent polymerization and growth process. The time course of fibrillogenesis includes a lag phase during which the concentration of ThT-positive aggregates is too low to be detected followed by a rapid exponential growth (elongation) of fibrils.[59, 60]

Results and discussion

Apolipoprotein corona around mannan nanogel

Samples of mannan nanogel incubated with human plasma for 24 h at 37 °C were separated by SEC. Two distinct peaks are seen in the elution profile (Figure 1a upper panel). The major peak that elutes at fraction 71 is also found in SEC of plasma only and corresponds to the elution of unbound proteins. A minor peak elutes at around fraction 26. This peak is not seen in experiments with plasma only and likely corresponds to mannan nanogel associated with plasma proteins. In order to characterize the proteins associated with the nanogel, individual fractions 22 to 37 from four different experiments were pooled, precipitated with trichloroacetic acid and the proteins visualized by coomassie blue after separation by SDS-PAGE (Figure 1a middle panel). Several proteins are found in the precipitated fractions. In control experiments without mannan nanogel no proteins are found in fractions 22 to 37 (Figure 1a lower panel), which strongly indicates that these proteins are associated and co-elute with the nanogel. The protein profile of human plasma is shown in Figure 1d, and clearly it is different from the profile of plasma proteins associated with mannan nanogel. One protein with a molecular weight around 68 kDa is seen in all fractions when nanogel is added. This is likely to be HSA, which is the most prominent protein in plasma (about 35 mg/mL). The high concentration of HSA means that even if it binds to the nanogel with low affinity it is likely to co-elute and continuously detach from the nanogel over the elution time.

Another common way to separate particles with bound proteins from unbound proteins is by centrifugation. The mannan nanogel was mixed with human plasma and incubated 1 h at 37 °C. The mixture was centrifuged, the pellets washed and bound proteins dissolved in buffer with SDS and separated by SDS-PAGE (Figure 1b). Several proteins are co-pelleted with the nanogel indicating that they are bound to the nanogel in plasma. Longer time of incubation, higher nanoparticle concentrations, or higher concentration of plasma produced larger pellets during centrifugation experiments. No pelleted proteins were seen in experiments without nanogel (data not shown). Nanogel in buffer will not pellet at the same centrifugation speed showing that the density and/or aggregation properties of the mannan nanogel are changed after plasma proteins have bound. To identify the bound proteins, the five major protein bands were cut out from a similar SDS-PAGE, the proteins digested with trypsin and the peptides subjected to mass spectrometry. The five major proteins after 1 h of incubation are identified as apolipoproteins B-100, A-I and E, and HSA (Figure 1b). One major protein band with an apparent molecular weight of 55 kDa is unidentified. This is a comparably simple protein corona. Most studied nanoparticles have a much more complex protein corona with a wide variety of proteins. One particle, the NIPAM:BAM copolymer, has a protein corona with mainly apolipoproteins, but without B-100.[11, 12] It would be interesting to compare the influence on the biocompatibility of the corona for these two materials with other nanoparticles.

A comparison of the bound proteins isolated by SEC and centrifugation, after incubation for 1 or 24 h, show several similarities but also differences. The five major proteins are present in all conditions but the ratios between the proteins are different. In the centrifugation experiments, apolipoproteins B-100 and A-I are the dominating proteins but after 24 h the ratio between HSA and apolipoproteins is larger than after 1 h of incubation (Figure 1b, c). This change in ratios is more pronounced in SEC in which mannan nanogel also was incubated for 24 h in plasma before separation. In SEC experiments there is an extra major protein band around 50 kDa. This protein band also appears in centrifugation after 24 h of incubation but in much smaller amounts. These differences in the corona between 1 and 24 h indicate that the corona is formed through a slow process and that equilibrium is reached only after a long time. A time dependent corona has been observed for sodium citrate stabilized gold nanoparticles.[22, 24] It was also shown that cell uptake of particles was different depending on the time particles were incubated in media before adding to the cells.[61] Consequently, time may be an important factor for how mannan nanogel interacts with the surrounding fluids and tissues after administration into the body.

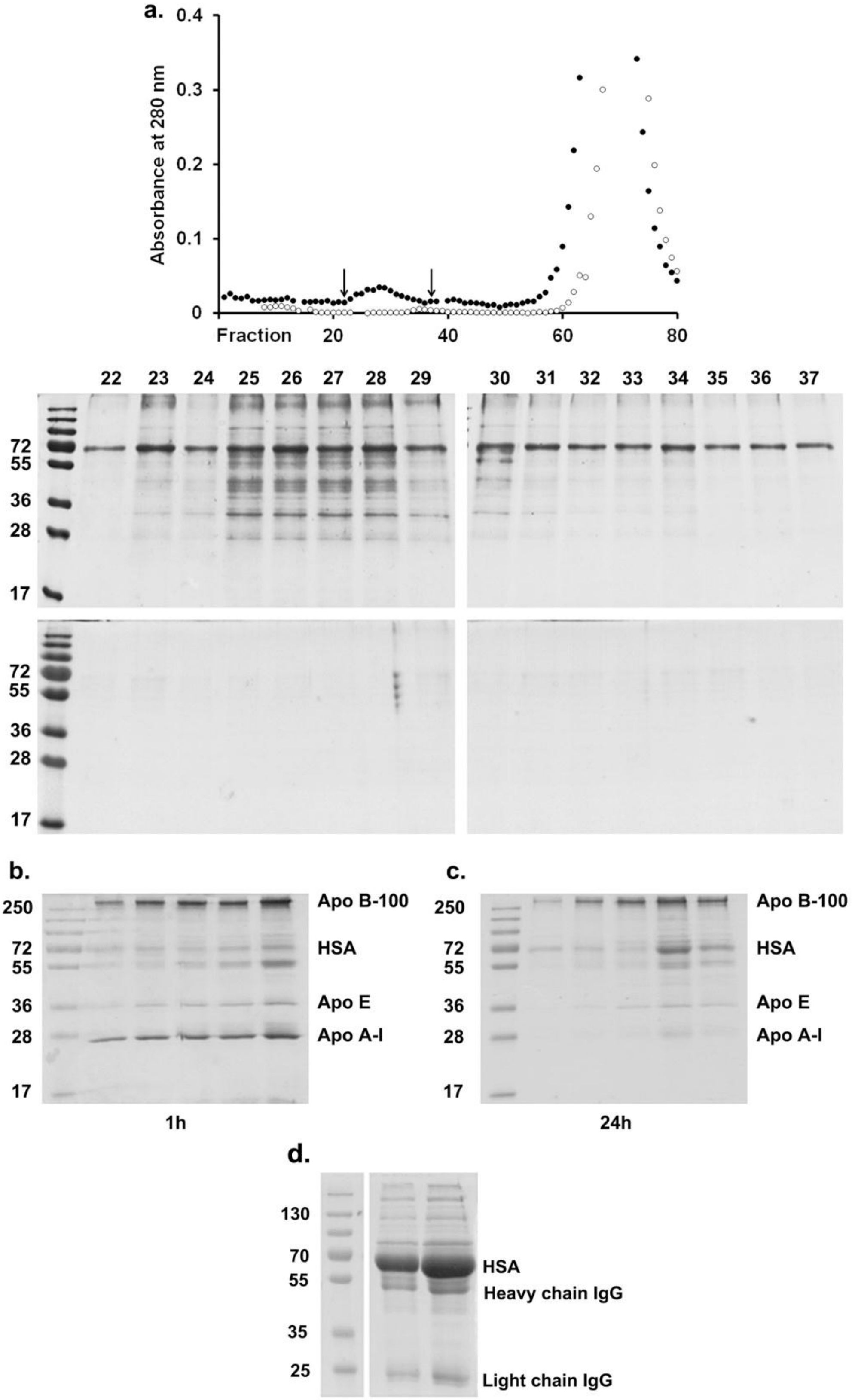

Figure 1. Protein corona around mannan nanogel. (*a*) Colloidal dispersion of mannan nanogel in PBS incubated with human plasma for 24 h at 37 °C or pure plasma as control were separated by size exclusion

chromatography: average absorbance at 280 nm of collected fractions of loaded human plasma in the absence (open circles) or in the presence (closed circles) of nanogel (upper panel); coomassie stained gels of plasma proteins associated with the nanogel (middle panel) and control with only plasma (lower panel), within individual fractions 22 to 37 pooled from four different experiments, precipitated with trichloroacetic acid. Coomassie stained gels of plasma proteins co-pelleted with mannan nanogel after (*b*) 1 h and (*c*) 24 h of incubation stirring at 37 °C of constant amount of mannan nanogel and increasing amount of plasma from left to right, in a fixed final volume. (*d*) Protein profile of the human plasma used in this study. Coomassie stained gel of proteins in 0.5 μL (middle lane) or 1 μL (right lane) of plasma.

Structural consequences of apoA-I and HSA binding to mannan nanogel

Protein binding to nanoparticles is often accompanied by a structural change in the proteins.[16, 37, 41, 62] Two proteins in the corona around mannan nanogel, apoA-I and HSA, were chosen for further analysis of the protein structure after binding to the nanogel. CD spectroscopy was used to follow changes in the secondary structure of the proteins. The CD spectrum of apoA-I has two minima at 222 and 208 nm, which are characteristic of the α-helical structure (Figure 2a). After adding mannan nanogel to apoA-I the negative signal at 222 and 208 nm is stronger, indicating an increase or stabilization of the α-helical structure. Also HSA has α-helical structure, but for HSA there are no significant changes in the structure after adding nanogel (Figure 2b).

Intrinsic tryptophan fluorescence spectroscopy is used to follow changes in the tertiary structure of the proteins. The fluorescence spectra of apoA-I and HSA have maxima at 340 and 344 nm, respectively (Figure 2d, e) indicating a folded protein structure in which the tryptophan side chain is buried in a hydrophobic internal environment. Adding mannan nanogel to the apoA-I causes a decreased intensity, indicating that the signal is quenched by nanogel or that the tryptophan side chain is buried in the interface between the protein and nanogel after protein binding. Adding mannan nanogel to HSA induces, in addition to the decrease in intensity, a blue shift in the wavelength maximum, indicating that the environment around the tryptophan side chains is more hydrophobic after binding to the nanogel.

ApoA-I is the main protein in high-density lipoprotein (HDL) particle and central in the lipid metabolism. A structural change in the protein altering the function of apoA-I could thereby influence the lipid metabolism in a potential harmful way. An increase of helical structure in apoA-I is also seen when it binds to phospholipids in HDL.[63-65] The structural change seen in both cases may be caused by stabilization of the protein structure normally occurring when apoA-I binds to a spherical surface.

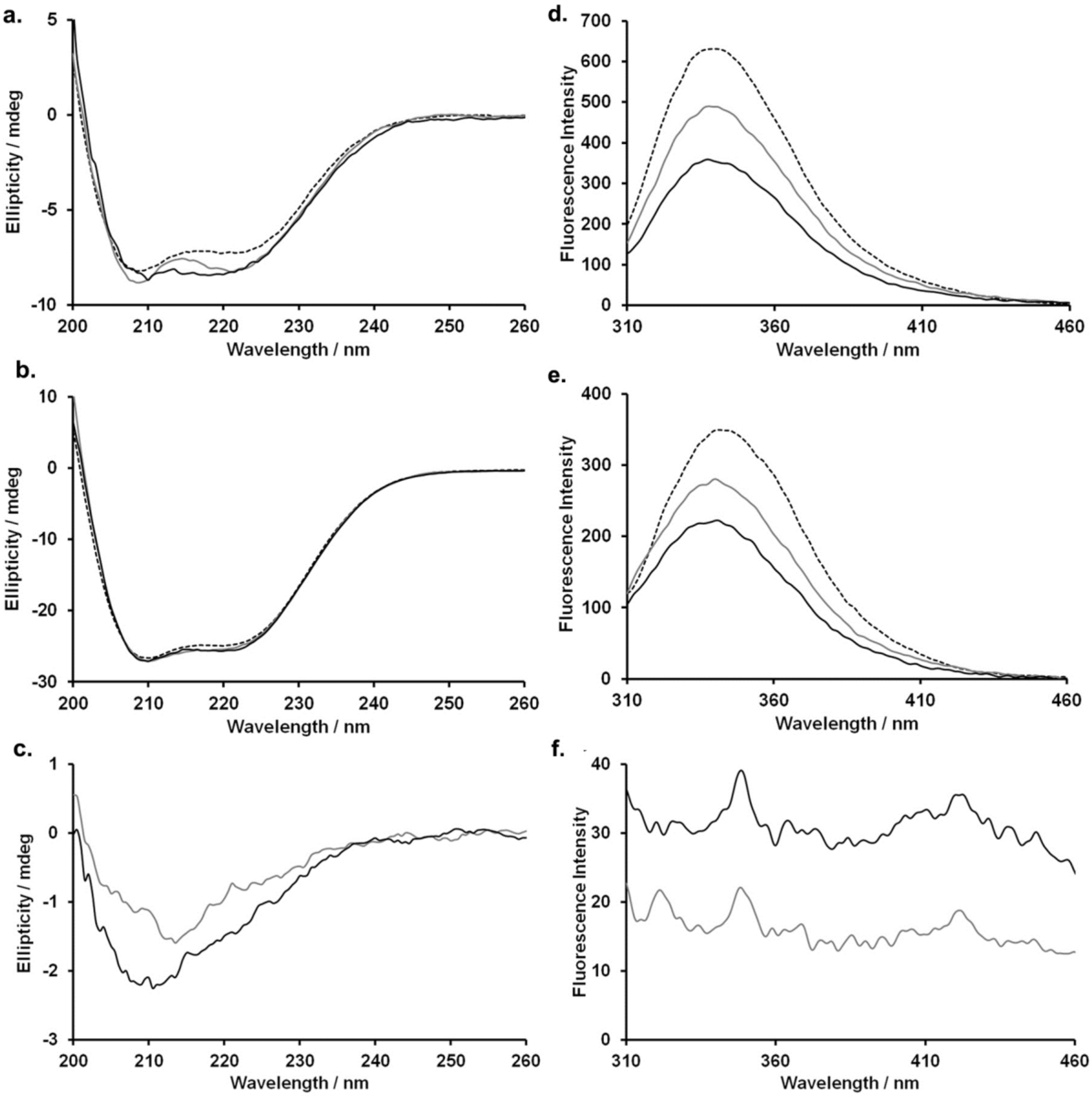

Figure 2. Far-UV CD (*a* and *b*) and tryptophan fluorescence emission (λ_{ex} 290 nm) (*d* and *e*) spectra of protein in the absence (black dashed line) or in the presence of a colloidal dispersion of mannan nanogel in PBS at 0.5 mg/mL (grey solid line) and at 1 mg/mL (black solid line) after subtraction of respective blank (*c* and *f*) recorded at 37 °C after 1 h of incubation stirring at 37 °C; (*a* and *d*) with apoA-I at 0.1 mg/mL or (*b* and *e*) with HSA 0.2 mg/mL.

Time dependent binding between apoA-I and mannan nanogel

The centrifugation experiments in human plasma showed that ratios between proteins in the corona change over time. In general this is expected as predicted by the Vroman effect; proteins present at high concentration in plasma will bind first but will be replaced over time by proteins with lower concentrations but higher affinity. However, for mannan nanogel also the total amount of proteins in the corona appeared to be lower after 24 h compared to after 1 h. A plausible scenario is that the proteins and/or the mannan nanogel structures are changed slowly over time whereby the time to reach equilibrium will be many hours. One such scenario could be that the proteins with time enter the nanogels and interact with the hydrophobic domains inside the nanogels. To test if the proteins' structural change is time dependent, the intrinsic tryptophan fluorescence was measured after 1 and 24 h. A clear difference in intensity is seen for apoA-I, but not for HSA after 1 and 24 h of incubation with nanogel (Figure 3). To further characterize the time dependency, the intensity from the proteins in the presence of nanogel at 0.6 mg/mL was obtained at different time points (Figure 4a). The intensity from HSA is constant while the intensity from apoA-I decreases over time. The most prominent change takes place within 1 h, but the intensity continues to decrease for several hours indicating that the process of apoA-I binding to the nanogel is slow. The affinity of the binding is compared by measuring the intensity at 345 nm after 1 h (open circles) and 24 h (closed circles) for apoA-I (black circles) and HSA (grey circles) in increasing concentrations of mannan nanogel (Figure 4b). The intensity decreases with increasing concentrations of nanogel for both apoA-I and HSA. No differences are seen between the titration curves for HSA after 1 and 24 h and at high concentrations of nanogel the intensity is constant indicating that all proteins are bound to the nanogel. In contrast there is a striking difference between titration curves after 1 and 24 h of incubation of nanogel and apoA-I. The intensity decreases more at nanogel concentrations over 0.3 mg/mL after 24 h of incubation than after 1 h, indicating that more proteins are bound to the nanogel or that a different structural change has occurred after 24 h of incubation. As the estimated amount of apoA-I on the particle is lower after 24 h than after 1 h of incubation (Figure 1b) the explanation that apoA-I undergoes a slow structural change, which may involve interactions with hydrophobic domains inside the mannan nanogel, is more plausible. The stability in size of nanogel over time was tested by measuring the mean hydrodynamic diameter of the mannan nanogel in the presence and in the absence of HSA (Figure 5). No significant changes were observed indicating that the nanogel is stable over the time frame of the measurement. The time dependent structural changes that were seen in the corona proteins emphasize the importance of studying the biocompatibility over time.

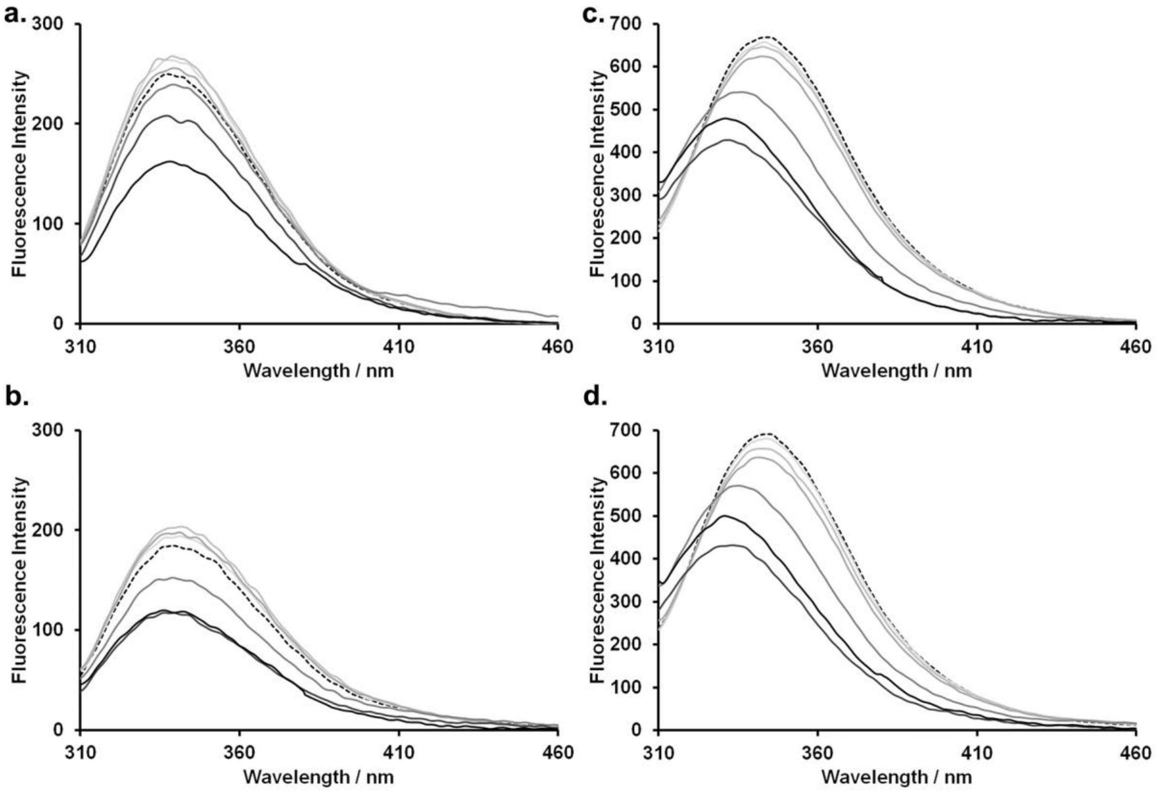

Figure 3. Tryptophan fluorescence emission (λ_{ex} 290 nm) spectra of apoA-I (0.1 mg/mL; *a* and *b*) and HSA (0.1 mg/mL; *c* and *d*) titrations after (*a* and *c*) 1 h and (*b* and *d*) 24 h of incubation stirring at 37 °C. Protein only (black dash line) and protein incubated with mannan nanogel colloidal dispersion in PBS in a range of concentrations (0.01–1.25 mg/mL; grey gradient from lower to higher concentrations).

Attempts were made to estimate the affinity from the titration experiments. The dissociation constant (K_D) of HSA-nanogel complex is estimated to be in µM range (not shown). A similar value of K_D, 6 µM, was obtained by isothermal titration calorimetry (Figure 6), indicating that HSA binds with low affinity to the mannan nanogel. The apoA-I data could not be fitted using Langmuir equation. Low affinity of albumin binding has been observed for other nanoparticles NIPAM:BAM copolymer, 0.83 µM,[66] 20 nm gold, 2.5 µM,[62] and polystyrene, 1.2 µM.[41] The low affinity, compared to for example the higher affinity, 1 nM, of apoA-I to NIPAM:BAM copolymer,[21] explains why only small amount of HSA is found on the particles although the plasma concentration is high.

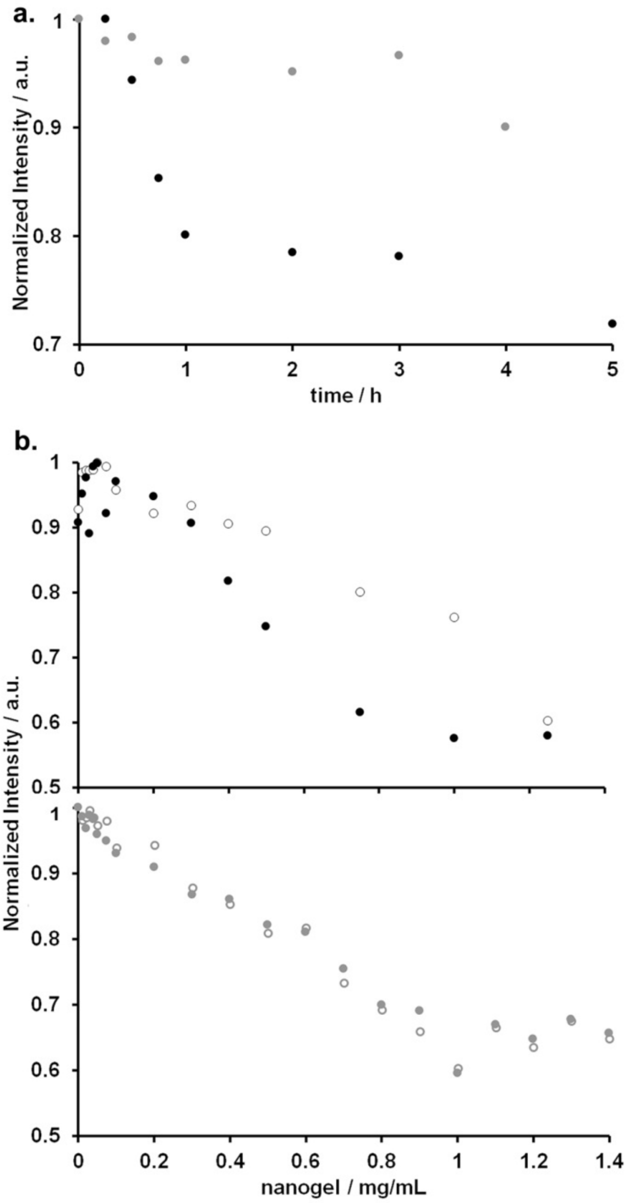

Figure 4. Time dependent binding (*a*) of apoA-I (black) and HSA (grey) at 0.1 mg/mL to mannan nanogel at 0.6 mg/mL in PBS at 37 ºC. Normalized tryptophan emission intensity (λ_{ex} 290 nm) at 345 nm as function of time. (*b*) Fluorescence titration of apoA-I (black) and HSA (grey) solutions at 0.1 mg/mL in the presence of colloidal dispersions of mannan nanogel at various concentrations in PBS after stirring 1 h (open circles) and 24 h (closed circles) at 37 °C; normalized fluorescence intensity at 345 nm as function of mannan nanogel concentration.

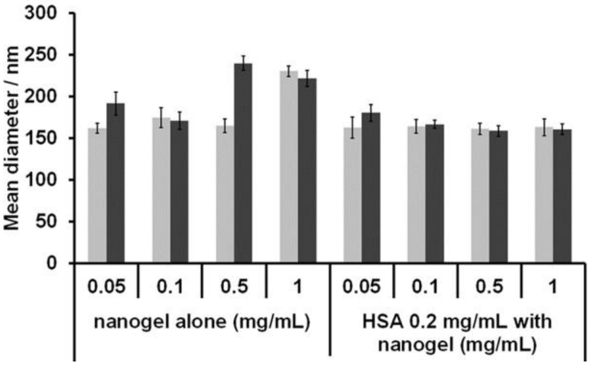

Figure 5. Non-influence of HSA (0.2 mg/mL) and concentration of mannan nanogel (0.05–1 mg/mL) on the z-average or mean hydrodynamic diameter of mannan nanogel colloidal dispersions in PBS after incubation stirring 1 h (bright grey) or 24 h (dark grey) at 37 °C. The results shown (mean ± S.D., *n* = 5) were calculated by DLS. The PdI of all samples ranged from 0.22 and 0.47.

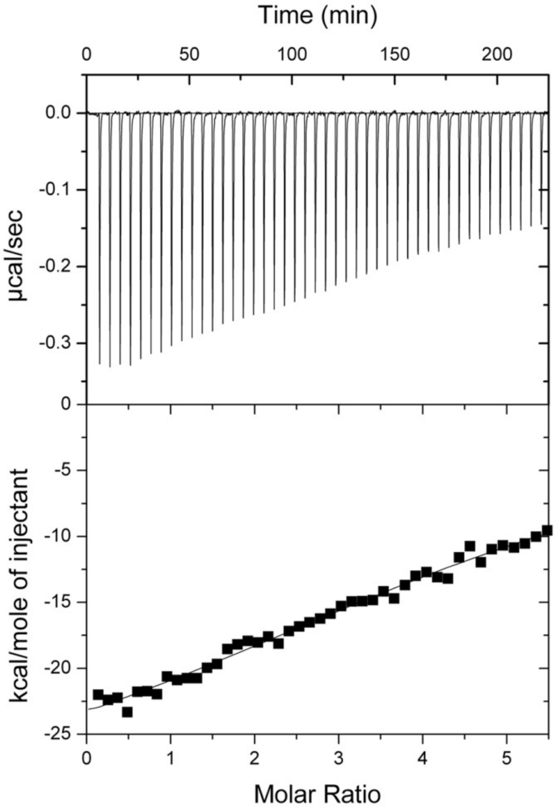

Figure 6. Isothermal titration calorimetry data at 37 °C from titration of HSA stock (5 mg/mL) into a colloidal dispersion of mannan nanogel (2 mg/mL). Each injection was 1 µL with a total of 45 injections. Raw data (upper panel) and integrated data (lower panel) of a representative experiment of four independent experiments. The black line shows the fitted curve assuming a simple 1:1 binding model with one kind of sites after adjusting the baseline, deleting the bad data, and subtracting the reference (injection of protein in buffer). The parameter values obtained were for heat change, ΔH = −25 ± 2 kcal/mol and for dissociation constant, K_D = 5.9 ± 4.6 µM (mean ± S.D., *n* = 4).

Mannan nanogel does not affect blood coagulation

The effect on blood coagulation by mannan nanogel was tested by the thrombin generation assay. No inhibition or stimulation of the thrombin generation is seen when mannan nanogel is added to the system (Figure 7). In another study, using the same assay, amine-modified polystyrene nanoparticles (0.5 mg/mL) inhibited the thrombin generation whereas 220 nm carboxyl-modified polystyrene nanoparticles (0.5 mg/mL) promoted the thrombin generation.[43] Several other nanoparticles can act as procoagulants in the same assay, for example carbon black, silicon dioxide, silicon carbide, titanium carbide and copper oxide nanoparticles.[44] As shown above the protein corona around mannan nanogel is, in contrast to most other nanoparticles studied, simple and consists mainly of apolipoproteins. For NIPAM:BAM copolymer nanoparticles, however, a similar protein corona of apolipoproteins was described.[11, 12] An increase of the more hydrophilic NIPAM part lead to decreased amount of proteins bound but that did not change the identity of the proteins.[11, 12] To compare two different polymer particles with similar protein corona, NIPAM coated gold nanoparticles were tested by the thrombin generation assay (Figure 8). No stimulation of the coagulation was seen. Maybe a simple corona of apolipoproteins is less prone to stimulate the coagulation and is a sign of biocompatibility from a coagulation perspective.

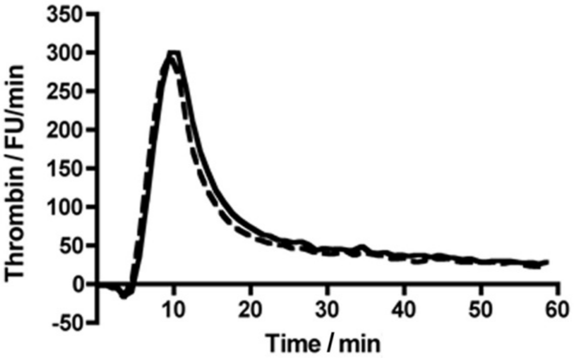

Figure 7. The effect on thrombin generation by mannan nanogel. Plasma was incubated in the absence (solid line) or in the presence (dashed line) of a colloidal dispersion of mannan nanogel at 1 mg/mL, and tested for thrombin generation using the thrombin generation assay. The first derivative, fluorescence units/min, is shown (mean, *n* = 3).

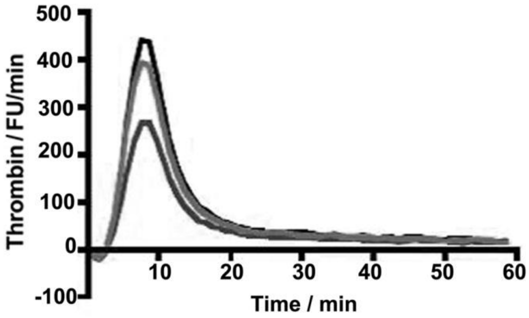

Figure 8. The effect on thrombin generation by NIPAM coated gold particles. Plasma was incubated in the absence (black line) or in the presence of NIPAM coated gold particles at 1.2×10^{-10} M (dark grey line) and at 2.4×10^{-11} M (bright grey line), and tested for thrombin generation using the thrombin generation assay. The first derivative, fluorescence units/min, is shown (mean, $n = 3$). The mean hydrodynamic diameter of the particles is 478 nm as measured by DLS.

Mannan nanogel retards Aβ(M1-40) and β2m fibrillation

The formation of amyloid aggregates was studied in the absence and in the presence of mannan nanogel using a continuous ThT binding assay. A significant increase in ThT fluorescence was observed over time, suggesting amyloid fibrils are formed both with and without nanogel present. However, the presence of mannan nanogel leads to a slight retardation of both Aβ(M1-40) and β2m fibrillation at nanogel concentrations in the range 0.03–0.9 mg/mL where the aggregation is delayed by at most a factor of two-three (Figure 9). An important result is that under no conditions do we see any acceleration of aggregation as has been observed for other nanoparticles.[49,50] Thus it appears that the nanogel acts to reduce the rate of nucleation, but the elongation rate is essentially unaffected by the presence of the nanogel. At constant Aβ(M1-40) and β2m concentration, the time required to reach half of the maximum fluorescence intensity ($t_{1/2}$), increases with the increase in mannan nanogel concentration suggesting that the formation of fibrils is delayed by interaction of Aβ(M1-40) and β2m with the nanogel. Moreover, the inhibitory effect is clearly concentration dependent. Addition of nanogel at a concentration 0.03 mg/mL is needed in order to see a significant effect. This is the first concentration tested above the cac or cmc equal to 0.01 mg/mL, which corresponds to the self-assembly of the amphiphilic monomers of MVC_{16}-31-20 and to the formation of the mannan nanogel.

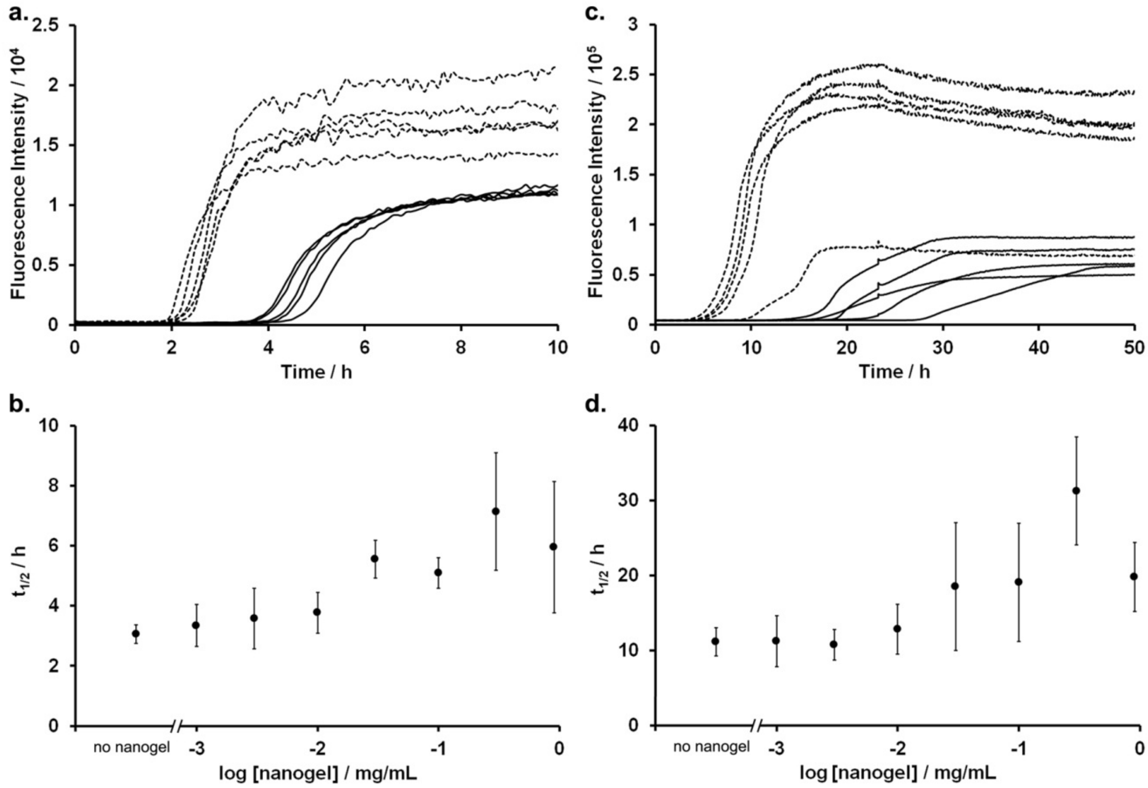

Figure 9. Fibrillation of Aβ(M1-40) (*a* and *b*) and of β2m (*c* and *d*) at 37 °C monitored by the temporal development of ThT binding. (*a*) ThT fluorescence intensity as function of time for 10 μM Aβ(M1-40), in 20 mM sodium phosphate buffer pH 7.4, 200 μM EDTA, 0.02% NaN_3 or (*c*) 40 μM β2m, in 20 mM sodium phosphate buffer pH 2.5, 50 mM NaCl, 0.02% NaN_3, in the absence (dash line) or in the presence (solid line) of mannan nanogel at 0.03 mg/mL, as an example. Each sample contained 20 μM ThT. Five replicates of a representative experiment are shown. Half-time of fibrillation ($t_{1/2}$) as function of the log of mannan nanogel concentration (0–0.9 mg/mL) for (*b*) Aβ(M1-40) and (*d*) β2m. Error bars indicate the S.D. of the mean of 11 replicates, 5 and 6 of two independent experiments.

So far studies indicate that it is the composition of nanoparticles and their surface characteristics that determine their impact on fibrillogenesis.[45] The mannan nanogel acts as artificial chaperones to inhibit the formation of Aβ(M1-40) and β2m fibrils. Hydrophobicity and hydrogen bonding between Aβ(M1-40) or β2m and mannan nanogel, through their hydrophobic domains and polar groups of polymer backbone, respectively, may play a role in binding and/or preventing the nucleation and elongation of the fibrils. The present study was performed using pure Aβ(M1-40) or β2m without competition from other proteins for binding to the nanoparticle surface, which are conditions dissimilar to those *in vivo* in terms of salts, metabolites and biological membranes and unlike any realistic clinical situation. Still, systematic investigation *in vitro* of the aggregation process shows evidence of a retardation effect of mannan nanogel in fibrillation, an extraordinary hint of its biosafety and promising biomedical applicability.

Conclusions

The corona around nanogel is quite specific and simple, and contains a small number of proteins including apolipoproteins B-100, A-I and E, and HSA. The protein corona evolves over time, is formed through a slow process and the equilibrium is reached only after ca. 24 h. Interaction with the mannan nanogel leads to an increased or unchanged α-helical structure for apoA-I and HSA, respectively. After binding of HSA to the nanogel, the environment around the tryptophan side chains is more hydrophobic. Moreover, blood coagulation is unperturbed and Aβ(M1-40) and β2m fibrillation is retarded by mannan nanogel suggesting biosafety, which is mandatory for nanomaterials to be used in biomedical applications.

References

1. Kabanov, A. V.; Vinogradov, S. V. Nanogels as pharmaceutical carriers: finite networks of infinite capabilities. *Angew Chem Int Ed* **2009**, 48, 5418-5429.

2. Oh, J. K. Engineering of nanometer-sized cross-linked hydrogels for biomedical applications. *Can J Chem* **2010**, 88, 173-184.

3. Ferreira, S. A.; Pereira, P.; Sampaio, P.; Coutinho, P. J. G.; Gama, F. M. Supramolecular assembled nanogel made of mannan. *J Colloid Interface Sci* **2011**, 361, 97-108.

4. Apostolopoulos, V.; Pietersz, G. A.; Loveland, B. E.; Sandrin, M. S.; McKenzie, I. F. Oxidative/reductive conjugation of mannan to antigen selects for T1 or T2 immune responses. *Proc Natl Acad Sci USA* **1995**, 92, 10128-10132.

5. Gu, X. G.; Schmitt, M.; Hiasa, A.; Nagata, Y.; Ikeda, H.; Sasaki, Y.; Akiyoshi, K.; Sunamoto, J.; Nakamura, H.; Kuribayashi, K*., et al.* A novel hydrophobized polysaccharide/oncoprotein complex vaccine induces in vitro and in vivo cellular and humoral immune responses against HER2-expressing murine sarcomas. *Cancer Res* **1998**, 58, 3385-3390.

6. Sihorkar, V.; Vyas, S. P. Potential of polysaccharide anchored liposomes in drug delivery, targeting and immunization. *J Pharm Pharm Sci* **2001**, 4, 138-158.

7. Gupta, A.; Gupta, R. K.; Gupta, G. S. Targeting cells for drug and gene delivery: Emerging applications of mannans and mannan binding lectins. *J Sci Ind Res* **2009**, 68, 465-483.

8. Avrameas, A.; McIlroy, D.; Hosmalin, A.; Autran, B.; Debre, P.; Monsigny, M.; Roche, A. C.; Midoux, P. Expression of a mannose/fucose membrane lectin on human dendritic cells. *Eur J Immunol* **1996**, 26, 394-400.

9. Fukasawa, M.; Shimizu, Y.; Shikata, K.; Nakata, M.; Sakakibara, R.; Yamamoto, N.; Hatanaka, M.; Mizuochi, T. Liposome oligomannose-coated with neoglycolipid, a new candidate for a safe adjuvant for induction of CD8+ cytotoxic T lymphocytes. *FEBS Lett* **1998**, 441, 353-356.

10. Apostolopoulos, V.; McKenzie, I. F. Role of the mannose receptor in the immune response. *Curr Mol Med* **2001**, 1, 469-474.

11. Cedervall, T.; Lynch, I.; Foy, M.; Berggard, T.; Donnelly, S. C.; Cagney, G.; Linse, S.; Dawson, K. A. Detailed identification of plasma proteins adsorbed on copolymer nanoparticles. *Angew Chem Int Ed Engl* **2007**, 46, 5754-5756.

12. Cedervall, T.; Lynch, I.; Lindman, S.; Berggård, T.; Thulin, E.; Nilsson, H.; Dawson, K. A.; Linse, S. Understanding the nanoparticle-protein corona using methods to quantify exchange rates and affinities of proteins for nanoparticles. *Proc Natl Acad Sci USA* **2007**, 104, 2050-2055.

13. Hellstrand, E.; Lynch, I.; Andersson, A.; Drakenberg, T.; Dahlbäck, B.; Dawson, K. A.; Linse, S.; Cedervall, T. Complete high-density lipoproteins in nanoparticle corona. *FEBS J* **2009**, 276, 3372-3381.

14. Aggarwal, P.; Hall, J. B.; McLeland, C. B.; Dobrovolskaia, M. A.; McNeil, S. E. Nanoparticle interaction with plasma proteins as it relates to particle biodistribution, biocompatibility and therapeutic efficacy. *Adv Drug Deliv Rev* **2009**, 61, 428-437.

15. Monopoli, M. P.; Walczyk, D.; Campbell, A.; Elia, G.; Lynch, I.; Bombelli, F. B.; Dawson, K. A. Physical-chemical aspects of protein corona: relevance to in vitro and in vivo biological impacts of nanoparticles. *J Am Chem Soc* **2011**, 133, 2525-2534.

16. Lundqvist, M.; Sethson, I.; Jonsson, B.-H. Protein adsorption onto silica nanoparticles: conformational changes depend on the particles' curvature and the protein stability. *Langmuir* **2004**, 20, 10639-10647.

17. Xia, X. R.; Monteiro-Riviere, N. A.; Riviere, J. E. An index for characterization of nanomaterials in biological systems. *Nat Nanotechnol* **2010**, 5, 671-675.

18. Shang, W.; Nuffer, J. H.; Muñiz-Papandrea, V. A.; Colón, W.; Siegel, R. W.; Dordick, J. S. Cytochrome c on silica nanoparticles: influence of nanoparticle size on protein structure, stability, and activity. *Small* **2009**, 5, 470-476.

19. Roach, P.; Farrar, D.; Perry, C. C. Surface tailoring for controlled protein adsorption: Effect of topography at the nanometer scale and chemistry. *J Am Chem Soc* **2006**, 128, 3939-3945.

20. Lundqvist, M.; Stigler, J.; Elia, G.; Lynch, I.; Cedervall, T.; Dawson, K. A. Nanoparticle size and surface properties determine the protein corona with possible implications for biological impacts. *Proc Natl Acad Sci U.S.A.* **2008**, 105, 14265-14270.

21. Dell'Orco, D.; Lundqvist, M.; Oslakovic, C.; Cedervall, T.; Linse, S. Modeling the time evolution of the nanoparticle-protein corona in a body fluid. *PLoS ONE* **2010**, 5, e10949.

22. Casals, E.; Pfaller, T.; Duschl, A.; Oostingh, G. J.; Puntes, V. Time evolution of the nanoparticle protein corona. *ACS Nano* **2010**, 4, 3623-3632.

23. Walczyk, D.; Bombelli, F. B.; Monopoli, M. P.; Lynch, I.; Dawson, K. A. What the cell "sees" in bionanoscience. *J Am Chem Soc* **2010**, 132, 5761-5768.

24. Maiorano, G.; Sabella, S.; Sorce, B.; Brunetti, V.; Malvindi, M. A.; Cingolani, R.; Pompa, P. P. Effects of cell culture media on the dynamic formation of protein-nanoparticle complexes and influence on the cellular response. *ACS Nano* **2010**, 4, 7481-7491.

25. Lundqvist, M.; Stigler, J.; Cedervall, T.; Berggård, T.; Flanagan, M. B.; Lynch, I.; Elia, G.; Dawson, K. The evolution of the protein corona around nanoparticles: A test study. *ACS Nano* **2011**, 5, 7503-7509.

26. Nagayama, S.; Ogawara, K.; Fukuoka, Y.; Higaki, K.; Kimura, T. Time-dependent changes in opsonin amount associated on nanoparticles alter their hepatic uptake characteristics. *Int J Pharm* **2007**, 342, 215-221.

27. Chithrani, B. D.; Chan, W. C. W. Elucidating the mechanism of cellular uptake and removal of protein-coated gold nanoparticles of different sizes and shapes. *Nano Lett* **2007**, 7, 1542-1550.

28. Oberdörster, G. Safety assessment for nanotechnology and nanomedicine: concepts of nanotoxicology. *J Intern Med* **2010**, 267, 89-105.

29. Ehrenberg, M. S.; Friedman, A. E.; Finkelstein, J. N.; Oberdörster, G.; McGrath, J. L. The influence of protein adsorption on nanoparticle association with cultured endothelial cells. *Biomaterials* **2009**, 30, 603-610.

30. Lynch, I.; Cedervall, T.; Lundqvist, M.; Cabaleiro-Lago, C.; Linse, S.; Dawson, K. A. The nanoparticle-protein complex as a biological entity; a complex fluids and surface science challenge for the 21st century. *Adv Colloid Interface Sci* **2007**, 134-135, 167-174.

31. Jiang, X.; Weise, S.; Hafner, M.; Rocker, C.; Zhang, F.; Parak, W. J.; Nienhaus, G. U. Quantitative analysis of the protein corona on FePt nanoparticles formed by transferrin binding. *J R Soc Interface* **2010**, 7 Suppl 1, S5-S13.

32. Lesniak, A.; Campbell, A.; Monopoli, M. P.; Lynch, I.; Salvati, A.; Dawson, K. A. Serum heat inactivation affects protein corona composition and nanoparticle uptake. *Biomaterials* **2010**, 31, 9511-9518.

33. Dobrovolskaia, M. A.; Aggarwal, P.; Hall, J. B.; McNeil, S. E. Preclinical studies to understand nanoparticle interaction with the immune system and its potential effects on nanoparticle biodistribution. *Mol Pharm* **2008**, 5, 487-495.

34. Lynch, I.; Dawson, K. A. Protein-nanoparticle interactions. *Nano Today* **2008**, 3, 40-47.

35. Faunce, T. A.; White, J.; Matthaei, K. I. Integrated research into the nanoparticle-protein corona: a new focus for safe, sustainable and equitable development of nanomedicines. *Nanomedicine (Lond)* **2008**, 3, 859-866.

36. Fenoglio, I.; Fubini, B.; Ghibaudi, E.; Turci, F. Multiple aspects of the interaction of biomacromolecules with inorganic surfaces. *Adv Drug Deliv Rev* **2011**, 63, 1186-1209.

37. Deng, Z. J.; Liang, M.; Monteiro, M.; Toth, I.; Minchin, R. F. Nanoparticle-induced unfolding of fibrinogen promotes Mac-1 receptor activation and inflammation. *Nat Nanotechnol* **2010**, 6, 39-44.

38. Kim, J.; Grate, J. W.; Wang, P. Nanostructures for enzyme stabilization. *Chem Eng Sci* **2006**, 61, 1017-1026.

39. Koutsopoulos, S.; Patzsch, K.; Bosker, W. T. E.; Norde, W. Adsorption of trypsin on hydrophilic and hydrophobic surfaces. *Langmuir* **2007**, 23, 2000-2006.

40. Gagner, J. E.; Lopez, M. D.; Dordick, J. S.; Siegel, R. W. Effect of gold nanoparticle morphology on adsorbed protein structure and function. *Biomaterials* **2011**, 32, 7241-7252.

41. Cukalevski, R.; Lundqvist, M.; Oslakovic, C.; Dahlbäck, B.; Linse, S.; Cedervall, T. Structural changes in apolipoproteins bound to nanoparticles. *Langmuir* **2011**, 27, 14360-14369.

42. Cedervall, T.; Hansson, L.-A.; Lard, M.; Frohm, B.; Linse, S. Food chain transport of nanoparticles affects behaviour and fat metabolism in fish. *PLoS ONE*, **2012**, 7, e32254.

43. Oslakovic, C.; Cedervall, T.; Linse, S.; Dahlbäck, B. Polystyrene nanoparticles affecting blood coagulation. *Nanomedicine*, **2012**, in press.

44. Laloy, J.; Robert, S.; Marbehant, C.; Mullier, F.; Mejia, J.; Piret, J. P.; Lucas, S.; Chatelain, B.; Dogne, J. M.; Toussaint, O*., et al.* Validation of the calibrated thrombin generation test (cTGT) as the reference assay to evaluate the procoagulant activity of nanomaterials. *Nanotoxicology* **2012**, 6, 213-232.

45. Fei, L.; Perrett, S. Effect of nanoparticles on protein folding and fibrillogenesis. *Int J Mol Sci* **2009**, 10, 646-655.

46. Brambilla, D.; Le Droumaguet, B.; Nicolas, J.; Hashemi, S. H.; Wu, L.-P.; Moghimi, S. M.; Couvreur, P.; Andrieux, K. Nanotechnologies for Alzheimer's disease: diagnosis, therapy, and safety issues. *Nanomedicine* **2011**, 7, 521-540.

47. Cleary, J. P.; Walsh, D. M.; Hofmeister, J. J.; Shankar, G. M.; Kuskowski, M. A.; Selkoe, D. J.; Ashe, K. H. Natural oligomers of the amyloid-β protein specifically disrupt cognitive function. *Nat Neurosci* **2005**, 8, 79-84.

48. Baglioni, S.; Casamenti, F.; Bucciantini, M.; Luheshi, L. M.; Taddei, N.; Chiti, F.; Dobson, C. M.; Stefani, M. Prefibrillar amyloid aggregates could be generic toxins in higher organisms. *J Neurosci* **2006**, 26, 8160-8167.

49. Ikeda, K.; Okada, T.; Sawada, S.-i.; Akiyoshi, K.; Matsuzaki, K. Inhibition of the formation of amyloid β-protein fibrils using biocompatible nanogels as artificial chaperones. *FEBS Lett* **2006**, 580, 6587-6595.

50. Cabaleiro-Lago, C.; Quinlan-Pluck, F.; Lynch, I.; Lindman, S.; Minogue, A. M.; Thulin, E.; Walsh, D. M.; Dawson, K. A.; Linse, S. Inhibition of amyloid β protein fibrillation by polymeric nanoparticles. *J Am Chem Soc* **2008**, 130, 15437-15443.

51. Linse, S.; Cabaleiro-Lago, C.; Xue, W.-F.; Lynch, I.; Lindman, S.; Thulin, E.; Radford, S. E.; Dawson, K. A. Nucleation of protein fibrillation by nanoparticles. *Proc Natl Acad Sci USA* **2007**, 104, 8691-8696.

52. Cabaleiro-Lago, C.; Quinlan-Pluck, F.; Lynch, I.; Dawson, K. A.; Linse, S. Dual effect of amino modified polystyrene nanoparticles on amyloid β protein fibrillation. *ACS Chem Neurosc* **2010**, 1, 279-287.

53. Oslakovic, C.; Krisinger, M. J.; Andersson, A.; Jauhiainen, M.; Ehnholm, C.; Dahlback, B. Anionic phospholipids lose their procoagulant properties when incorporated into high density lipoproteins. *J Biol Chem* **2009**, 284, 5896-5904.

54. Walsh, D. M.; Thulin, E.; Minogue, A. M.; Gustavsson, N.; Pang, E.; Teplow, D. B.; Linse, S. A facile method for expression and purification of the Alzheimer's disease-associated amyloid beta-peptide. *FEBS J* **2009**, 276, 1266-1281.

55. Krisinger, M. J.; Guo, L. J.; Salvagno, G. L.; Guidi, G. C.; Lippi, G.; Dahlback, B. Mouse Recombinant Protein C Variants With Enhanced Membrane Affinity and Hyper-Anticoagulant Activity in Mouse Plasma. *FEBS J* **2009**, 276, 6586-6602.

56. LeVine, H., 3rd Thioflavine T interaction with synthetic Alzheimer's disease β-amyloid peptides: detection of amyloid aggregation in solution. *Protein Sci* **1993**, 2, 404-410.

57. Naiki, H.; Gejyo, F. Kinetic analysis of amyloid fibril formation. *Methods Enzymol* **1999**, 309, 305-318.

58. Levine, H. Thioflavin-T interaction with amyloid beta-sheet structures. *Amyloid* **1995**, 2, 1-6.

59. Chiti, F.; Dobson, C. M. Protein misfolding, functional amyloid, and human disease. *Annu Rev Biochem* **2006**, 75, 333-366.

60. Jarrett, J. T.; Lansbury, P. T. Amyloid fibril formation requires a chemically discriminating nucleation event: studies of an amyloidogenic sequence from the bacterial protein OsmB. *Biochemistry* **1992**, 31, 12345-12352.

61. Safi, M.; Courtois, J.; Seigneuret, M.; Conjeaud, H.; Berret, J. F. The effects of aggregation and protein corona on the cellular internalization of iron oxide nanoparticles. *Biomaterials* **2011**, 32, 9353-9363.

62. Lacerda, S. H. D. P.; Park, J. J.; Meuse, C.; Pristinski, D.; Becker, M. L.; Karim, A.; Douglas, J. F. Interaction of gold nanoparticles with common human blood proteins. *ACS Nano* **2009**, 4, 365-379.

63. Saito, H.; Dhanasekaran, P.; Nguyen, D.; Deridder, E.; Holvoet, P.; Lund-Katz, S.; Phillips, M. C. α-helix formation is required for high affinity binding of human apolipoprotein A-I to lipids. *J Biol Chem* **2004**, 279, 20974-20981.

64. Fang, Y.; Gursky, O.; Atkinson, D. Lipid-binding studies of human apolipoprotein A-I and its terminally truncated mutants. *Biochemistry* **2003**, 42, 13260-13268.

65. Kono, M.; Okumura, Y.; Tanaka, M.; Nguyen, D.; Dhanasekaran, P.; Lund-Katz, S.; Phillips, M. C.; Saito, H. Conformational flexibility of the N-terminal domain of apolipoprotein A-I bound to spherical lipid particles. *Biochemistry* **2008**, 47, 11340-11347.

66. Lindman, S.; Lynch, I.; Thulin, E.; Nilsson, H.; Dawson, K. A.; Linse, S. Systematic investigation of the thermodynamics of HSA adsorption to N-iso-propylacrylamide/N-tert-butylacrylamide copolymer nanoparticles. Effects of particle size and hydrophobicity. *Nano Lett* **2007**, 7, 914-920.

Chapter 8

Adjuvant effect of mannan nanogel on the immune response to ovalbumin in mice

The ovalbumin (OVA)-mannan nanogel formulation was characterized physicochemically (size, zeta potential, and loading efficiency) and its immunogenicity was assessed by determining the serum OVA-specific antibody titres in intradermally immunized mice and *ex vivo* splenic proliferative response to OVA or mitogenic stimuli.

OVA-mannan nanogel formulation had a mean hydrodynamic diameter around 240 nm and a near neutral surface charge, similar to mannan nanogel itself. The OVA loading efficiency was around 25% after 24 h of incubation at 25 °C. Intradermal vaccination using the OVA-mannan nanogel formulation elicited a humoral immune response in which OVA-specific immunoglobulin (Ig)G1 was produced, but not IgG2a, indicating a T helper 2-type bias. In addition, the OVA-specific IgA was not detected and low OVA-specific IgG3 titer was detected in the serum.

Introduction

Discovery of novel efficacious and safe adjuvants, vehicles or immunopotentiators, capable of boosting cellular plus humoral immunity, is a primary goal in vaccine design.

Adjuvant activity to B cells provided by T helper (T_H) cells can be evaluated by measuring total immunoglobulin (Ig)G levels in a secondary immune response. T_H cells can be divided into different subsets of effector cells. In particular, the T_H1 subset is associated to cell-mediated immune responses while the T_H2 subset induces essentially a humoral-type immune responses.[1] T_H1 cells secrete cytokines, such as interleukin (IL)-2, tumor necrosis factor β (TNF-β) and interferon (IFN)-γ, and preferentially stimulate the production of IgG2a. They provide help for cytotoxic T-cells production. The T_H1 response is required for protective immunity against intracellular pathogens and tumors. In turn, the T_H2 subset characteristically produces IL-4, besides IL-5 and IL-10, and stimulates the production of IgG1.

Alum (aluminum salts) are extensively used in vaccines but they are not suitable for all antigens, have variable or poor antigen adsorption, and are difficult to lyophilize. Alum-based vaccines have been described to induce only weak T-cell mediated immune responses, poor maturation of antigen-presenting cells (APC), to cause sporadic occurrence of granulomas, hypersensitivity reactions, or neurotoxicity and to be inappropriate for needle-free delivery routes. Alum are T_H2-biased adjuvants that can effectively enhance IgG1 antibody responses in mice, but they fail to induce T_H1 type immune responses.[2, 3] Alum adjuvanticity has been attributed to the intracellular NOD-like receptor family, pyrin domain containing 3 (NLRP3) inflammasome complex activation leading to the processing of several proinflammatory cytokines including IL-1β.[4, 5] Other studies suggest an indirect inflammasome activation *via* an alum induced release of the danger signal uric acid[6] or enzymes from lysosomes of damaged cells.[7] Nevertheless results on the requirement of NLRP3 activity for alum adjuvanticity are still contradictory.[5, 6, 8]

Encapsulation of the antigen into polymeric particulate carrier systems has currently been explored widely, to develop potential novel vaccines in order to enhance the delivery or immunogenicity of an antigen, as a promising alternative to alum. While soluble antigen is poorly presented on major histocompatibility complex (MHC) class I, it has been demonstrated that antigen encapsulated in polymeric particles can be effectively cross-presented yielding an effective $CD8^+$ T-cell response.[9] Nanoparticles with specific physicochemical characteristics can be designed and conjugated with immunopotentiators, providing control on the immunogenicity of the vaccine[10, 11] on the strength and quality of the immune response. This also is influenced by the administration route,[12, 13] and amount of antigen and delivery system used.[12, 14]

In this work, a mannan nanogel, previously developed and comprehensively characterized, was investigated as potential vaccine delivery/adjuvant system. Ovalbumin (OVA) has been commonly used as a model antigen to study the potential of polymeric nanogels to be used in subunit vaccines.[10-17] Our strategy consisted in placing the particulate immunogen intradermally, close to the more efficient APC: the specialized population of dendritic cells (DC) of the epidermis (Langerhans cells). These cells capture the antigen *in situ,* and migrate to T-dependent lymphoid organs, wherein they present the antigen and sensitize antigen-specific T-cells eliciting humoral and cellular immune responses. The nanogel-based immunogenic preparation was physicochemically characterized in terms of size, surface charge and loading efficiency. Furthermore, the extent and type of immune response elicited after intradermal administration of the OVA-nanogel formulation in mice was evaluated assessing the serum OVA-specific antibody titres, the *ex vivo* splenic proliferative response to OVA or mitogenic stimuli and the production of cytokines from splenocytes.

Experimental

Mannan nanogel

Mannan-VMA-SC_{16} (VMA: vinyl methacrylate, SC_{16}: hydrophobic alkyl chain) was synthesized, as described previously,[18] with 31 acrylate groups (DS_{VMA} 31%) and 20 alkyl chains (DS_{C16} 20%) per 100 mannose residues. Resultant amphiphilic mannan is named MVC_{16}-31-20. Each sterile stock colloidal dispersion of mannan-C_{16} was prepared stirring the lyophilized mannan-C_{16} in sterile apyrogenic phosphate buffered saline, pH 7.4 (PBS), for 3–5 days at 50 °C, followed by sterilized filtration (Minisart® Syringe Filters, Sartorius stedim biotech, Germany; pore size 0.22 μm). The nanogel formation was confirmed by dynamic light scattering (DLS). The size distribution and zeta potential measurements were performed in a Malvern Zetasizer NANO ZS (Malvern Instruments Limited, UK) as previously described.[4]

Complement activation

To determine if mannan nanogel activated the complement cascade, the protocol described by the Nanotechnology Characterization Laboratory for qualitative determination of total complement activation by Western blot analysis[19] was performed with slight modifications. Briefly, equal volumes (50 μL) of human plasma from healthy donors, veronal buffer and sample – mannan nanogel colloidal dispersion in PBS (1 mg/mL), cobra venom factor (Quidel Corporation, California, USA) as positive control, or PBS as negative control − were mixed together and incubated 1 h at 37 °C. Proteins were resolved using 10% sodium dodecyl sulphate polyacrylamide gel electrophoresis (SDS-PAGE), and then transferred to a Immun-Blot PVDF membrane using the Trans-Blot® SD semidry transfer equipment (Bio-Rad, California, USA). The membranes were incubated 90 min with a mouse monoclonal antibody against human C3 (Abcam, Cambridge, UK) diluted 1:1000 followed by washes and incubation with secondary polyclonal antibodies goat anti-mouse IgG conjugated with alkaline phosphatase (Dako, Glostrup, Denmark) diluted 1:2000. The membrane was finally revealed with 5-bromo-4-chloro-3-indolyl phosphate (BCIP; Sigma, St Louis, Missouri, USA). The C3 degradation was evaluated by densitometry using image analysis software (NIH Image J software).

Antigen

OVA (Grade III, Mw 45 KDa; Sigma) solutions in PBS were depleted of contaminating endotoxin using a polymixin B column (Pierce, Illinois, USA), and tested by the limulus amebocyte lysate test (E-toxate™; Sigma). All OVA preparations used in this study tested endotoxin free.

Preparation and characterization of OVA-mannan nanogel formulation

The OVA (0.2 mg/mL) incorporation in mannan nanogel colloidal dispersion (4 mg/mL) in PBS, after 24 h of incubation at 25 °C was evaluated using an ultrafiltration method – 5 min at 10,000 g to collect the filtrate and 2 min at 1,000 g to collect the retentate – using Heraeus® Pico™ & Fresco™ 17 microcentrifuge (Thermo Scientific) and Microcon Centrifugal Filter devices with molecular weight cut-off, 1×10^5 (Millipore). The retentate was subjected to 3 washes in PBS. Initial sample and all collected filtrate and retentate samples had a fixed final volume adjusted with PBS. Empty nanogel colloidal dispersion (4 mg/mL) and OVA solution (0.2 mg/mL) in PBS were used as controls and subjected to the same procedure. The association of OVA with nanogel was evaluated by analyzing initial sample, filtrate and retentate fractions by SDS-PAGE and protein assays. Each sample (10 µL) was diluted with PBS (10 µL) and proteins were desorbed from the nanogel by adding SDS loading buffer (4 µL) followed by 6–10 min boiling. Samples were resolved using 12% SDS-PAGE. Each gel run included one lane of a molecular weight protein ladder standard (PageRuler Prestained Protein Ladder; Fermentas). Gels were silver-stained. For all samples in study, the OVA concentration was determined with bicinchoninic acid (BCA) protein assay kit (Pierce, Illinois, USA) and Bio-Rad protein assay (Bio-Rad, California, USA) following manufacturer instructions. Each sample was assessed in duplicate in two independent experiments; the results were expressed as the amount of protein (µg) per milligram of mannan nanogel. Besides, the loading efficiency was defined as the percentage of OVA loaded relating to the initial amount of protein. The absorbance obtained for colloidal dispersion of mannan nanogel fractionated samples, was subtracted from that obtained for each OVA-mannan nanogel fractionated samples.

Mice

Male BALB/c mice (15 weeks old) were purchased from Charles River (Barcelona, Spain). Animals were kept at the animal facilities of the Institute Abel Salazar during the experiments. Hiding and nesting materials were provided as enrichment. Procedures involving mice were performed according to the European Convention for the Protection of Vertebrate Animals used for Experimental and Other Scientific Purposes (ETS 123) and 86/609/EEC Directive and Portuguese rules (DL 129/92).

Immunization

Mice were trice immunized intradermally with 20 µg of OVA formulated with one of the following delivery vehicles (100 µL): PBS; control adjuvant 1:1 PBS/alum suspension (Aluminium hydroxide Gel; Brenntag, Frederikssund, Denmark, a kind gift of Dr Erik Lindblad, Biosector, Frederikssund, Denmark); and mannan nanogel (400 µg) colloidal dispersions in PBS: the OVA was either mixed immediately before injection (OVA-mannan nanogel-M) or allowed to incorporate in the nanogel for 24 h at 25 °C (OVA-mannan nanogel-I). As control, mannan nanogel (400 µg/100 µL) colloidal dispersion in PBS was also injected, completing the five groups in study. All formulations injected were evaluated by silver-stained SDS-PAGE gels prepared as described above. The mannan nanogel and OVA-mannan nanogel size distribution and zeta potential were studied in DLS.

The first boost was given 16 days after priming and the second one in the following 26 days. Blood samples were collected 12−15 days post immunization. After incubation overnight at 4 °C till clot formation, samples were centrifuged for 15 min at 10,000 g at 4

°C (Heraeus® Pico™ & Fresco™ 17 microcentrifuge, Thermo Scientific) and collected sera were stored at −20 °C until used in antibody assessment by quantitative enzyme-linked immunosorbent assay (ELISA).

Titration of OVA-specific antibody in serum

OVA-specific IgM, IgG, IgG1, IgG2a, IgG3 and IgA in serum were detected by ELISA. In brief, microtiter flat-botton 96-well plate (MaxiSorp™, Nunc, Denmark) were coated overnight at 4 °C with 5 µg/mL OVA solution in PBS (50 µL/well). After washing with 0.05% Tween 20 in Tris-buffered saline (10 mM Tris base, 150 mM NaCl), pH 8.0 (TST buffer), the block solution – TST buffer with 2% bovine serum albumin (BSA, Sigma) – incubated for 1 h at room temperature (200 µL/well). After discarding the block solution, serial dilutions of the serum samples in TST with 1% BSA were then plated (50 µL/well) and incubated for 1 h at room temperature. After washing with TST buffer, the secondary antibody goat anti-mouse IgG, IgG1, IgG2a, IgG3 and IgA conjugated to alkaline phosphatase human adsorbed (SouthernBiotech, Alabama, USA) diluted 1:500 was incubated 1 h at room temperature (50 µL/well). After washing with TST buffer, the bound antibodies were detected by development at room temperature, protected from light, using a substrate solution (50 µL/well) of 4-nitrophenylphosphate disodium salt hexahydrate (5 mg/tablet, Sigma) dispersed in 5 mL of alkaline phosphatase buffer (50 mM Na_2CO_3, 1 mM $MgCl_2$), pH 9.8. The reaction was stopped by the addition of 0.1 M ethylenediaminetetraacetic acid (EDTA), pH 8.0 (50 µL/well). The absorbance was measured at 405 and at 570 nm as reference with an ELISA spectrophotometer (Original Multiskan Ex; Thermo Electron Corporation). The ELISA antibody titres were expressed as the reciprocal of the highest dilution giving an absorbance of 0.1 above that of the control (no serum added).[15, 20, 21]

Splenocytes assays

Mice were sacrificed 26 days after third immunization. The spleens were excised aseptically and lymphocytes isolated. Briefly, single cell suspensions were prepared by teasing the tissue between two glass slides and cells were centrifuged for 10 min at 240 g at 4 °C (Sigma 3-16k Refrigerated Centrifuge). Erythrocytes present were lysed using an ACK lysis buffer (155 mM NH_4Cl, 10 mM $KHCO_3$, and 0.1 mM EDTA) for 5 min. After centrifugation, the pelleted cells were washed twice with Hank´s balanced salt solution (HBSS; Sigma) and resuspended in complete medium (cRPMI) – RPMI 1640 medium (Sigma) supplemented with 4-(2-hydroxyethyl)-1-piperazineethanesulfonic acid (HEPES;

10 mM; Sigma), 10% heat-inactivated fetal bovine serum (FBS; Sigma), penicillin (60 IU/mL), streptomycin (60 µg/mL; Sigma), β-mercaptoethanol (0.5 mM; Sigma). Each cell suspension was normalized after accurate calculation of cells per microliter in the sample using a same volume of known concentration of flow cytometry cell counting beads (microparticles based on polystyrene monodisperse, 10 µm; Fluka) by flow cytometric analysis (fluorescence-activated cell sorting [FACS]) in a flow cytometer (Beckman Coulter) with supplied software (EXPO 32 ADC V1.2). Spleen cell suspension was plated ($2x10^5$ cell/200 µL/well) into 96-well round-bottomed culture plates (Nunc, Denmark). Splenocytes were cultured for 72 h at 37 °C in a 95% humidified air containing 5% CO_2 in the absence of stimuli (cRPMI only), or stimulated with *a*) OVA (25 µg/mL), *b*) the unspecific mitogen concanavalin A (con A; 5 µg/mL; Sigma) that can activate T-cells, or *c*) hamster anti-mouse CD3 (0.5 µg/mL; BD Pharmingen™), that can activate either unprimed (naive) or primed (memory/preactivated) T-cells, in the presence of Fc receptor-bearing accessory cells. All the tests were carried out in duplicates.

Determination of cell concentration

The cell suspension in each well was homogenized and the cell concentration assessed using flow cytometry cell counting beads, as described above. The results are expressed as stimulation index (SI) calculated as follows: SI = the cell concentration for stimulated cultures divided by the cell concentration for nonstimulated cultures.

Analysis of cytokines in splenocyte culture supernatants

The plates were centrifuged 7 min at 1200 g (Alc 4236 centrifuge) and the culture supernatants were collected and stored at −80 °C for the estimation of cytokines. The T_H1 (IFN-γ) and T_H2 (IL-4) cytokines were measured with mouse IFN-γ DuoSet® ELISA Development System (R&D Systems) and mouse IL-4 ELISA Ready-SET-Go!® (eBioscience), respectively, according to the manufacturer’s instructions.

Colorimetric assay for splenocyte proliferation

Splenocytes were resuspended in fresh cRPMI (200 µL/well), subsequently added with 3-(4,5-dimethylthiazol-2-yl)-2,5-diphenyltetrazolium bromide (MTT; Sigma) solution in PBS (final concentration: 0.5 mg/mL) and then incubated for 3 h at 37 °C in a 95% humidified air containing 5% CO_2. The plates were centrifuged 7 min at 1200 g (Alc 4236 centrifuge); the untransformed MTT was carefully removed and the formazan crystals solubilized with dimethyl sulfoxide. Finally, the UV absorbance was measured at 570 nm after 15 min in

ELISA spectrophotometer (Original Multiskan Ex; Thermo Electron Corporation). The results shown are from one experiment performed in duplicate. The results are expressed as SI calculated as follows: SI = the absorbance value for stimulated cultures divided by the absorbance value for nonstimulated cultures.

Statistical analysis

The results were expressed as mean ± standard deviation (S.D.) for each group ($n = 3$, OVA in 1:1 PBS/alum; $n = 4$, in other groups) and statistical analysis was carried out using one-way analysis of variance (ANOVA) with Bonferroni's multiple comparison post-test using GraphPad Prism version 4.00 for Windows (GraphPad Software, California, USA).

Results and discussion

OVA-mannan nanogel formulation

Mannan from *Saccharomyces cerevisiae,* used to produce self-assembled mannan nanogel, is a mannose-rich glycan able to bind mannose-binding lectin, also known as mannan-binding protein, leading to complement activation via the lectin pathway.[22, 23] Complement activation can promote inflammation, macrophage phagocytosis, anaphylaxis, B-cell activation, and T-cell response, as well as enhance antigen presentation to B-cells by follicular DC.[24] As uncontrolled complement activation can induce many inflammatory and life threatening disorders,[25, 26] the mannan nanogel degree of complement activation was examined in an *in vitro* assay in human plasma aliquots pretreated with mannan nanogel. Mannan nanogel did not induce complement activation, as compared to control (Figure 1).

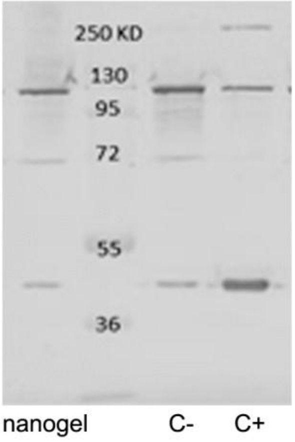

Figure 1. Analysis of complement system activation by Western blot. The upper band of ~115 KDa corresponds to C3 (α chain) and the lower band ~43 KDa corresponds to C3-cleavage product(s) (C3c, iC3b[C3α'] for mannan nanogel (nanogel), PBS as negative control (C-) and cobra venom factor as positive control (C+). C3 degradation was evaluated by densitometry using image analysis software (NIH Image J software), after normalizing the percentage of the lower band of the positive control as the maximum degradation that can be achieved (100%): 41 ± 8% for negative control and 33 ± 7% for mannan nanogel.

Considering the mannan ability to target mannose receptor expressed on the surface of APC,[27, 28] and the ability of nanogels to carry biologically active agents,[29] we conceived the mannan nanogel as vaccine delivery/adjuvant system, which is tested in the current work. Following loading of nanogel with OVA, preparations were subjected to ultracentrifugation, to determine how efficiently the OVA was associated with the nanogel. Initial and fractionated samples were evaluated by SDS-PAGE (Figure 2) and by the Bio-Rad and BCA protein assays. As previously studied by phenol-sulfuric acid method, using mannose as standard, 75% of the initial amount of the mannan nanogel is collected in the retentate.[4] Free protein was in the filtrate. In contrast, when the OVA-nanogel preparations were employed, part of OVA was associated with the nanogels in the retentate – 16.6 ± 7.2 or 16.7 ± 0.5 μg OVA/mg mannan nanogel – with a loading efficiency of 24.9 ± 6.1% or 23.3 ± 3.1% as assessed by BCA or Bio-Rad protein assay, respectively.

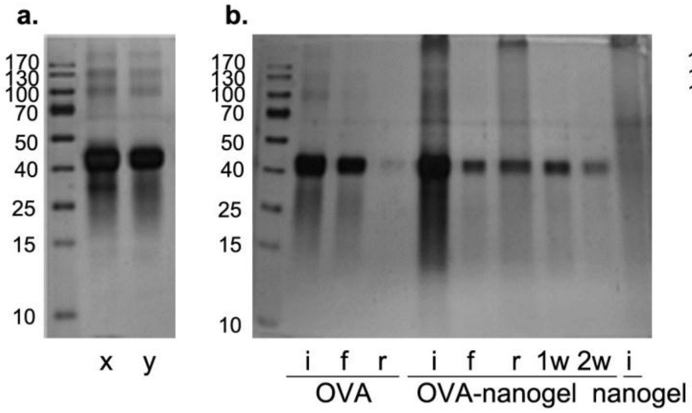

Figure 2. Characterization of OVA-mannan nanogel formulation with silver-stained SDS-PAGE gels: (*a*) OVA (0.2 mg/mL) integrity in formulation, examined comparing the freshly prepared (x) with the incubated 24 h at 25 °C (y); (*b*) ultrafiltration of OVA-mannan nanogel formulation obtained by incorporation (24 h at 25 °C) of OVA (0.2 mg/mL) in mannan nanogel colloidal dispersion (4 mg/mL) in comparison with OVA solution (0.2 mg/mL) and empty nanogel colloidal dispersion (4 mg/mL) in PBS – initial sample (i), first filtrate (f), and retentate (r) obtained after washing (filtrates 1w and 2w); (*c*) OVA-mannan nanogel samples used to immunize mice intradermally obtained by mixture (M) or incorporation (I) in comparison with OVA (O) and nanogel (N) in PBS.

The size distribution and zeta potential of mannan nanogel and OVA-mannan nanogel formulation was evaluated by DLS (Table 1). OVA-mannan nanogel formulation had a mean hydrodynamic diameter around 240 nm and a near neutral surface charge, similar to those obtained for mannan nanogel. These samples and OVA formulated in PBS were analyzed by SDS-PAGE (Figure 2c).

Table 1. Size and zeta potential measurements obtained in DLS at 37 ºC for mannan nanogel colloidal dispersion in PBS (4 mg/mL) and for OVA (0.2 mg/mL) formulated with mannan nanogel colloidal dispersion in PBS (4 mg/mL), immediately after mixture (OVA-mannan nanogel-M) or after 24 h of incorporation at 25 °C (OVA-mannan nanogel-I)

	mannan nanogel	OVA-mannan nanogel-M	OVA-mannan nanogel-I
Z-average (nm)	240.9 ± 6.7	239.6 ± 9.0	234.3 ± 8.5
Polydispersity Index (PdI)	0.618 ± 0.099	0.565 ± 0.101	0.702 ± 0.022
Zeta potential (mV)	-9.69 ± 2.00	-11.10 ± 1.09	-10.90 ± 1.43

(mean ± S.D., *n* = 10)

Immune response induced by immunization using OVA-mannan nanogel formulation

Specific antibody response in serum

The effect of mannan nanogel on the induction of humoral immune response in OVA-immunized mice was evaluated by ELISA. The production of antibodies of different isotypes is associated with different types of T_H cells. IgG3 was not detected 12 days after first boost and IgA was not detected 15 days after second boost (data not shown). IgG2a, associated with T_H1-type immune response, was not detected in any immunized group after priming, first and second boost (data not shown), denoting little evidence of activation of the cellular arm of the immune system. The serum OVA-specific IgM, IgG, IgG1 and IgG3 antibody levels in the OVA-immunized mice are shown in Figure 3. After priming, OVA-specific IgM was equally detected in all groups. Similarly to alum, mannan nanogel adjuvant formulated with OVA enhanced OVA-specific IgG1 subclass associated with T_H2-type immune response but significant differences were only detected when using OVA-mannan nanogel-I after third immunization, as compared with OVA in PBS immunized group. However, there were no observed significant differences between the total serum IgG1 levels in mice groups immunized with OVA-mannan nanogel-M or OVA-mannan nanogel-I. OVA in 1:1 PBS/alum suspension produced significantly higher OVA-specific IgG1 titres, as compared with OVA in PBS immunized group. After third immunization significant differences in OVA-specific levels of IgG3 were also detected when using alum. From the above findings, we can draw that mannan nanogel can enhance serum antibody production in mice immunized with OVA.

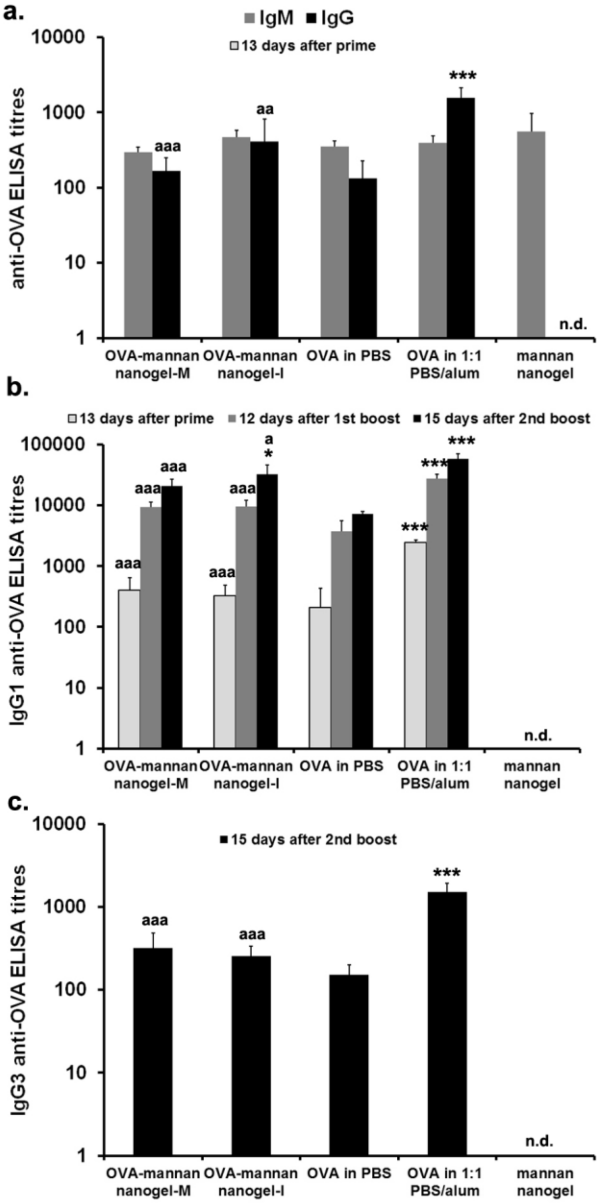

Figure 3. Effect of mannan nanogel on serum OVA-specific antibody titres. Groups of male BALB/c mice were trice immunized intradermally on days 1, 16 and 42 with 20 µg OVA formulated with one of the following delivery vehicles (100 µL): mannan nanogel (400 µg) colloidal dispersion in PBS, immediately mixed before injection (OVA-mannan nanogel-M) or obtained after 24 h of incubation at 25 °C (OVA-mannan nanogel-I); PBS; control adjuvant 1:1 PBS/alum suspension. As control, mannan nanogel (400 µg) colloidal dispersion in PBS was also injected, completing the five groups in study. The titres are presented as mean ± S.D. (*n* = 3, OVA in 1:1 PBS/alum; *n* = 4, in other groups) for (*a*) IgM, IgG (13 days after priming), (*b*) IgG1 (13 days after priming, 12 day after first boost, and 15 days after second boost) and (*c*) IgG3 (15 days after second boost). Statistical significant differences with regard to the OVA in PBS group were designated as *p < 0.05 and ***p < 0.001 and those with OVA in 1:1 PBS/alum group were designated as ^{a}p < 0.05, ^{aa}p < 0.01 and ^{aaa}P < 0.001; not detected (n.d.).

Splenocyte proliferation and cytokine secretion

Stimulation index (SI) assessed by flow cytometry using cell counting beads (Figure 4a) and MTT method (Figure 4b) in isolated and re-stimulated splenocytes from mice previously immunized indicate slight differences in proliferative response to OVA.

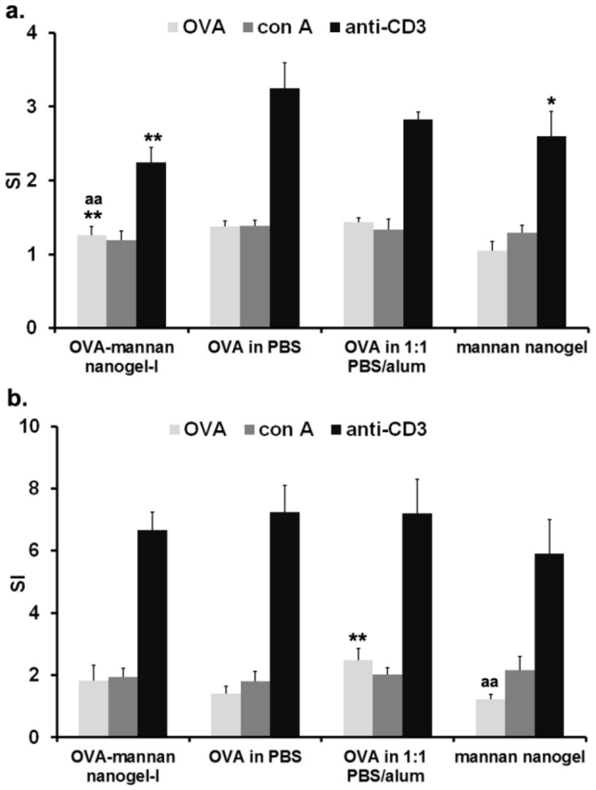

Figure 4. Effect of mannan nanogel on OVA, concanavalin A (con A) and anti-CD3 stimulated splenocyte proliferation. Groups of male BALB/c mice were trice immunized intradermally on days 1, 16 and 42 with 20 µg OVA formulated with one of the following delivery vehicles (100 µL): mannan nanogel (400 µg) colloidal dispersion in PBS after 24 h of incubation at 25 °C (OVA-mannan nanogel-I); PBS; and control adjuvant 1:1 PBS/alum suspension. As control, mannan nanogel (400 µg) colloidal dispersion in PBS was also injected, completing the four groups in study. Splenocytes were prepared 26 days after the last immunization, and cultured with OVA (25 µg/mL), Con A (5 µg/mL), anti-CD3 (0.5 µg/mL), or cRPMI, for 72 h. Splenocyte proliferation was measured (*a*) by flow cytometry using cell counting beads and (*b*) by the MTT method. The stimulation index (SI) is presented as mean ± S.D. (*n* = 3, OVA in 1:1 PBS/alum; *n* = 4, in other groups). For each treatment, statistical significant differences with OVA in PBS group were designated as *p < 0.05 and **p < 0.01 and those with OVA in 1:1 PBS/alum group designated as ^{aa}p < 0.01.

Similar levels of IFN-γ were detected in all groups in *ex vivo* splenic response to OVA, con A and anti-CD3 stimulation (Figure 5). When the mice were challenged with antigen (OVA) the development of the T_H2-type response could have resulted in a lower production of INF- γ than in control group challenged with mannan nanogel as shown by the results obtained in unstimulated cultures. All unstimulated and OVA- or Con A-stimulated cultures secreted undetectable levels of IL-4 (< 8 pg/mL), except OVA-stimulated culture in OVA in 1:1 PBS/alum group (33 ± 8 pg/mL). Only anti-CD3 stimulated detectable levels IL-4, ranging around 112 ± 28 pg/mL in all groups (data not shown).

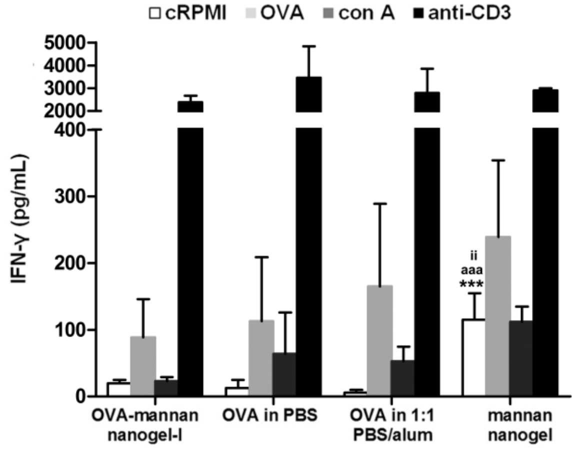

Figure 5. IFN-γ profile of mice immunized with OVA formulated with proposed adjuvant mannan nanogel. Groups of male BALB/c mice were trice immunized intradermally on days 1, 16 and 42 with 20 µg OVA formulated with one of the following delivery vehicles (100 µL): mannan nanogel (400 µg) colloidal dispersion in PBS after 24 h of incubation at 25 °C (OVA-mannan nanogel-I); PBS; and control adjuvant 1:1 PBS/alum suspension. As control, mannan nanogel (400 µg) colloidal dispersion in PBS was also injected, completing the four groups in study. Splenocytes were prepared 26 days after the last immunization, and stimulated *in vitro* with OVA (25 µg/mL), Con A (5 µg/mL), or anti-CD3 (0.5 µg/mL) for 72 h. The production of IFN-γ was measured in the culture supernatants by ELISA according to manufacturer instructions. The values are presented as mean ± S.D. (*n* = 3, OVA in 1:1 PBS/alum; *n* = 4, in other groups). For each treatment, significant differences with OVA in PBS group were designated as ***p < 0.001; those with OVA in 1:1 PBS/alum group were designated as $^{aaa}p < 0.001$; and those with OVA-mannan nanogel-I group were designated as $^{ii}p < 0.01$.

Conclusions

Based on findings presented herein, preliminary results indicate that mannan nanogel has potential immunological adjuvant activity on the specific immune response to OVA, predominantly humoral, in intradermally immunized mice. Antibody subtyping indicates a T_H2 bias.

References

1. Constant, S. L.; Bottomly, K. Induction of Th1 and Th2 CD4+ T cell responses: the alternative approaches. *Annu Rev Immunol* **1997**, 15, 297-322.

2. Gupta, R. K. Aluminum compounds as vaccine adjuvants. *Adv Drug Deliv Rev* **1998**, 32, 155-172.

3. Harm, H. Mechanisms of stimulation of the immune response by aluminum adjuvants. *Vaccine* **2002**, 20, Supplement 3, S34-S39.

4. Eisenbarth, S. C.; Colegio, O. R.; O/'Connor, W.; Sutterwala, F. S.; Flavell, R. A. Crucial role for the Nalp3 inflammasome in the immunostimulatory properties of aluminium adjuvants. *Nature* **2008**, 453, 1122-1126.

5. Li, H.; Willingham, S. B.; Ting, J. P.; Re, F. Cutting edge: inflammasome activation by alum and alum's adjuvant effect are mediated by NLRP3. *J Immunol* **2008**, 181, 17-21.

6. Kool, M.; Soullié, T.; van Nimwegen, M.; Willart, M. A. M.; Muskens, F.; Jung, S.; Hoogsteden, H. C.; Hammad, H.; Lambrecht, B. N. Alum adjuvant boosts adaptive immunity by inducing uric acid and activating inflammatory dendritic cells. *J Exp Med* **2008**, 205, 869-882.

7. Hornung, V.; Bauernfeind, F.; Halle, A.; Samstad, E. O.; Kono, H.; Rock, K. L.; Fitzgerald, K. A.; Latz, E. Silica crystals and aluminum salts activate the NALP3 inflammasome through phagosomal destabilization. *Nat Immunol* **2008**, 9, 847-856.

8. McKee, A. S.; Munks, M. W.; MacLeod, M. K.; Fleenor, C. J.; Van Rooijen, N.; Kappler, J. W.; Marrack, P. Alum induces innate immune responses through macrophage and mast cell sensors, but these sensors are not required for alum to act as an adjuvant for specific immunity. *J Immunol* **2009**, 183, 4403-4414.

9. Wang, X.; Uto, T.; Akagi, T.; Akashi, M.; Baba, M. Induction of potent CD8+ T-cell responses by novel biodegradable nanoparticles carrying human immunodeficiency virus type 1 gp120. *J Virol* **2007**, 81, 10009-10016.

10. Hamdy, S.; Elamanchili, P.; Alshamsan, A.; Molavi, O.; Satou, T.; Samuel, J. Enhanced antigen-specific primary CD4+ and CD8+ responses by codelivery of ovalbumin and toll-like receptor ligand monophosphoryl lipid A in poly(D,L-lactic-co-glycolic acid) nanoparticles. *J Biomed Mater Res A* **2007**, 81, 652-662.

11. Sarti, F.; Perera, G.; Hintzen, F.; Kotti, K.; Karageorgiou, V.; Kammona, O.; Kiparissides, C.; Bernkop-Schnurch, A. In vivo evidence of oral vaccination with PLGA nanoparticles containing the immunostimulant monophosphoryl lipid A. *Biomaterials* **2011**, 32, 4052-4057.

12. Mohanan, D.; Slutter, B.; Henriksen-Lacey, M.; Jiskoot, W.; Bouwstra, J. A.; Perrie, Y.; Kundig, T. M.; Gander, B.; Johansen, P. Administration routes affect the quality of immune responses: A cross-sectional evaluation of particulate antigen-delivery systems. *J Control Release* **2010**, 147, 342-349.

13. Bal, S. M.; Slutter, B.; Verheul, R.; Bouwstra, J. A.; Jiskoot, W. Adjuvanted, antigen loaded N-trimethyl chitosan nanoparticles for nasal and intradermal vaccination: Adjuvant- and site-dependent immunogenicity in mice. *Eur J Pharm Sci* **2011**, 45, 475-481.

14. Verheul, R. J.; Slütter, B.; Bal, S. M.; Bouwstra, J. A.; Jiskoot, W.; Hennink, W. E. Covalently stabilized trimethyl chitosan-hyaluronic acid nanoparticles for nasal and intradermal vaccination. *J Control Release* **2011**, 156, 46-52.

15. Yoshikawa, T.; Okada, N.; Oda, A.; Matsuo, K.; Matsuo, K.; Kayamuro, H.; Ishii, Y.; Yoshinaga, T.; Akagi, T.; Akashi, M.*, et al.* Nanoparticles built by self-assembly of amphiphilic [gamma]-PGA can deliver antigens to antigen-presenting cells with high efficiency: A new tumor-vaccine carrier for eliciting effector T cells. *Vaccine* **2008**, 26, 1303-1313.

16. Slütter, B.; Bal, S.; Keijzer, C.; Mallants, R.; Hagenaars, N.; Que, I.; Kaijzel, E.; van Eden, W.; Augustijns, P.; Lowik, C.*, et al.* Nasal vaccination with N-trimethyl chitosan and PLGA based nanoparticles: nanoparticle characteristics determine quality and strength of the antibody response in mice against the encapsulated antigen. *Vaccine* **2010**, 28, 6282-6291.

17. Wen, Z.-S.; Xu, Y.-L.; Zou, X.-T.; Xu, Z.-R. Chitosan Nanoparticles Act as an Adjuvant to Promote both Th1 and Th2 Immune Responses Induced by Ovalbumin in Mice. *Marine Drugs* **2011**, 9, 1038-1055.

18. Ferreira, S. A.; Pereira, P.; Sampaio, P.; Coutinho, P. J. G.; Gama, F. M. Supramolecular assembled nanogel made of mannan. *J Colloid Interface Sci* **2011**, 361, 97-108.

19. Dobrovolskaia, M. A.; Neun, B. W. NCL Method ITA-5.1 - Qualitative analysis of total complement activation by western blot. http://ncl.cancer.gov/NCL_Method_ITA-5.1.pdf

20. Okahashi, N.; Takahashi, I.; Nakai, M.; Senpuku, H.; Nisizawa, T.; Koga, T. Identification of antigenic epitopes in an alanine-rich repeating region of a surface protein antigen of Streptococcus mutants. *Infect Immun* **1993**, 61, 1301-1306.

21. Vilanova, M.; Teixeira, L.; Caramalho, Í.; Torrado, E.; Marques, A.; Madureira, P.; Ribeiro, A.; Ferreira, P.; Gama, M.; Demengeot, J. Protection against systemic candidiasis in mice immunized with secreted aspartic proteinase 2. *Immunology* **2004**, 111, 334-342.

22. Takahashi, K.; Ip, W. E.; Michelow, I. C.; Ezekowitz, R. A. The mannose-binding lectin: a prototypic pattern recognition molecule. *Curr Opin Immunol* **2006**, 18, 16-23.

23. Thiel, S. Complement activating soluble pattern recognition molecules with collagen-like regions, mannan-binding lectin, ficolins and associated proteins. *Mol Immunol* **2007**, 44, 3875-3888.

24. Look, M.; Bandyopadhyay, A.; Blum, J. S.; Fahmy, T. M. Application of nanotechnologies for improved immune response against infectious diseases in the developing world. *Adv Drug Deliv Rev* **2010**, 62, 378-393.

25. Sjöberg, A. P.; Trouw, L. A.; Blom, A. M. Complement activation and inhibition: a delicate balance. *Trends Immunol* **2009**, 30, 83-90.

26. Moghimi, S. M.; Andersen, A. J.; Ahmadvand, D.; Wibroe, P. P.; Andresen, T. L.; Hunter, A. C. Material properties in complement activation. *Adv Drug Deliv Rev* **2011**, 63, 1000-1007.

27. Avrameas, A.; McIlroy, D.; Hosmalin, A.; Autran, B.; Debre, P.; Monsigny, M.; Roche, A. C.; Midoux, P. Expression of a mannose/fucose membrane lectin on human dendritic cells. *Eur J Immunol* **1996**, 26, 394-400.

28. Apostolopoulos, V.; McKenzie, I. F. Role of the mannose receptor in the immune response. *Curr Mol Med* **2001**, 1, 469-474.

29. Kabanov, A. V.; Vinogradov, S. V. Nanogels as pharmaceutical carriers: finite networks of infinite capabilities. *Angew Chem Int Ed* **2009**, 48, 5418-5429.

Chapter 9

Concluding remarks and future perspectives

Self-assembled mannan and pullulan nanogels were successfully produced using a versatile, simple, reproducible and low-cost method. Spherical polydisperse nanogels reveal long-term colloidal stability in aqueous medium up to six months, with a nearly neutral negative surface charge and mean hydrodynamic diameter in the nanoscale range, depending on the polymer degree of substitution.

Mannan nanogel reveals no cytotoxicity up to about 0.4 mg/mL in mouse embryo fibroblast cell line 3T3 and mouse bone marrow-derived macrophages (BMDM), and no DNA damage in fibroblasts, although possibly in BMDM, under the tested conditions.

A time-, concentration- and energy-dependent uptake profile of the mannan nanogel involving mannose receptor-mediated phagocytosis and clathrin-mediated endocytosis and possibly some endolysosomal escape, is observed in BMDM.

The protein corona formed in human plasma around mannan nanogel consists of a very specific set of proteins, apolipoproteins B-100, A-I and E and human serum albumin, slowly formed following a dynamic protein exchange process.

The mannan nanogel does not affect blood coagulation, does not induce complement activation and retards the fibril formation of both Alzheimer’s disease-associated amyloid β peptide and haemodialysis-associated amyloidosis β2 microglobulin.

Mannan nanogel has potential immunological adjuvant activity on the specific immune response to ovalbumin, predominantly humoral, in intradermally immunized mice. Ovalbumin-specific antibody subtyping indicates a T helper 2-type bias.

Following this opening encouraging study, further tests need to be performed in order to clarify the potential applicability of mannan nanogel as an effective vaccine delivery/adjuvant system, with ability to elicit both cellular and humoral specific immune responses codelivering different antigens possibly covalently linked, optimized combining immunopotentiators, and testing different number of and interval between administrations in adequate murine models, or adapting the amount of antigen and nanogel administered. Moreover, the mechanism of mannan nanogel adjuvant effect – still not clearly elucidate – requires to be studied in detail.

Mannan nanogel spontaneously incorporates proteins and hydrophobic drugs, suggesting its potential as targeted delivery system of therapeutic molecules to macrophages. The development of this strategy requires the performance of biodistribution assays. Further, the ability of the mannan nanogel to cross biological barriers requires also additional studies on the endocytosis and intracellular transport of the labeled nanogel loading the therapeutic molecules, combining the use of different inhibitors, mutated proteins, small interfering RNA and colocalization experiments with specific markers that identify cellular structures.

Mannan nanogel has promising properties for macrophages targeted delivery of vaccines or drugs suggested by its distinct physicochemical characteristics, loading ability of biological agents, cytocompatibility and macrophage uptake profile, biosafety and biocompatibility at molecular level, and adjuvant activity.